Corrected + augmented
with three photographs

SUPERSONIC FLOW OVER LOW ASPECT-RATIO WINGS

by

I.C. RICHARDS, M.A. (Oxon)

Submitted for the degree of Doctor of Philosophy
of the Cranfield Institute of Technology

- - - - - - - o O o - - - - - -

Cranfield Institute of Technology
College of Aeronautics
CRANFIELD
Bedfordshire

November 1976

data are presented as upper and lower surface pressure distributions and as oil flow, vapour screen and schlieren photographs, at angles of attack up to 50 degrees. A later version of thin shock-layer theory, which employs a physically more acceptable method to solve the governing equations, is also described. The predictions for shock wave angle, streamline pattern and pressure distributions are compared with experiments for a wing with flat compression surface. Suggestions for further work are made.

S U M M A R Y

An attempt has been made, by means of experimental work, to consolidate and augment existing knowledge of high-speed flows over delta wings. Particular emphasis is placed on the investigation of flows which did not confirm to the 'accepted' pattern.

In Part 1 the flow regimes on a caret wing are discussed with particular emphasis placed on the occurrence of 'strong' oblique shocks. Results are presented which demonstrate that when viewed in a direction normal to the leading edge, shocks of both the 'weak' and the 'strong' families can be said to exist. An experiment designed to produce a single strong shock by means of a caret wing of large anhedral, instead gave rise to a complex multiple shock pattern which could not be adequately explained by exact inviscid theory.

In Part 2 the unexpected pressure rises reported on the lee surfaces of various delta wings (References 22 and 23) are shown to be, at least in part, the result of interference from the model support and base-mounted instrumentation. The physical reason for the pressure rise is discussed. 'Correct' leeside pressure distributions are presented for one of the models used in Reference 23 for angles of attack up to 50 degrees.

In Part 3 the different flow regimes on delta wings are discussed together with the methods of defining the boundaries between them. The conjecture that thin shock-layer theory can be used to predict the onset of leading-edge separation is carefully investigated by means of tunnel tests on a particular wing with triangular cross-section. The

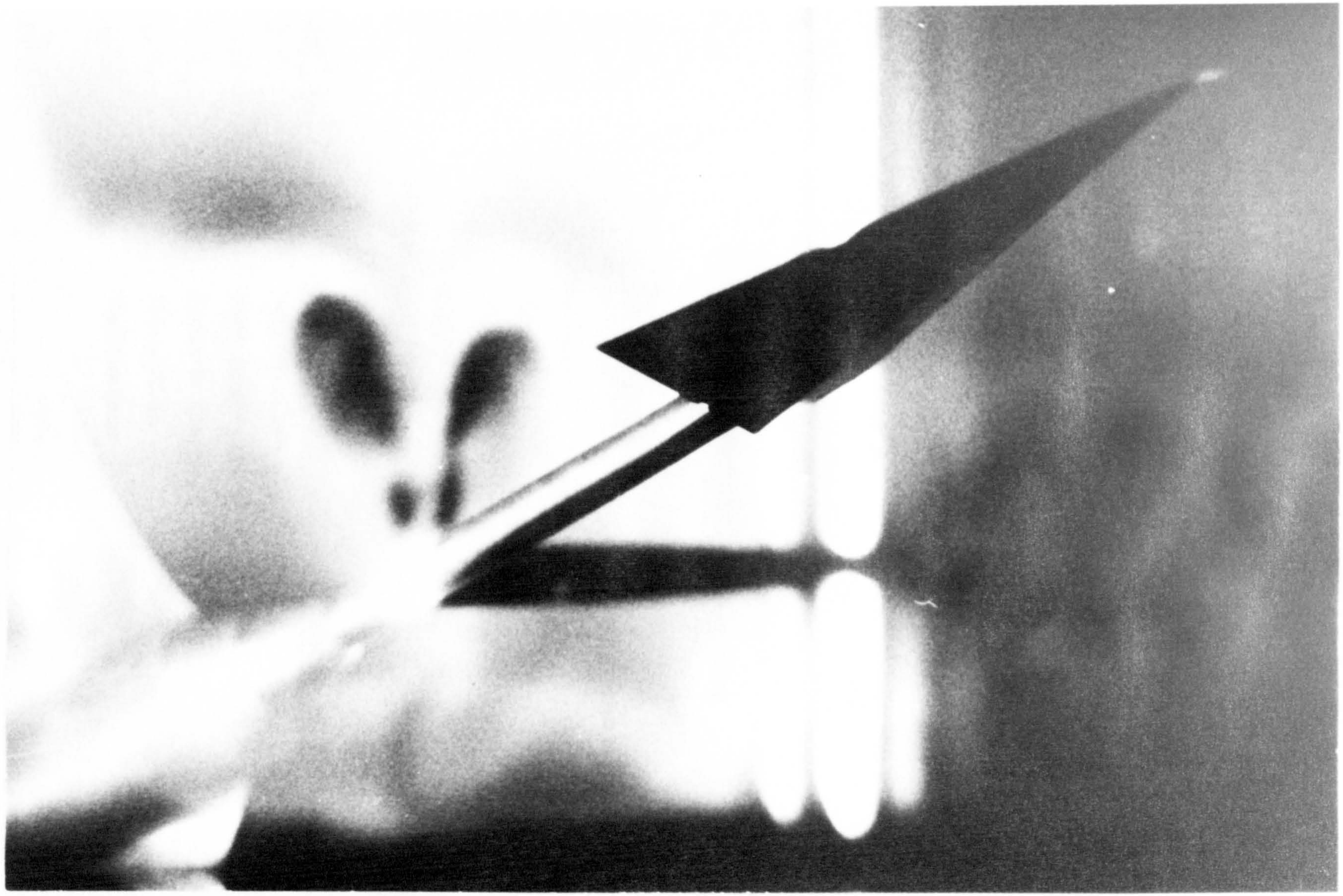

The testing of a delta wing - The trailing vortices and shock wave are made visible by means of a 'vapour screen' positioned behind the trailing edge. In the intense cold of the working section the water vapour freezes and an icicle grows from the tip of the model.

LIST OF CONTENTS

List of contents - continued :

LIST OF FIGURES

List of figures - continued :

- - - - - - - - o O o - - - - - - - -

N O T A T I O N

Cp	Non dimensional pressure coefficient
Cp(vac)	Pressure coefficient 'in vacuo' = $^{-2}/_{\gamma M^2}$
M	Mach Number
P	Pressure
P_t	Total pressure
$\underline{q}$	Velocity vector
Re_ℓ	Reynolds Number based on model length
T_t	Total temperature
x, y, z	Natural coordinates of figure 2
u, v, w	Velocity components
α	Angle of incidence relative to leading-edge plane
α_r	Semi-vertex angle of wedge, angle of incidence of lower ridgeline of caret wing
β	$(M^2 - 1)^{\frac{1}{2}}$
γ	Ratio of specific heats
χ	Sweepback angle in planform (caret wing, $\alpha_r = 0$)
Λ	Sweepback angle in leading-edge plane
ρ	Density
σ	Local body inclination
ω	Angle of 'undercut' (caret wing)

Subscripts

b	value at wing surface
s	value immediately behind shock
∞	value in undisturbed stream

I N T R O D U C T I O N

Before the advent of the modern, high speed aeroplane, a typical aircraft wing would have large aspect ratio, moderate taper and little or no sweepback. With the exception of the immediate vicinity of the tips and the junction with the fuselage the local flow on such a wing is substantially parallel to that of the mainstream and the surface pressures close to those predicted by two-dimensional strip theory. The wing designer would choose as his starting point, one or more aerofoil sections selected from a standard catalogue in which the geometry of numerous sections would be listed together with their most important aerodynamic characteristics. The sections themselves would have been derived mainly from wind tunnel tests, possibly with the assistance of potential flow theory.

The development of the practical gas turbine led to great increases in aircraft speeds and hence to the adoption of the swept wing (conceived originally by Busemann in 1929) to ward off the effects of compressibility; consideration of an 'infinite swept wing' of uniform chord suggested that, in the absence of viscous effects, the magnitude of the velocity component of the onset flow parallel to the leading edge was irrelevant, being equivalent to a translation of the wing parallel to itself. Two-dimensional results could therefore be applied to swept wings provided that the section thickness was suitably factored to take account of the sweep (for an infinite wing the factor would simply be the secant of the leading edge sweep; for wings of more general planform, a corresponding result can be obtained).If we assume that the maximum Mach number which can be reached by an unswept wing of 'subcritical' design before serious drag rise occurs is, very roughly, 0.7, then in order to reach a Mach number of unity an aircraft will require about 45 degrees of sweep and to reach Mach 2, about 70 degrees of sweep.

At these higher sweep angles the upper surface flow becomes prone to separation; an undesirable characteristic which leads in general to a limit on the useable lift because of unsteadiness in the flow (buffet). Airfield performance also becomes critical due to a combination of the above with the reduction in lift-curve slope which accompanies increasing

sweep. Although the use of 'supercritical' sections allows the sweep requirements to be relaxed somewhat, the fact remains that for aircraft designed to fly at Mach numbers much above 2.0, it will not be possible to maintain a 'classical' type of attached flow throughout the flight envelope.

The solution to this problem lies in making constructive use of the inevitable flow separation by forcing it to occur along a highly swept line defined by a sharp leading edge; under these conditions the separated vortex sheet rolls up to form a steady, tightly-bound vortex lying above the wing. This type of flow proves to be well suited to the design of aircraft in which it is desired to combine high supersonic capability with acceptable airfield performance since, in contrast to the highly swept 'classical' wing, the leeside vortices provide a stable, low pressure region up to very large angles of attack.

The simplest case of a leading edge vortex flow, and the only one which seems theoretically tractible at present, is that developed by a sharp-edged wing with triangular planform, in which the flow vectors are constant along rays through the apex; such a flow is termed 'conical'.

Although, as will be discussed later, flow conditions normal to the leading edge still retain some significance, vortex flows have no counterpart in two dimensions and it is therefore the simple delta wing with conical thickness distribution which has come to play much the same analytical role at high speeds as has the two-dimensional aerofoil at lower speeds. Although a highly idealised approximation to a practical slender aircraft wing, many of the features of the flow predicted for these simple wings will be mirrored in the more complicated flows which are at present beyond the scope of theoretical methods.

SCOPE OF THE PRESENT WORK

In the case of the delta wing research described here it was thought desirable to consolidate existing knowledge of the subject by attempting to answer specific questions rather than to slavishly add to the available data.

Three main areas of supersonic flow on delta wings were thought to require systematic investigation. The nature of each problem is discussed briefly below, in the order in which it is treated in the text.

1. STRONG AND WEAK SHOCK SOLUTIONS FOR CARET WINGS

In order to realise the complete design curve on certain caret wings it is necessary to accept that, in the plane normal to the leading edges, both 'weak' and 'strong' oblique shocks will occur. This has led Venn and Flower to question the existence of such flows and to propose alternative solutions which involve only weak oblique shocks. On a broader front, there has been speculation that it might be possible to produce on oblique shock that was 'strong' not only in the sense implied above, but also with respect to the free stream. Although never observed in an unbounded, two-dimensional flow, strong oblique-shocks have been observed in external compression jet intakes. It was surmised that a suitably designed caret wing might support such a shock, its position being stabilised by the presence of the leading edges.

2. ANOMALOUS LEESIDE FLOWS

Leeside flows in general have received little specific attention. Above moderate supersonic Mach numbers, leeside pressures on lifting wings are usually close to the vacuum limit and are often neglected in the calculation of aerodynamic loads. Experimental work by Hillier and by Szodruch and Squire however showed that under certain conditions leeside pressures could rise above that of the freestream at moderate incidences.

Neither they nor earlier workers who have observed a similar phenomenon, were able to suggest, except in a very general way, the reason for this pressure rise.

3. ONSET OF LEADING-EDGE SEPARATION

At supersonic speeds, flow incident upon the leading edge of a slender wing may either separate and roll up to form a vortex as described earlier, or, under suitable conditions of low incidence and high Mach number, may remain attached to the wing surface, negotiating the leading edge by means of a centred expansion fan. There were (and are) no theoretical models for leeside flows capable of predicting which type of flow would occur under given conditions and reliance has to be placed on a rather diffuse and restricted empirical boundary. Squire has attempted to use a simple theory to predict changes in the compression surface flow which may accompany the onset of leading-edge separation on the lee surface. The theory needed experimental verification, especially for wings of finite thickness.

Notwithstanding the remarks made at the beginning of this section a considerable volume of (mainly pressure) data is included in part 3, in the expectation that it may prove useful to, amongst others, designers of guided weapons, where combinations of high Mach number and high incidence are commonplace and where flying surfaces are often not far removed from the simple delta wings tested here.

THE EXPERIMENTAL FACILITIES

The College of Aeronautics at Cranfield has two major high speed facilities. The first is a continuous running, supersonic tunnel with a working section measuring 230 mm x 230 mm and a Mach number range from M=1.6 to M=2.5 or exceptionally M=2.8. The second is an intermittent hypersonic Helium tunnel with a core diameter of 100 mm. This hypersonic facility is unique in the United Kingdom and was the subject of

considerable development during the course of the contract, particularly with regard to the design of a 'glow discharge' flow visualisation apparatus. The work had not been completed when the contract ended but an account of the progress made may be found in the Appendix. References made in the text to hypersonic testing by the Author refer to the Imperial College hypersonic gun-tunnel, a short duration facility with a Mach number capability of M = 8 or M = 12.2

A C K N O W L E D G M E N T S

The work reported in this thesis was carried out under the Ministry of Defence, Procurement Executive contract entitled 'The Flow over Low Aspect-Ratio Wings at Supersonic and Hypersonic Speeds'. The Author duly records his thanks.

Throughout the tenure of his contract the Author was supervised by Professor J.L. Stollery, who always found time to take an active part in the research. For his advice and guidance, which have proved literally invaluable, the Author is deeply grateful.

Regular meetings with the Contract Monitor, Mr. P.L. Roe, and Dr. L.C. Squire, have provided the theoretical 'back-up' necessary for any research programme, and the form in which the work appears is in no small measure due to their assistance. The same may be said of Professor B.A. Woods, whose timely arrival from New Zealand enabled the last sections of this thesis to be written.

Especially when he first arrives, a student is deeply dependent on the help of the technical staff and in this, the Author feels that he has been unusually fortunate. For steering him around some pitfalls and patiently watching him drop into others, he would like to thank the Division's workshop staff, especially Mr. D.F. Sibley and Mr. M.F. Goodridge but above all Mr. S.W. Clarke who, amongst many other things, missed his lunch probably more times than he cares to remember, in order to run the supersonic tunnel.

The Author would like to thank Mrs. J. Holloway for her careful and accurate typing in this and previous papers.

This thesis is dedicated to Mr. J.R. Busing who died shortly before it was completed and in whom much of the Division's experimental expertise resided. His help and friendship will be sadly missed.

- - - - - o O o - - - - -

P A R T 1

THE CARET WING

1.1. THE CONCEPT OF A WAVE RIDER

Consider the two dimensional wedge in supersonic flow shown in Figure 1a. The upper surface, being parallel to the onset flow, produces no disturbance whilst the lower surface turns the flow parallel to itself by means of a plane shock attached to the leading edge. Now imagine two 'splitter plates' to be placed on finite distance apart on the infinite wedge as shown in Figure 1b. As long as the line of intersection of the plates with the lower surface of the wedge is streamwise when viewed in planform (i.e. lies in a plane of constant z), the plates will, regardless of their orientation, be stream surfaces of the flow behind the shock and will therefore create no disturbance in the flow (ignoring for the time being, the effects of viscosity, finite plate thickness, etc). For the purposes of this argument, we will assume that the plates satisfy the above conditions but are 'tilted' towards each other at the top. If, in addition, we arrange for the leading edges of the plates to extend forward until they just reach the shock, then by the 'principle of independence', no disturbances can propagate around the leading edges of these plates; in other words the outboard sections of the wedge may be removed without affecting the flow in the region between the plates. Finally, imagine the plates to be moved towards each other so that the width of wedge between them shrinks and finally becomes a line (Figure 1c). As nothing which could affect the flow in the region between the plates has been changed in this operation, the flow must still be 'two-dimensional' though now being supported by a definitely three dimensional shape having a triangular (delta) planform and inverted 'V' cross-section.

The shape derived here is called a 'caret wing' and is the simplest member of a class of lifting bodies known as 'waveriders', so called because they are designed to support a prescribed and usually simple shock shape - in this particular case, a plane shock.

The caret wing was conceived by Nonweiler[1] in 1963 though the principle of generating segments of plane shock waves on three-dimensional bodies had been discovered four years earlier by Maikapar[2], who had applied the idea to a non-lifting body consisting essentially of four caret wings mounted 'back to back' in the form of a star.

The initial appeal of the caret wing was that it enabled accurate flowfield calculations to be made on shapes thought to be representative of those that might be used at hypersonic speeds, at a time when the methods available for treating arbitrary body shapes at high Mach numbers were still very crude, e.g. simple Newtonian theory. It was soon realised however, that the caret wing also offered aerodynamic advantages over the conventional delta wing. These derived fundamentally from the position of the shock on the caret wing which,being inclined at a greater angle to the surface than that of a flat delta wing, gave greater lift at a given incidence and hence a more favourable value of lift-to-drag ratio. Had this not been the case, it is likely that the waverider would have suffered an early demise as the simple 'design' flow-field just described belied a rather complex 'off-design' behaviour.

The waverider concept was in time extended to flowfields other than that of the simple wedge. Townend[3], for example, has proposed a body which utilises the 'shockless' compression of a curved wedge and Jones[4] a body which incorporates part of the flowfield of a right circular cone. More recently, Schwartz[5] has designed wings which will support parbaloidal shocks and Pike[6] wings which will support part of the shock of more general axisymmetric bodies. In addition to this there have been many attempts to produce shapes more representative of real aircraft, incorporating more volume near the centreline for instance, whilst retaining the design philosophy of the simple caret wing (eg. Squire[7], Townend[8]).

The brunt of the research effort has never the less been directed towards the simple caret wing, it having been, to the Author's knowledge, the subject of over thirty papers. There still exist some points in need of clarification, particularly with regard to the off-design behaviour and the existence, or otherwise, of 'strong' oblique shocks.

These will be covered in the next section where the flow over the compression surface of a caret wing is considered in more detail. The problem of leeside flows are discussed separately in Part 3.

1.2. FLOW REGIMES ON CARET WINGS

1.2.1. The Design Curve

It will be appreciated from the previous section that whilst a caret wing is capable of supporting a two-dimensional flowfield, it will only do so for conditions of Mach number and incidence which are such as to produce a 'stand-off' angle for the wedge shock equal to the design angle of the wing (denoted by ω in Figure 2). For a particular wing, the locus of these points is known as the 'design-curve', the form of which may be determined by solving the two dimensional oblique shock relations for the flow deflection angle α_r and the shock angle θ

viz :
$$\tan \alpha_r = \cot \theta \; \frac{M_\infty^2 \sin^2 \theta - 1}{(\gamma + 1) M_\infty^2/2 - (M_\infty^2 \sin^2 \theta - 1)} \quad \ldots (1.1)$$

together with the condition that the shock must lie in the plane of the leading edges,

viz :
$$\theta - \alpha_r = \omega$$

The resulting equation, being an implicit function of α_r and M_∞ can be rather tedious to solve and it is convenient to use compressible flow charts (e.g. Reference 9) if high accuracy is not required.

The design curve may be arrived at by a different route by considering the plane shock to spring not from the 'vestigal' wedge, but from the leading edges of the wing panels, which are themselves inclined to the onset flow. Making use of the 'infinite swept wing analogy' (See, for example, Reference 10), we consider only

the component of flow normal to the leading edges (which will be subsequently referred to as the 'normal plane') and obtain the following expressions for the Mach number and incidence in this plane (See Figure 2 for notation).

$$Mn = M\infty \ (1 - \cos^2 \alpha \ . \ \sin^2 \Lambda)^{\frac{1}{2}} \qquad \ldots\ldots(1.3)$$

$$\sin \alpha_{nc} = \frac{\sin (\alpha - \omega) \ \cos \Lambda}{(1-\cos^2 \omega \ \sin^2 \Lambda)^{\frac{1}{2}} \ (1-\cos^2 \alpha \ \sin^2 \Lambda)^{\frac{1}{2}}} \qquad \ldots\ldots(1.4)$$

Where $\alpha = \alpha_r + \omega$ - i.e. the angle of incidence measured relative to the plane of the leading edges, the equivalent design angle in the 'normal plane' is given by :

$$\omega_n = \tan^{-1} \left(\frac{\tan \omega}{\cos \Lambda} \right) \qquad \ldots\ldots(1.5)$$

Since both methods are 'exact' for the design case, the results of solving equations 1.3, 1.4, and 1.5, with the oblique shock relations, 1.1 are identical to those obtained earlier. The extra complication of this approach is justified by the fact that the method of analysis continues to have some significance when the wing is 'off-design' and the flowfield too 'three-dimensional' for the 'vestigal wedge' method to give useful results.

For given values of α_r and $M\infty$, equation 1.1 will yield either two or no values of θ. The latter correspond to a detached shock (on the equivalent wedge) and the former to the 'weak' and 'strong' oblique shock solutions. Only the 'weak' solution is observed in steady, two-dimensional flow and it is this solution which is assumed in the design of a conventional caret wing. When using the second method however, it is in general necessary to consider both the 'weak' and 'strong' solutions in the 'normal plane' in order to produce the complete design curve and this has led Venn and Flower[11] to question the existence of a single shock solution for that part of the design curve for which the shock in the 'normal plane' is 'strong'. This point will be further discussed in a later section.

1.2.2. The Detachment Curve

A two-dimensional wedge will only support an attached shock wave up to a certain wedge angle after which a detached, curved shock will appear. This angle varies from zero at M=1 to approximately 45.4 degrees at $M = \infty$. As explained in the previous section, the ridgeline incidence α_r of a caret wing ceases to have any special significance away from the design curve and it is the conditions normal to the leading edge which we must consider in determining when shock detachment will occur. In principle, equation (1.1) may be used (with α_r and $M\infty$ replaced by α_{nc} and Mn) to find the condition for shock detachment, which is indicated by the degeneracy of the 'weak' and 'strong' shock solutions; in practice, it is usually more convenient to use the flow charts (e.g. Reference 9) referred to in the previous section.

An example of the design and detachment curves for a 'typical' caret wing is shown in Figure 3. By definition, the design curve is independent of aspect ratio whereas the detachment curve is not. The point Q in Figure 3, at which the two curves touch, is significant in that it marks the changeover from 'weak' to 'strong' shock solutions in the 'normal plane'. The foot of the detachment curve incidentally is usually shown to lie at P_1, where the normal component of Mach numbers is equal to :-

$$M\infty \left(1 - \cos^2\omega \sin^2\Lambda \right)^{\frac{1}{2}}$$

but this is only the case for wings of zero thickness. The effect of a finite leading-edge angle is to increase the minimum Mach number for which an attached shock wave can occur. This topic will be discussed in some detail in Section 3.1.2b.

1.2.3. Possible Types of Flow on Caret Wings

An inspection of Figure 3 shows that the design and detachment curves divide the (M, α) space into four regions as follows :

REGION 'A' : lying to the right of, and bounded by, the design curve.

REGION 'B' : the area to the left of the design curve and extending to the detachment curve.

REGION 'C' : the area extending from the 'strong' branch of the design curve (QT) to the detachment curve.

REGION 'D' : lying above the shock detachment curve.

(a) Flow in Regions 'B' and 'D'

All Authors are in agreement with regard to the flow in these regions and little description is necessary.

Throughout Region 'B' the shock is bowed outwards though attached to the leading edges. The shock shape at very small incidences can be calculated by assuming that it is the envelope of the Mach cones from the leading-edges of the wing. Venn and Flower[11] have shown that the shock shape found in this way consists of straight (plane) segments extending from the leading edges to the Mach cone from the apex, to which they are tangential.

The effect of increasing incidence at constant Mach number depends to some extent on the starting point though the shock is qualitatively as described above throughout the region. This is illustrated in Figure 3. At a Mach number M_1, the plane leading-edge shocks described above, move closer to the wing panels with increasing incidence but the shock is still bowed outwards when the detachment curve is reached at X_1. Starting at a higher Mach number M_2, the plane shocks again move closer to the wing with increasing incidence but this time, the curved central part of the shock disappears entirely as the design curve is reached at, D_1, and a single plane shock is formed. Further increases in incidence cause the shock(s) to move 'inside' the wing (Region 'A') but at some stage this inward progression is

halted as a single plane shock occurs again at D_2. Above this incidence, the shock becomes increasingly convex before detaching at X_2.

It should be noted that a dual design condition at a given Mach number does not necessarily imply that one shock solution is 'weak' and the other 'strong', either in the sense of the 'equivalent wedge' flow or in the 'normal plane'. As stated in the previous Section, the design curve is independent of aspect ratio whereas the detachment curve is not and therefore a family of wings with the same value of the design angle, ω, but different sweeps, will have identical design incidences at a given Mach number. The point, Q, at which the design and detachment curves touch will however, change from one member of the family to the next, moving to lower Mach numbers as the sweepback is increased (See P.345 of Reference 12 for example). Since the point of coincidence of the two curves makes the change from the 'weak' to the 'strong' shock solution in the 'normal plane' it follows that the two solutions are only of a different type if the point Q lies between D_1 and D_2. In Figure 3, Q lies to the right of both D_1 and D_2 and both solutions are therefore 'weak'.

In Region 'D', above the detachment curve, the shock is detached and 'stands-off' from the leading edges. It is generally held (e.g. Reference 12) that the shock is convex throughout this region but Venn and Flower[11] suggest that at sufficiently high Mach numbers and incidences the shock may be concave inboard of the leading edges.

An examination of the schlieren photographs obtained by Richards[13] and Coleman[14] at Mach numbers of 12 and 8 respectively, shows no obvious evidence of this effect (See Figure 5e for example) but a conical schlieren or shadowgraph photograph would be necessary to place the matter beyond doubt.

(b) Flow in Region 'A'

To the right of the design curve SQT the shock structure lies 'within' the wing and for wings of low aspect ratio (taken in this case to imply an included angle of less than 90 degrees between the wing panels) can be very complex (See Reference 11 for example). For wings of more moderate aspect ratio a 'bifurcated shock' occurs as shown in Fig.3. The shock is again composed of plane segments from the leading edges intersecting with the shock from the ridgeline but the situation is complicated by the existence of two 'inner shocks' which extend from the intersection to the wing panels. These shocks are necessary to satisfy the boundary conditions at the wing surface and may be thought of as a development of the 'Mach cone from the apex' at zero incidence. In order to visualise this shock structure explicitly a conical schlieren or shadowgraph technique needs to be used. Crabtree and Treadgold[15] and Alekseev and Gonor[16] have published results obtained from such a system which confirm that the flow is as described above although in Reference 16 the results were complicated by the presence of shock-induced separations.

At Mach numbers higher than that corresponding to the change-over from 'weak' to 'strong' shock solutions (point Q in Figure 2) opinions differ as to how the shock pattern changes with increasing incidence. Squire[17] believes (and has supporting evidence from the results of Treadgold[15] and Keldysh[18] that the central shock 'slides-down' the outer shocks, reaching the leading edges at the design incidence. The existence of a 'strong' shock in the 'normal plane' is thus accepted although it occurs only as a limit. Venn and Flower [11] contend (though it is possible that their opinions may have changed in the light of the results presented by Squire) that the strong shock does not occur in practice and that the bifurcated shock structure persists up to (and indeed beyond) the design curve SQT.

Results are presented in Figures 4 and 5, which were obtained by the Author in the Imperial College No. 1 gun tunnel at a Mach number of 12.2. The wing tested had a root chord of 76.2mm, leading edge sweep, Λ , equal to 63 degrees and a design angle, ω, of 14 degrees; the wing thickness normal to the leading-edge was 8.4 degrees. As can be seen from Figure 4, the design and detachment curves touch at a Mach number of approximately 5. For free-stream Mach numbers between about 3.5 and 4.0 a dual design condition exists, both solutions being of the 'weak' family. At the test Mach number there is only a single solution, this being of the 'strong' variety.

Figures 5(a) - (c) show how the flow develops in Region 'A'. At the lowest incidence tested ($\alpha_r = 21^o$) two distinct shocks are visible in the schlieren photograph, one, clearly the central shock, is nearly plane and persists for a chord length downstream of the model with virtually no deflection, whilst the other apparently springs from the tip and is much more curved (in the XZ plane). There is no evidence from the photograph to suggest that the shocks 'interfere' to any extent and it may therefore be inferred that they are separated in a 'lateral' sense. As no reference to the downstream behaviour of such shocks could be found in the published literature it was decided to roll the model at constant incidence whilst keeping the knife-edge horizontal in order to build up a picture of the three-dimensional shock. Rather surprisingly, the detail revealed by the schlieren decreased rapidly as the model was rolled; in particular, with the model rolled so that one wing panel was parallel to the direction of viewing, only a very weak shock (or perhaps wake) could be observed whilst with the model rolled through 90 degrees, no detail at all could be seen. It was therefore inferred that the constituent parts of the downstream shock system are nearly plane and moverover, are inclined only slightly in the YZ plane. The Author is uncertain whether or not the results are particular to the caret wing tested here which was unusual in that the upper surface was designed to produce a strong Prandtl-Meyer expansion when the lower surface was 'on design'.

In Figure 5(b) taken at α_r = 35 degrees, the central shock has moved outwards and apparently become stronger whilst the 'tip' shocks have become much fainter and more highly curved. (suggesting attenuation by an expansion fan).

The wing is 'on design' for α_r = 39 degrees. Figure 5(c) shows a single plane shock lying in the plane of the leading edges with no evidence of the 'tip' shocks observed at lower incidences. It is thought that this photograph provides unambiguous evidence for the existence of a 'strong' oblique shock in the 'normal plane'. The experimentally observed design incidence of the wing is some two degrees lower than predicted by the exact oblique shock relations though the implied error in terms of design angle, ω, is only 0.7 degrees. For the flow behind the shock, the Reynolds number based on root chord was approximately equal to 4×10^4 and the boundary layer would therefore have been laminar over the lower surface. Using a 'data sheet method' (Reference 19) to calculate the growth of a flat plate boundary layer under these conditions, the displacement thickness at the trailing edge was found to be 0.39 mm; equivalent to a decrease in ω of about 0.3 degrees. The discrepancy, which is thought to be greater than the experimental error, was probably due to the approximate nature of the calculation which made no allowance for the thickening of the boundary layer in the 'ridge corner'.

We conclude that the flow in this region is as described by Squire in Reference 17 and that the full design curve of a caret wing can be realised even though, in practice, it may involve the formation of a 'strong' oblique shock in the plane normal to the leading edge.

(c) Flow in Region 'C'

In the region between the design curve SQT and the detachment curve PQR a shock pattern similar to that in Region 'B', i.e. a bowed shock lying outside the plane of the leading edges* but attached to them, can in theory occur but the Author has been unable to find any results in the published literature where this can defininitely have been said to occur. The alternative is a detached shock wave as in Region 'D'.

In the previously described tests carried out by the Author in the Imperial College gun tunnels, the shock is seen to move outside the plane of the leading edges at α_r = 41degrees (Figure 5d), there is no evidence of shock detachment in the planview schlieren photograph taken at α_r = 42 degrees but at α_r = 45 degrees the shock is clearly detached. This method for detecting shock detachment is known to be rather insensitive but an alternative technique used by Stetson and Scaggs[20], in which shock detachment is indicated by a flow of oil round the leading edges from the lower to the upper surface, could not be successfully adapted to the gun tunnel. The question as to whether or not an attached shock can exist in this region must therefore, remain open to some doubt. As the results of the Imperial College tests have never been published in their entirity, a summary of the relevant experimental details is given in Figure 6.

1.3. An experiment with a caret wing of large anhedral

1.3.1. Introduction

In the previous section it was concluded that for a caret wing 'on design' the shock wave in the plane normal to the leading edges could be either 'weak' or 'strong'. This led to speculation that by designing a wing of sufficiently large anhedral, it might be possible to produce an oblique shock that was 'strong' both in the normal plane and in the

* though with the shock inclined inwards at the leading edges

sense of the equivalent wedge. Although as stated earlier, such a shock is never observed in steady, two-dimensional flow it is an accepted feature in external compression jet intakes (See e.g. Neale and Lambe[21]) where the flow may be described as 'bounded two dimensional'.

1.3.2. Details of the model and test conditions

The model was to be tested in the Cranfield 230mm x 230 mm supersonic wind tunnel and was therefore designed to support a plane 'strong' shock at a Mach number of 2.45. A large degree of latitude was, of course, possible in the choice of geometric parameters, those finally chosen (See Figure 7) giving a theoretical inviscid design incidence of α_r = 20 degrees. The design and detachment curves are also shown in Figure 7 and are seen to be quite different to those of a conventional caret wing.

Because of the low aerodynamic loads imposed upon the model, 18 swg (1.27 mm) stainless steel sheet was used for the construction, the upper surface being chamfered over a distance of 10 mm to produce the desired sharp leading edge. It was initially intended to use the model only for flow visualisation but after the first series of tests a row of compression surface pressure tappings were installed parallel to the leading edge and 10 mm behind it.

The original pressure measuring system in the supersonic tunnel consisted of vertical mercury manometer banks which were found to be rather insensitive for the low stagnation pressures generally used and improvements to the system were therefore sought. The first modification was to convert one bank of manometers from mercury to ethylene glycol; this conferred a better than tenfold increase in sensitivity and still allowed pressures lower than 0.8 Cp (vac).

to be measured without risk of the fluid boiling. These manometers were used successfully throughout the tests on the caret wing, but it was found that the high viscosity of the ethylene glycol seriously limited the rate at which readings could be taken. During the tests on the flat cone model described in Part 2, the possibility of replacing them by pressure transducers was investigated, with encouraging results and a complete system, consisting of pressure scanning switch, data logger and teletype was subsequently installed. This resulted in a large increase in both the speed and the accuracy of the measurements, both of which were to prove very necessary in the delta wing work described in Part 3, where a large volume of data had to be collected and the pressures were often close to the vacuum limit.

Throughout the tests described in this thesis, the Mach number was kept constant at a nominal 2.5. The actual test conditions were as follows :

$M_\infty = 2.45$

$P_t = 3.5 \times 10^4$ Nm^{-2} (5 psia)

$R_{e/l} = 7.2 \times 10^5$ m^{-1}

T_t = ambient

adiabatic wall.

A conventional, single-pass schlieren system was used with the beam perpendicular to the tunnel axis.

1.3.3. Results

An inspection of the schlieren photographs in Figure 8 shows immediately that the design aim, of producing a single, strong oblique-shock, has not been achieved. Instead, a complex, multiple shock pattern, apparently similar to that described by Venn and Flower[11] for wings of low aspect ratio has formed. Probably because such wings are considered unrealistic for any practical application, many of the results for 'crossed-shocks' remain speculative and it was therefore decided to

pursue the testing to the extent that useful comparisons with theory could be made. A row of pressure tappings was therefore installed, as described in 1.3.2. and the model pressure-plotted over an incidence range $10^{\circ} \leq \alpha_r \leq 30^{\circ}$. The mean values of three sets of readings are shown in Table 1. below. In keeping with the assumptions of conical flow, the positions of the pressure tappings are described by the non-dimensional value ζ/ζ_{max} where ζ is the distance from the ridgeline to the tapping and ζ max the corresponding distance to the leading edge.

TABLE 1 p/p_{∞} on the compression surface of the caret wing

α_r \ ζ/ζ_{max}	0.0	0.300	.465	.559	.624	.676	.712	.741
10°	1.96	1.99	1.61	1.48	1.31	1.32	1.33	1.36
15°	2.49	2.50	1.88	1.76	1.53	1.51	1.49	1.51
20°	3.24	3.39	2.13	2.04	1.94	1.79	1.66	1.65
25°	4.45	5.18	2.55	2.34	2.35	2.30	2.14	1.76
30°	6.01	6.68	6.58	4.01	3.65	3.02	2.46	2.29

1.3.4. Theory

In principle the 'building-up' of a multiple shock pattern from segments of plane shocks is straightforward, though in practice Venn and Flower[11] describe it as 'complicated and lengthy' without the aid of a computer, a view which the Author will endorse.

Physically, multiple shocks arise when a wing has sufficiently large anhedral for the shocks from the leading edge to intersect and cross, before they enter the region of influence of the ridgeline. These shocks may subsequently reflect from the wing panels and re-cross, perhaps several times, the total number of shocks increasing with the anhedral and with

the Mach number. All but the innermost shock of the family must be 'weak' in order to preserve the supersonic flow behind them; the innermost shock may be either 'strong' or 'weak' in a suitably defined 'normal plane', (these cases are analogous to 'on-design' behaviour) or, more generally, will be of the 'bifurcated' type as described in 1.2.3b)

The starting point for the 'exact' calculation is the set of equations 1.1, 1.3, and 1.4, which allows the angle between the leading edge shock and the wing panel to be determined and hence the line of intersection of the leading-edge shocks. The local flow behind each of these shocks will be parallel to the wing panel and its magnitude and direction may be determined from the oblique-shock relations (it is in general necessary to solve all these equations explicitly, as the shock charts referred to earlier do not provide sufficient accuracy for more than a rough calculation). In order to continue with the solution it is helpful to adopt the idea proposed by Venn and Flower[11] and to treat the line of intersection of the leading edge shocks as the leading-edge of a 'new' caret wing, whose plane of symmetry is defined by one panel of the existing wing. Some fairly straightforward trigonometry will produce values for the sweepback and design angle of the virtual wing which, in conjunction with the previously calculated post-shock Mach number and incidence can be used in equations 1.1, 1.3, and 1.4 to produce the angle between the second shock and the plane of symmetry of the original wing. These calculations can obviously be repeated for an arbitrary number of shocks and a question therefore arises as to how the innermost shock should be constructed. Only a limited number of solutions can be computed exactly; these correspond to those cases where the calculation is terminated automatically by an angle of incidence of zero being predicted for the following stage in the calculation.

Since the flow behind these inner shocks must be parallel both to the wing panels and to the plane of symmetry, the situation is analogous to the design condition for a conventional caret wing and is in fact referred to by Venn and Flower[11] as the 'nth design condition' where n is the total number of shocks between the leading edge and the inner shock.

For the more general case of 'off-design' behaviour the inner shock will be of the 'bifurcated' type and therefore not ammenable to simple oblique-shock theory. An approximation for the shock from the ridgeline therefore has to be used to complete the solution.

1.3.5. Discussion

At the test Mach number of 2.45, the caret wing described in 1.3.2. has a 'first' design incidence of $\alpha_r = 20^\circ$ and a 'second' design incidence of $\alpha_r = 27.3^\circ$. As the results cover the range $10^\circ \leqslant \alpha_r \leqslant 30^\circ$ in increments of 5 degrees and because the 'first' design condition was not realised, all the results obtained were for 'off-design' incidences. For reasons which will be discussed shortly however, it is thought extremely unlikely that this 'second' design condition could have been achieved.

Using the method described in the previous section shock patterns were calculated for all of the incidences tested. In each case exact 'weak' solutions were continued inboard, up to the estimated position of the shock from the ridgeline. The flow inclination and Mach number behind the last calculated shock-segment were then used in conjunction with tangent-wedge theory to produce a more accurate value for the final shock position.

The theoretical and experimental pressure distributions are compared in Figure 9 and show large differences not only in the absolute values but also in the general

shape. In particular, although the measured pressures appear to be approaching the theoretical value near the leading edge there is no real evidence of the constant pressure region which is predicted to extend from the leading edge to the first shock impingement on the wing at approximately $\zeta/\zeta_{max} = 0.3$. The pressures instead tend to rise fairly steadily to almost twice the predicted values at the inboard end of this region. Ridgeline pressures on the other hand are consistently over-predicted by the tangent wedge approximation but high accuracy was not expected from this simple approach; a change to a tangent cone approximation (not shown) causes consistent under-prediction of the pressures.

After the difficulties experienced in interpreting the rather simple schlieren photographs shown in Figure 5, the task of analysing those in Figure 8 was approached with some trepidation. Taking first the position of the inner shock; this moves slowly outboard from $\zeta/\zeta_{max} = 0.30$ at $\alpha_r = 10^\circ$ to $\zeta/\zeta_{max} = 0.32$ at $\alpha_r = 25^\circ$ and then jumps suddenly to $\zeta/\zeta_{max} = 0.42$ at $\alpha_r = 30^\circ$. This jump is accompanied by the appearance of a curved detached bow shock which crosses the trailing edge at $\zeta/\zeta_{max} = 0.63$ and obviously has the effect of reducing the Mach number in the flow over a large portion of the compression surface. The formation of a detached shock wave was not unexpected as the shock detachment angle for a wedge at this Mach number is about 29 degrees. The remaining shocks are very hard to explain, being more numerous and complicated than would be expected from the crossed-shock model, though conversely large surface pressure changes occur where there are apparently no shocks. The only freedom within the 'exact' method concerns the choice of 'weak' or 'strong' shock solutions; the effect of having the second shock 'strong' was therefore investigated even though it appeared to be excluded by the evidence of the schlieren photographs which showed other shocks in the flow behind

the 'strong' shock. The calculation for $\alpha_r = 10^\circ$ showed that the flow was in fact just supersonic behind the second shock but the predicted pressure levels were over twice those measured at the ridgeline. It was concluded that the exact theory is incapable of explaining the observed results which must therefore in part be due to viscous effects.

In Reference 16, Aleekseev and Gonor report on tests on a caret wing with design angle $\omega = 31.2$ degrees and sweepback $\Lambda = 73.3$ degrees at a Mach number of 4.0. Their results, which are confined to conical shadowgraph photographs, show that it is possible for the shock impinging on the wing panel to separate the boundary layer and hence cause large changes in the effective wing geometry and the shock structure. Unfortunately, Reynolds number of these tests is not mentioned, nor any information from which it may be estimated and it is therefore not possible to say how closely their tests compare with the current work. The two main effects of interaction between the shock and boundary layer are as follows :

1. The position of the shock may be substantially changed from that in inviscid flow.

2. The sudden pressure rise through the shock will become 'blurred'; that is, on the surface under the shock, the pressures will rise at a more gradual rate, the start of the pressure rise possibly lying upstream of the shock position.

It is thought that a combination of these two effects is adequate to explain the discrepancies which exist between the theory, the measured surface pressures and schlieren photographs. Firstly, the theory is restricted to conical flows and the experimental results are presented in a way which assumes that the flow is conical but at the low Reynolds number of the tests, there may be significant regions of laminar separation especially

towards the apex of the wing which will cause the flow to depart from a conical condition. Under these circumstances the practice of measuring the shock positions at the trailing edge from schlieren photographs and then extrapolating to the apex is also unreliable and poor agreement is likely to be obtained between an observed pressure rise and the calculated position of the shock which is thought to be causing it. Finally, there is the 'blurring' effect on the shock which allows the surface pressures to rise in a region apparently upstream of where the shock is acting.

In the present tests, it is suggested that at least over part of the wing, the shock from the leading edge having crossed the plane of symetry impinges on the opposite wing panels and separates the boundary layer, perhaps with the formation of a ' λ shock'. At lower incidences the flow may become turbulent and re-attach before reaching the shock from the ridgeline whilst at high incidences, it is probable that an involved interaction between shocks and the boundary layer occurs leading to the complex downstream behaviour observed in the schlieren photographs.

1.3.6. Conclusions

The caret wing which was originally designed to support a single strong oblique-shock when 'on-design', did not achieve this objective; it is thought that it was the careful control of downstream conditions which allowed other workers to produce such a shock in rectangular intakes. The 'crossed-shock' structure which did occur was analysed by means of 'exact' theory which, whilst predictably giving good answers near the leading edge, failed to produce agreement with experiment further inboard. This has been attributed to the presence of shock induced boundary-layer separation. For this reason it is thought highly unlikely that the 'second design condition', which involves the formation of a 'strong' inner shock, could have been realised at the test Reynolds number.

P A R T 2

THE ANOMALOUS LEESIDE PRESSURE RISE

2. INTRODUCTION

Hillier[22] and Szodruch and Squire[23] have tested families of wings with delta planforms and have observed unusual trends in the development of leeside flows with increasing incidence. As the inci dence increased from zero, the leeside pressure at first fell as expected but then, at about 12 degrees, began to rise and by 14 degrees had reached the free stream static value. Subsequent increases in incidence produced further small rises in pressure. Complementary schlieren photographs showed this pressure rise to be accompanied by an apparent movement of the vortex away from the lee surface and the appearance of a shock from the apex of the wing. The same qualit-ative behaviour was shown when the models were tested in the 3ft x 4ft supersonic tunnel at the Royal Aircraft Establishment, Bedford.

A similar phenomenon had been observed some years previously in the Cranfield supersonic tunnel by Edney and Stevenson[24] and the work later pursued by Craven and Alexander[25].

At the suggestion of L.C.Squire, one of the models was brought to Cranfield to investigate the effect of support interference on the leeside flow. Details of the model are shown in Figure 10.

2.1. Test procedure and results

The mounting lug on the model proved incompatible with the model support system in the supersonic tunnel and was therefore removed and replaced by a sting as shown in Figure 11. The pressure plotting tubes were unchanged and those on the flat upper surface were connected by 3 mm O.D. PVC tubing to the tunnel pressure measuring system. The results of this initial test showed the flow to be developing in an orderly manner up to an incidence of 22 degrees; the leeside pressure falling steadily with increasing incidence. The schlieren photographs in Figure 12 show that for positive incidences up to this value

there is a vortex lying above the wing (appearing as a diffuse dark line) and between this and the wing, a shock (revealed as a bright line) almost parallel to the upper surface and resulting from the strong downwash between the vortices. Above and behind the trailing edge oblique shock(s) return the flow to a streamwise direction. At α = 23.5 degrees the flow became suddenly unsteady with large pressure fluctuations occuring. Observations of the schlieren showed the flow to be 'switching' between two types, the first typical of that observed at lower incidences and the second exhibiting a shock from the model apex and the 'vortex' apparently well away from the wing. The impression gained was that the flow did not change discontinuously from one type to the other, but that the shock which was initially close to the lee surface, moved rapidly away from the wing to its new position, having 'passed through' the vortex. At α = 24 degrees the second type of flow became steady and the leeside pressure rose above the free stream static level.

The length of the sting was then increased by 70mm; this produced no detectable change in the flow pattern, and indicated that it was not the proximity of the incidence crescent which affected the flow.

Finally, the flexible tubing was removed from the back of the model and the free ends of the hypodermic tube bent slightly inwards. A comparative schlieren photograph (Figure 13) taken at α = 24 degrees shows a significant change in the flow with no evidence of the apex shock observed earlier. A second sting was then constructed to allow the incidence to be increased to 50 degrees; a single, small diameter flexible tube was used to monitor the pressure on the leeside centreline. Schlieren photographs (Figure 14) show no abrupt change in the flow pattern; the apex shock finally appearing at about α = 35 degrees. Further thin flexible tubes were then joined to the hypodermic tubes. Schlieren photographs indicated that the flow had not been significantly disturbed. With the aid of these smaller tubes some pressure distributions were measured; the results for 55% chord are shown in Figure 15 for the incidence range $0 \leqslant \alpha \leqslant 50$ degrees. As can be seen, the pressure falls to approximately 0.7 C_p(vac) at

α = 35 degrees and thereafter rises gradually to reach the free stream static value at α = 50 degrees. The results for 80% chord were generally very similar though away from the vacuum limit the suction levels were generally some 10% higher than those at the forward station.

Figure 16 shows a specimen results from Squire and Szodruch's[23] investigation for comparison. The particular test was conducted at M = 3.5 and therefore the numerical value of the pressure coefficients cannot be directly compared with those in the previous figure. The divergence in the results for α = 12 degrees is clearly visible however.

An inspection of the schlieren photographs shows that the leeside vortices 'bend' away from the wing surface at some point. This 'bend', which Szodruch[26] associates with vortex burst, lies close to the trailing edge at moderate incidences and begins to move upstream at about α = 20 degrees. The measured pressure distributions though seem to indicate that the pressure rise occurs simultaneously at 55 and 80% chord. More chordwise pressure measurements would be necessary to clarify the connection between the state of the vortex and the leeside pressure.

2.3. Further tests

The leeside pressure rise observed in the earlier tests at the RAE and Cambridge would appear to have been the result of interference from some part of the model support. To artificially produce an adverse pressure gradient such as may have existed, three rectangular flaps were constructed (Figure 17) and tested successively on the model. Flap 'A' was set at zero incidence (relative to the lee surface) and extended backwards a distance of equal to 20% root chord. Flaps 'B' and 'C' were 20 degree wedges of 10% and 20% root chord respectively. They extended forward from the trailing edge of the model.

The model was re-tested in the range $20^{\circ} \leq \alpha \leq 50^{\circ}$. Flap 'A' was found to have little effect, the apex shock and pressure rise occurring much as before at $\alpha = 35$ degrees. Flaps 'B' and 'C' produced local regions of separated flow in the compression corner (Figure 18) but otherwise had little effect on the leeside flow. In particular there was no evidence of the separated region extending upstream with increasing incidence.

At this stage it was decided to restore the model to its original configuration, i.e. as in Figure 12, to check that the initial observations could be reproduced. At the maximum incidence obtainable with the straight sting ($\alpha = 25$ degrees) there was no evidence of leeside flow separation. This proved a serious problem. In the original tests the sudden pressure rise had occurred very close to the limit of incidence adjustment and the critical incidence was known to be very sensitive to small changes in the model and its support, which would not therefore be altered to increase the incidence range.

An examination of the model revealed that at some time during the tests the tip had become rather blunted and this was therefore built up and re-sharpened; a suggested mechanism for the observed pressure rise had been asymmetrical vortex shedding which is known to depend strongly on the tip geometry. In this case however, the sharpening was not found to have any effect. Finally, a large wedge was placed in the wake of the model just behind and above the trailing edge (Figure 17). (Szodruch[26] had found this effective in promoting the leeside pressure rise). A schlieren photograph (Figure 19) taken at $\alpha = 25$ degrees shows no evidence that the flow over the wing has been substantially altered.

2.4. Discussion

Although we have been unable to pinpoint the cause of the leeside pressure rise and its subsequent disappearance it is instructive to examine the results for evidence of the nature

of the flow breakdown. The pressure distributions in Figures 15 and 16 are remarkably similar at least for low incidences, in view of the difference in Mach number between the Cambridge and Cranfield tests. The combination of subsonic leading edges and large leading-edge angle makes it unlikely that there would have been attached flow around the leading edges in the Cranfield tests and the similarity may be somewhat misleading, though schlieren photographs on the current work and Reference 23 leave little doubt that the same breakdown mechanism was at work in both cases.

Szodruch[26] suggests vortex burst as the reason for the observed leeside pressure rise and to support their argument have oil-flow photographs strongly resembling those obtained by Earnshaw and Lawford[27] for their low speed experiments on vortex breakdown. In addition, the schlieren photographs in Reference 23 show an apparent broadening of the vortex after the pressure rise has occurred, which would again be consistent with breakdown.

Against this argument, we note that although in the Cambridge tests the pressure rise at the trailing edge <u>generally</u> occurred at a lower incidence than that at the forward station, this was certainly not the case in the Cranfield tests where there were two, quite different, types of flow at a particular incidence. Further, if the interpretation of the schlieren photographs is correct then the burst actually occurs at the apex. It is generally accepted that vortex breakdown is the result of stagnation of the axial flow in the vortex core and it might be expected that different mechanisms would be required for the burst to move upstream depending upon whether the core is subsonic or supersonic. In a series of tests intended to explain the results of Edney and Stevenson[24], Craven and Alexander[25] investigated vortex burst on a delta wing with 75 degrees of sweep at a Mach number of 2,0. They discovered that the existence of a supersonic vortex core did not inhibit the steady upstream progression of the breakdown with increasing incidence and that the results were not unlike those obtained at low speeds, the vortex burst crossing the trailing edge at α = 26 degrees and reaching x/l = 0.3 at the incidence limit of α = 34degrees. The associated pressure rise always occurred somewhat downstream of the burst, reaching only x/l=0.5 at the incidence limit. These results may be compared with those obtained by Earnshaw & Lawford[27] at low speeds for wings of 70 and 76degrees of sweep. For the lower sweep wing the vortex burst crossed the trailing edge at α = 28degrees and reached x/l=0.3 at α =35degrees; the corresponding results for the 76° wing were 35degs and 47degs. In these low speed tests the breakdown had not

reached the apex of the wing at the incidence limit (α = 50°) Wentz and Kohlman[28] find very similar results and point out that the progression of the burst depends upon the pressure gradient along the vortex core and will in general become more gradual as the apex is approached, the pressure gradient tending to zero as the flow becomes conical.

In References 25 and 26, as well as in the current investigation, the effect of placing obstacles in the wake was examined, the intention being to promote burst by direct action on the vortex. In each case, the result was the same; the position of breakdown was forced upstream but there was no general pressure rise over the lee surface. The Author therefore feels that alternative reasons for the pressure rise should be considered.

The original Cranfield tests, in which the flow was seen to oscillate between two distinct types, were strongly reminiscent of the flow over a bluff-body with 'spike' forebody and it is thought that the analogy can be usefully pursued. Figure 20 taken from Reference 29, shows the two types of flow which may occur with such a configuration. In 20(a) a weak shock extends from the tip of the spike to the detached bow shock of the bluff body. In 20(b) the boundary layer has separated from the tip forming a region of conically separated flow; the conical shock from the spike has become much stronger and there is a commensurate reduction in the strength of the bow shock. In Figure 20(c) the corresponding case for a body at incidence (taken from Reference 30) is shown. In this case separation has only occurred on one side of the spike, the compression surface flow remaining attached. It will be noted that this figure bears a strong resemblance to Figure 12(iv) and suggests that the dark line in that figure may be associated with a mixing layer rather than a vortex. In other respects the model also appears to be consistent with the experimental observations; the weak vortex flow which in Reference 23 was observed to persist after the pressure rise can be explained as recirculation within the separated region, and the 'bluff body effect' produced by the adverse pressure gradient over some part of the support (the existence of which seems to be necessary for either model). The

separation itself results from the influence of this pressure gradient propagating upstream through the leeside boundary layer. The suggestion in Reference 23 that the leeside pressure rise is ultimately the result of the tip shock is supported by this model. A final piece of evidence for the model proposed here comes from unpublished results obtained by undergraduates at Cambridge under Squire who found that the application of transition bands to the models of Reference 23 delayed the pressure rise by several degrees compared with the 'transition free tests. This implies that the state of the boundary layer is important to this effect; an observation which is more easily explained by the 'conical separation' model than by the 'vortex burst' model.

2.5. Conclusions

The investigation into the leeside pressure rise on delta wings observed by various workers has failed to pinpoint the exact cause. The usual explanation, that the pressure is the result of vortex breakdown, has been shown to have several shortcomings and it has instead been suggested that the pressure rise is due primarily to a large scale separation of the leeside flow similar in type to that observed on 'spiked' forebodies at supersonic speeds.

- - - - - o O o - - - - -

P A R T 3

The Supersonic Delta Wing

3.1.1 Introduction

In this section, two pieces of experimental work are described together with two versions of thin shock-layer theory from substantially independent authors. Had the later version of the theory been available when the experimental programme was being planned, its content would have been markedly altered. In order to preserve the correct sequence of events therefore, the work presented here is arranged in chronological order.

3.1.2 Flow regimes on delta wings

a) Thin wings

The supersonic flow over a delta wing is complicated and depends on sweepback, thickness, leading-edge radius, incidence, Mach number and Reynolds Number. In order to reduce the number of variables and to develop a 'feel' for the type of flows encountered, we will initially restrict our discussion to thin wings with sharp leading edges. This permits a further simplification into two significant parameters, viz. the component of Mach number normal to the leading edge (M_n) and the flow inclination in this plane (α_n). These are related to sweep, Mach number and incidence by:

$$\alpha_n = \tan^{-1}\left(\frac{\tan \alpha}{\cos \Lambda}\right) \qquad (3.1)$$

$$\text{and} \quad Mn = M_\infty(1 - \cos^2 \alpha \sin^2 \Lambda)^{\frac{1}{2}} \qquad (3.2)$$

(see figure 21). With the aid of this redefinition of variables, the data for thin wings may be represented on a single graph (see figure 22), and three flow regimes identified, corresponding to:

a) detached shock on compression surface / separated flow on expansion surface

b) detached shock on compression surface / attached flow on expansion surface

c) attached shock on compression surface / attached flow on expansion surface

The shock detachment boundary separating regions B and C is obtained by applying the two dimensional oblique shock relations in a plane normal to the leading edges (as in section 1.2.2) The detachment condition is 'exact' and may be obtained from either a complicated analytical expression or from shock charts (e.g. reference 9). It will be noted that shock detachment can occur either as a result of the leading edges of the wing becoming subsonic (i.e. $M_n < 1$) or because the equivalent wedge angle (α_n) exceeds the detachment angle.

Accompanying a detached shock there may be either attached or separated flow around the leading edge (regions B and A in figure 22 respectively). In region B the flow remains attached around the leading edge, turning by means of a Prandtl Meyer expansion. The streamlines on the leeside are directed towards the centreline and there will in general be a shock to return the flow to the free-stream direction. This shock may separate the boundary layer and result in the formation of an inboard vortex.

In region A, the leeside flow is similar to the 'low-speed' case. The boundary layer separates at the leading edge and rolls up to form a vortex lying above the wing. There will in general be an attachment line inboard, with a region of streamwise flow between this and the wing centreline. With increasing incidence this region will diminish in extent until the attachment line reaches the centreline.

Separation at a sharp leading edge exists in order to satisfy the Kutta condition there. In region 'C', where the shock is attached, the flow is not required to negotiate the leading edge and separation will not occur, the leeside flow therefore being qualitatively similar to that in region 'B'.

The boundary between regions A and B, shown cross-hatched in figure 22, was proposed by Stanbrook and Squire[31] from their compilation of delta wing data published originally in 1952 (see figure 25). To the left of the boundary (region A) no instances of attached leeside flows had been recorded and to the right of the boundary (region B) no instances of separated flows. Within the boundary region both separated and attached flow had been observed (including mixed flows on a single wing). Although the data used by Stanbrook and Squire are for 'thin' wings, this does not imply that the wings had zero thickness. This finite thickness, of which no account was taken in reference 31, could at least partly explain the diffuse nature of the boundary; a plot in (α_n, M_n) (where α_n is measured relative to the leading-edge plane) cannot be expected to correlate data for a range of wing thicknesses.

Since 1952 the Squire-Stanbrook boundary has been somewhat extended in the light of further experimental work but there is currently no theoretical model for leeside flows capable of predicting its position.

In 1975 Squire[32] suggested that the onset of leading edge separation would be accompanied by marked changes in the compression surface flow. He used thin shock-layer theory to predict the conditions under which such changes may occur. This will be discussed in detail in Section 3.2.

The exact mechanism by which leading edge separation occurs is also open to conjecture. According to Squire[32] the sequence of events in crossing from region B to region A (say by reducing the Mach number) is as follows:- In region B in figure 22, the flow expands around the leading edge in a Prandtl Meyer wave and there will in general be a region of constant pressure on the leeside, terminated by a shock. As the Mach number falls the flow is unable to expand completely and leading edge separation occurs, though the vortex remains close to the wing surface and the inboard flow is still terminated by a shock. With further decreases in Mach number the expansion fan fades out leaving a fully developed vortex flow.

In Rein's[33] model, the region of uniform pressure inboard of the leading-edge is explained by the presence of a leeside separation bubble which forms as soon as the shock detaches from the lower surface. This bubble is analogous to that observed on a wedge in transonic flow and is assumed to be of constant width. It therefore interacts with the inboard shock near the apex, resulting in a vortex being shed over the inner part of the wing. As the Mach number falls, the bubble increases in width and the vortex in extent. Eventually the region of attached flow inboard of the bubble vanishes and the leading edge vortex covers the whole wing.

Both these models have corroborative experimental evidence though Rein's results could also be explained by a 'transition' argument in which the laminar boundary layer near the apex is separated by the inboard compression, whereas the turbulent layer farther downstream is not.

b) Effect of thickness

As long as the leading edge remains sharp the two-dimensional shock detachment conditions can be easily modified to take account of finite wing thickness. Assuming α and α_n are defined as before relative to the plane of the leading edges and that, in the normal plane, the wing has thickness δ_u above and δ_ℓ below the leading edge plane (see figure 23) then the results for a family of wings will collapse in a plot of $(\alpha_n + \delta_\ell)$ vs. M_n for $(\alpha_n + \delta_\ell) \geq (\delta_n + \delta_\ell)/2$. The equality sign represents the condition that the 'equivalent wedge' is symmetric with respect to the direction of the normal component of the free stream.

For normal incidences below this, the conventionally 'leeward' surface controls the shock detachment and a family of curves result. The effective incidence of the leeside plane is given by $(\delta_n - \alpha_n)$ and it is this value of α (effective)which must be used in the equation (e.g. reference 9) for shock detachment. Some examples are shown in figure 24.

For incidences above $\alpha_n + \delta_\ell = (\delta_n + \delta_\ell)/2$, Squire[32] finds that the $\{(\alpha_n + \delta_\ell), M_n\}$ representation satisfactorily correlates the available data for leading-edge separation. The apparently weak dependence of the leeside flow on leeside shape is interesting and supports the view that changes in the compression surface flow are responsible for leeside separation. It should be noted that even with a detached shock wave, the upper surface cannot influence the lower surface flow (beyond the boundary layer) so long as there exists a sonic line between the shock and the leading-edge region of the wing, and so long as the changes to the leeside shape are not so gross as to change significantly the position of this sonic line. The data for two dimensional, sharp edged aerofoils in transonic flow cannot apparently be correlated in this way. In Figure 26 the separation boundaries for a number of symmetrical aerofoils (taken from Reference 34 and Reference 35) are plotted both as functions of mean incidence and lower surface incidence. In neither instance can the data said to be 'collapsed' and it is therefore inferred that some mechanism is at work in the two dimensional case which compensates for increases in the incidence of the lower surface by a corresponding change in the leeside flow. This 'mechanism' is presumably the leading edge separation bubble, a device usually denied the delta wing, (though Drougge[36] has demonstrated its existence) which allows a separated flow to become re-attached very close to the leading edge.

(c) Effect of leading-edge radius

The question of leading edge bluntness can be conveniently divided into two catagories according to whether the leading-edge radius is very much smaller than the thickness of the wing or of a similar order of magnitude. All real wings will of course, fall into one of the two catagories because of the impossibility of producing an 'absolutely' sharp leading-edge; the shock will be locally detached on any wing. It would appear that the 'principle of independence' is only rigorously justifiable when the leading-edge radius is less than the mean free path of the fluid (about 1 μm in air at sea level conditions); in practice it is found (see Ref 36) that the effect of small amounts of blunting is only felt over a distance comparable with the leading-edge radius.

Delta wings with a 'conventional' aerofoil section fall into the second catagory and in the early days of delta wing research received much attention. Separation boundaries proved to be extremely sensitive to leading edge shape and a further complication arises because attached flow at the leading edge is possible even without the agency of a supersonic type of expansion. Results collected by Stanbrook and Squire[31] are shown in Figure 25; presented in the same way as those for sharp-edged wings they reflect the limitations of the (M_n , δ_n) representation by producing a poorly defined boundary.

After Weber[37] and later workers had shown that sharp-edged wings could produce acceptably low drag if suitably twisted and cambered, interest in round nosed wings lapsed for some years until the start of the 're-usable' space shuttle program. Because of the extremely high speeds ($M \simeq 30$) at which the orbiter will re-enter the Earth's atmosphere, the problems of heat transfer to sharp leading edges become insuperable and very rounded leading edges have to be used. The problems of unpredictable separation which led earlier designers to abandon this type of wing are still present but the effects are suppressed by means of artificial stability augmentation.

(d) Effect of Reynolds Number

Little systematic work has been conducted to investigate the effects of Reynolds number on delta wing flow fields, most of the experiments treating only the 'transition fixed' and 'transition free' cases (e.g. Reference 38).

The state of the boundary layer on the compression surface has only a minimal effect on the compression surface pressure distributions because of the favourable pressure-gradients existing there. In cases where the compression-surface shock is detached though, fluid will be spilled around the leading edges and therefore a turbulent compression-surface boundary layer may cause transition in that of the lee surface.

Our lack of knowledge of scale effects is reflected for instance, in an inability to predict when shock induced separation will occur in otherwise attached leeside flows. When a vortex flow occurs on the leeside, the theoretical work of Cooke[39] leads us to expect a 'saw tooth' type of transition front, different mechanisms causing transition in the attached central region between the attachment lines, and in the region of strong cross-flow. The main effect of increasing Reynolds number in this model will be an outboard shift of the suction peaks as the boundary layer becomes turbulent and secondary separation is delayed.

3.2.1. Thin shock-layer theory

In 1963 Messiter[40] published a paper entitled 'Lift of slender delta wings according to Newtonian theory'. In it, he describes a prediction method, later to be referred to as 'thin shock-layer theory', for the forces on thin delta wings at hypersonic speeds. Since then, thin shock-layer theory has been developed by Squire, Hida, Roe, Woods and others, into a most versatile and powerful technique. In particular, the range of validity has been extended to include moderate supersonic Mach numbers and low incidences, and the restriction to thin wings (and indeed to conical wings) has been lifted. Pressure distributions and shock shapes are accurately predicted and recently Squire has suggested that changes in the compression surface streamline patterns, calculated from thin shock layer theory, may provide theoretical justification for the Stanbrook-Squire boundary.

In this chapter we will describe, in chronological order, development of Messiter's theory.

The semi-empirical Newtonian force law, which predicts a surface pressure coefficient of the very simple form, $C_p = 2 \sin^2 \sigma$, where σ is the local body slope, has been found to give surprisingly good agreement with experiment at hypersonic speeds, though the physical model used originally to derive the expression seems to be unrealistic. The incident fluid is considered to consist of massy, non-interacting, inelastic particles which, on collision with the body, are assumed to have their normal component of momentum destroyed. We therefore picture a flow in which the fluid strikes the body and turns abruptly to flow around the body in an infinitesimally thin layer. Although the concept would not have occurred to Newton, we now see that this is tantamount to saying that the shock and body surface are coincident.

The same result may be more credibly derived from the oblique shock relations. In the dual limit $M_\infty \to \infty$, $\gamma \to 1$, the shock wave angle becomes equal to the flow deflection angle and the pressure coefficient behind the shock equal to the Newtonian value.

In 1963 Messiter[40] published a paper in which he set out to improve the accuracy of Newtonian theory by assuming that the shock layer was not of infinitesimal thickness but merely 'thin' (i.e. the shock lay close to the body surface). Figure 2 shows the Cartesian coordinate system used, the wing, which is flat, lies in the plane defined by $y = 0$. For the steady isentropic flow of an ideal gas, we require to satisfy the following equations of motion:

$$\begin{aligned} &\text{continuity,} && \operatorname{div} \rho \underline{q} = 0 \\ &\text{momentum,} && \underline{q}.\nabla\underline{q} + (1/\rho)\nabla P = 0 \\ &\text{entropy,} && \underline{q}.\nabla(P/\rho^\gamma) = 0 \end{aligned} \qquad (3.3)$$

together with the shock relationships:

$$\begin{aligned} (\rho(\underline{q}.\underline{n})) &= 0 \\ (P + \rho(\underline{q}.\underline{n})^2) &= 0 \\ (\underline{q} \times \underline{n}) &= 0 \end{aligned} \qquad (3.4)$$

where the larger brackets denote the change in the enclosed quantity across the shock, and $\underline{n}$ is the unit normal to the shock wave.

Since the shock layer is assumed to be thin, the shock inclination must be approximately equal to the wing incidence, α. The inverse density ratio across it is given by :

$$\varepsilon = \rho_\infty/\rho_s \approx \frac{\gamma - 1}{\gamma + 1} + \frac{2}{(\gamma+1)\, M_\infty^2 \, \sin^2 \alpha} \qquad (3.5)$$

It is next required to scale the natural coordinate system so that it will be described by quantities of order unity. For a chord of unit length, the shock stand off distance at the trailing edge $y_s \propto \varepsilon\tan\alpha$. The choice of scaling for Z is less obvious but it is assumed that in the region of interest the aspect ratio of the wing will be of the same order as the Mach angle in the shock layer, which can be shown to be $O(\varepsilon^{\frac{1}{2}})$. The following coordinate 'stretching' is therefore adopted:

$$\left.\begin{aligned} x^* &= x \\ y^* &= y/\varepsilon\tan\alpha \\ z^* &= z/\varepsilon^{\frac{1}{2}}\tan\alpha \end{aligned}\right\} \qquad (3.6)$$

where $\tan\alpha$ in the third equation has been introduced to simplify the later algeba.

To estimate the order of magnitude of the independent variables the related solutions for the flow over a swept wing with an attached shock wave is considered and the flow quantities are assumed to have the same order of magnitude everywhere as they have there. The following equations are derived from the shock relations (equation 3.4) with the assumption that $\bar{y}_{s_{\bar{x}}}$, $\bar{y}_{s_{\bar{z}}}$ and $\rho_\infty/\rho \ll 1$.

$$
\left.
\begin{aligned}
u/U &= \cos\alpha + \varepsilon(\sin^2\alpha/\cos\alpha)u^* + \ldots. \\
v/U &= \varepsilon \sin\alpha\, v^* + \ldots. \\
w/U &= \varepsilon^{\frac{1}{2}} \sin\alpha\, w^* + \ldots. \\
\frac{P-P_\infty}{\rho_\infty U^2} &= \sin^2\alpha + \varepsilon \sin^2\alpha\, p^* \\
\frac{\rho_\infty}{\rho} &= \varepsilon - \frac{\gamma-1}{2}\varepsilon(2u^* + w^{*2}) - \varepsilon^2(1+p^*) + \ldots.
\end{aligned}
\right\} \qquad (3.7)
$$

where u^*, v^*, w^* and p^* are the corrections to the Newtonian values.

Substituting equations(3.7) back into the exact equations of motion and shock relations and retaining only the lowest order terms in ε, the following very simple relations are obtained:

$$
\left.
\begin{aligned}
&\text{Continuity} && \frac{\partial v^*}{\partial y^*} + \frac{\partial w^*}{\partial z^*} = 0 \\
&\text{x-mom.} && \frac{\partial u^*}{\partial x^*} + v^*\frac{\partial u^*}{\partial y^*} + w^*\frac{\partial u^*}{\partial z^*} = 0 \\
&\text{y-mom.} && \frac{\partial v^*}{\partial x^*} + v^*\frac{\partial v^*}{\partial y^*} + w^*\frac{\partial v^*}{\partial z^*} = -\frac{\partial p^*}{\partial y^*} \\
&\text{z-mom.} && \frac{\partial w^*}{\partial x^*} + v^*\frac{\partial w^*}{\partial y^*} + w^*\frac{\partial w^*}{\partial z^*} = 0
\end{aligned}
\right\} \qquad (3.8)
$$

$$
\left.
\begin{aligned}
\text{Shock relations} \quad u_s^* &= -\partial y_s^*/\partial x^* \\
v_s^* &= (\partial y_s^*/\partial x^*) - (\partial y_s^*/\partial z^*)^2 - 1 \\
w_s^* &= -\partial y_s^*/\partial z^* \\
p_s^* &= 2(\partial y_s^*/\partial x^*) - (\partial y_s^*/\partial z^*)^2 - 1
\end{aligned}
\right\} \qquad (3.9)
$$

As a final simplification, a restriction is made to conical flows, writing,

$$
\left.
\begin{aligned}
\bar{y} &= y^*/x \\
\bar{z} &= x^*/x
\end{aligned}
\right\} \qquad (3.10)
$$

Equations (3.8) and (3.9) then become:

$$\left.\begin{aligned} &\bar{v}_{\bar{y}} + \bar{w}_{\bar{z}} = 0 \\ &(\bar{v} - \bar{y})\,\bar{u}_{\bar{y}} + (\bar{w} - \bar{z})\,\bar{u}_{\bar{z}} = 0 \\ &(\bar{v} - \bar{y})\,\bar{v}_{\bar{y}} + (\bar{w} - \bar{z})\,\bar{v}_{\bar{z}} = -\,p_{\bar{y}} \\ &(\bar{v} - \bar{y})\,\bar{w}_{\bar{y}} + (\bar{w} - \bar{z})\,\bar{w}_{\bar{z}} = 0 \end{aligned}\right\} \qquad (3.11)$$

where $\bar{u}_{\bar{y}} \equiv \dfrac{\partial \bar{u}}{\partial \bar{y}}$ etc.

$$\left.\begin{aligned} \text{and} \quad \bar{u}_s &= -\bar{y}_s + \bar{z}\,d\bar{y}_s/d\bar{z} \\ \bar{v}_s &= \bar{y}_s - \bar{z}\,d\bar{y}_s/d\bar{z} - (d\bar{y}_s/d\bar{z})^2 - 1 \\ \bar{w}_s &= -\,d\bar{y}_s/d\bar{z} \\ p_s &= 2\bar{y}_s - 2\bar{z}\,d\bar{y}_s/d\bar{z} - (d\bar{y}_s/d\bar{z})^2 - 1 \end{aligned}\right\} \qquad (3.12)$$

The equations (3.11) have two sets of real characteristics given by:

$$\bar{z} = \text{const.} \quad : \quad \zeta = \text{const.}$$

where ζ satisfies

$$(\bar{v} - \bar{y})\,\frac{\partial \zeta}{\partial \bar{y}} + (w - z)\,\frac{\partial \zeta}{\partial \bar{z}} = 0$$

The first of these characteristics is an unrealistic feature of the equations, implying as it does that disturbances may be transmitted instantaneously across the shock layer. (Hillier and Woods[41] point out that in thin shock-layer theory the compressible aspect of the flow is modelled only at the shock. Within the shock-layer the equations describe a Newton-Busemann type of flow in which interaction between particles is felt only in centrifugal effects normal to the body, i.e. in the $\bar{z} = 0$ direction.) The second characteristic path is the streamline and therefore has a counterpart in the full equations.

Fixing the constant on the ζ characteristics by setting $(\bar{y}_s, \bar{z}) = \bar{z}$, the solution for equations (3.8) and (3.9) can be shown to depend only on the cross-flow velocity $\bar{w}(\zeta)$. For a detached shock wave, $\bar{w}(\zeta) = \bar{z}_b$ and the relationship between body slope and shock shape is given by the following integral equation:

$$\left(\frac{d\bar{y}}{d\bar{z}}\right)_{body} = -\bar{w}(\bar{z}_b) - \frac{1}{\bar{w}(\bar{z}_b) - \bar{z}_b} + \int_{\zeta}^{\bar{z}_b} \frac{ds}{(\bar{w}(s) - s)^2} \qquad (3.13)$$

This is the basic equation for the solution of $\bar{w}(\zeta)$, once it is known the pressure distribution can be determined from equation (3.14).

The boundary conditions of equation (3.13) are

$$\left.\begin{aligned} \bar{w}(o) &= 0 \\ \bar{w}(\Omega) &= 1 + \Omega \end{aligned}\right\}$$

where $\Omega = b/\ell\ \epsilon^{\frac{1}{2}} \tan\alpha$ and is the 'non-dimensional span' (or aspect ratio) in thin shock-layer coordinates.

The first of the boundary conditions expresses the fact that there is to be zero cross-flow in the plane of symmetry, the second that the singularity in the shock curvature should occur on the normal characteristic through the leading edge ($\bar{z} = \Omega$).

Because Ω and $\bar{z}$ are the only parameters appearing in the expression for the cross-flow velocity (and hence the pressure distribution and shock shape), Ω has the rôle of similarity parameter in thin shock-layer theory and will be referred to frequently in later pages.

It is not intended to pursue further the solution of equation (3.13). It will be sufficient to note that Messiter computed solutions for several thin wings and used his results to predict normal force coefficients (with the approximation of zero leeside pressure).

The next modification of the theory was due to Hida[42] who included the effect of thickness (diamond and circular arc cross-sections) in the theory. Unfortunately because of the small radius of convergence of the power series chosen, his analytical solutions for pressure distributions gave poor agreement with experiment. In 1967 Squire[43] used a more precise numerical method to improve the accuracy of the solution.

For the diamond section wing, the body slope is given in physical coordinates by

$$\left(\frac{dy}{\partial z}\right) = -\,{}^{h}/_{b}$$

or in the 'stretched' coordinate system:

$$\left(\frac{d\bar{y}}{d\bar{z}}\right)_{body} = -\,{}^{h}/_{b}\,\epsilon^{\frac{1}{2}} = -C \qquad (3.14)$$

This result, with the sign of C changed, also applies to caret wings.

The wing thickness appears explicitly in the expression for the pressure at the body surface:

$$P(\bar{z}_b) = 1 - \bar{w}^2(\bar{z}_b) + 2\left(\Delta_o - \int_o^{\bar{z}_b} \bar{w}(s)ds\right) + 2\bar{z}_b\,\bar{w}(\bar{z}_b)$$

$$+ \left[-1 + \frac{1}{\left(\bar{w}(\bar{z}_b)-\bar{z}_b\right)^2}\right]\frac{\partial \bar{w}(\bar{z}_b)}{\partial \bar{z}} \int_{\zeta}^{z_b} \frac{\left(\bar{w}(s)-\bar{z}_b\right)^3}{\left(\bar{w}(s)-s\right)^2}\,ds + 2C\Omega \qquad (3.15)$$

which can be evaluated after $\bar{w}(s)$ has been found from equation (3.13), subject to the same boundary conditions as before. Squire's results for pressure distributions show good agreement with experiment over a wide range of the parameters Ω and C and Mach numbers as low as $M = 4$. The predicted and measured pressures diverge close to the leading edge though, the theory tending to predict too high a pressure in this region.

The most obvious unrealistic feature of thin shock-layer theory is the assumption that the inverse density ratio ϵ, across a basic shock in the leading edge plane, is representative of that across the real shock. The credibility of this assumption diminishes with increasing wing thickness and decreasing Mach number, i.e. as the real shock moves away from the wing.

In 1974 Squire[44] proposed a method for improving the accuracy of the theory by moving the basic shock away from the plane of the leading edges.

The expressions for pressure and shock shape may be written in functional form:

$$P(\bar{y}\ ,\ \bar{z}) \;=\; 2C\Omega + P^{\bigstar}(\bar{z}/\Omega\ ,\ \Omega\ ,\ C) \qquad (3.16)$$

$$\bar{y}_S(\bar{z}) \;=\; \bar{y}_S^{\bigstar}(\bar{z}/\Omega\ ,\ \Omega\ ,\ C) \qquad (3.17)$$

If the expansion procedure is carried out about any other basic shock position, the approximate equations are unchanged but new values of Ω and C must be used because of the change in ε and hence in the coordinate stretching. In addition, because equation (3.15) contains a term in which the shock shape $\bar{y}_S$ is defined relative to the basic shock, the equation must be amended to read:

$$P(\bar{y}\ ,\ \bar{z}) \;=\; 2C\Omega - \frac{2\tan\phi}{\varepsilon\tan(\alpha+\phi)} + P^{\bigstar}(\bar{z}/\Omega\ ,\ \Omega\ ,\ C) \qquad (3.18)$$

where the basic shock makes angle ϕ with the leading-edge plane.

If the basic shock is moved through a small angle ϕ, then the expression for pressure coefficient in the unmodified theory,

$$Cp \;=\; 2\,\mathrm{Sin}^2\,\alpha\,\left(1 + \varepsilon\,P^{\bigstar}(\bar{z}/\Omega\ ,\ \Omega)\right)$$

becomes

$$Cp \;=\; 2\,\mathrm{Sin}^2\,\alpha + 2\,\mathrm{Sin}^2(\alpha+\phi)\varepsilon'\,P^{\bigstar}(\bar{z}/\Omega'\ ,\ \Omega')$$

where the amended parameters are shown primed.

Only the correction term has been changed, but because $\varepsilon' < \varepsilon$, the range of validity of the theory appears to have been increased.

By careful comparison with experiment, Squire attempted to find the best position for the 'basic shock'. Considering only the detached shock case he investigated three alternatives:

1. Basic shock in leading-edge plane.

2. Basic shock midway between the leading-edge plane and the plane through the calculated shock on the centreline.

3. Basic shock in the plane of the calculated shock on the centreline.

These are respectively termed the 'unmodified','half-modified' and 'full-modified' theories. In the 'half-modified' and 'full-modified' theories, the basic shock position is calculated by an iterative procedure; this converges rapidly as the shock shape is only weakly sensitive to basic shock position, especially if the value of ε is small in the first approximation.

The comparison in reference 44 covered the Mach number range $2 < M < 10$ and the results can be readily summarised

1. The accuracy of t.s.ℓ.t. <u>can</u> be improved by moving the basic shock.

2. Where the shock is detached use the 'half-modified' theory.

3. Where the shock is attached use the fully modified theory.

4. Close to shock detachment ($\Omega \simeq 2$) use the 'full-modified' theory - but exercise discretion.

From now on the 'prime' will be omitted from the representation for Ω and it will be assumed that:

$$\Omega = b/\ell \, \varepsilon^{\frac{1}{2}} \tan \alpha \text{ shock}$$

where α shock is the inclination of the basic shock. The previous definition in which $\alpha = \alpha$ shock is to be seen as a particular case ('unmodified' theory).

In his concluding remarks to reference 44 Squire suggests a reason for the sometimes unexpected accuracy of thin shock-layer theory:- "It is interesting to find that for flat wings the initial movement of the shock below the wing produces only small changes in the surface pressure distribution but, particularly at low incidence, even a small movement of the basic shock can produce a marked reduction in the value of the inverse density ratio ε. This suggests that the real governing parameter is the inverse density-ratio across the calculated shock wave rather than across the arbitrarily chosen basic shock position". For iterative procedures, in which the position of the calculated shock wave influences that of the basic shock, this point may well be valid but for the 'unmodified' theory, whose accuracy when $\varepsilon > 1$ is cited at the

beginning of the paper, this explanation does not seem to apply and an expansion in a power series in ϵ is hard to justify, though all investigations of the higher order terms may reveal that this coefficients are always small.

For the delta wing tested at Cranfield, the shock is detached for all incidences and therefore the 'half-modified' theory would be expected to give the best results. Figure 27 shows the variation of ϵ with α for this wing in the three versions of the theory.

3.2.2 Extension to the prediction of leeside flows

Recently, Shanbhag[45] has written a program for the solution of equation (3.13) for the cross-flow velocity $\bar{w}(\Omega, c)$. The numerical method used to solve the equation is different from that used previously by Squire and very much quicker. Considering first, the case $C = 0$ (thin wings), the solutions for $\bar{w}$ are shown in Figure 28, together with the corresponding streamline patterns and pressure distributions. The striking feature is that at $\Omega = \bar{\Omega} = 0.5$ the streamline pattern appears to change abruptly from a situation in which there is only a single attachment line at the centreline (Figure 28a) to one in which there are three attachment lines (Figure 28b). In 28a, the streamlines are conically divergent everywhere; in 28b, the streamlines are conically divergent outboard of the outer attachment lines and convergent inboard of them. An inspection of Figure 28c suggests that the change in streamline pattern may occur as a result of a singularity when part of the solution becomes tangential to $\bar{w}(s) = s$. The mathematical reason for the jump is not really clear however, and in the real flow the movement of the attachment lines would be expected to occur over a finite incidence range.

In the case of thick wings, Squire[32] was only able to compute solutions for w corresponding to the single attachment-line type of flow. The solutions lying about the line $\bar{w}(s) = s$ were well behaved but no method could be discovered to produce solutions lying below the line. Hence it was inferred that, by analogy with the thin wing behaviour, the flow pattern changed to the three attachment-line type when the solutions crossed this line. The maximum value of Ω

for which the solutions always lie above $\overline{w}(s) = s$ has been found to be closely given by:

$$\overline{\Omega} = 0{\cdot}5 + 1{\cdot}2\ C$$

The curve $\Omega = \overline{\Omega}$ is plotted in figure 24 and shows it heading encouragingly for the Stanbrook-Squire boundary. The two curves do not intersect because of the requirement $\varepsilon < 1$, which limits us to high values of incidence when Ω is small. We are apparently presented with an attractive model in which leading-edge separation occurs because of a sudden increase in the outflow around the leading edges. This outflow is the result of a change in flow pattern on the compression surface which may be predicted by thin shock-layer theory. The available data for <u>thin</u> wings (e.g. references 46 and 47) tends to support the theory that leading-edge separation occurs for a particular value of Ω, though not precisely $\Omega = 0{\cdot}5$. The outboard attachment lines have been observed (again on thin wings) by Bashkin[48] although unfortunately he does not relate their movement to the start of leading-edge separation.

The data for thick wings are extremely sparse and the present investigation arose from one of the suggestions for 'further work' in reference 32. Figure 29 shows the locus of $\Omega = \overline{\Omega}$ for the C.I.T. model together with the exact shock detachment boundary and the Stanbrook-Squire boundary. At $M = 2{\cdot}5$, $\Omega = \overline{\Omega}$ for $\alpha = 10^0$.

3.3 Tunnel Investigation of a Particular Delta Wing

3.3.1 Aims of the Investigation

The objectives of the experimental investigation were twofold:-

i) To produce a delta wing model which could be tested over a wide range of incidences ($0 < \alpha < 50^0$) without serious support interference. The model also had to be capable of being extensively and accurately pressure plotted.

ii) To investigate the boundary between regimes of attached and separated leeside flows and in particular to relate the results to the movement of the attachment lines on the compression surface.

3.3.2 The Models

Due to the difficulty in accommodating the pressure tubes, two models were constructed; Model 1 with pressure tappings in the flat expansion surface and Model 2 with tappings in the 'V' compression surface. The models were otherwise identical (see figure 30). The pressure tubes were led away through a small diameter hollow sting. This method of construction was adopted because earlier work by the Author[49] had shown that a combination of large sting and multiple pressure tubes in the base region could profoundly affect the leeside flow field. A photograph of the models is shown in figure 31. The surface pressures were measured by means of 2mm diameter hypodermic tube recessed into the model surface and rendered flush using Araldite. Two stings were constructed, one straight and the other bent through 25 degrees. In conjunction with the tunnel incidence adjustment of 30 degrees, this covered the required range with a useful 5 degree overlap to check for possible sting interference. To ensure alignment, the stings were fixed permanently into the model bases. The models themselves were in two parts, split just forward of the trailing edge to allow the sting assemblies to be interchanged; the two halves were secured by dowels and screws. This arrangement had the additional merit of providing a very 'clean' base area.

After machining, the models were set up on a surface table and carefully measured. Slight 'bowing' was found to have occurred as a result of the installation of the pressure tubes. The table below shows the deviation from design of the two models at the centreline of the flat face. The datum is a line through the tip and parallel with the sting. In both cases the flat surfaces were slightly concave.

	Δ y mm					
x/ℓ	0	0·2	0·4	0·6	0·8	1·0
Model 1	0	0·40	0·60	0·70	0·75	0·75
Model 2	0	0·31	0·47	0·57	0·60	0·60

The bend is greatest near the tip, but a line drawn from tip to trailing edge intersects the sting at an angle of less than ½ degree.

No attempt to allow for this is made in the reduction of the data; all quoted incidences refer to the sting inclination.

3.3.3 Test Prodecure

a) Pressure Plotting

The surface pressure tubes were initially drilled 2mm from the leading edges to produce static pressure tappings. This represented the closest approach to the leading edges with this tube layout and was equivalent to about 95% of the semispan at 90% chord. The hole diameter was 0·25mm. The eight or nine ports per model were scanned sequentially by a Statham 0-10 psia transducer using an NPL pressure scanning switch mounted external to the tunnel. Free stream total and static pressures were also scanned and the output fed via a Dynamco data logger to a teletypewriter. The results were reduced to the nondimensional ratio P/p_∞.

Figure 32 shows a general view of the tunnel working section and pressure measuring system.

On subsequent runs the pressure tubes were drilled successively nearer the model centreline and the outboard holes were plugged with beeswax.

b) Schlieren Photographs

A conventional single-pass schlieren system was used. The knife-edge was aligned with the free-stream for all the photographs shown here. Other orientations were investigated but provided little extra information. Polaroid film was used initially but was not found to give consistent picture quality. Ilford blue-sensitive plates (type LN) were used subsequently with good results. A continuous mercury vapour source was used and exposure times of $\sim$ 1/200 S were provided by the camera shutter.

c) Vapour Screen Technique

The static temperature in the working section of a supersonic tunnel is, as a rule, very much lower than ambient temperature. It is therefore usual to dry the air in the tunnel to prevent a mist of condensation forming in the working section. If illuminated by a

'sheet' of light (such as may be provided by a narrow slit and cylindrical lens) however the condensation can act as a useful tracer for the flow and will reveal the position os such features as shock waves and vortices (see for example reference 50). Figure 33 identifies the major features in a typical vapour screen photograph.

In the Cranfield tunnel it was necessary to introduce additional moisture to produce a visible mist. An attempt to saturate the air in the tunnel proved fruitless because of action of the drying plant. Injecting steam just upstream of the nozzle throat worked well and required typically only one litre of water for a two-hour run.

The vapour screen was photographed using a 35mm camera on full aperture. Exposure times of around 60 seconds were required for monochrome film.

d) Oil Flow Tests

A mixture of titanium dioxide, Hypoy 90 gear oil and a few drops of oleic acid, applied uniformly to both sides of the model, was found to give satisfactory results.

The tunnel was run up to speed with the model at zero incidence to remove excess mixture. Then the model was set to the required incidence and kept there for typically 15 minutes until a suitable pattern had formed. Earlier tests had shown that as long as the pressure was sufficiently low, the pattern was only slightly degraded during the shutting-down procedure. The model was therefore removed from the tunnel after each run to be photographed.

3.3.4 Results

a) Flow over the Compression Surface

The measured compression surface pressures distributions are shown in figures 34-41 together with the predictions of the 'half-modified' thin shock-layer theory. The agreement is seen to be generally excellent even at incidences as low as 10 degrees, when $\varepsilon = 1{\cdot}3$ in this version of the theory. At high incidences the pressure over the inboard part on the wing is accurately predicted but in the region of large transverse pressure gradient near the leading edges the theory is in slight error. The error is not

systematic however; at $\alpha = 40^0$ the measured pressures are higher than the theoretical line, at $\alpha = 50^0$ they are lower.

The pressure distributions show no evidence of a change in the nature of the flow at $\alpha = 10^0$. However, as Squire[3] points out, a jump in the mathematical solution to the governing equations does not necessarily imply a sudden change in the real flow.

Thin shock-layer theory assumes conical flow; this assumption is justified for the compression surface as is shown in figure 42 where the measured pressures from all the chordwise stations are superimposed and compared with the simple Newtonian and thin shock-layer theories.

The shock wave angle measured from the schlieren photographs (figure 43) is compared with the exact inviscid cone and wedge values as well as with the predictions of thin shock-layer theory in figure 44. Thin shock layer theory correctly predicts the trend of the data but underestimates the magnitude of the shock angle by some 3 degrees. The cone and wedge values are those of an uninclined cone/wedge of semivertex angle equal to the incidence of the lower ridgeline of the wing.

The oil flow photographs are shown in figure 45. At high incidences the outflow on the compression surface is clearly visible but at low incidences the 'extra' attachment lines cannot be detected even though the flow is conically convergent inboard.

b) Flow over the expansion surface

The pressure distributions on the expansion surface indicate that the flow field is not conical. Figures 45-53 show the spanwise pressure distributions at various chordwise stations.

Close to the apex, the pressure is nearly uniform across the span. For all other chordwise stations, the pressure distributions indicate the early onset of leading edge separation. The suction peak associated with the vortex is already well defined at $\alpha = 5^0$ and grows progressively with increasing incidence. Above $\alpha = 15^0$, the peaks become flatter due to the influence of the vacuum limit, the minimum pressure reached being about 0·8 C_p(vac). The line drawn through the results for $\alpha = 24^0$ is representative of all the results in $25^0 \leqslant \alpha \leqslant 45^0$. At the highest incidences (close to

$\alpha = 50^{\circ}$) the pressure begins to rise although in these tests it never exceeds the free stream static value. The scatter in the results for $\alpha = 50^{\circ}$ is quite marked, especially towards the rear of the model and suggests that there may have been some unsteadiness in the flow. At these incidences the leeside flow is highly three dimensional and similar to the wake of a 'bluff body'.

The pressure distributions for the rearmost station (Figure 53) show a more complicated pattern with generally higher pressures (for a given incidence) than at other chordwise stations. Whether this is due to upstream influence from the base or to a secondary vortex is not clear from the pressure distributions alone. In Figure 54 the pressure distributions at three chordwise stations are superimposed to emphasise the non-conical nature of the flow.

Sting interference does not appear to pose any problem in these tests. In the region $20^{\circ} \leqslant \alpha \leqslant 25^{\circ}$ it was possible to measure pressure distributions with both straight and 'cranked' stings. The differences were quite small and of the same order as the overall scatter on the results.

Surface oil flow visualisation is not straightforward in a continuous running supersonic tunnel without the aid of some form of model injection and the Author is aware that the photographs shown in Figure 45 leave something to be desired, particularly in reproduction. Nevertheless, it is felt that they are of adequate quality to reveal the characteristic pattern of an attached leading edge flow (parallel surface streamlines leaving the leading edge with an inboard component of velocity) had this occurred. The photographs show evidence of leeside separation at all positive incidences. Over the forward part of the wing the flow appears to be conical (though the pressure distributions are at variance with this) but towards the trailing edge non-uniformities occur.

The departure from conical flow is first observed at about 60% chord and moves upstream with increasing incidence. By analogy with the results of Squire, Jones and Stanbrook[51] we recognise the flow as being characterised by leading edge separation and the formation of a vortex, followed by re-attachment further inboard and a secondary separation of the boundary layer in the outflow under the primary vortex. The primary

attachment lines occur at about 50% of the semispan at $\alpha = 5^{\circ}$ and move towards the centreline with increasing incidence. At $\alpha = 25^{\circ}$ there is only a single attachment line along the root chord. Attachment and separation points taken from the oil flow photographs are marked on the pressure distributions in Figures 46, 49, and 53 and show that the secondary separation occurs in regions of apparently favourable pressure gradient. This is probably the result of smooth (but not necessarily correct) curves being drawn through the experimental data, though some results published by Squire[52] show a similar effect.

In the region towwards the trailing edge the photographs are less easy to interpret. At low incidences the oil flow seems to indicate a complex system of vortices and tertiary separation. At higher incidences it can only be said that the flow is extensively separated outboard of the region of high shear associated with the primary vortex. The departure from conical flow is thought to be an 'upstream' effect from the base though the results quoted in Part 2 suggest that natural vortex breakdown could influence the flow near the trailing edge at incidences as low as $\alpha = 20$ degrees.

The vapour screen photographs are shown in Figure 55. The slit illuminated the model at about 60% chord. The upper surface vortices are clearly visible at $\alpha = 5^{\circ}$ and grow steadily in size up to $\alpha = 25^{\circ}$. Above this incidence, further photographs (not included here) show that the vortices begin to merge and cannot be resolved above $\alpha = 40^{\circ}$. The enveloping shock is well defined for all incidences. Photographs with the vapour screen close to the trailing edge show no evidence of a secondary vortex. This is not unexpected; other authors have noted the inability of the technique to show up internal vortex structure.

In the schlieren photographs, the presence of the vortices is shown by a diffuse dark line above the wing. To find out to which part of the vortex this corresponds, the height of the line above the wing surface was plotted against incidence. A similar exercise was carried out for the vapour screen photographs, this time measuring to the edge of the dark region, which was shown in Reference 51 to be the envelope of streamlines which, passing close to the leading edge are brought to attachment on the wing surface. The results are compared in Figure 56. The two sets of data lie almost on the same line showing that the dark line in the schlieren photographs represents the 'top' of the vortex sheet from the leading edge. The vortex height is seen to grow almost linearly with incidence up to $\alpha = 25^{\circ}$ and thereafter to grow more slowly.

3.3.5 Conclusions

a) Modified thin shock-layer theory predicts pressure distributions on the compression surface of delta wings with high accuracy in the incidence range investigated ($10^0 \leq \alpha \leq 50^0$). The agreement is good even at low incidences where certain assumptions of the theory would appear to be invalid.

b) The theory is in slight numerical error in its predictions of shock position, however the trend is closely followed. The results are more satisfactory than those of simpler prediction techniques.

c) The correlation between leading-edge separation and the movement of attachment lines on the compression surface has not been proven. All the techniques employed suggest that leading-edge separation occurs at very low incidences and certainly on the 'wrong' side of the existing Stanbrook-Squire boundary.

3.4 The Importance of the Numerical Scheme in Thin Shock Layer Theory

Shortly after the work described in the last chapter was undertaken, Hillier and Woods[41] came independently to the conclusion that the various numerical schemes used up to that time to solve equation (3.13), viz.

$$\left(\frac{d\bar{y}}{d\bar{z}} \right)_{body} = - \bar{w}(\bar{z}_b) \frac{1}{\bar{w}(\bar{z}_b) - \bar{z}_b} + \int_{\zeta}^{\bar{z}_b} \frac{ds}{(\bar{w}(s) - s)^2}$$

were invalid for certain values of Ω.

To overcome the problem of the singularity at the wing centreline, Hida, Squire, Hillier and Shanbhag had all assumed an analytical form for the cross-flow velocity in that region, viz.

$$\bar{w}(\zeta) = \sum_{i=1}^{i=n} a_i \zeta^i \qquad (3.19)$$

Using only the first three terms of this series, Hida had evaluated the coefficients explicitly by assuming that this expression for $w(\zeta)$ held right to the leading edge and invoking the relevant

boundary condition there. Following the failure of this method, later authors restricted themselves to the inboard region of the wing and obtained an expression for the cross-flow velocity in terms of the single unknown a_1 (the first coefficient in equation 3.18). The calculation was then 'marched' towards the leading edge. At the leading edge the boundary condition $\overline{w} = 1 + \Omega$ has to be satisfied and this is achieved for a chosen value of Ω by iterating on a_1. As described in section 3.2.2, two possible flow patterns may be obtained depending on the value of Ω. It is in the interesting region of $0.5 < \Omega < 2.0$ (where there are three attachment lines) that this scheme appears to violate causality. A simple argument due to Woods illustrates this point. Consider the wing shown in figure 57a, let there be a small bump on the surface at $\overline{z}_d$ inboard of the attachment line S_2. As the solution is marched out from the centreline, the flow field is unaffected until the bump is reached. The disturbance it produces is transmitted to the shock a) directly along the $\overline{z}$ = constant characteristic and b) to a more outboard part of the shock, along the streamline (ζ = constant) characteristic. Further, this second disturbance is 'reflected' at the shock, back onto the wing surface, 're-reflected' along a streamline and so on. Therefore in this scheme, the disturbance propagates away from the centreline (and against the stream direction) as shown in figure 57a. The rôle of the streamline characteristics is the same in this approximate theory as in the real flow; along them, vorticity is convected in the stream direction. Clearly the disturbance produced by the bump at $\overline{z}_d$ should propagate inboard as in figure 57b. The 'bump' is merely a device to aid our understanding of a 'propagating disturbance', the important point being made is that solutions to equation (3.12) should be calculated along the conical streamline and in the local stream direction. Hillier and Woods refer to this as the 'restriction principle'.

For a delta wing, this involves 'marching' both inboard and outboard from the outer attachment line S_2 (the position of which is unknown), satisfying the boundary conditions at the leading edge and at the centreline, and iterating on a_1. Clearly a more difficult task than the scheme used previously.

Hillier and Woods have compared their results for flat wings with those of Shanbhag for similar flight conditions. The most interesting result to emerge, from the point of view of the present investigation, is that the discontinuity in the flow variables at $\Omega = 0{\cdot}5$ has vanished and the outboard attachment lines are predicted to collapse progressively onto the centreline with decreasing Ω. Thus the simple model proposed by Squire, in which leading edge separation is seen as the result of an abrupt change in the compression-surface flow, will have to be reconsidered.

Pressures and shock shapes are also compared. For $\Omega = 1{\cdot}2$, the results of Hillier and Woods' method are indistinguishable from those of Shanbhag. However, for $\Omega = 0{\cdot}9$ Shanbhag's pressures are generally some 5% higher than Hillier's and Woods'. For $\Omega = 0{\cdot}6$, the discrepancy has grown to approximately 20% and the shape of the distributions differ markedly close to the leading edge. The quoted results refer to the function p in

$$C_p = 2 \sin^2 \alpha (1 + \varepsilon p) \qquad (3.20)$$

and therefore the discrepancies in the calculated values of pressure coefficient are very much smaller.

Squire's results for pressure distributions show excellent agreement with those of Hillier and Woods and suggest that it may have been a straight forward numerical error in Shanbhag's work (rather than the 'incorrect' method of solution of equation (3.13) which led to these differences. In spite of this, Woods and Hillier feel that it would be prudent to observe the 'restriction principle' in future work.

3.5 Further Experiments to Validate the Amended Theory

3.5.1 Aim and description of tests

Following the discovery of the error in Shanbhag's numerical procedure it was decided to carry out further experiments to test Woods' predictions for the movement of the compression surface attachment lines. Due to the restricted length of time Woods was spending in this country, results have only been computed for the

flat compression surface case and it was therefore necessary to re-test the wing in the 'inverted' position.

The experimental techniques used in the previous work had been generally satisfactory but it was felt that the surface oil flow method could be improved, particularly with regard to the compression surface flow. The version of thin shock-layer theory available to us at the time advised us to look for attachment lines which were initially 'close to the leading edges' and which 'suddenly collapsed onto the centreline' as the incidence was increased. This lack of quantitative information regarding the position of the attachment lines made the choice of pigments and oils very difficult and the outboard attachment lines were not observed.

Woods'[53] results show a progressive movement of the attachment lines from 80% span to the centreline over an incidence range of some 20 degrees and their experimental detection seemed more hopeful. It was decided to use an 'oil-dot' technique; although a 'coarser' method than the surface coating, the 'tail' on each dot clearly defines the local flow direction. By drawing a ray through each dot, the flow can be classified as "conically divergent" or "conically convergent" and the limits for the position of the attachment line obtained. A mixture of NACA 77 oil and titanium dioxide was used for the 'dots', which were applied with a hypodermic syringe. To crudely take account of the thicker boundary layer and lower shear, larger drops of oil were used towards the trailing edge of the model.

3.5.2 Results

A series of photographs showing the flat compression surface flow are shown in figure 58. The inferred positions of the attachment lines are shown in figure 59 as a plot of s/Ω vs. α. The 'error bars' reflect the limitations of the 'oil dot' technique.

The predictions for the 'half-modified' thin shock layer theory (which gives the best agreement with measured pressure distributions) are seen to follow the trend of the experiment but to underestimate the angle of incidence by about 6 degrees. The 'unmodified' theory passes right through the data; the 'full-modified' theory (not shown) gives the poorest agreement of all.

The experimental results show that the attachment lines reside within 20% of the semispan of the leading edges until approximately 30 degrees of incidence, they then start to move inboard at an increasing rate and reach the centreline at $\alpha = 45^{\circ}$.

The corresponding vapour screen photographs are shown in Figure 60. The slit illuminated the model close to the trailing edge. The leeside vortices are clearly visible at $\alpha = 10^{\circ}$ but the detection of their first appearance was rather subjective. A mean value taken from many observations of both increasing and decreasing incidence cases, is 7 degrees. The spread in the results is $\pm$ 1 degree. Compression surface pressures were also measured. In view of the conical nature of the flow found previously, it was deemed unnecessary to distinguish between chordwise stations and the results are presented on a single graph (Figure 61).

3.5.3. Conclusions

(1) The predictions of Woods give an accurate qualitiative description of the compression surface flow. The picture may also be made quantitative but the choice of basic shock position is difficult; the version of thin shock-layer theory which best predicts the measured pressure distributions is found to be in error with regard to the outboard attachment-line position and conversely.

(2) The movement of the attachment lines and the onset of leading edge separation are probably related but not in the simple way predicted by the earlier version of thin shock-layer theory. In this particular experiment leading-edge separation occurred for $\mathcal{N} \simeq 0.82$ (half-modified) or $\mathcal{N} = 0.96$ (unmodified); the corresponding values of ε are 1.0 and 8. It seems unlikely that this result would have any general validity.

3.5.4. Discussion

The declared aims of the work just described were set out in 3.3.1 and may be summarised as follows :

(i) To carefully and accurately test a typical delta wing over a wide incidence range.

(ii) To compare the onset of leading-edge separation with theoretical predictions.

It is thought that generally speaking, the first objective has been achieved, though the non-conical leeside flow revealed by the flow visualisation gives rise to some concern, as it is certainly not

typical of the results which appear in the literature. The attention paid to producing a sting of small dimensions however, together with the fact that the departures from the expected flow pattern occur well outboard of the centreline, lead to some confidence that this effect is not the result of support interference.

With the discovery of an error in Shanbhag's calculations much of the point of the second objective has been lost and it is only left to compare the results with the empirical boundary of Figure 25. As was stated earlier, all the techniques employed suggested that leading-edge separation was well established at α = 5 degrees (conditions corresponding to α_n = 14.3 degrees, M_n = 0.862 at M = 2.45) and that this would place an experimental point to the right of the existing Stanbrook-Squire boundary. Three points should be borne in mind before enquiring too deeply as to why this should be so. Firstly, because of the way in which the boundary is defined (see 3.1.2) it can only become more diffuse as increasing amounts of data become available. Secondly, the right hand limit of the boundary is defined by a very small number of points, especially at low incidences. In fact, below α_n = 7 degrees (corresponding to α = 2.5 degrees in the current tests) there are no 'attached flow' points at all on the limiting line which must therefore be considered to be speculative. The third point is more contentious and concerns the accuracy of the experimental results. When the models were originally designed it was intended that they should be tested at a Mach number of 2.8 using a pair of existing but untried liners for the supersonic tunnel; under these conditions the change from attached to separated leeside flows was expected to occur in the range $10^\circ < \alpha < 15^\circ$. It was later discovered that the use of these liners would run the compressor dangerously close to surge conditions and the Mach number therefore had to remain at 2.45. Even at this Mach number this shock-layer theory predicted that the onset of leading-edge separation would occur at α = 10 degrees. In the event, with separation occurring below α = 5 degrees there is a possibility that the small geometrical errors in the models (see 3.3.2) for instance, could make a significant difference to the measurement of the onset of separation. It is therefore thought that a sensible tolerance should be allowed when estimating the incidence at which the leeside vortices first make their appearance. With the wing flown 'inverted' incidentally, the vapour screen technique (see Figure 60) indicated that leading edge separation occurred between α = 5 and α = 10 degrees, though the representation

of Figure 25 does not distinguish between these two cases.

A systematic investigation of the Stanbrook Squire boundary, as opposed to a check on thin shock-layer theory, would obviously have required the construction of a number of purpose-designed wings, covering various aspect ratios and thicknesses, and was not considered feasible in the time available.

4.0. Final Conclusions and Suggestions for Further Work

(1) The simple caret wing when 'on design' is capable of supporting an oblique shock wave which is 'strong' when viewed in a plane normal to the leading edge but not one which is 'strong' with respect to the complete flow. It is possible however that by analogy with the results of Neale and Lambe, such a shock may occur on a caret wing which forms part of a more complicated internal flow system.

Tests on a caret wing of large anhedral showed that a system of 'crossed-shocks' was formed at all the incidences tested. The position and strength of these shocks were not well predicted by 'exact' theory due, it is thought, to interaction between the shocks and the boundary layer.

(2) The abnormally high leeside pressures observed by Szondruch and Squire have been reproduced at Cranfield and subsequently 'cured' by the removal of the pressure tubes from the base of the model. Later, attempts to induce the pressure to rise by various flaps and obstructions in the wake, failed and the exact cause of the original pressure rise cannot therefore be said to have been located. An analysis of the available data for both natural and forced vortex burst showed the behaviour to be quite unlike that observed by Szodruch and Squire or the Author; it is suggested that the effect should be regarded as the result of a large scale boundary layer separation.

(3) The appealingly simple conjecture that sudden changes in the compression surface flow, predicted by thin shock-layer theory, should promote leading edge separation has not been found and indeed later versions of the theory do not predict a sudden movement of the attachment lines.

It is still attractive to postulate that leading edge separation will occur when the outflow from the compression surface exceeds a certain value and three avenues for future work present themselves :

(a) The results of Woods allow us to predict the movement of the outboard attachment lines with some confidence, but at low angles of incidence (where the transition to a leeside vortex flow occurred in the current tests), they are suspect because the range of validity of the theory has been exceeded. Nothing is known of how the attachment lines start to move as the incidence is increased from zero. A straightforward experiment is proposed in which, using a more refined version of the 'oil dot' technique and probably a larger model, the behaviour of the attachment lines at very low incidences is investigated. Should it be revealed that the attachment lines leave the leading edge, in some sense, 'abruptly' at a particular incidence, a simple correlation between this and the onset of leading edge separation may again be sought.

(b) It has already been remarked (paragraph 3.4) that in thin shock-layer theory the flow in the shock layer retains many of the features of the simple Newtonian model. It is not therefore an obvious candidate for the prediction of surface streamlines. Following discussions with Hillier and Roe, two approaches are suggested in order to improve the prediction of leading edge separation.

(i) In spite of the foregoing remarks, the outboard attachment lines <u>do</u> exist and will therefore feature in the solution to the full equations of motion. With the assumptions $v = w = 0$ at the attachment line, these equations may be amenable to solution, at this line, without the drastic alterations implicit in the shock-layer approximation.

(ii) Leading edge separation may depend not so much on the position of the attachment lines as on the amount of fluid 'spilled' around the leading edge. Thin shock-layer theory is well suited to this type of problem and it is suggested that the product of shock stand-off distance at the leading edge and cross-flow velocity may correlate the experimental data for leading-edge separation.

A P P E N D I X

THE HYPERSONIC HELIUM TUNNEL

INTRODUCTION

The hypersonic helium tunnel at Cranfield has had rather a chequered history since being commissioned in 1964. It started life as a closed-jet facility, the working section being cylindrical and fitted with NPL designed traversing gear, and in this guise performed satisfactorily, though with rather short running times. Both total-pressure regulation and starting were originally left to a pneumatically operated valve but this, in due course, was relieved of its second duty when a burst diaphragm was installed. The passage of the normal shock through the working section established hypersonic flow almost instantaneously and hence led to an increase in the duration of steady flow.

In an effort to produce a more uniform Mach number distribution, the original conical nozzle was replaced by a 'contoured' nozzle in the late sixties. Although the throat area could be changed, by means of a series of inserts, to provide Mach numbers between 10 and 30, the nozzle was designed to give uniform flow at M = 10. The modification was by-and-large successful though traverses through the nozzle boundary layer showed this to be much thicker than had been assumed in the design calculations. Unfortunately, details of much of the testing were not formally reported and have since been lost.

The final major modification before the start of the current work, was to convert the working section to an 'open-jet' type with glass windows to permit the use of a schlieren system. The design and construction of the new working section had to be completed in a very short time and the resulting article had several serious short-comings.

GENERAL DESCRIPTION

Like its not defunct 'sister' tunnel at RAE Farnborough, the Cranfield helium tunnel is of the intermittent, 'blow-down' type, though, of œourse, a sealed, return-circuit is provided to conserve the expensive working fluid. High pressure helium is stored in and fed from, a maximum of fifty bottles connected to a manifold which leads in turn, to a pressure-regulating servo-valve, a settling chamber, a ball valve housing the starting diaphragm, and , finally, the nozzle and working section. As in most hypersonic facilities, a parallel diffuser is employed. Down-stream of this is a large vacuum tank, the volume of which sets a limit to the maximum time for which hypersonic flow can be maint-ained, before the 'back pressure' becomes too high. A large industrial vacuum pump removes the gas from the dump tank and supplies it, at one atmosphere, to a four-stage compressor which returns the gas to the manifold up to a maximum working pressure of about 150 atmospheres. Although the return circuit is operational during tunnel running, its contribution to running times, which are of the order of 15 seconds, is small.

Contamination of the helium is monitored by means of a gas chromatograph; periodic purification is effected by absorbing the contaminants (mainly air) in activated charcoal, cooled with liquid nitrogen.

THE CASE FOR A NEW WORKING SECTION

The initial tests carried out by the Author consisted of setting up a schlieren system to measure the shock angle on a small cone and measurement of the post-shock total pressure in the working section using a pitot rake. The results were most discour-aging, the schlieren photographs suggesting that the 'average' Mach number in the region of the cone was about 5, whilst the more explicit pressure measurements showed that the desired Mach number was realised only in the central 20 mm of the nominally 100 mm diameter core. As the tunnel had previously been operating successfully it was assumed that the problems must be associated with the new working section. A closer inspection revealed that the diffuser inlet was of smaller diameter than the nozzle exit; even in the absence of the mixing layer

effect this could be expected to lead to an increase in pressure in the working section box and a resulting collapse of the hypersonic flow.

There was no simple way of increasing the diffuser diameter and this, coupled with the poor model accessibility and lack of space within the existing working section, led to the decision to produce an entirely new working section based broadly on the design of that of the Imperial College No.2. gun tunnel.

At the outset it was decided that to construct a large working section, stressed to anything like the tunnel stagnation pressure was quite unreasonable and that therefore a safety 'by-pass' would have to be constructed in order to keep the working section pressures low in the event of a downstream blockage. Simple calculations assuming maximum working stagnation pressure and choked flow in the nozzle throat and by-pass, suggested that it would be quite feasible to construct a box which would need to be only stressed to two atmospheres gauge. As the construction was still rather massive, the use of a large aluminium caseing was considered but rejected, after discussions with Townsend who had suffered porosity problems with the RAE working section. Steel plate was finally adopted for the construction of the main box, electrically welded both internally and externally, with aluminium alloy used for the doors. All the detail design was left in the hands of M.F.Goodridge of the Aerodynamics Workshop, Cranfield.

The end product is shown in Figure 62. Two large doors on hinges are secured by catches, thus allowing rapid model changes. The models themselves are mounted on machine tables from either the roof or floor of the tunnel. To avoid any possible recurrence of the previous problems the inlet of the sliding diffuser is twice the diameter of the nozzle exit and parallel-sided, though it may be modified in the future. Four large plugs in the tunnel floor permit the leading-through of pressure or electrical connections. The safety by-pass is mounted on top of the tunnel and leads directly into the vacuum tank. A perforated plate and 'melanex' diaphragm prevent the flow of gas down the by-pass in normal circumstances. The diaphragm was found to rupture naturally at about 3.5×10^4 Nm^{-2} (5 p.s.i.g) when tested on the bench; in the tunnel installation a 'pricker' is installed for further security.

TUNNEL DEVELOPMENT - FLOW VISUALISATION

In a tunnel with a core diameter of only 100mm the models tested have to be correspondingly small and the extent of 'conventional' measurements, such as pressure plotting, is necessarily limited. It was for this reason, rather than because the densities were too low to permit the use of a schlieren system, that the possibility of using a 'glow discharge' technique was investigated; such a method is considerably more powerful for the visualisation of three-dimensional flows.

The available methods can be divided into two catagories depending upon whether the gas is excited directly in the region in which it is desired to visualise the flow, or if the excitation is upstream of the region of interest. In both cases, the principle is similar; a certain proportion of the ions, atoms, or molecules in a given volume will be in an excited state and will decay back to their ground state by the emission of radiation; the intensity of this radiation will be in proportion to the density of the excited particles and therefore, to the density of the gas itself. The two cases are distinguished by the manner in which the particles decay to their ground state. In the method of direct excitation, transition back to the ground state occurs by the emission of a photon and is effectively instantaneous; in the 'afterglow' method, it is the decay of the long-lived 'meta stable' states, for which the selection rules prohibit the emission of a single photon, which provide the visible radiation. In this instance de-excitation must occur as the result of a collision process (or possibly the emission of more than one photon) and the gas may be swept some way downstream before this happens.

It is also possible to excite the gas by means, not of a strong electric field, but by an 'electron beam'. Such methods have been frequently employed (See for example, Lévy[54]) but the apparatus is neither simple to set-up nor to use and installation in the C.I.T tunnel would have presented serious difficulties.

The simplest and most attractive method for a glow discharge system is that described by Metcalf, Walliker and Berry[55]. Two identical circular electrodes were placed a short distance apart just downstream of the nozzle exit plane. An alternating potential of 5KV at 50 Hz was applied to these electrodes and led to a discharge path extending across the nozzle exit plane. Under running conditions, ($M=6.5$, $\rho_\infty = 4 \times 10^{-5}$ Amagat) a bright afterglow plume would extend for over a metre downstream of the nozzle. The method was used successfully for both nitrogen and helium. Unlike the tunnel described by Metcalf et al, the C.I.T. tunnel has no resevoir heating and the density in the working section is therefore very much higher. Typical values, for stagnation conditions of 4.14×10^6 Nm^{-2} (40 amagat) are in fact :-

$$P_\infty = 6 \times 10^{-3} \text{ Amagat}$$

$$\rho_\infty = 0.2 \text{ Amagat}$$

$$T_\infty = 8.5 \text{ K}$$

Under these conditions it was thought likely that the afterglow would be quenched.

The alternative, of direct excitation, was known to be effective up to higher densities and it was this method which was adopted for the C.I.T. tunnel. The usual technique (See, for example Horstmann and Kussoy[56]) is to use the model as one of the electrodes but this can lead to aerodynamic features becoming obscured by the 'plume' from the leading edge. Froebel[57] has demonstrated that excellent flow visualisation can be achieved by using a circular electrode upstream of the model in conjunction with a conical electrode downstream, the model being immersed in the positive column of the discharge. It was decided to copy this method as closely as possible and a full D.C. power supply was therefore constructed along the lines suggested in Reference 57.

The arrangement of the electrodes is visible in Figure 62. The toroidal, upstream electrode is set in a 'Paxolin' insulator and secured to the tunnel wall by nylon screws - its diameter is the same as that of the nozzle exit. The downstream electrode is conical and is carried on a 'Paxolin' strut. Both electrodes are made

of aluminium and have the same surface area. Power is brought in through two vacuum 'lead-throughs' passing through the previously mentioned plugs in the working section floor. The power supply produces 100 mA at 10KV, well in excess of that found to be necessary in Reference 57.

Initial problems shown during testing consisted of the current taking unauthorised paths between the electrodes and breakdown of the insulation within the power supply. All the testing was done at pressures around 10^{-3} Amagat and the discharge within the working section was therefore of the corona type. Judicious use of a file to remove sharp edges from the electrodes, together with the use of shrink-on insulating sleeves cured most of these problems but the lead-throughs persisted in giving trouble.

At sufficiently low pressures (below say 1.5×10^{-3} Amagat) a strong, steady discharge almost filling the working section could be maintained in quiescent air. As the pressure was allowed to rise, the discharge retreated towards the electrodes eventually occuring only at the tip of the conical electrode (where the field strength was highest) and on a small region of the circular electrode. This would generally change abruptly to an unsteady arc between the circular electrode and the tunnel wall. Various modifications and extensions to the insulator did not effect any great improvements. As the power supply was 'floating' with respect to earth, any steady discharge from one electrode to the tunnel wall must have been matched by a similar discharge from the other electrode. As the conical electrode was remote from any metallic part of the tunnel, the breakdown was almost certainly occuring at the lead-through. The significance of this was not realised at the time, and much effort was wasted in modifications to the insulation.

In spite of these problems it was decided to persist with a 'wind-on' run, even though the expected densities were much higher than those at which breakdown had occurred in the quiescent gas. The effect of the moving fluid seems to be something of an unknown quantity, Fisher and Bharathan[58] believing that even at hypersonic speeds the change should be negligible whilst Froebel[57] states without discussion, that a discharge will only occur with the cathode upstream of the anode. In the event a satisfactory discharge was not obtained, the current 'arcing' between the circular electrode and the tunnel wall.

TUNNEL DEVELOPMENT - EVALUATION OF THE WORKING SECTION

In parallel with the work just described, plans were made to calibrate the new working section. Progress was seriously hampered by the many leaks which developed after the tunnel had laid idle for over a year, and, at the completion of the contract, the calibration had not been attempted, though all the equipment was available to do so. The new working section had proved satisfactory under vacuum however, and the operation of the safety burst diaphragm had also been tested with the diffuser fully blocked (with a resevoir pressure of 40 Amagat the working-section pressure did not exceed 1 Amagat absolute).

CONCLUSIONS

The C.I.T. hypersonic facility is unique in this country and is now equipped with a modern and practical working section. The most immediate need is for a thorough overhaul of the ancillary plant and pipe work to overcome the problems of leakage and consequent contamination of the helium. After this has been done, calibration should be a straightforward task. Attention should be paid to 'potting' the lead-throughs for the glow discharge apparatus followed by initial running at a stagnation pressure of ~ 10 Amagat to reproduce as closely as possible the conditions of Reference 57, under which Froebel obtained excellent results.

- - - - - o O o - - - - -

REFERENCES

1. Nonweiler, T.R.F. — Delta wings of shapes amenable to exact shock wave theory. Journ. Roy. Aero. Soc. Vol.67, No.39 1963

2. Maikapar, G.I. — On the wave drag of axisymmetric bodies at supersonic speeds. Prikl, Mat. Mek., Vol.23, p.528 1959 Transl. Journ.Appl.Math.Mech. Pergamon

3. Townend, L.H. — On lifting bodies which contain two-dimensional supersonic flows. RAE Report Aero 2675 (ARC R&M 3383) 1963

4. Jones, J.G. — A method for designing lifting configurations at high supersonic speeds using the flow fields of non-lifting cones. RAE Report Aero 2674 (ARC 24846) 1963

5. Schwartz, L.W. — Hypersonic flows generated by parabolic and paraboloidal shock waves. Physics of fluids Vol.17, p.1816 1974

6. Pike, J. — Wing body shapes from known flow fields RAE TR 70235 (ARC.33157) 1970

7. Squire, L.C. — The effects of recessed lower surface shape on the lift and drag of conical wings at high incidence and high Mach number. Aero Quart. Vol.XXVI, p.1 1975

8. Townend, L.H. — Some design aspects of space shuttle orbiters Prog. Aero Sci. Vol.13, pp.81-136.Pergamon 1972

9. Equations, tables and charts for compressible flow. NACA 1135

10. Kuchemann and Weber — Aerodynamics of propulsion. McGraw-Hill 1953

11. Venn, J and Flower, J.W. — Shock patterns for simple caret wings. Aeron. Journ. Vol.74, pp.339-348, 1970

12. Squire, L.C. — A comparison of the lift of flat delta wings and waveriders at high angles of incidence and high Mach number. Ingenieur - Archiv Vol.40, pp.339-352 1971

13. Richards, I.C. — Tests on a caret wing at M=12.2 Unpublished.

References continued :

14. Coleman, G.T. — Force measurements on caret and delta wings at high incidences. Imperial College Aero Report 72-16 1972

15. Crabtree, L.F. and Treadgold, D.A. — Experiments on hypersonic lifting bodies. RAE TR 67004 1966; ICAS Paper 66-24 1966

16. Alekseev, V.N. and Gonor, A.L. — Some results of an optical investigation of supersonic three-dimensional flows. Mekhanik, Zhidkosti i Gaza Vol.1, pp.179-185 1974; RAE Translation 1828 (1975)

17. Squire, L.C. — Experimental results for waveriders in certain off-design conditions. Aero Quart. Vol. XXII pp.225-232 1971

18. Keldysh, V.V. — The investigation of the flow in the vicinity of V-shaped wings formed by stream surfaces behind a plane shock wave. Mikhanika Zhidkosti i Gaza Vol.4. 1976; RAE Translation 1407 (1969)

19. ESDU Data Sheets Article 68019 December 1968

20. Stetson, K.F.and Scaggs, N.E. — Shock detachment from the leading edges of delta wings. ARL. 72-0079 1972

21. Neale, M.C. and Lambe, P.S. — Tests with a two dimensional intake having all external compression and a design Mach number of 2.0. ARC CP No.937 1963

22. Hillier,R. — Pressure distributions at M=3.51 and at high incidences on four wings with delta planform. ARC. CP 1198 1972

23. Szodruch, J. and Squire, L.C. — Pressure distributions on the suction surface of some delta wings at M=3.5 ARC. 35 008 1974

24. Edney, B.E and Stevenson, M.A. — Vortex breakdown at Mach 2. College of Aeronautics unpublished thesis 1963

25. Craven, A.H. and Alexander, A.J. — An investigation of vortex breakdown at Mach 2. College of Aeronautics Note Aero 158.

26. Szodruch, J. — Leeside flowfields on delta wings with detached shock waves. Euro Mech 74, Colloquim 12. Cambridge. 1976

References continued :

27. Earnshaw, P.B. and Lawford, J.A. — Low speed wind tunnel experiments on a series of sharp-edged delta wings. Part 1. Forces moments, normal force fluctuations and positions of vortex breakdown. RAE TN Aero 2780 (ARC R & M 3424) 1961

28. Wentz, W.H. and Kohlman, D.L. — Vortex breakdown on slender sharp-edged wings. Journ. of Aircraft Vol.8, p.156 1971

29. Mair, W.A. — Experiments on separation of boundary layers on probes in front of blunt-nosed bodies in a supersonic air stream. Phil. Mag., Vol. 43 Seventh series 1952

30. Hunt, G.K. — Supersonic wind tunnel study of reducing the drag of a bluff body at incidence by means of a spike. RAE Report Aero 2606 1958

31. Stanbrook, A. and Squire L.C. — Possible types of flow at swept leading edges. Aero Quart. Vol.XV, pp.72-82 1964

32. Squire, L.C. — Flow regimes over delta wings at supersonic and hypersonic speeds. Aero Quart. Vol. XXVII 1976

33. Rein, J.A. — Flow over the suction surface of delta wings with detached shock waves AWRL TN HSA 102, 1964

34. Lindsey, W.F. and Landrum, E.J. — Compilation of information on the transonic attachment of flows at the leading edge of aerofoils. NACA TN 4204 1958

35. Henshall, B.D. and Cash, R.F. — Obervations of the flow past a two-dimensional 4% thick biconvex aerofoil at high subsonic speeds. ARC 19, 057 1957

36. Drougge, G. — Experimentell bestämning av omslaglinjens läge på deltavingar vid överljudfart FFA Report AU-11-113.1 1963

37. Weber, J. — Design of warped slender wings with the attachment line along the leading edge. ARC R&M 3406 1965

38. Sutton, E.P. — Some observations on the flow over a delta-winged model with 55 degrees leading edge sweep at Mach numbers between 0.4 and 1.8 ARC R&M 3190 1960

References continued :

39. Cooke, J.C.
Boundary layer flow between the attachment lines on a flat plate delta wing at incidence.
Aero Quart. Vol.XIII, pp.1-16 1962

40. Messiter, A.F.
The lift of slender delta wings according to Newtonian theory.
AIAA Journ. Vol.1. p.794 1963

41. Hillier, R and Woods, B.A.
A note on the thin shock-layer approximation
Aero Quart. Vol.XXVIII, pp.85-89 1977

42. Hida, K.
Thickness effects on the force of slender wings in hypersonic flow.
AIAA Journ. Vol.3 p.427 1965

43. Squire, L.C.
Calculated pressure distributions and shock shapes on thick conical wings at high supersonic speeds.
Aero. Quart. Vol. XVIII, pp.185-206 1967

44. Squire, L.C.
Some extensions to thin shock-layer theory
Aero. Quart. Vol. XXV pp.1-13 1974

45. Shanbhag, V.V.
Numerical studies on hypersonic delta wings with detached shock waves.
ARC CP 1277 1974

46. Michael, W.H.
Flow studies on a flat plate delta wing at supersonic speeds.
NACA TN 3472 1955

47. Fellows, K.A and Carter, E.C.
Results and analysis on two isolated slender wing and wing-body combinations at supersonic speeds.
ARC CP 1131 1972

48. Bashkin, V.A.
Experimental study of flow about that delta wings at M=5 and at angles of attack from 0 to 70°
Izs A.N. SSSR Mekhanika Zhidkosti i Gaza
Vol. 23. pp.102-108 1967

49. Richards, I.C.
Pressure measurements on the suction surface of a flat cone at M=2.5
College of Aeronautics memo 7509 1975

50. McGregor, I.
The vapour screen method of flow visualisation
J.F.M. Vol.1 pp.481-511 1961

51. Squire, L.C. and Jones, J.C. and Stanbrook, A.
An experimental investigation of the characteristics of some plane and cambered delta wings at Mach numbers from 0.7 to 2.0
ARC R&M 3305 1963

References continued :

52. Squire, L.C. — Pressure distributions and flow patterns on some conical shapes with sharp edges and symmetrical cross sections at M=4.0 ARC. R&M 3340 1963

53. Woods, B.A. — Private communication

54. Lévwy, S. — Visualisations d' ecoulemonts en soufflerie a l'aide d'un faisceau d'electrons. Rech. Aerosp. No.1970-3, 155-166 1970

55. Metcalf, S.C. Walliker, D.A.J. and Berry, C.J. — A new method of afterglow visualisation for low density high Mach number flows. NPL Aero Report 1291 1969

56. Horstmann, C.C. and Kussoy, M.I. — Hypersonic viscous interactions on slender cones AIAA Journ. Vol. 6, No.12 1968

57. Froebel, A.T. — Glow discharge flow visualisation in a hypersonic helium wind tunnel. National Aeronautical Establishment (Canada) Report 4.03.02

58. Fisher, S.S. and Bharathan, D. — Glow discharge flow in low density free jets. J.Spacecraft. Vol.10 No.10 1973

- - - - - - - - o O o - - - - - - - -

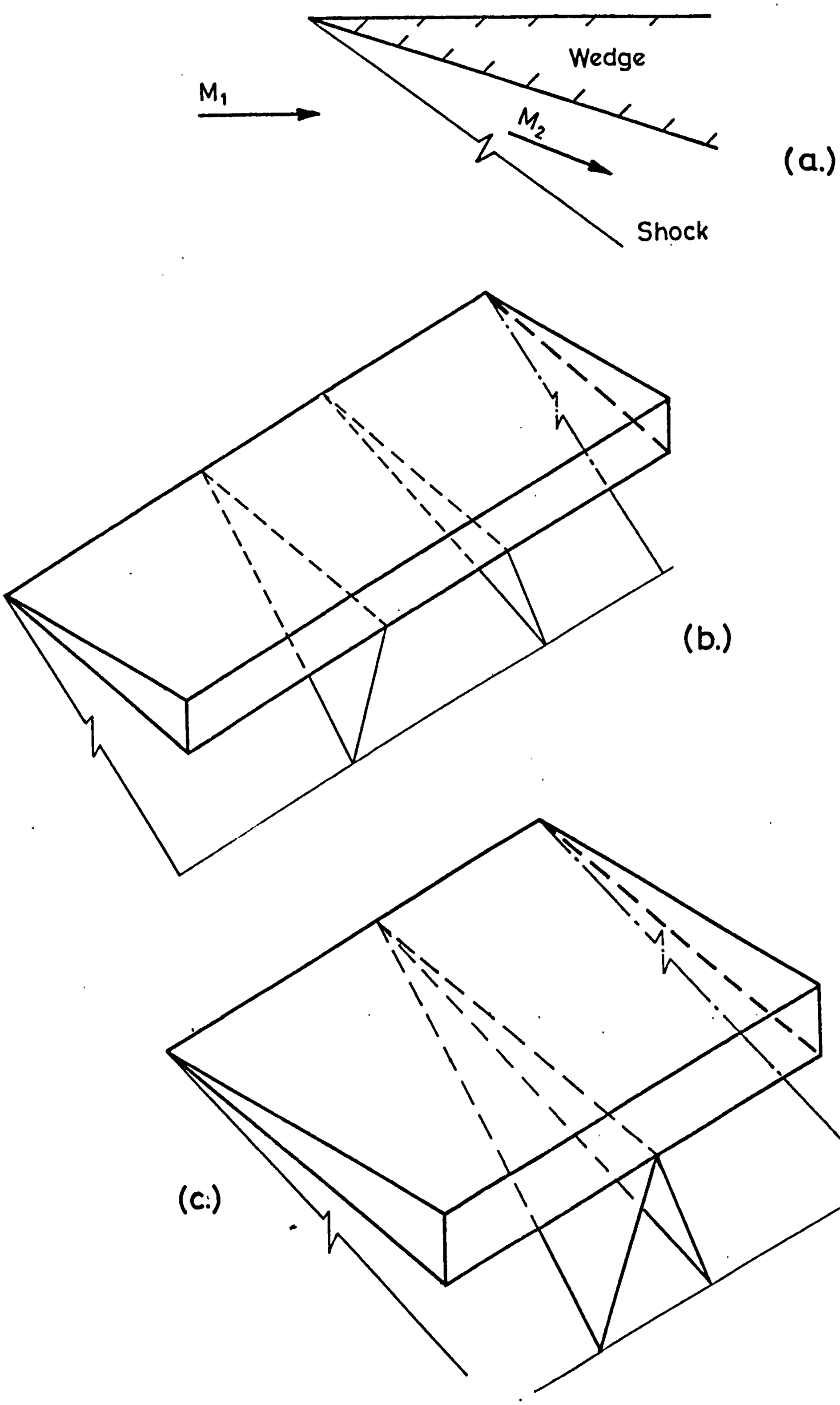

Fig. 1. The concept of a Caret Wing.

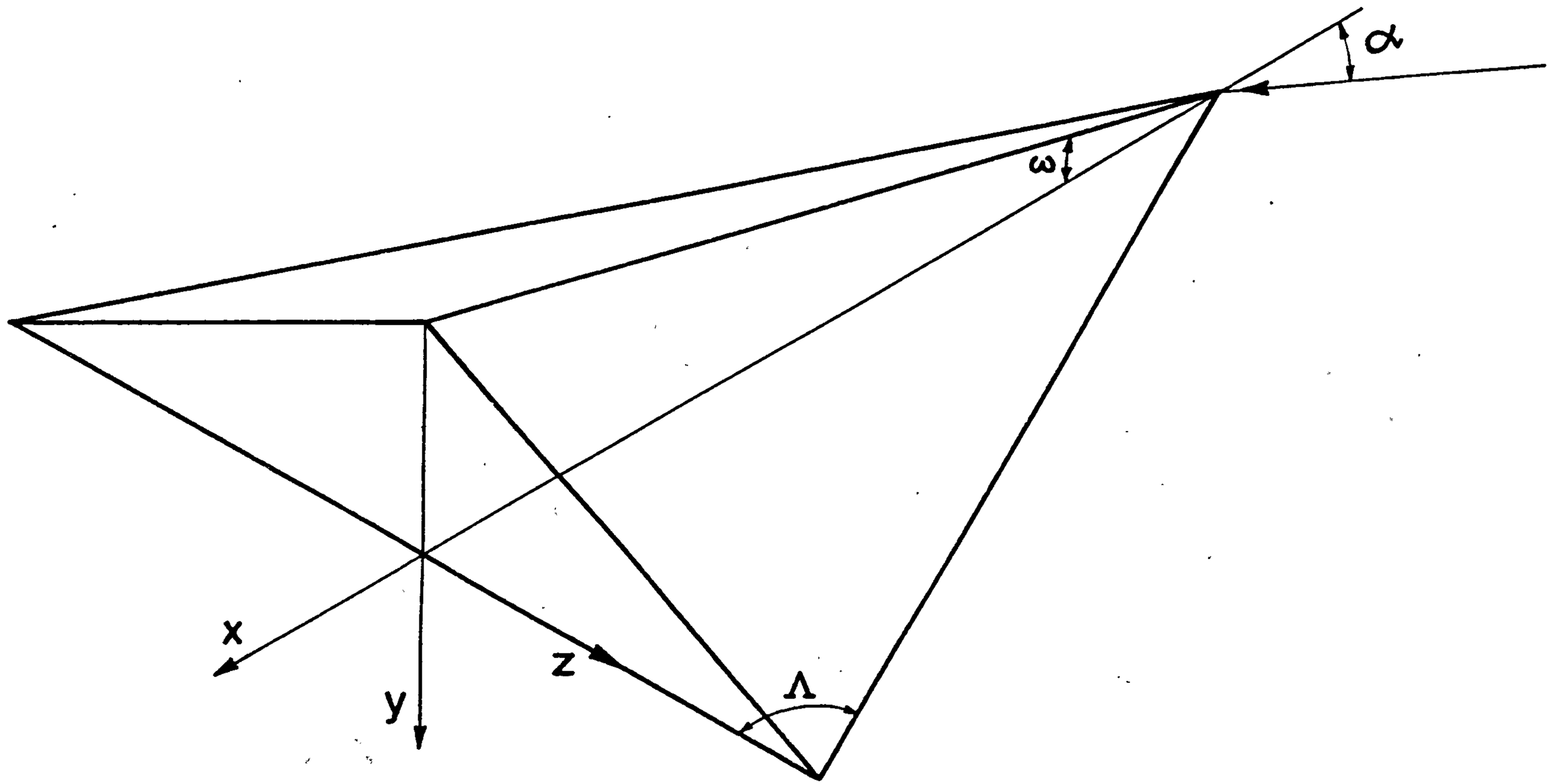

Fig. 2. Co-ordinate system

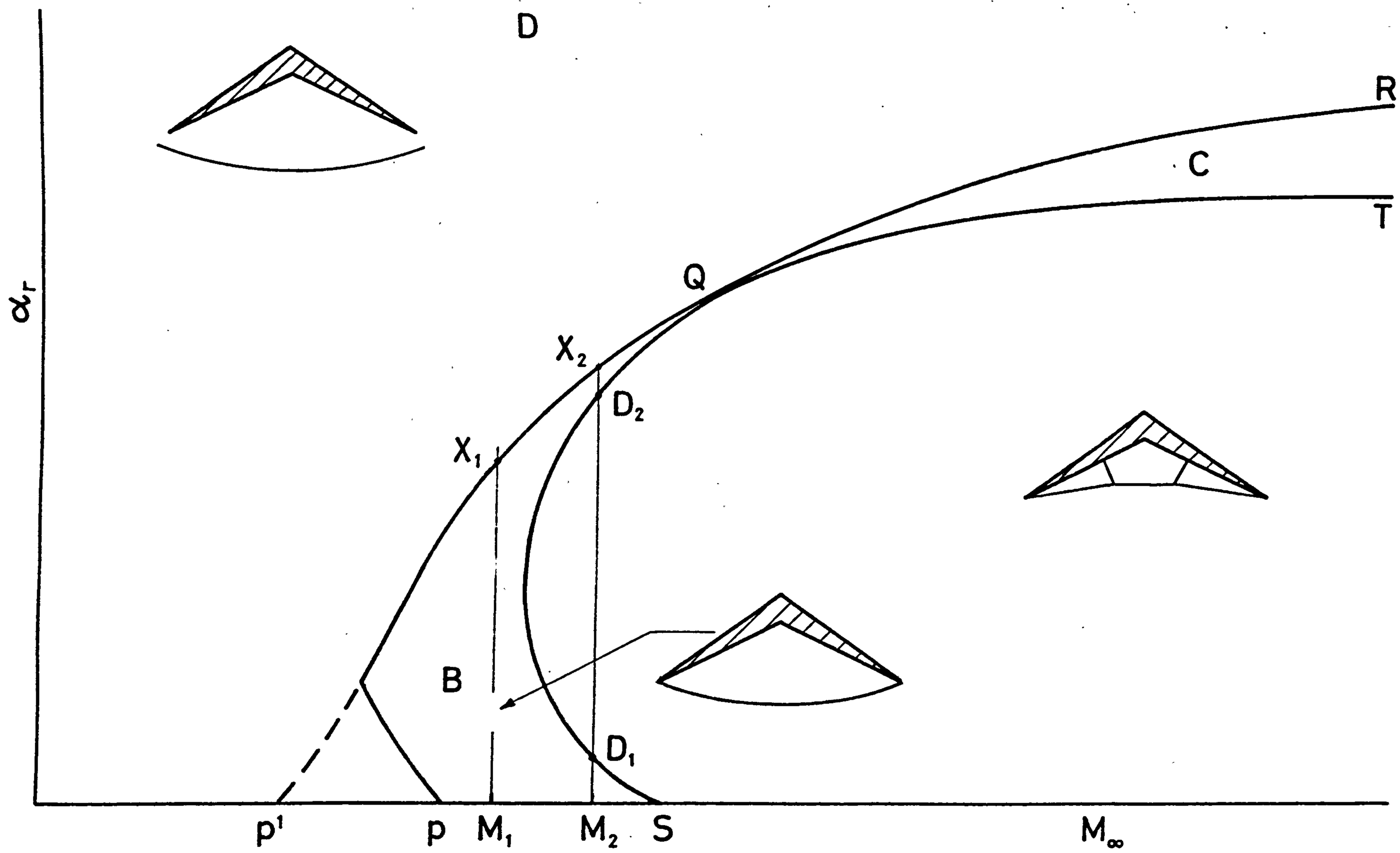

Fig. 3. Flow regimes on a Caret Wing.

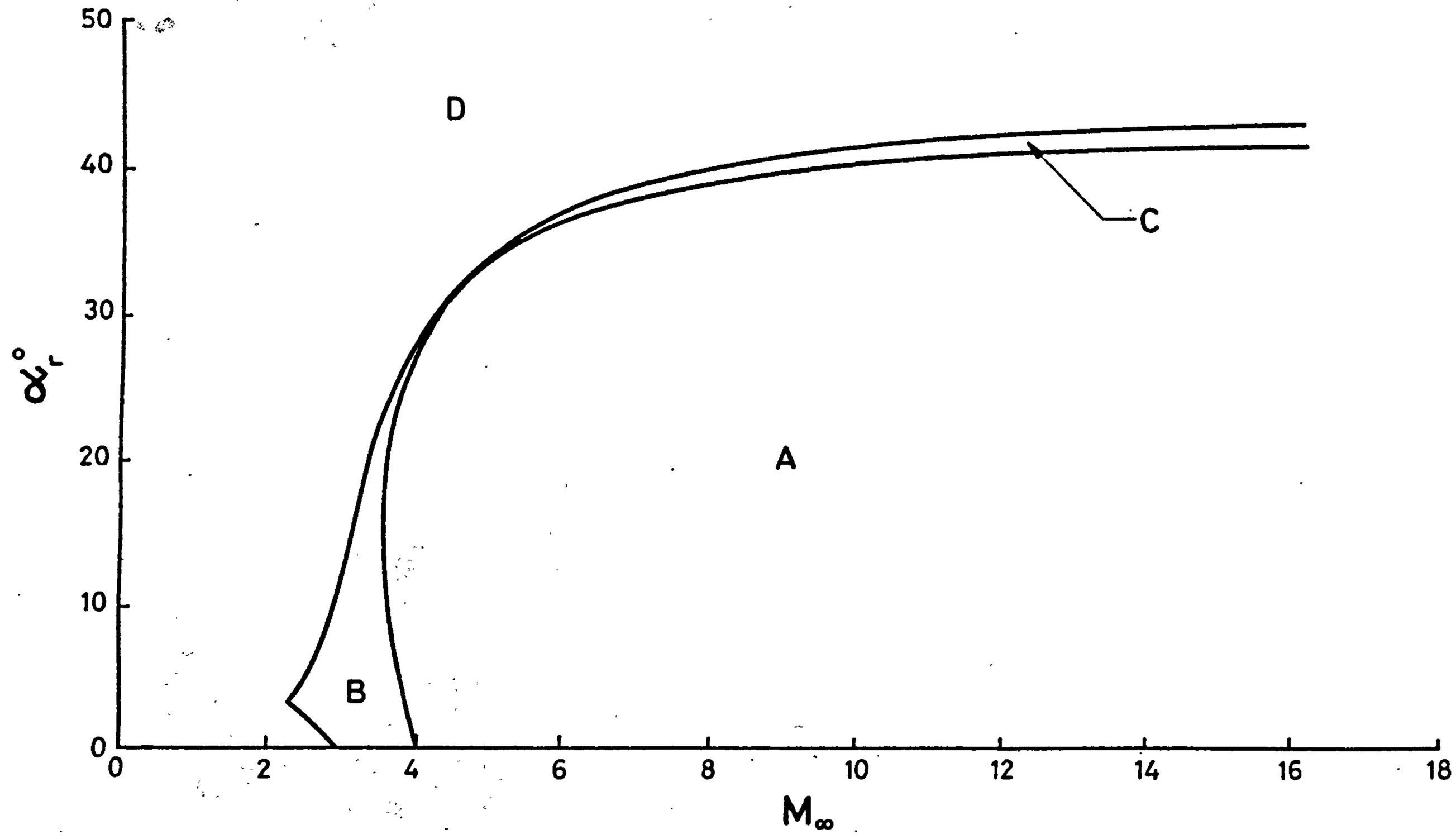

Fig. 4. Design and detachment curves for the $\Lambda = 63°$ Caret Wing.

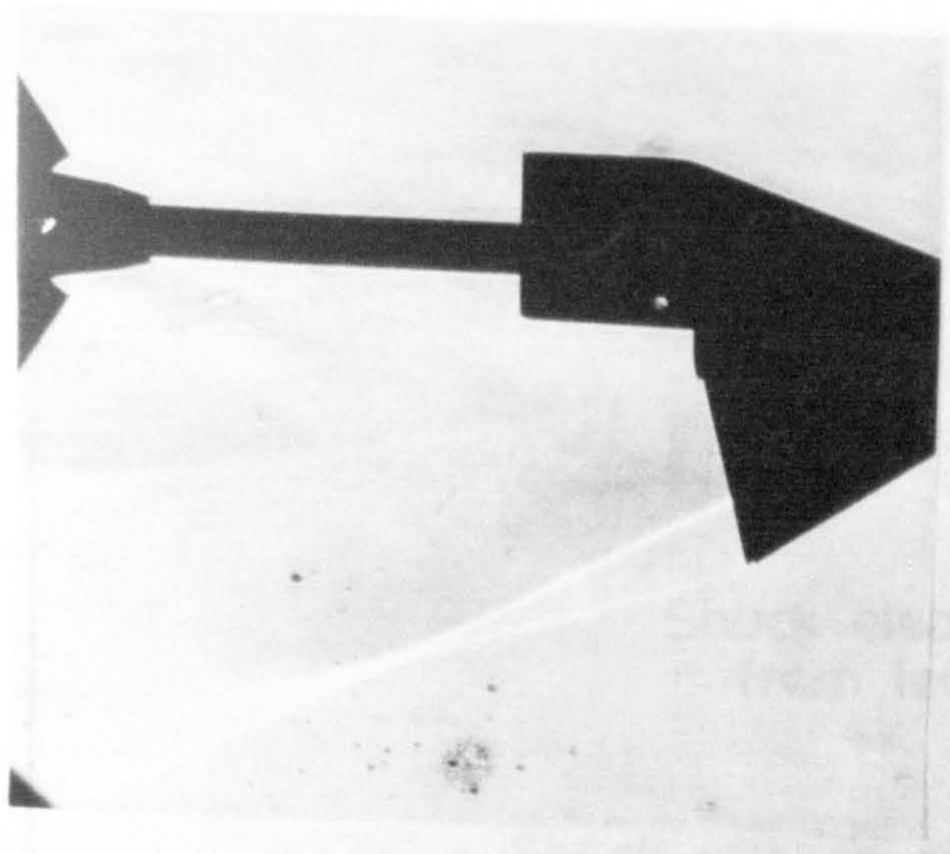

$\alpha_r = 21°$

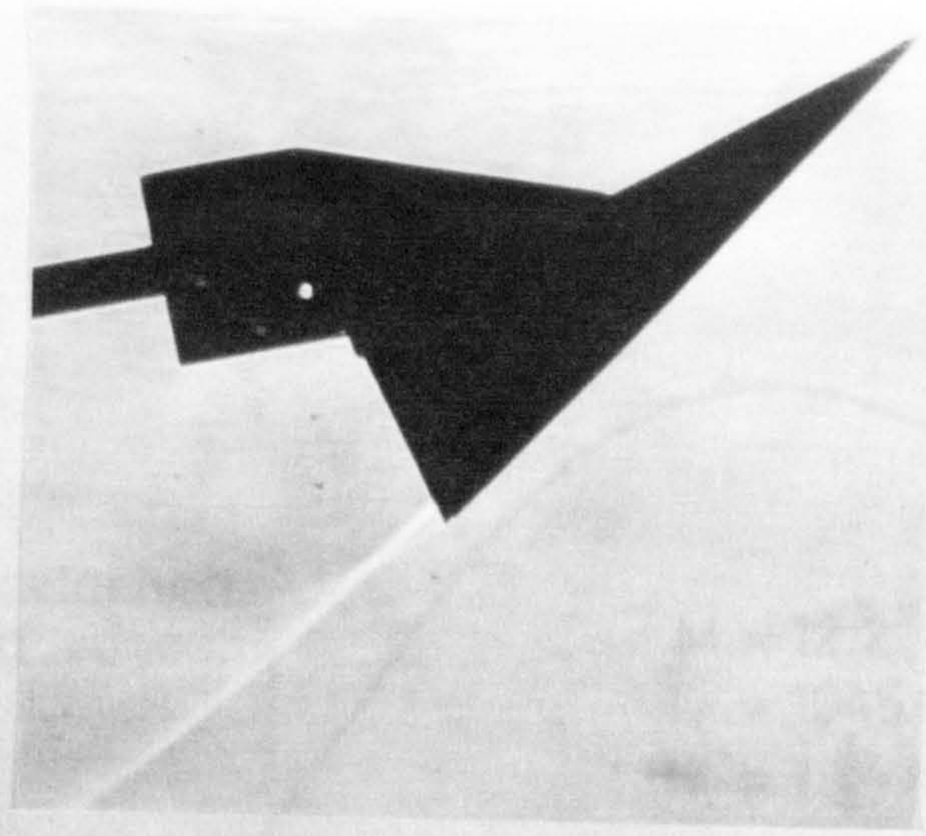

$\alpha_r = 35°$

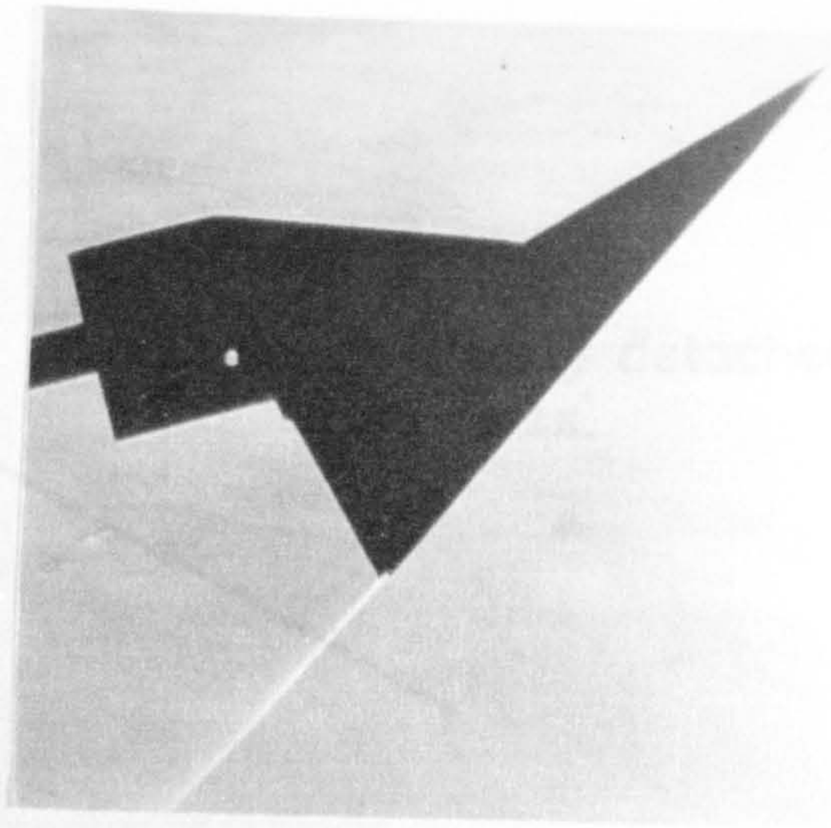

$\alpha_r = 39°$

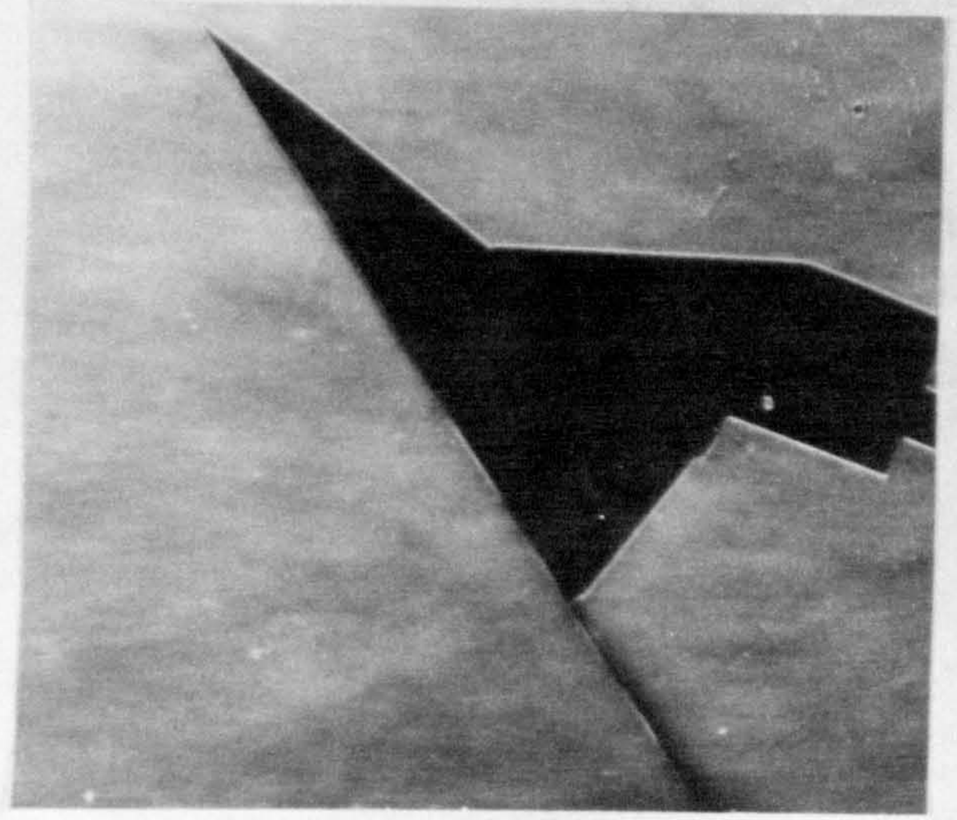

$\alpha_r = 41°$

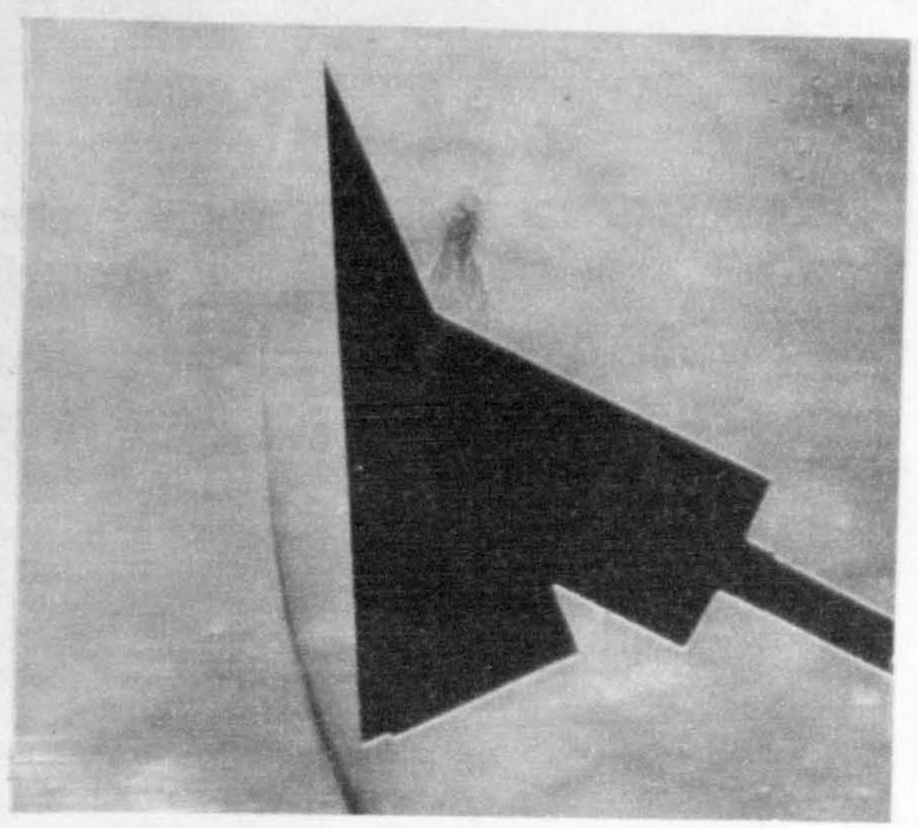

$\alpha_r = 70°$

Fig. 5. $\Lambda = 63°$ Caret Wing at M = 12.2

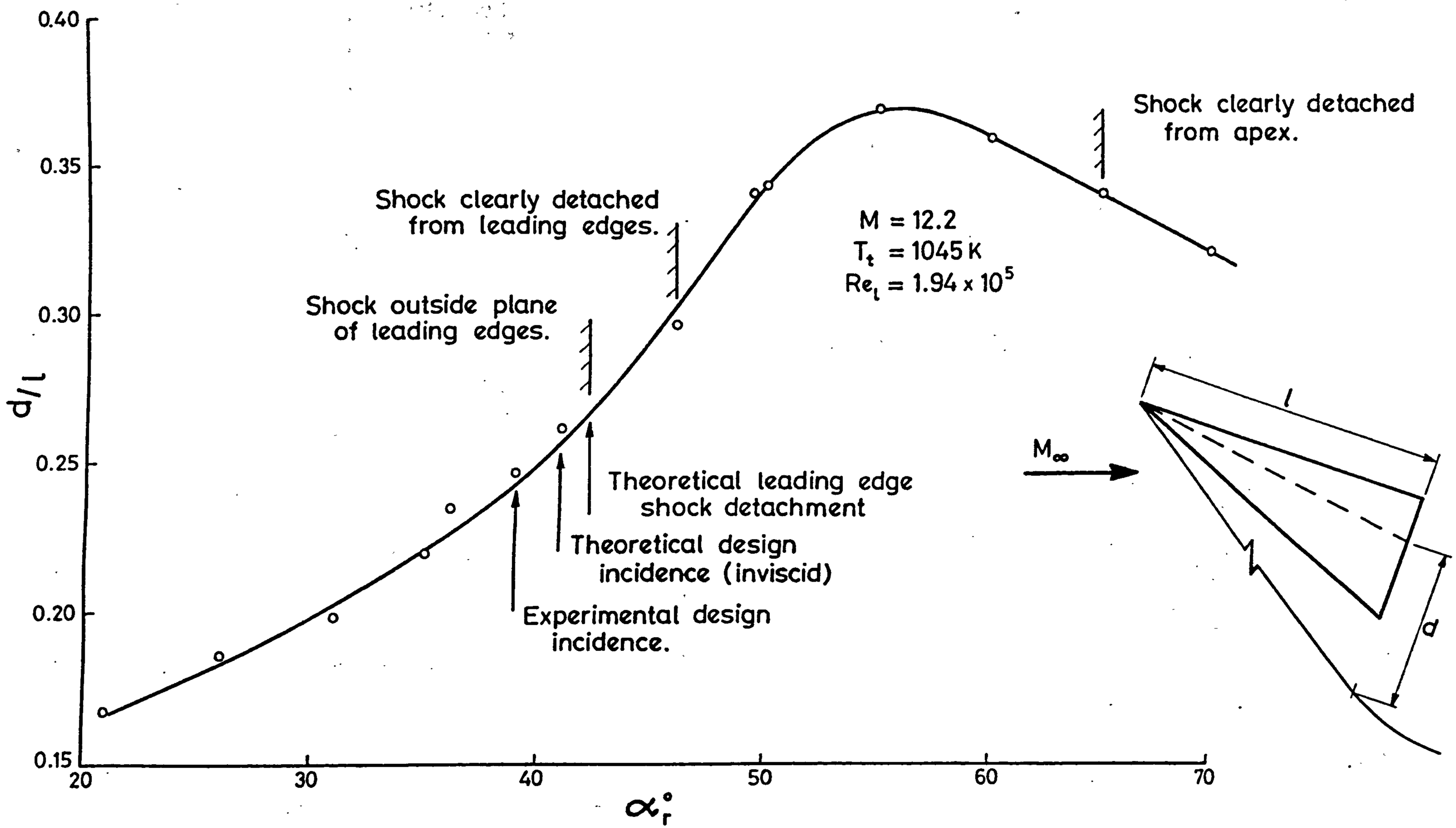

Fig. 6. Summary of results of the tests at M = 12.2

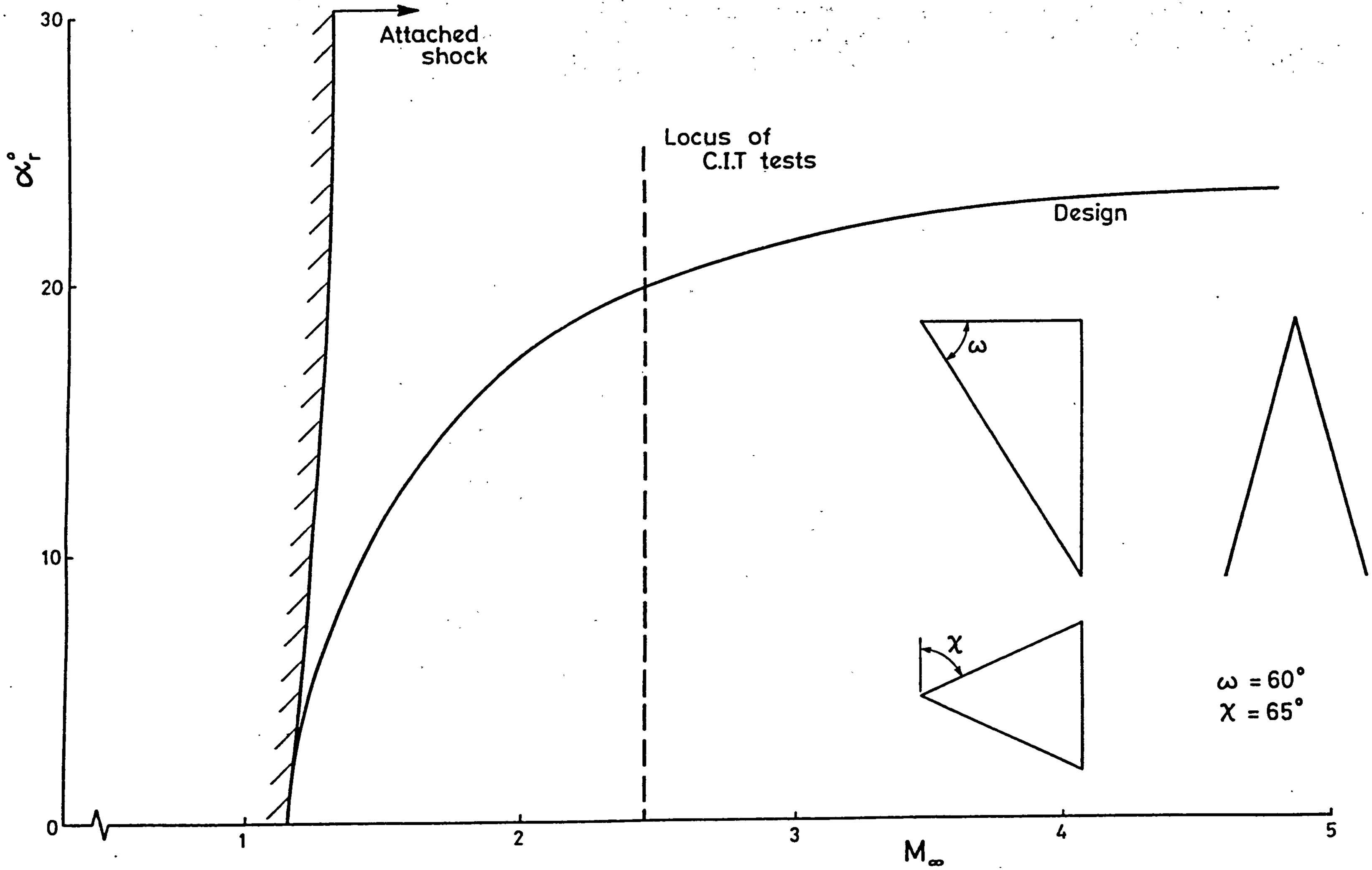

Fig. 7. Caret Wing to support strong oblique shock.

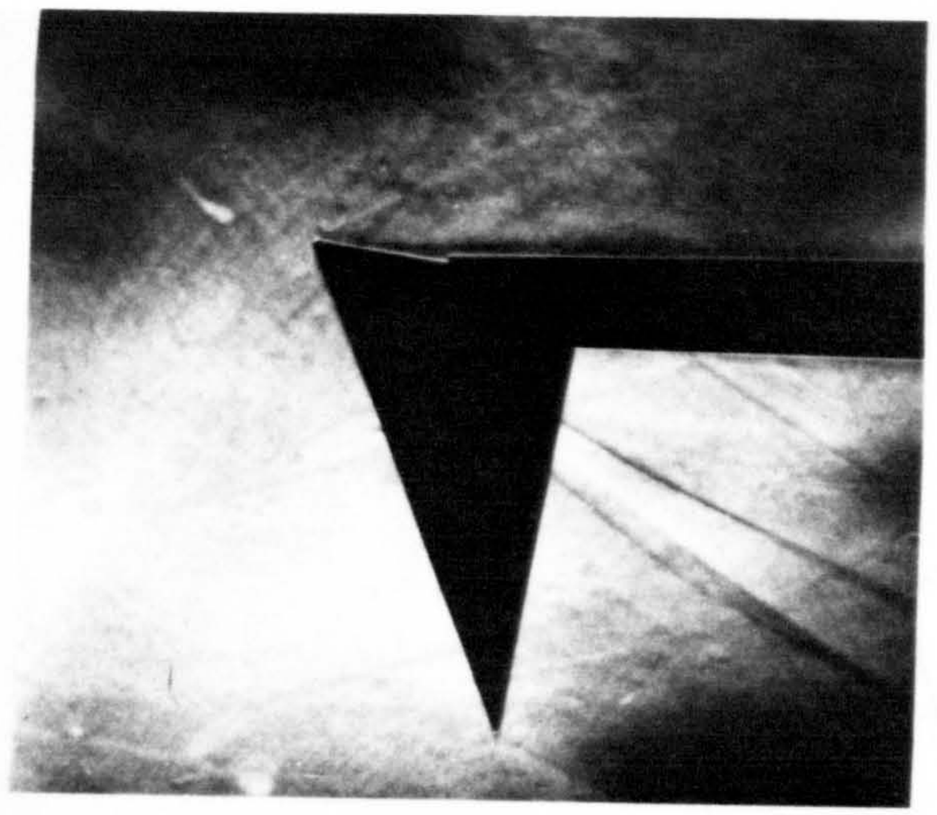

$\alpha_r = 10°$

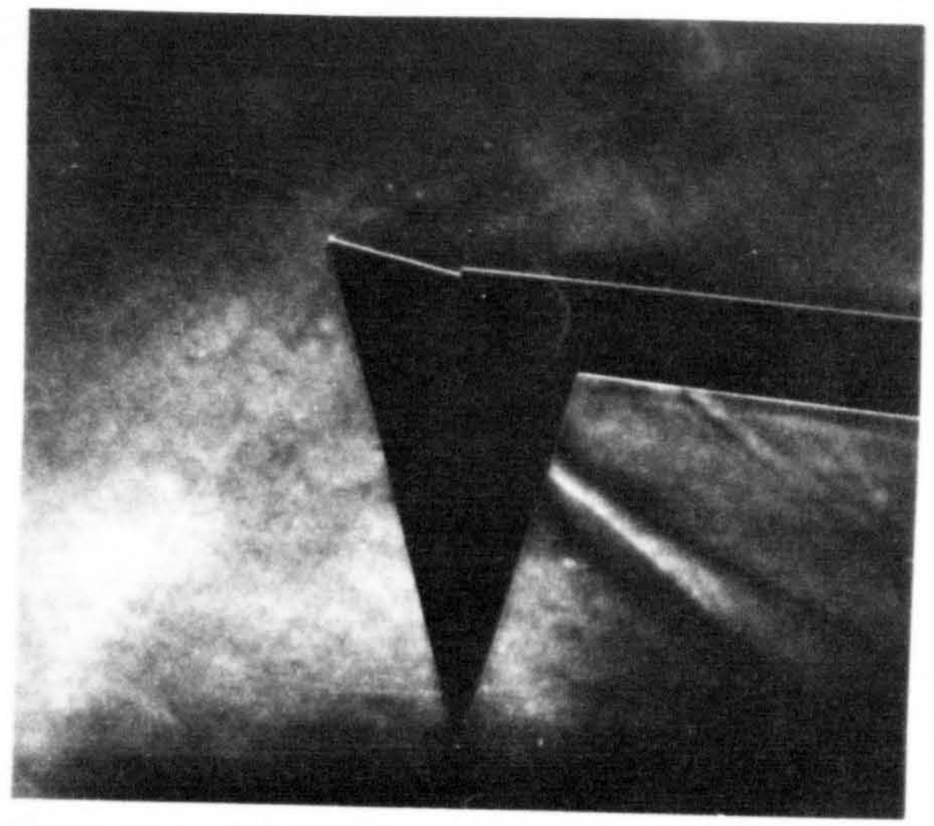

$\alpha_r = 15°$

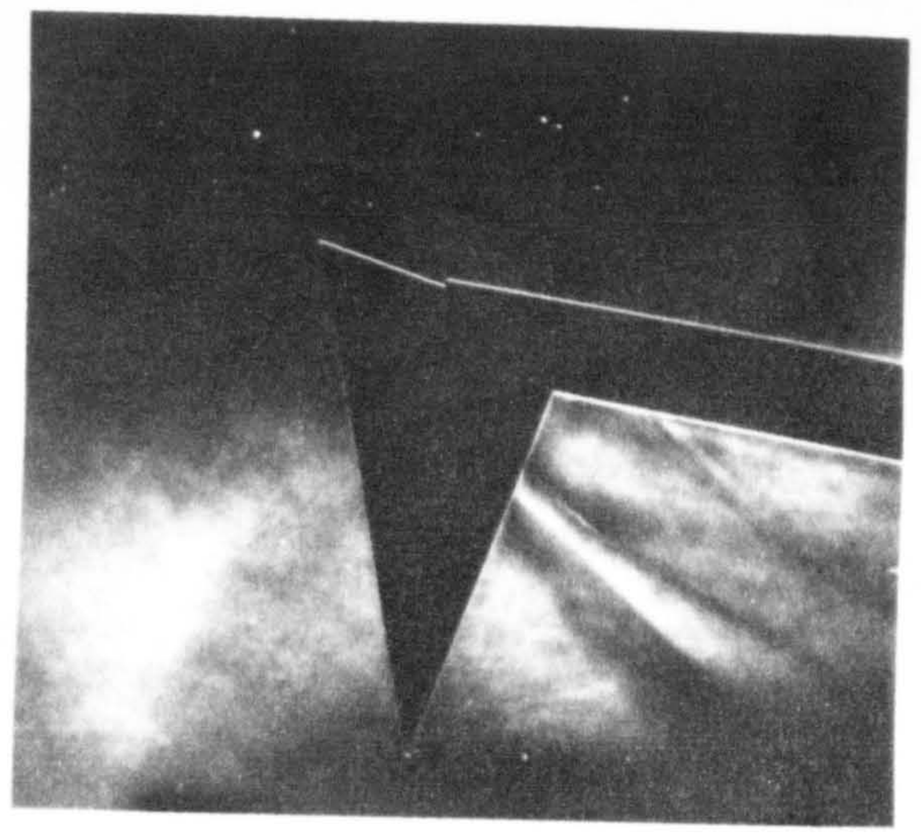

$\alpha_r = 20°$

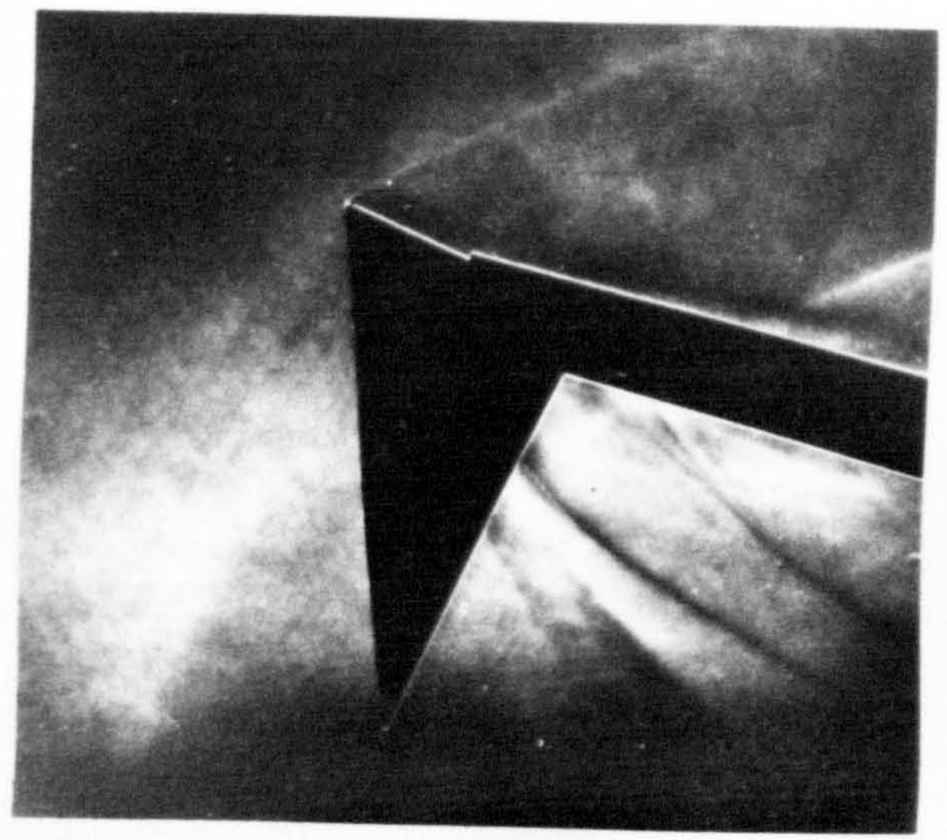

$\alpha_r = 25°$

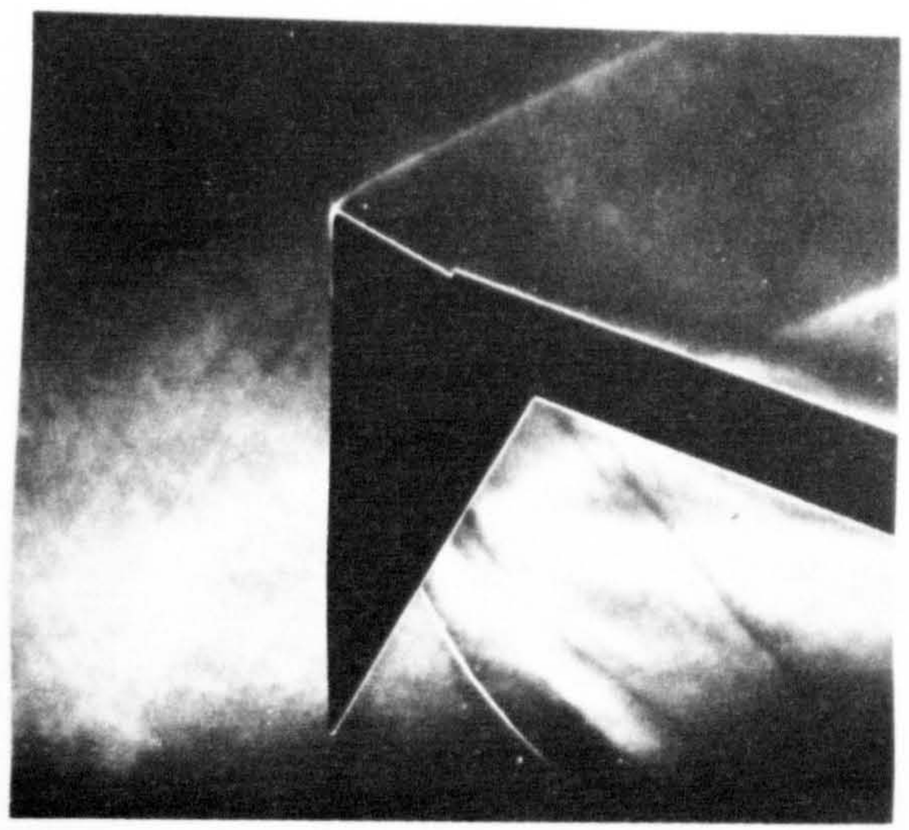

$\alpha_r = 30°$

Fig. 8. Schlieren photographs of large anhedral Caret Wing.

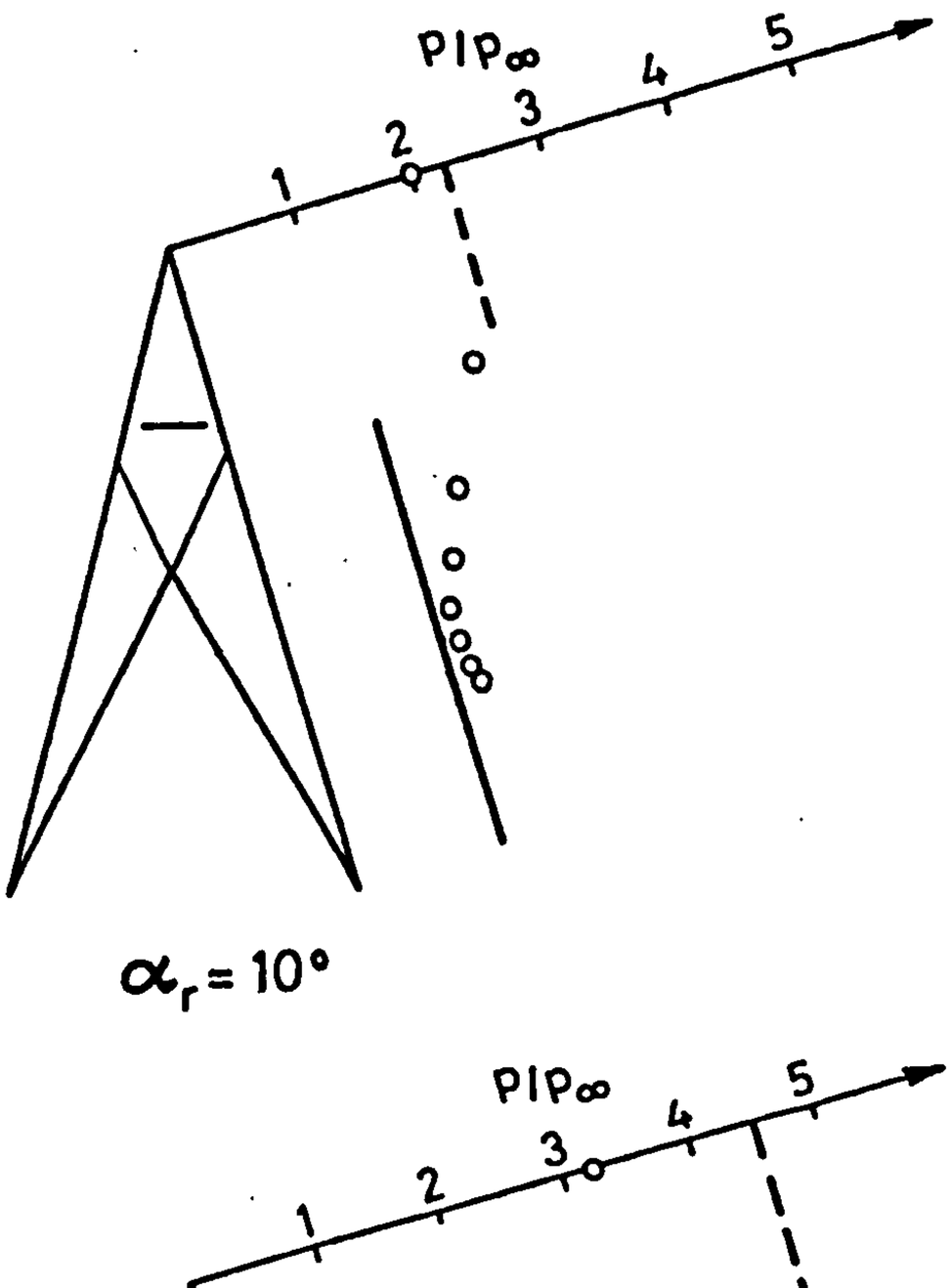

$\alpha_r = 10°$

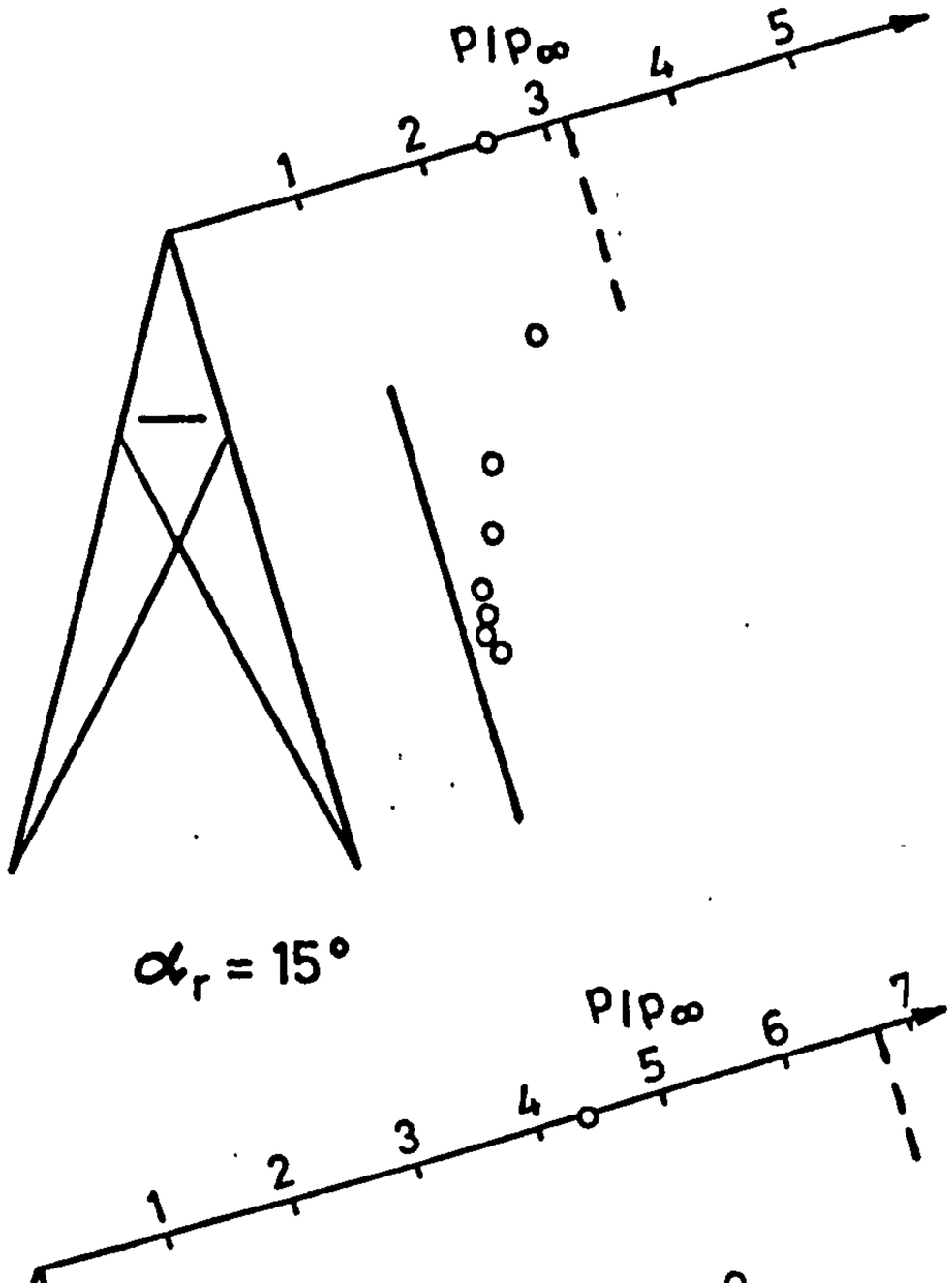

$\alpha_r = 15°$

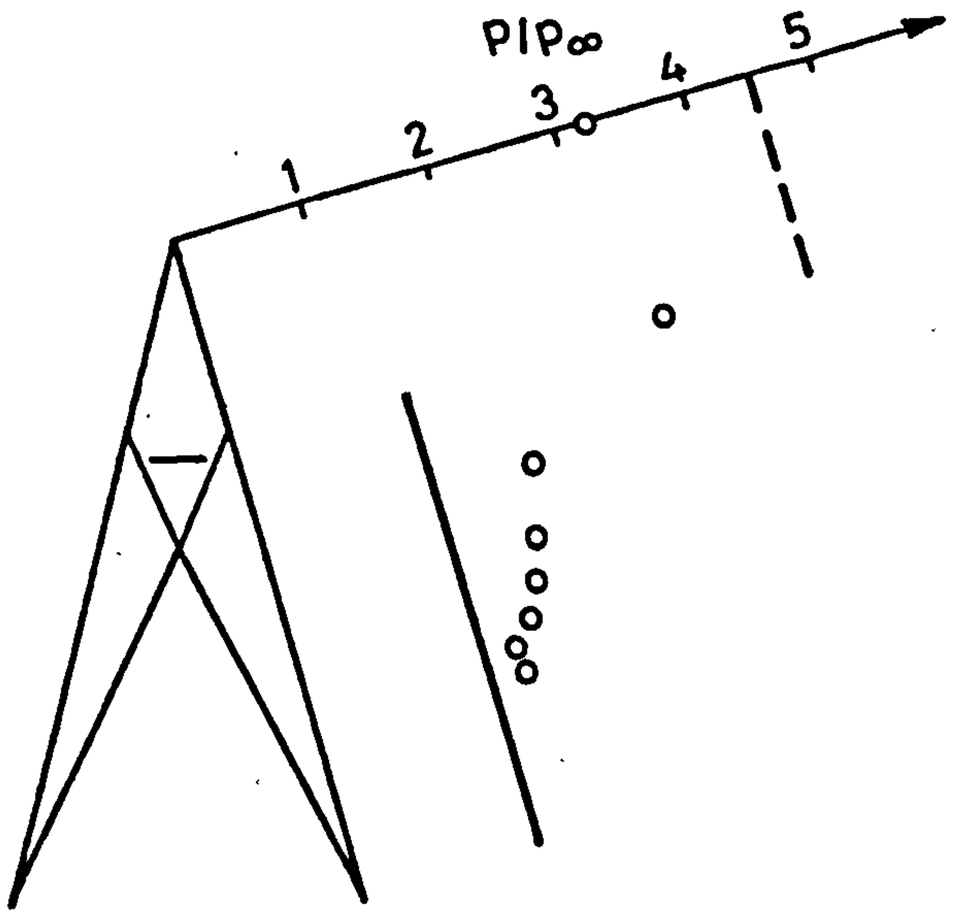

$\alpha_r = 20°$

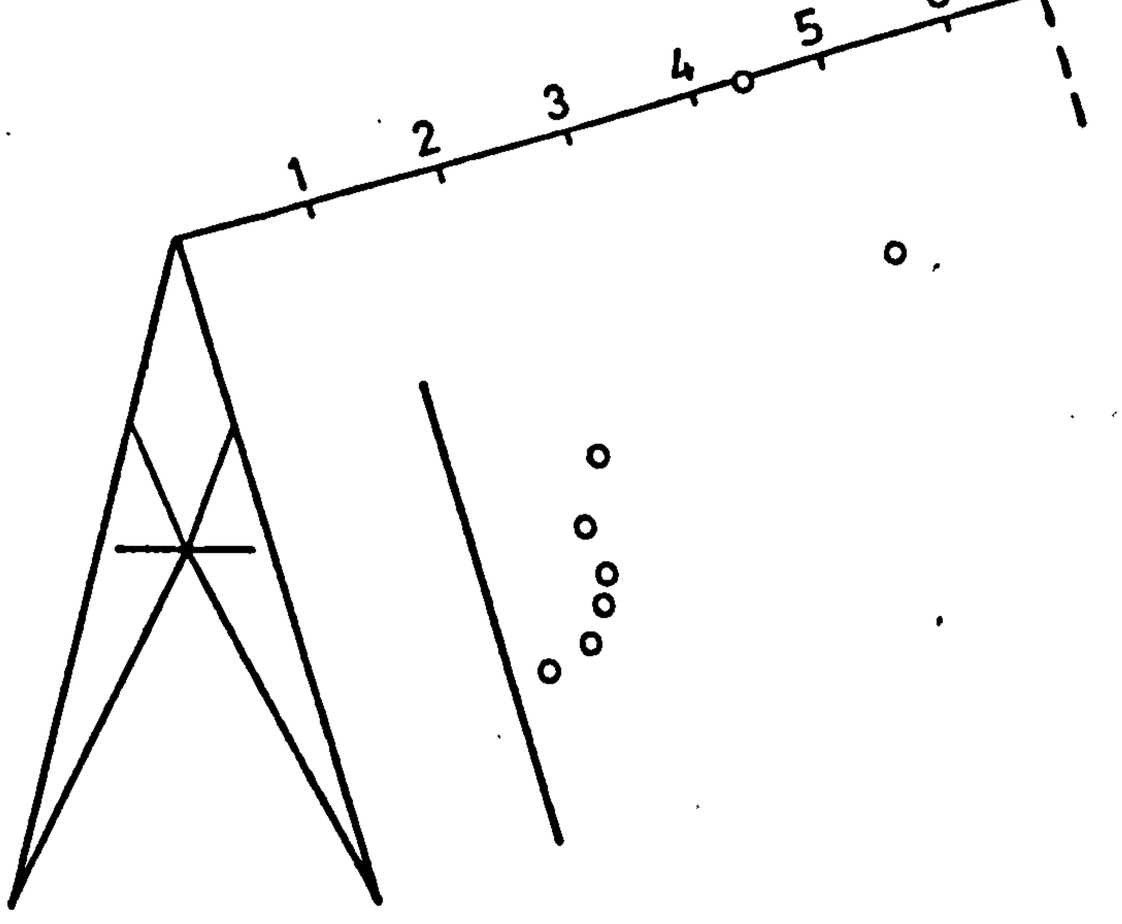

$\alpha_r = 25°$

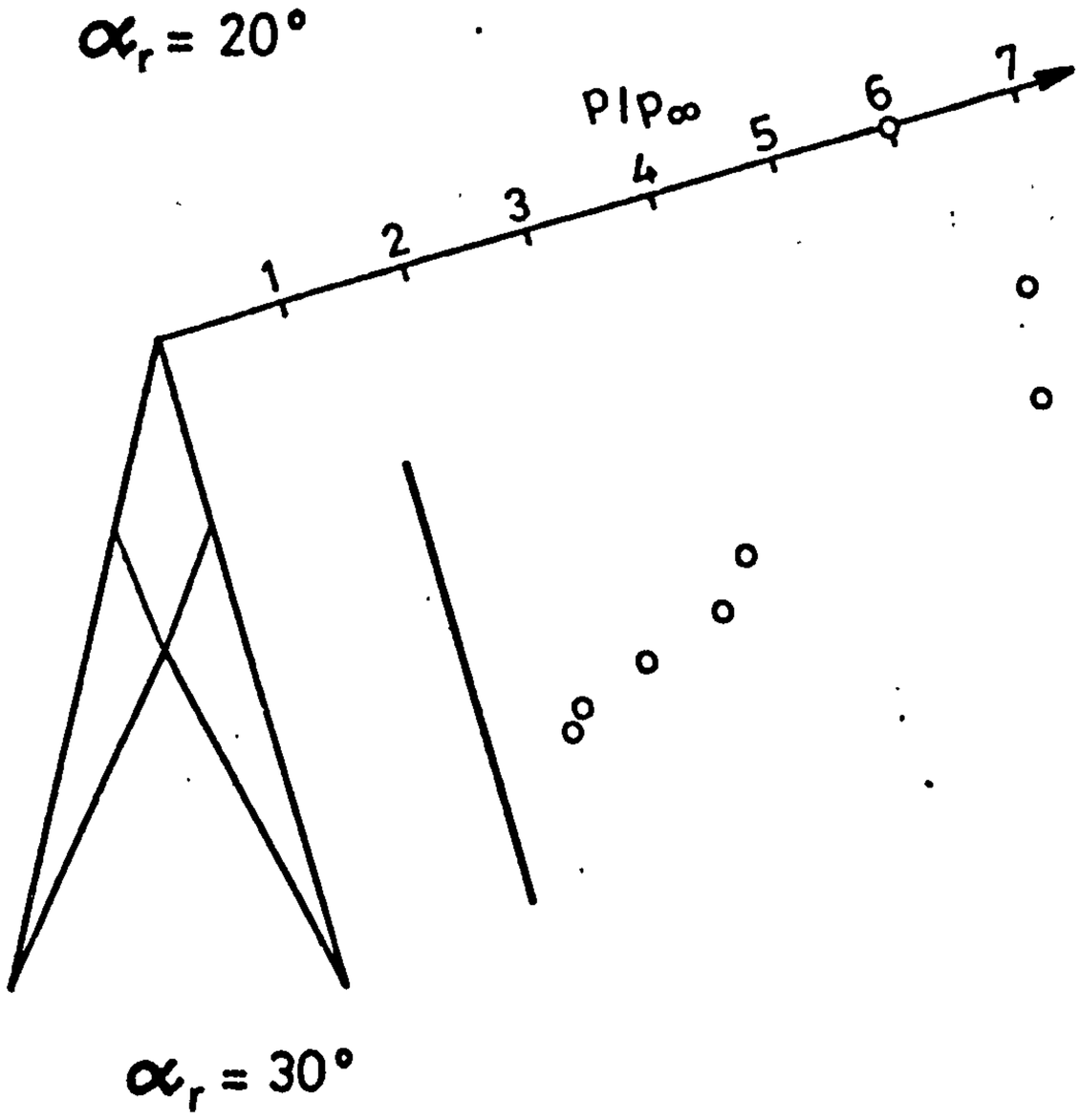

$\alpha_r = 30°$

p/p_∞ for various α_r

Experiment

Exact theory

Approximate solution for inner shock

Fig. 9. Pressure distribution on large anhedral Caret Wing.

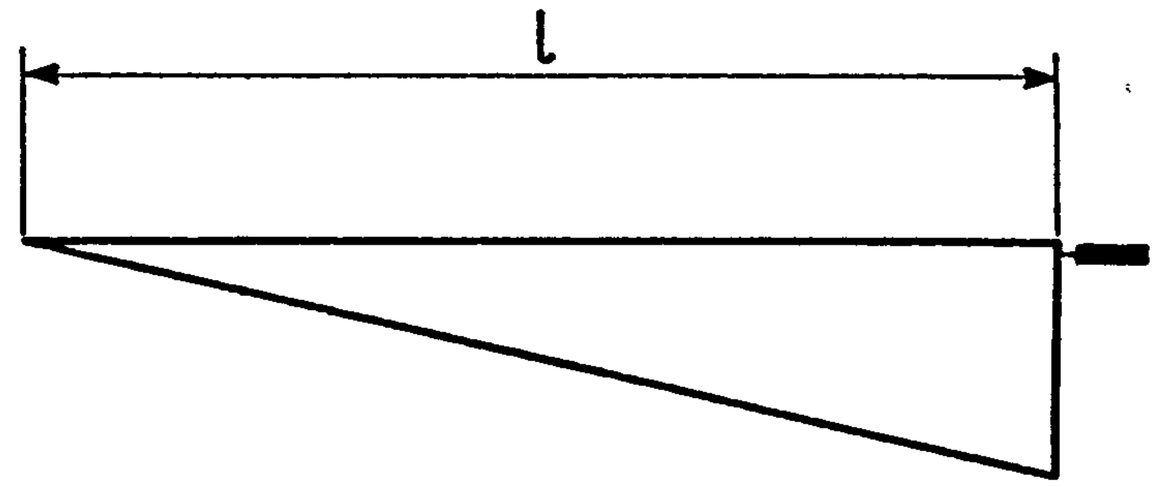

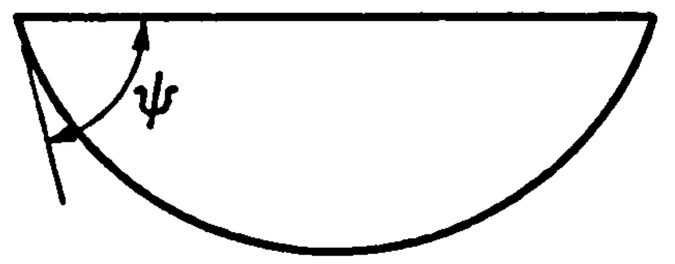

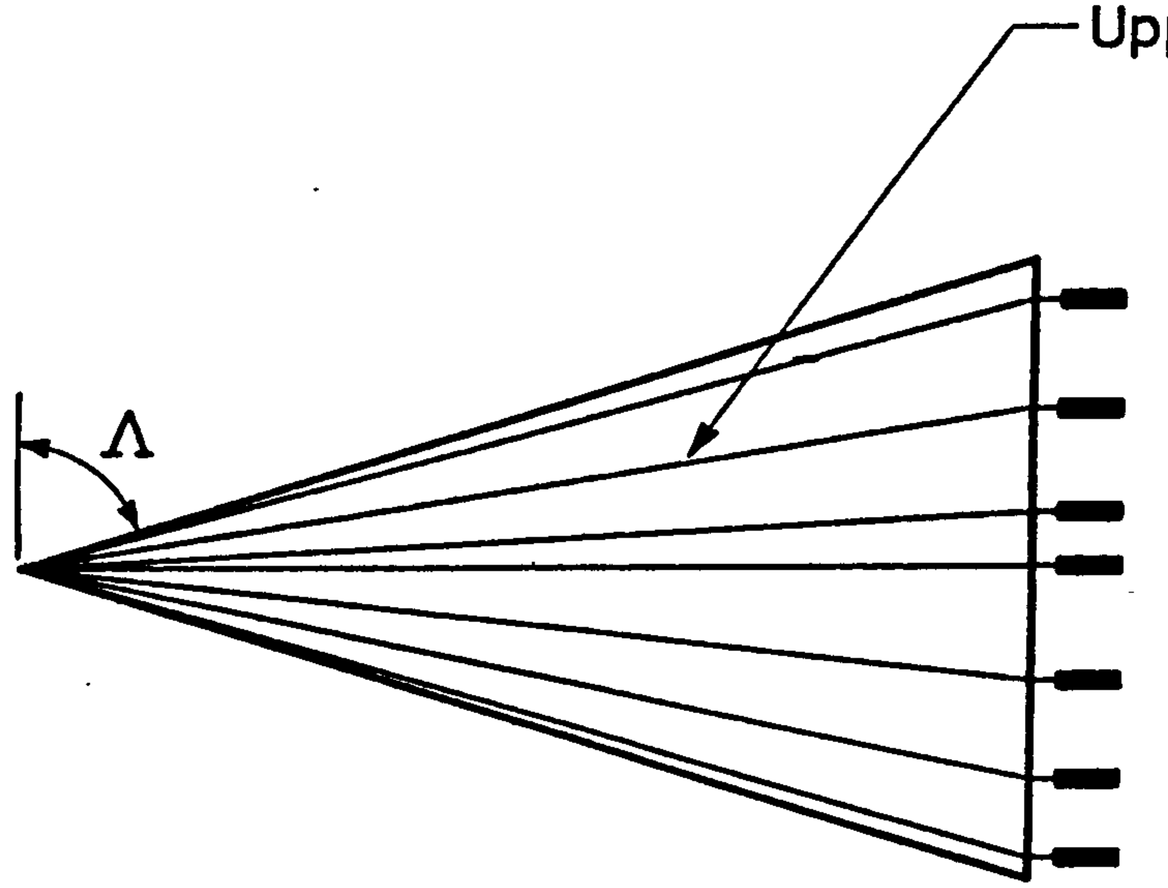

$\Lambda = 72.5°$
$\psi = 75.0°$
$l = 100\,mm$

Fig. 10. Details of the Flat Cone model.

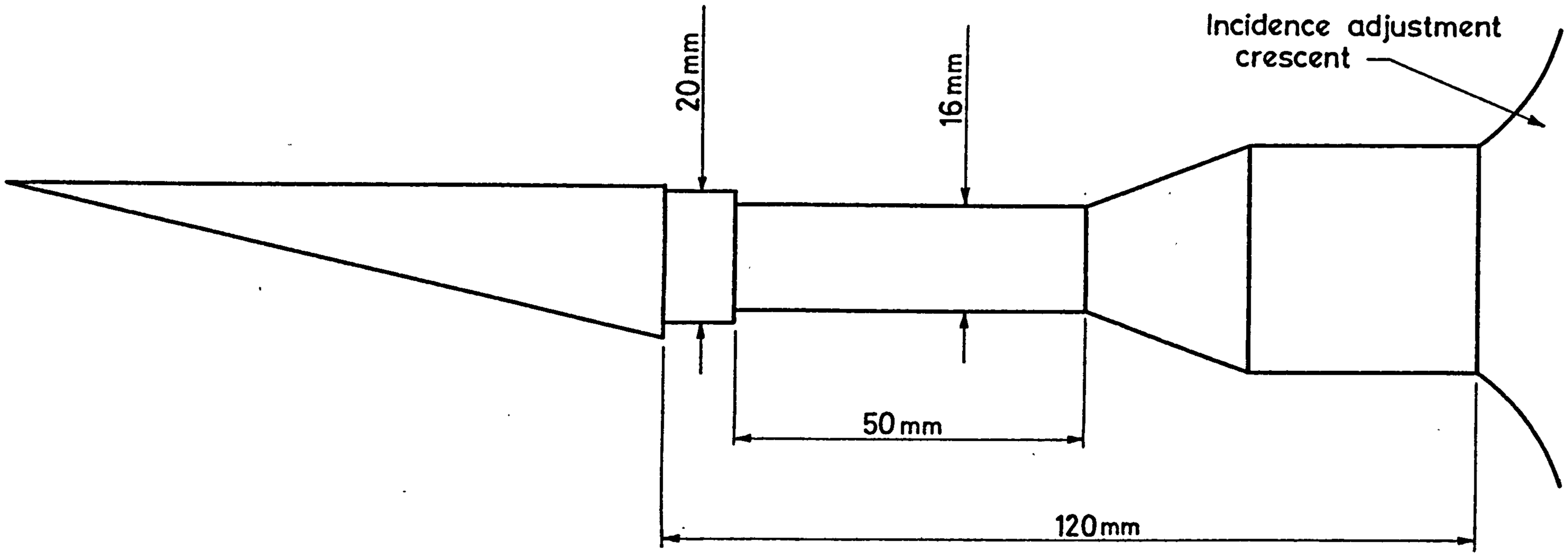

Fig. 11. Model support system in C.I.T. tunnel.

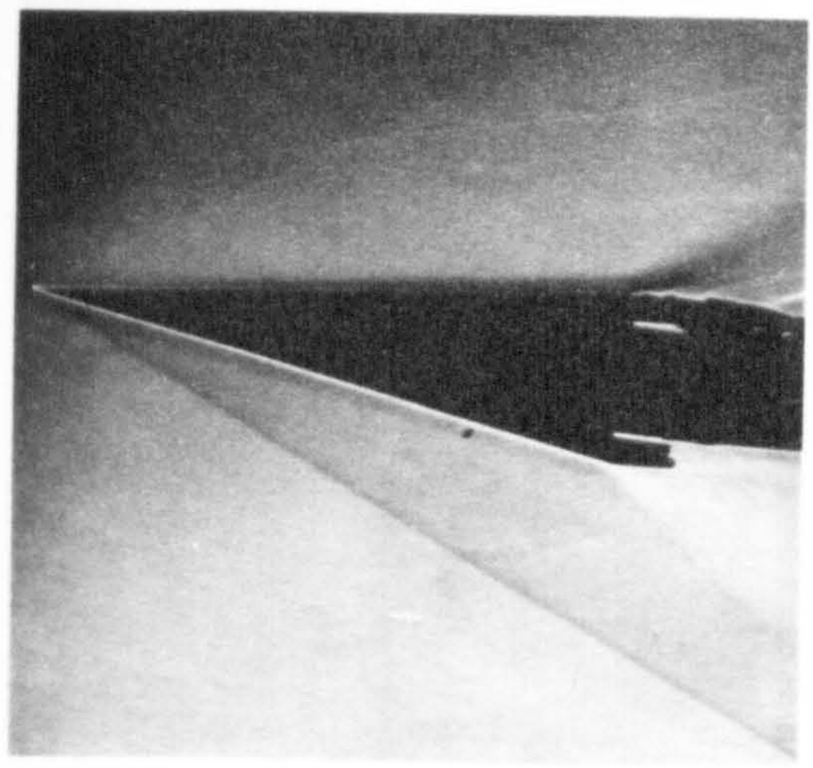

$\alpha = 0°$

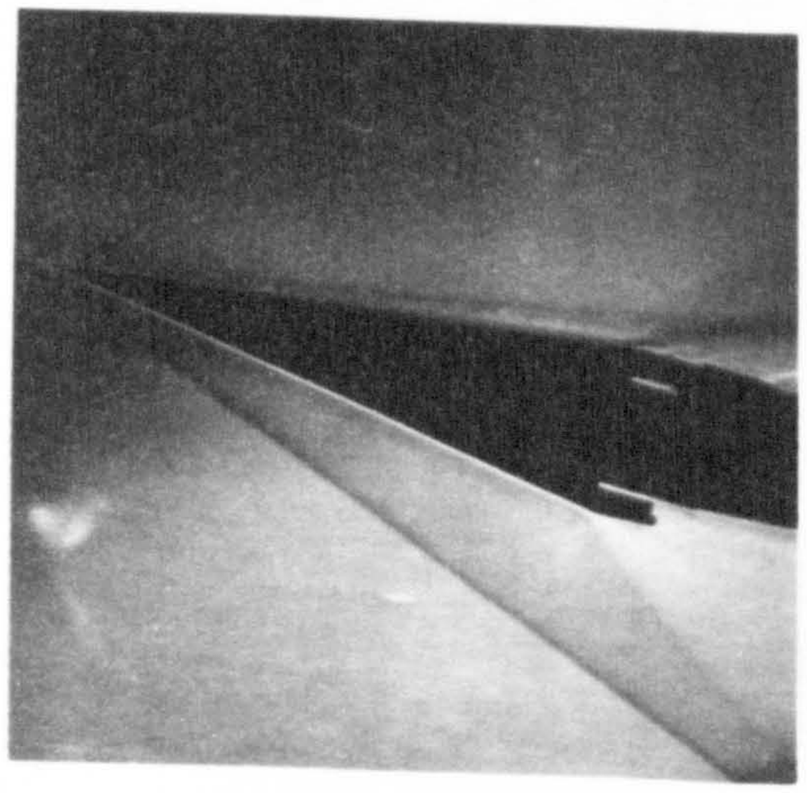

$\alpha = 6°$

$\alpha = 12°$

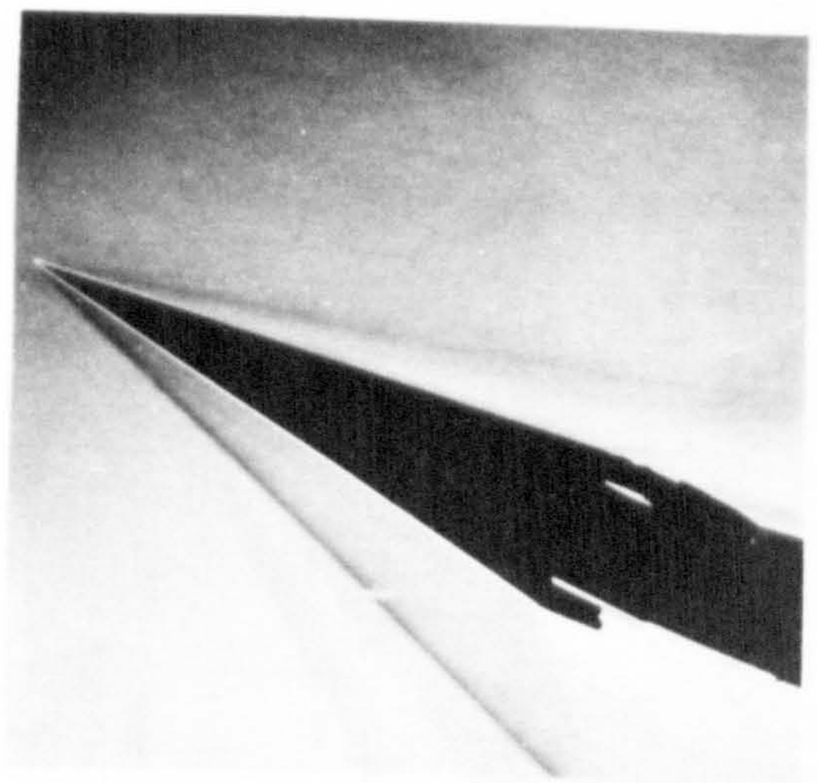

$\alpha = 16°$

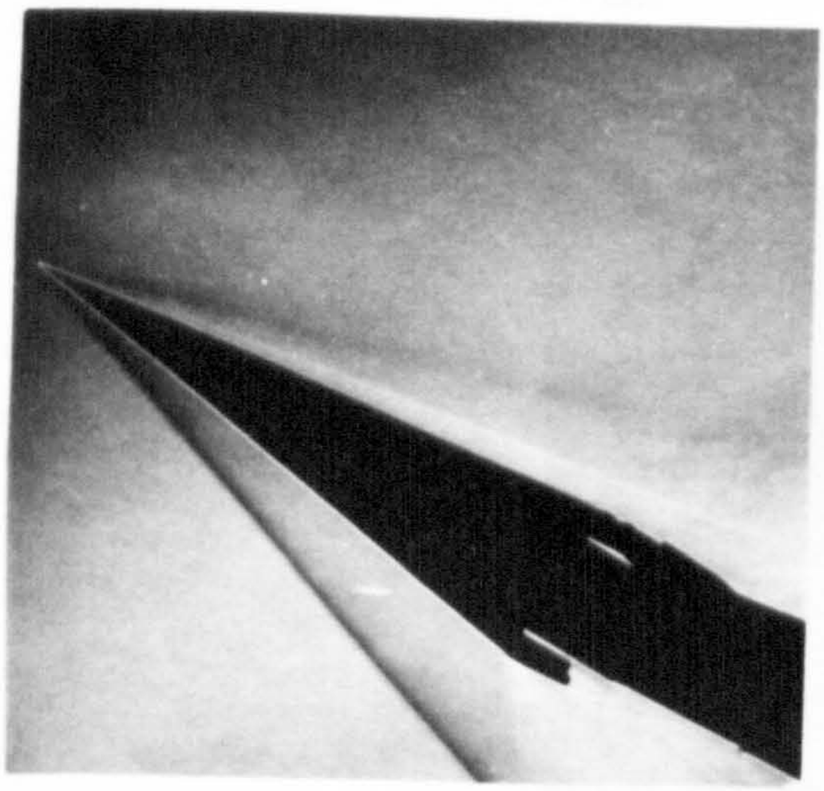

$\alpha = 22°$

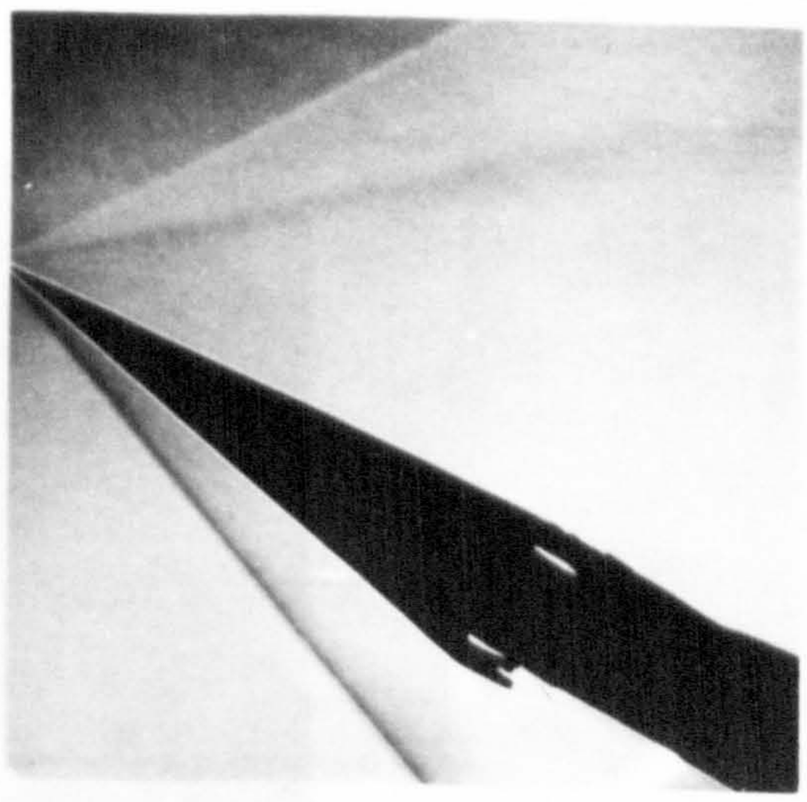

$\alpha = 24°$

Fig. 12. Flat Cone with original sting and pressure tubes.

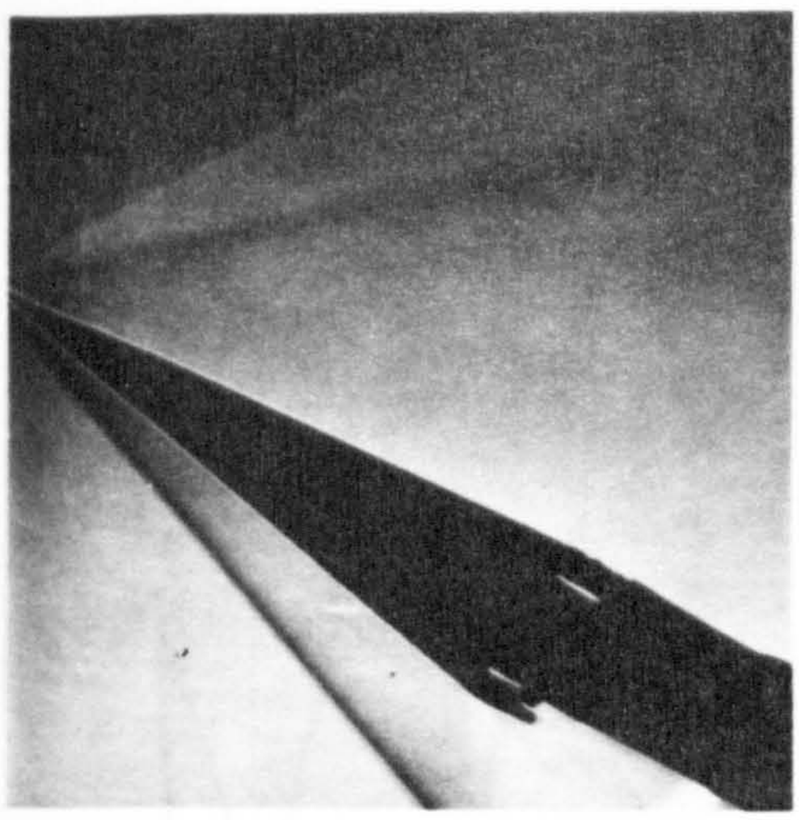

$\alpha = 24°$

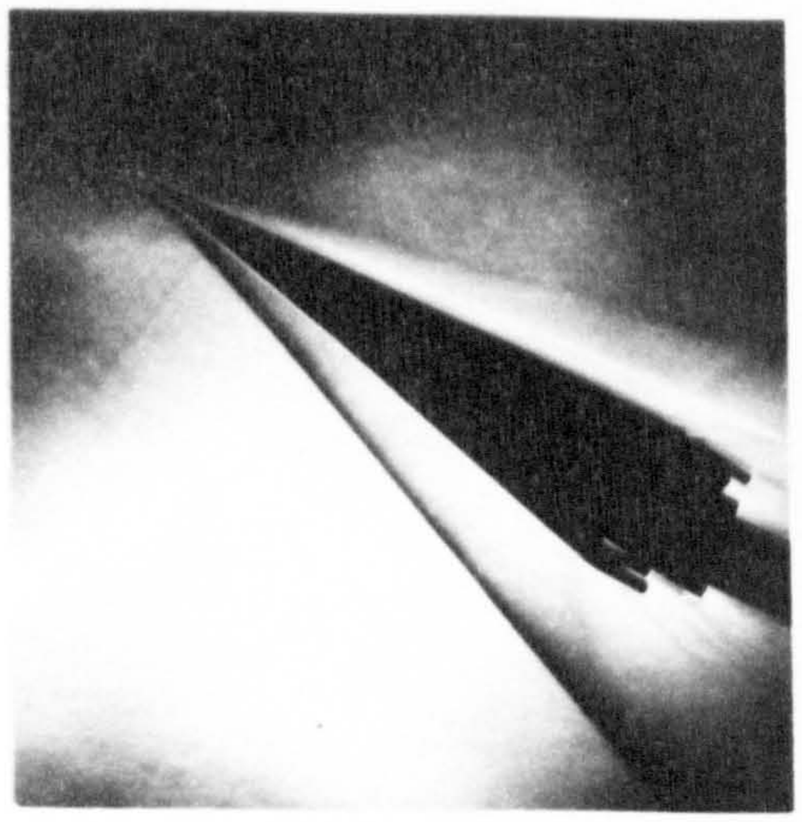

Fig.13. **Different flow types at 24 Deg**

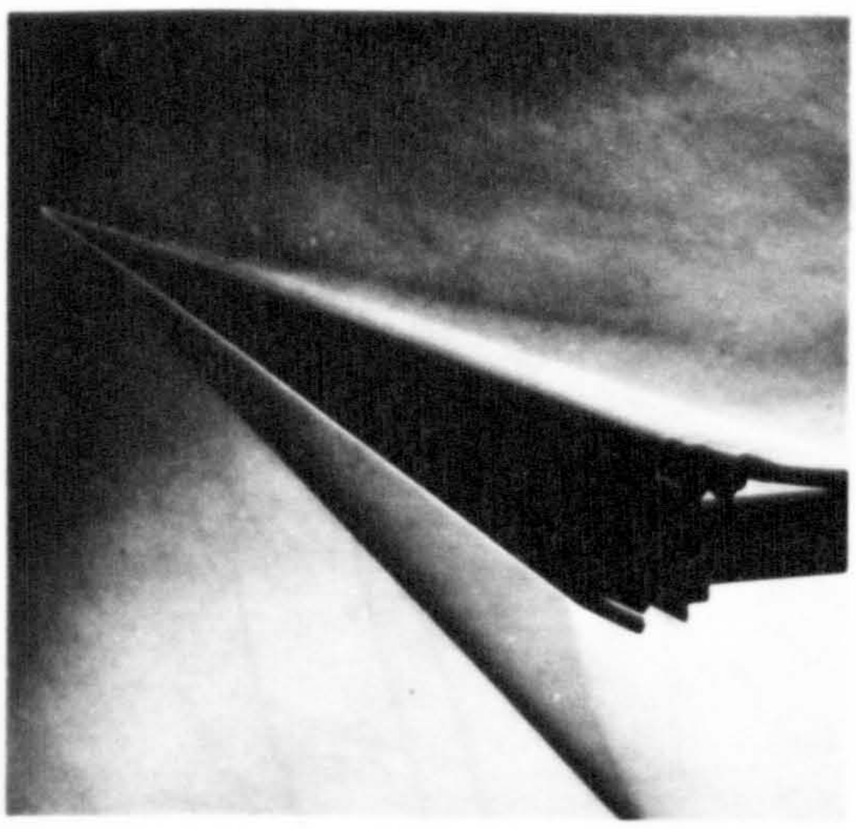

$\alpha = 20°$

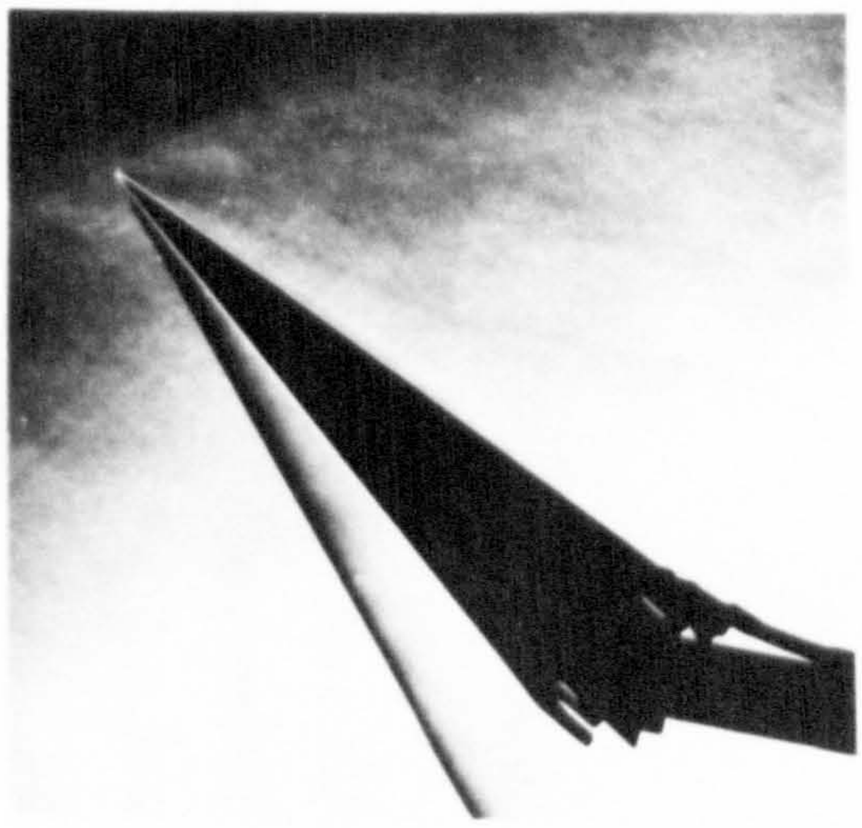

$\alpha = 35°$

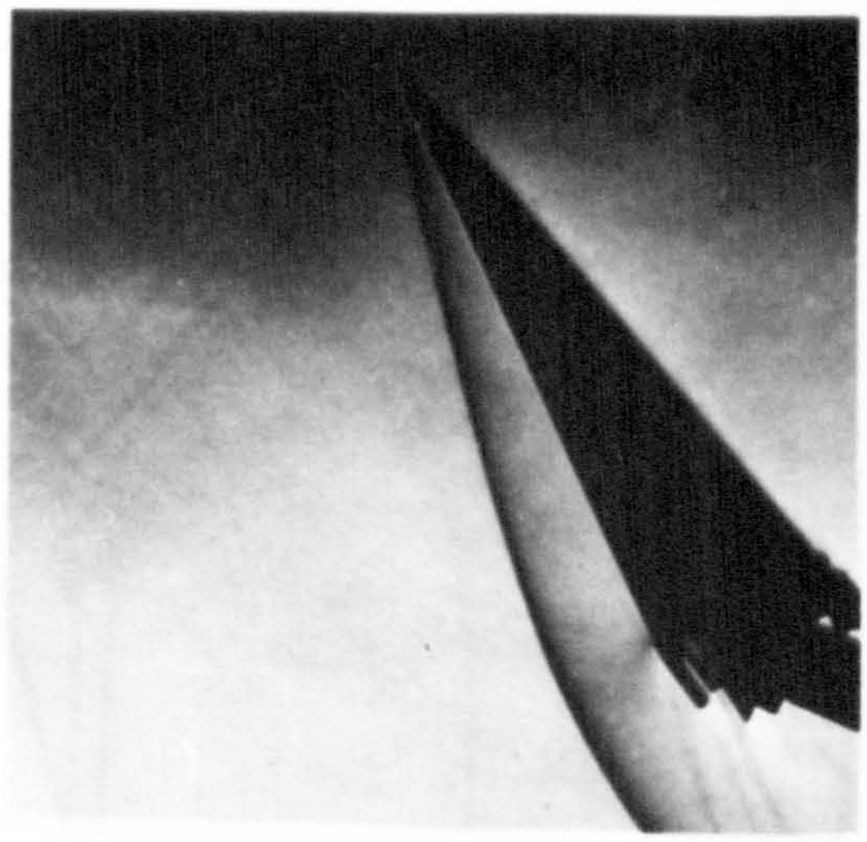

$\alpha = 50°$

Fig. 14. Model with angled sting.

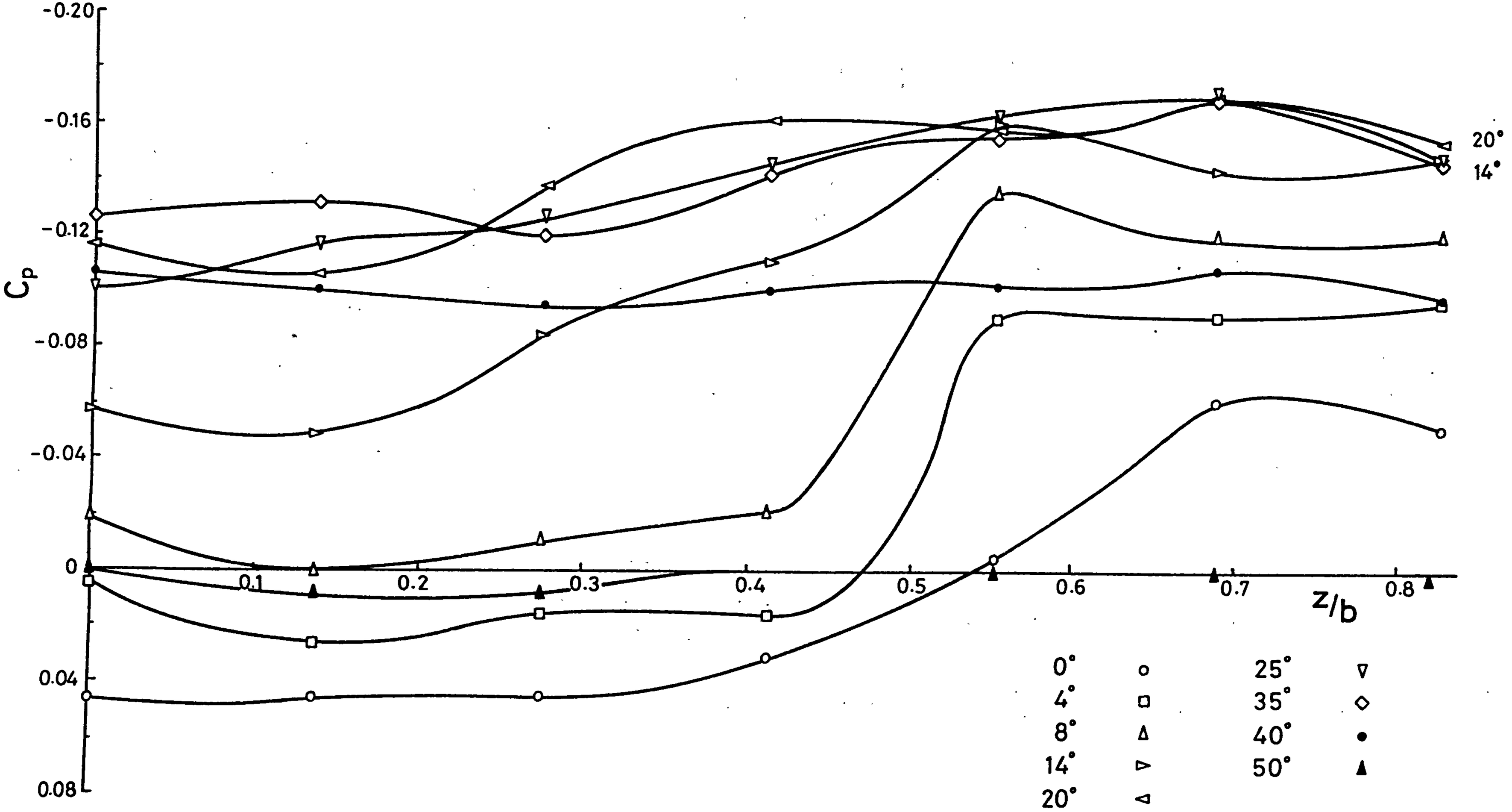

Fig. 15. Pressure distribution at 55 % chord.

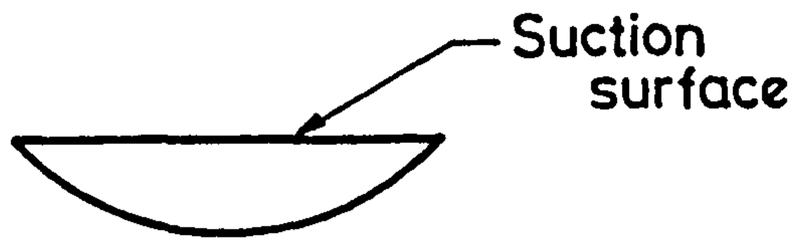

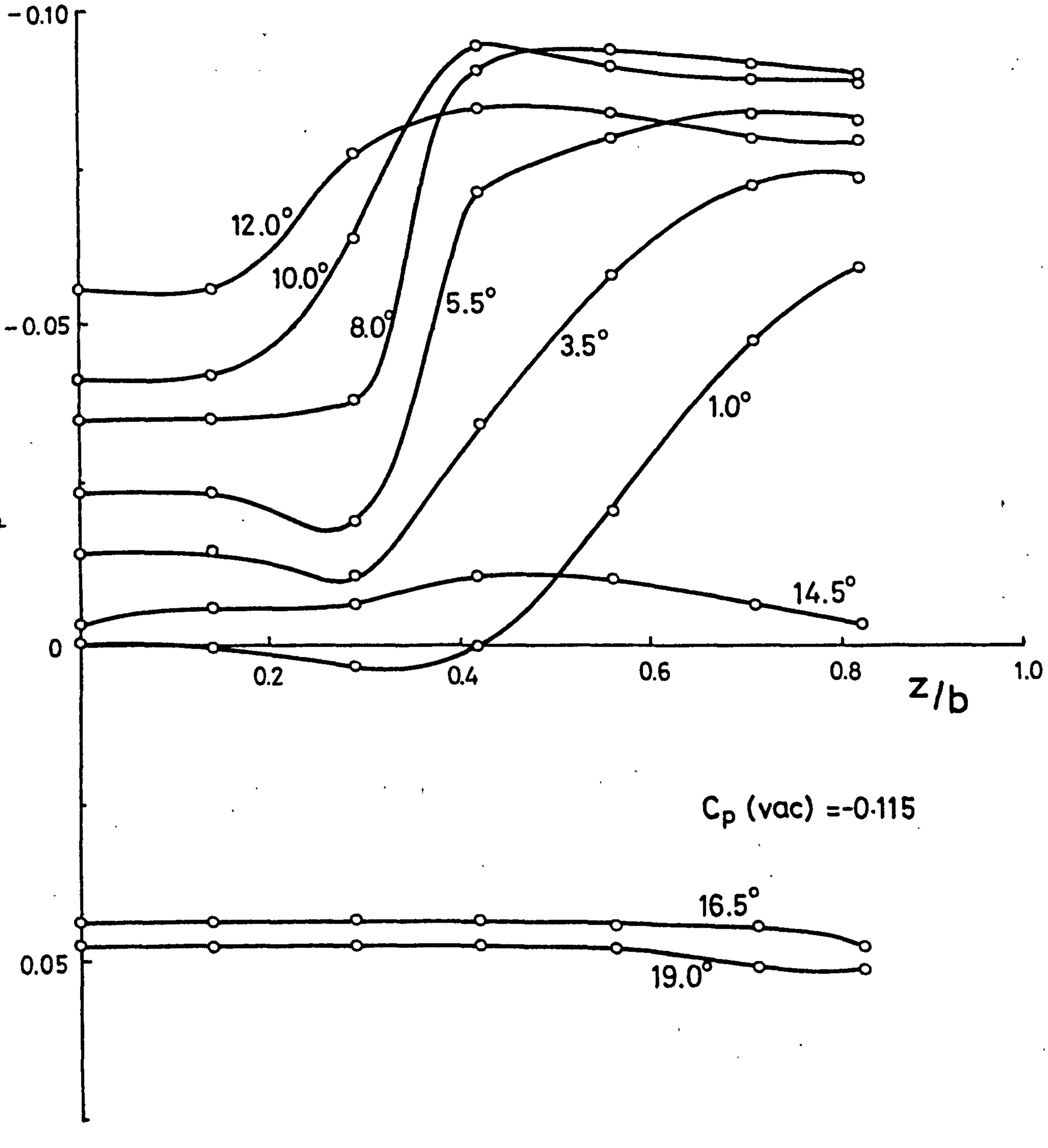

Fig.16. Model 3: Pressure distribution over the span at different angles of incidence.
(Lee-side = flat surface , $x/l = 0.55$, $M_o = 3.5$.)

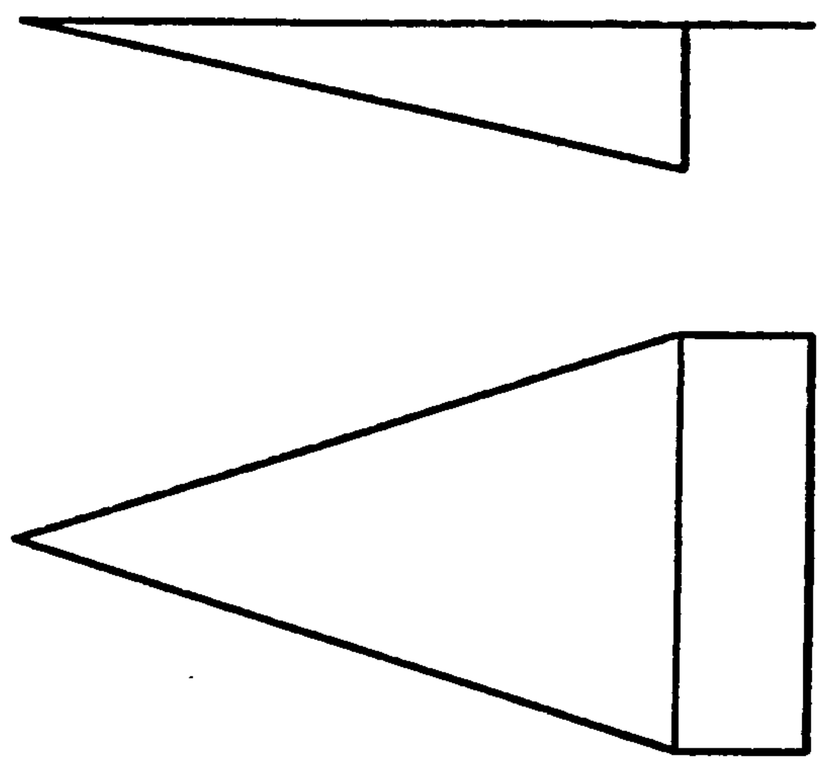

Flap

0°
20 % Chord

A

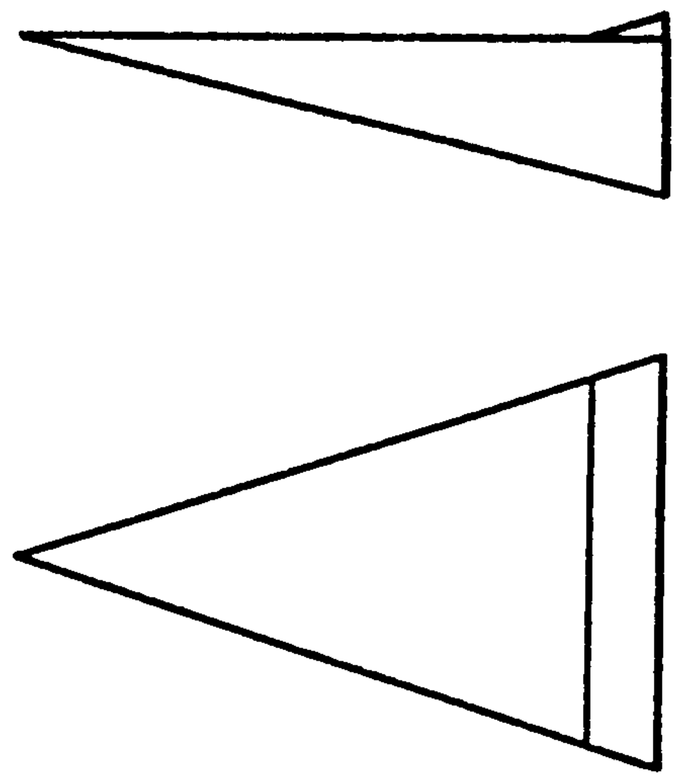

Flap

20°
10 % Chord

B

C

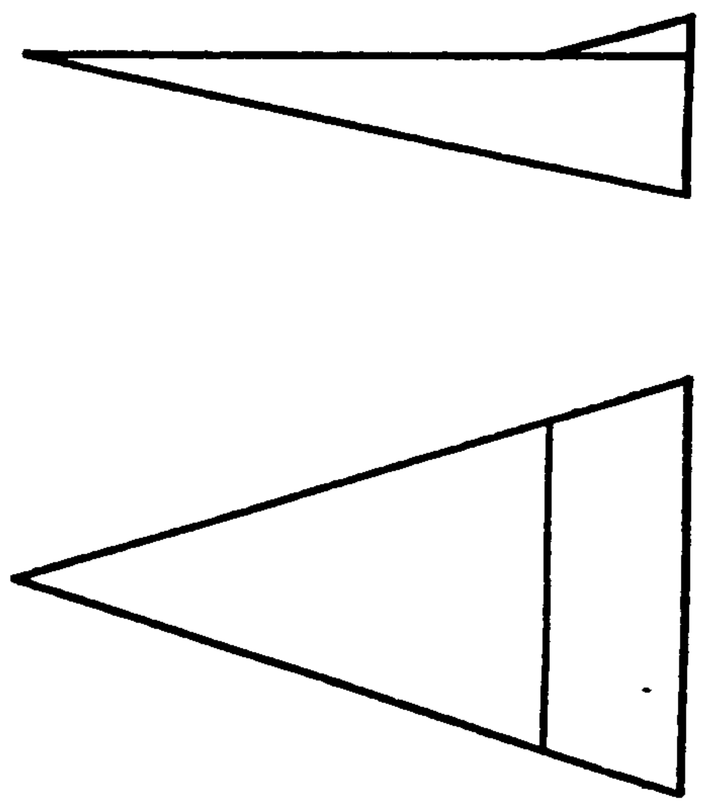

Flap

20°
20 % Chord

D

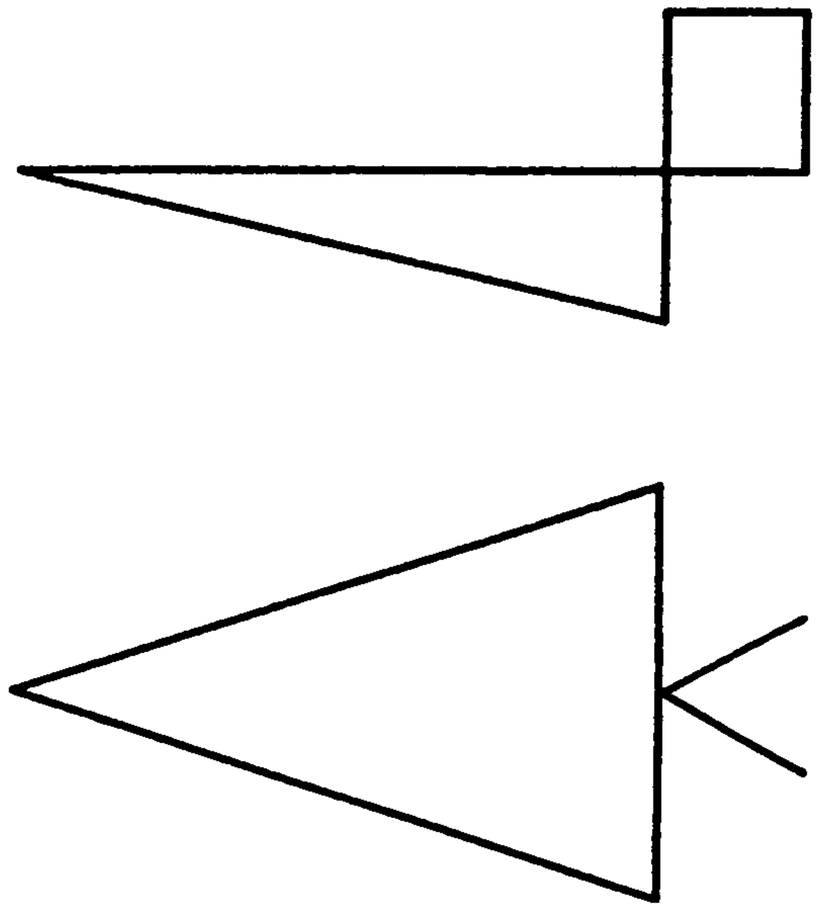

Wedge

Fig. 17. Attempts to promote leeside pressure rise.

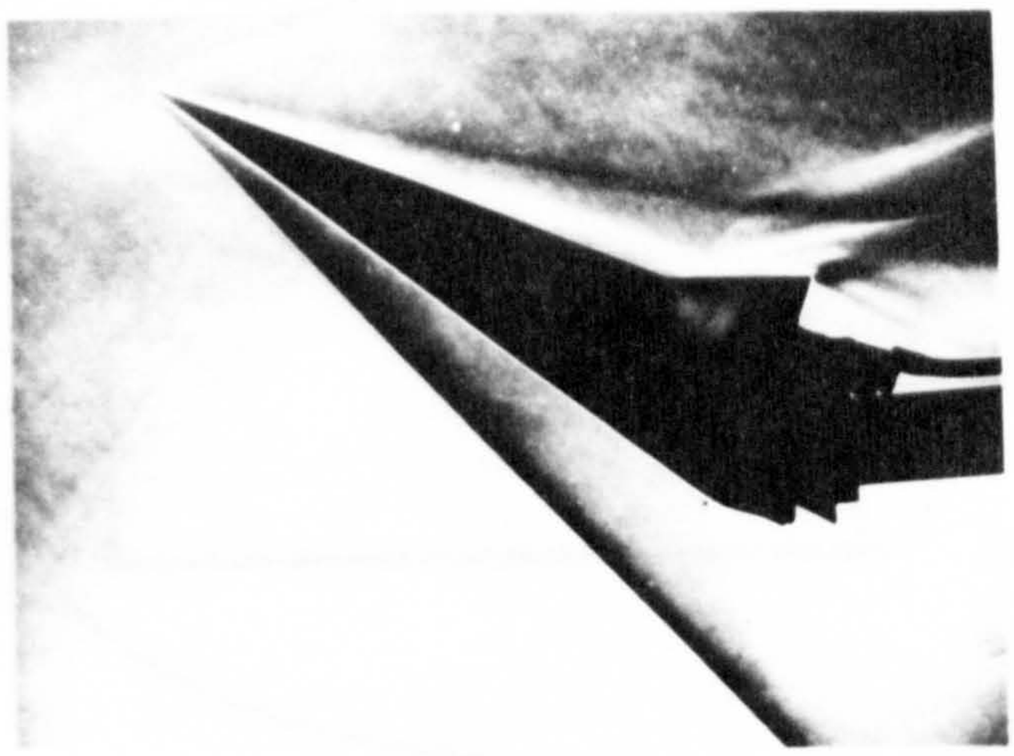

Fig. 18. Model with 20°, 20% chord flap showing separated flow in compression corner.
$\alpha = 20^\circ$

Fig. 19. Model with wedge in wake.
$\alpha = 25^\circ$

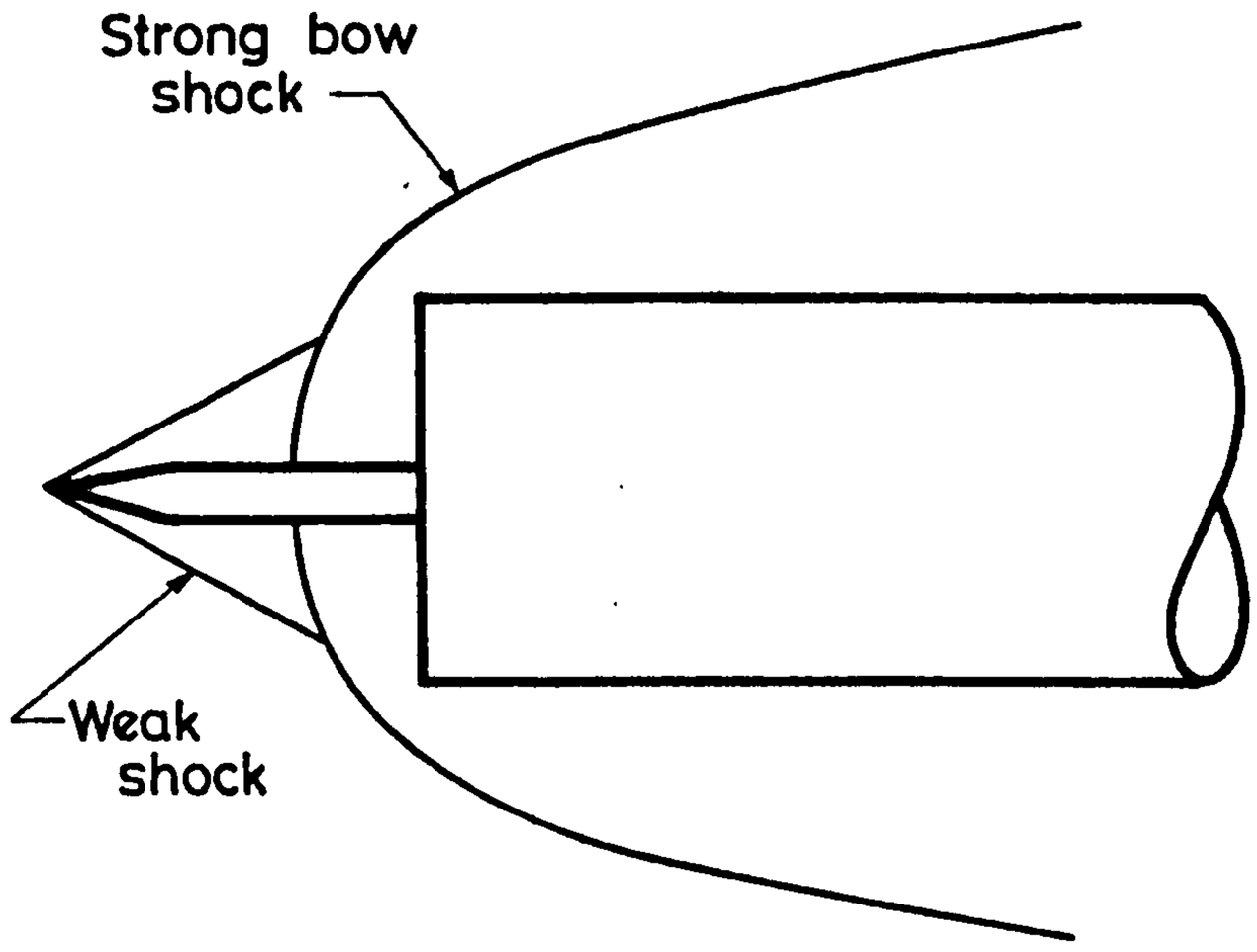

(a.)

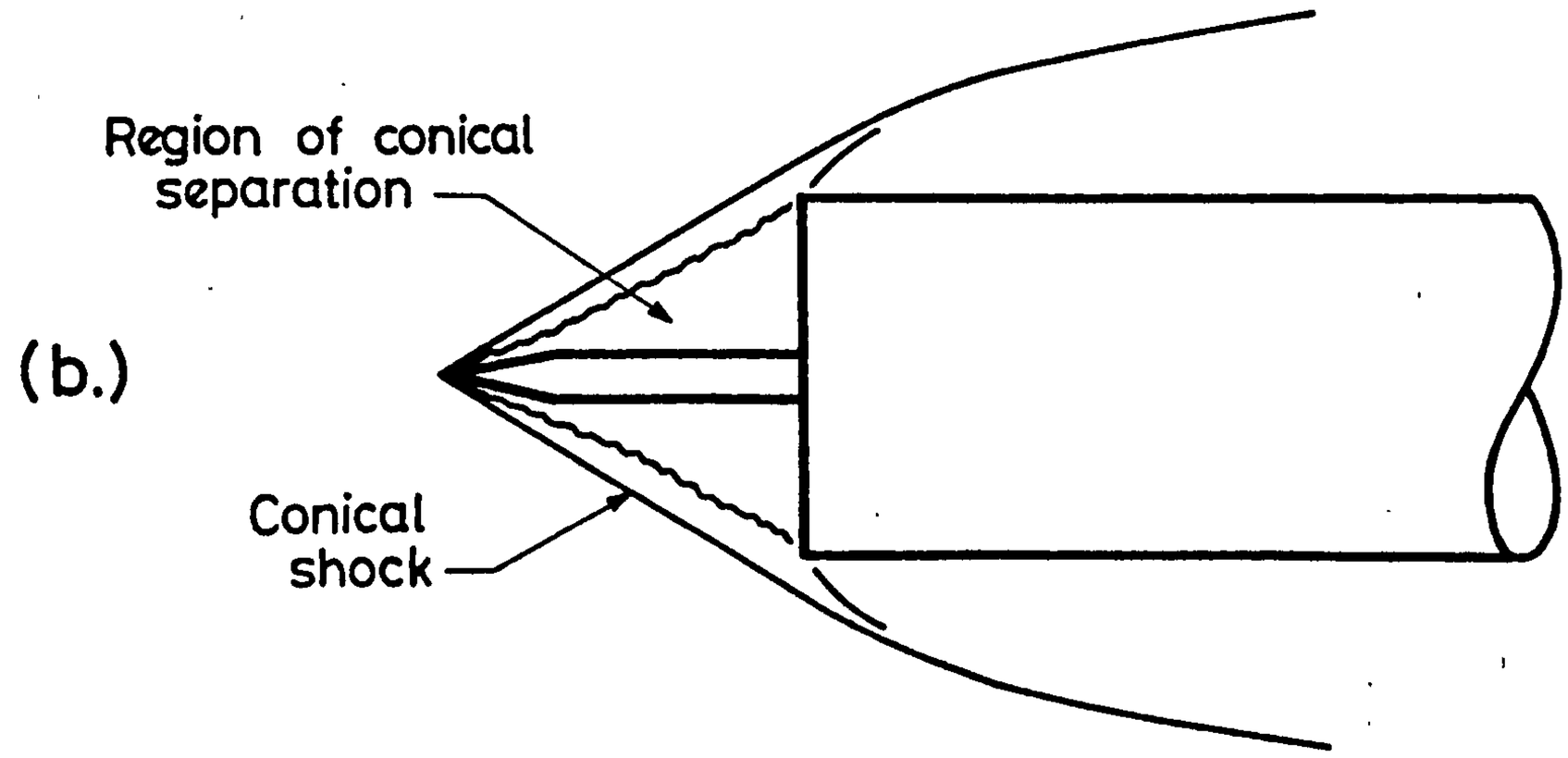

(b.)

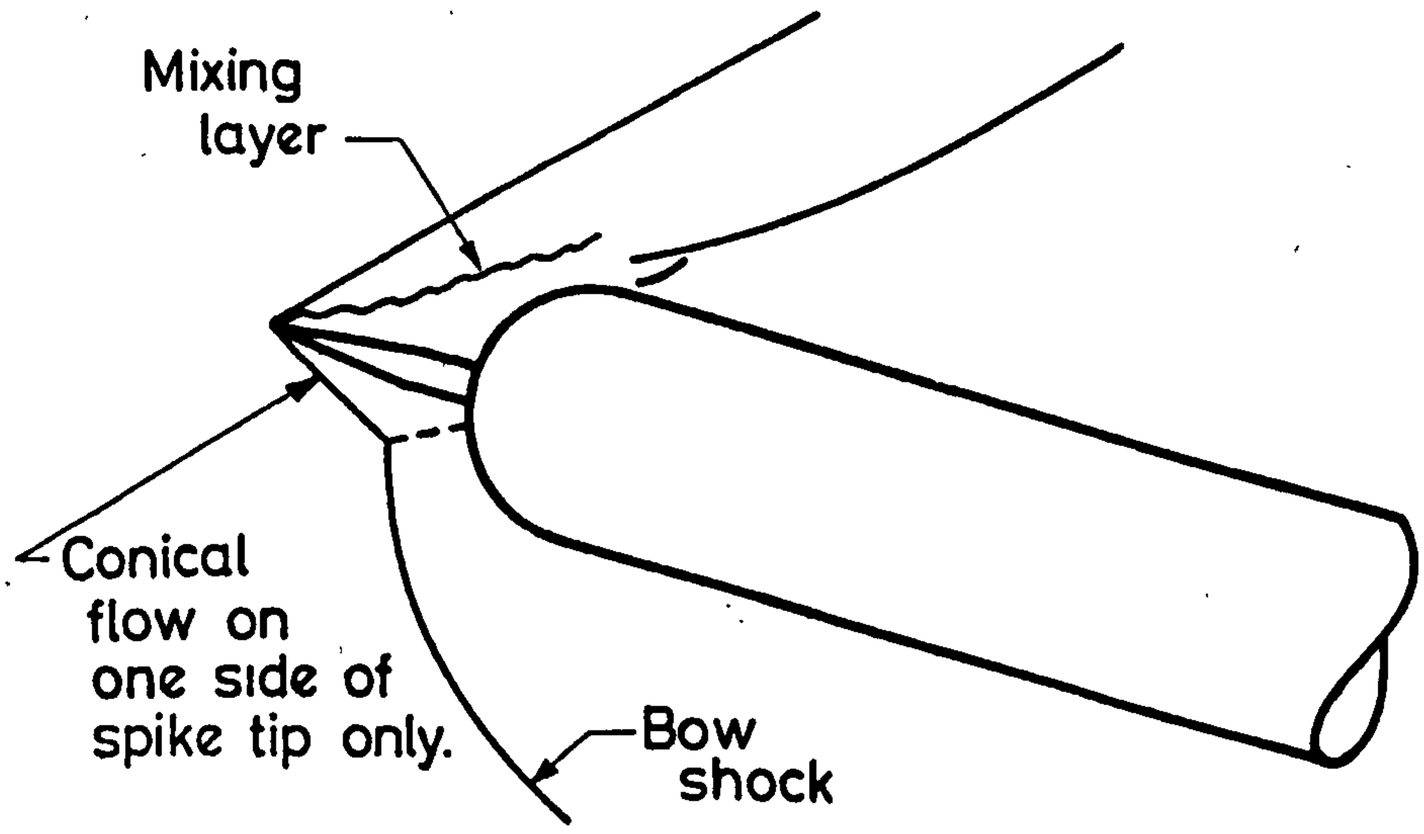

(c.)

Fig. 20. Conical separation.

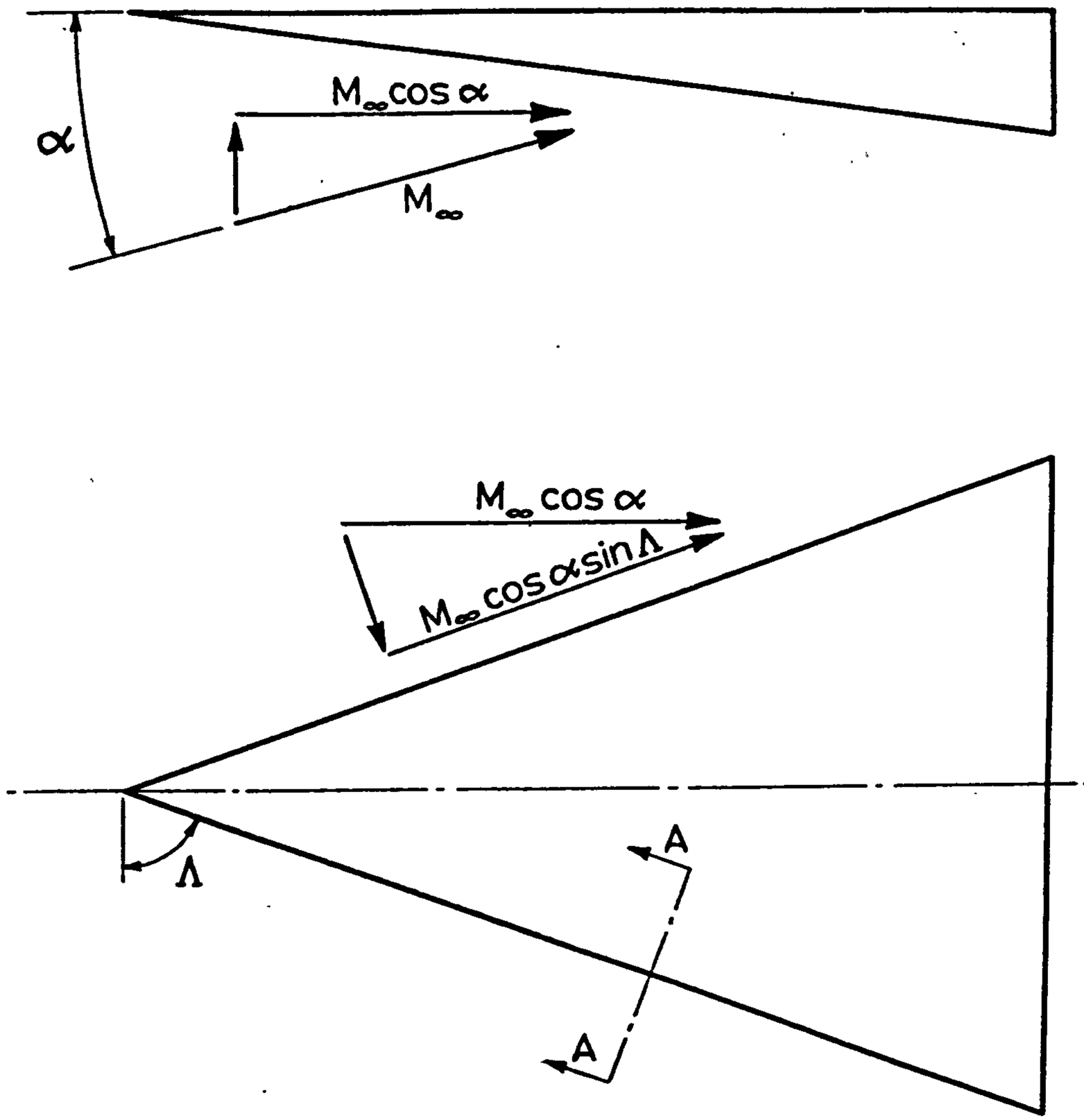

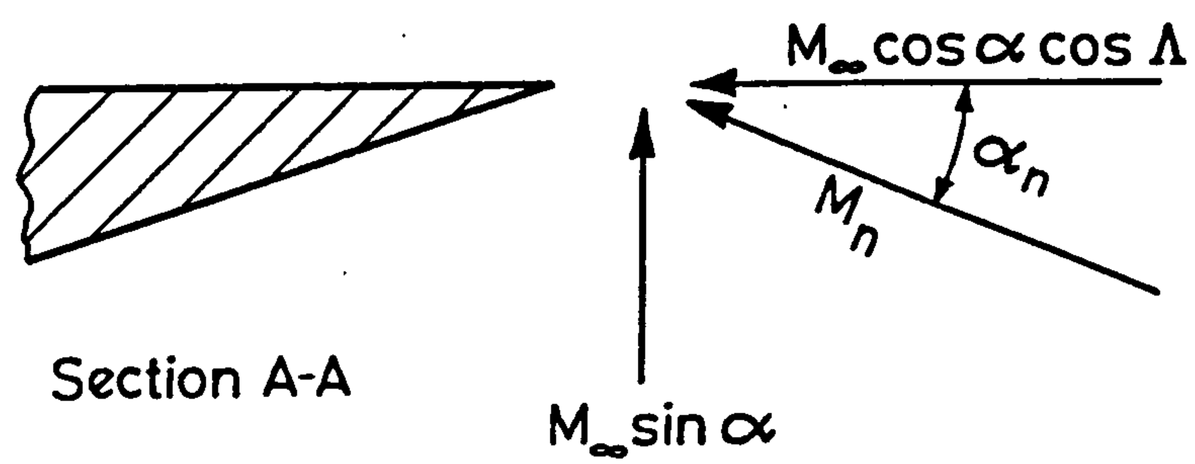

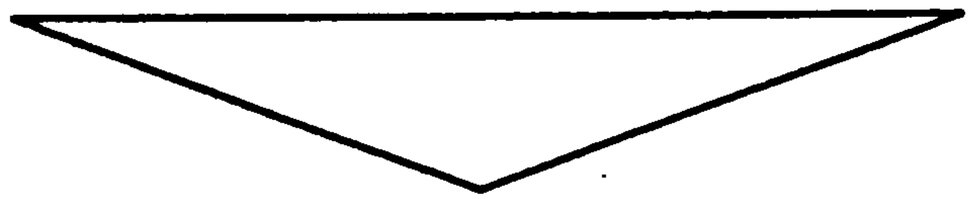

$$M_n = M_\infty (1 - \sin^2 \Lambda . \cos^2 \alpha)^{1/2}$$

$$\alpha_n = \tan^{-1} \frac{\tan \alpha}{\cos \Lambda}$$

Fig. 21. Construction of effective Mach Number and incidence.

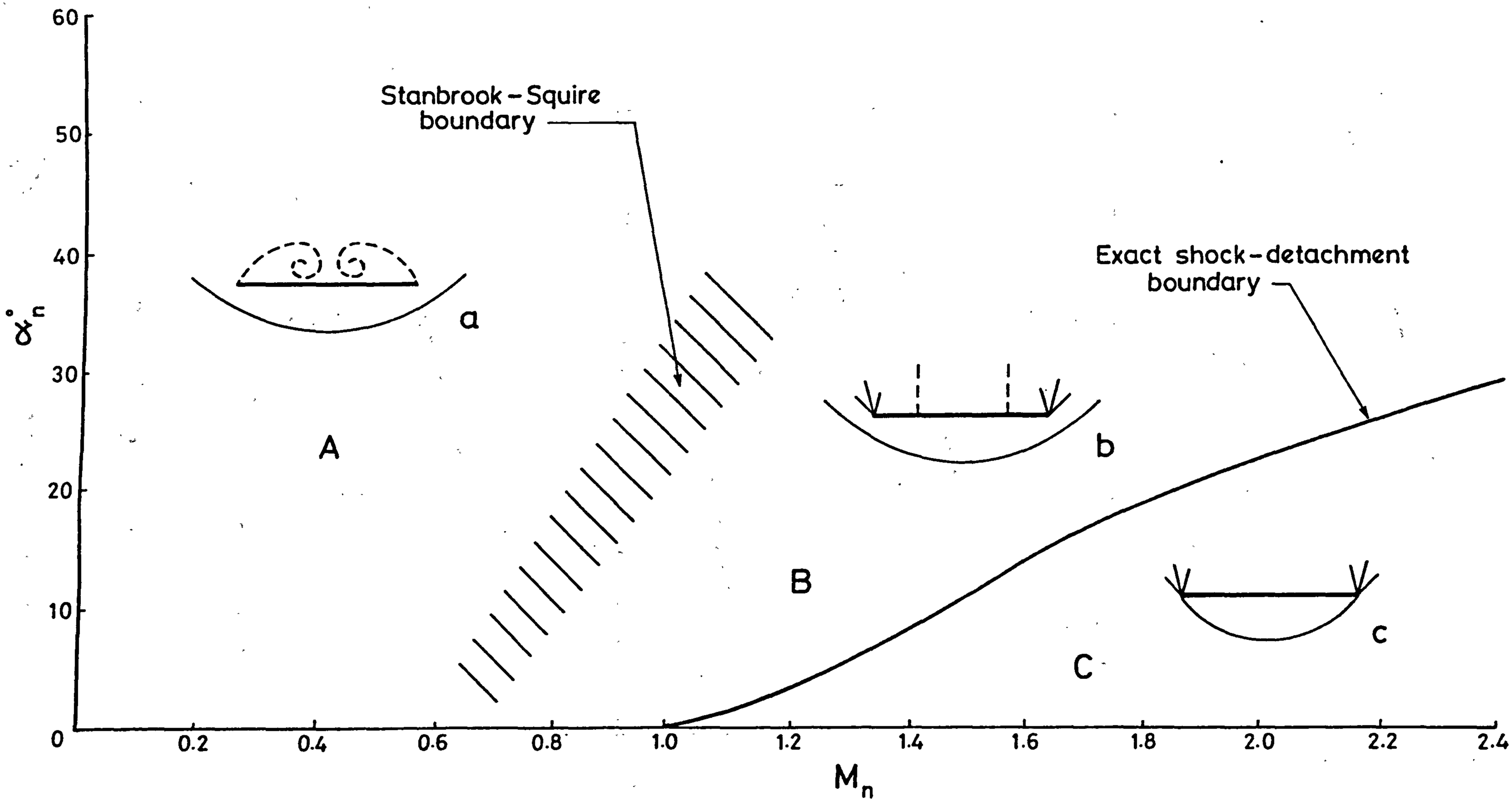

Fig. 22. Flow regimes on thin delta wings.

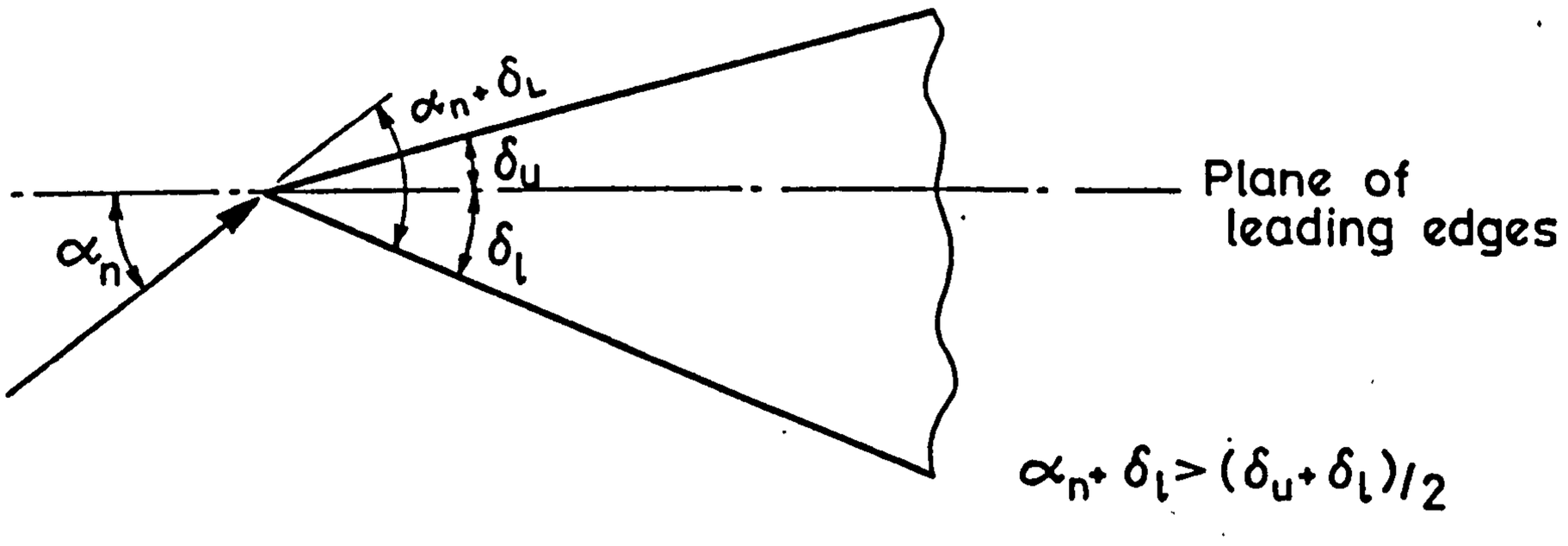

a. Lower surface controlling shock detachment.

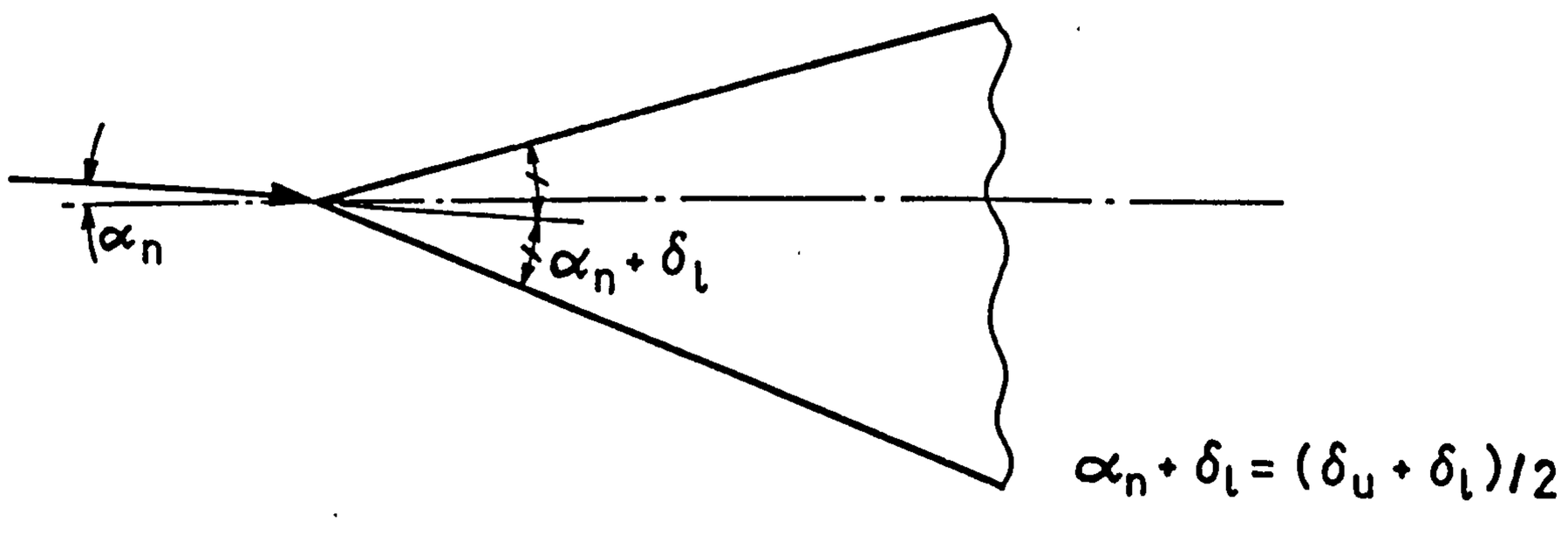

b. Minimum Mach number for shock attachment.

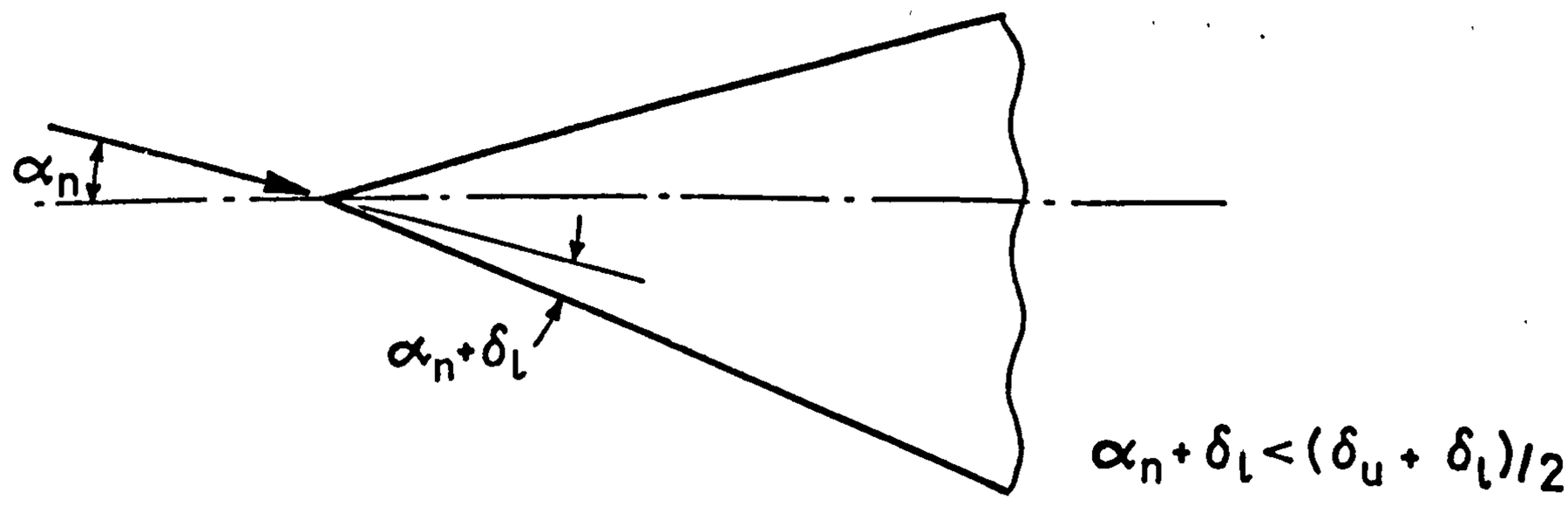

c. Upper surface controlling shock detachment.

Fig. 23. The effect of thickness on shock detachment.
(Sections normal to leading edge)

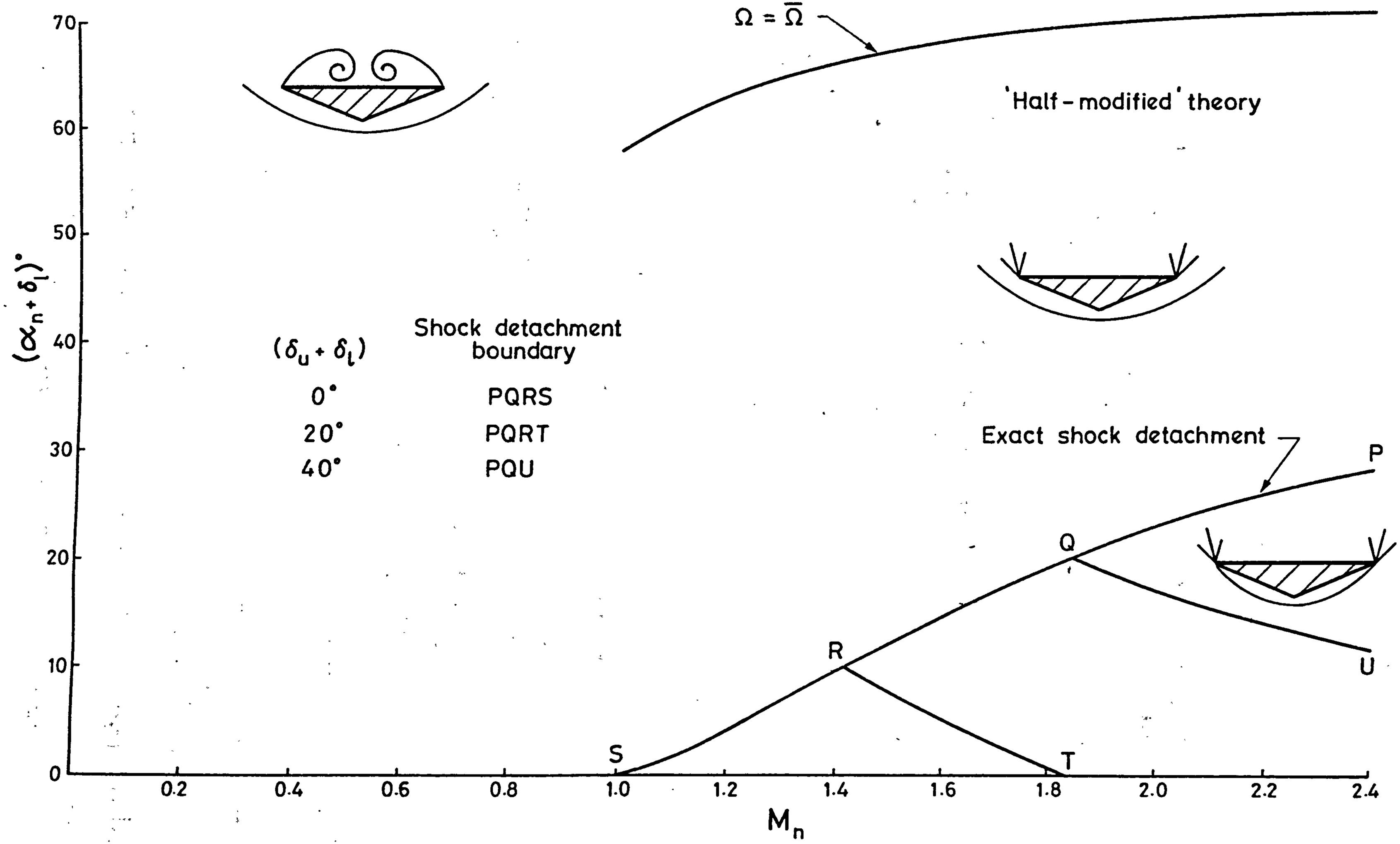

Fig. 24. Flow regimes on wings of finite thickness.

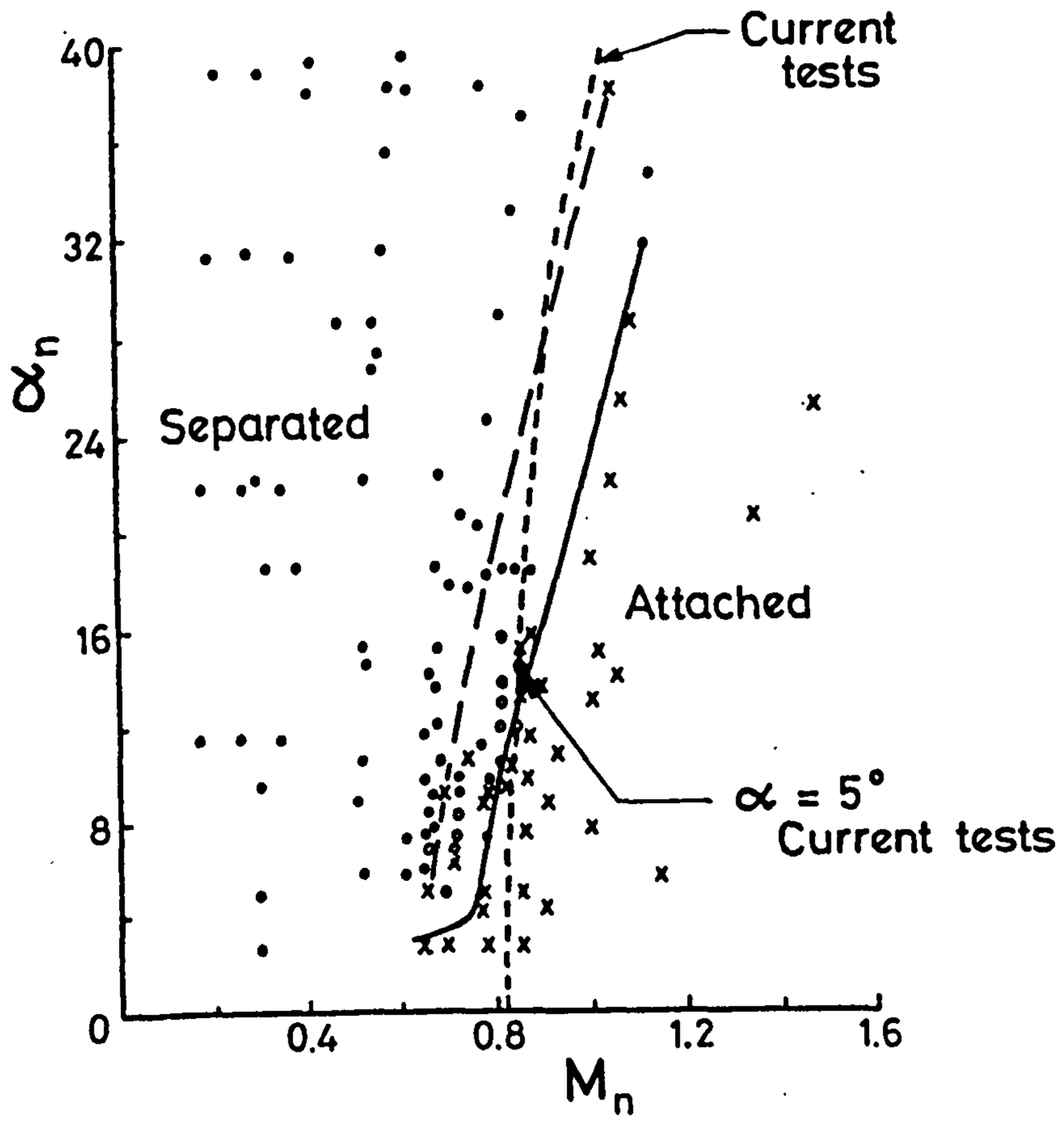

Wings with sharp leading-edges

Wings with rounded leading-edges.

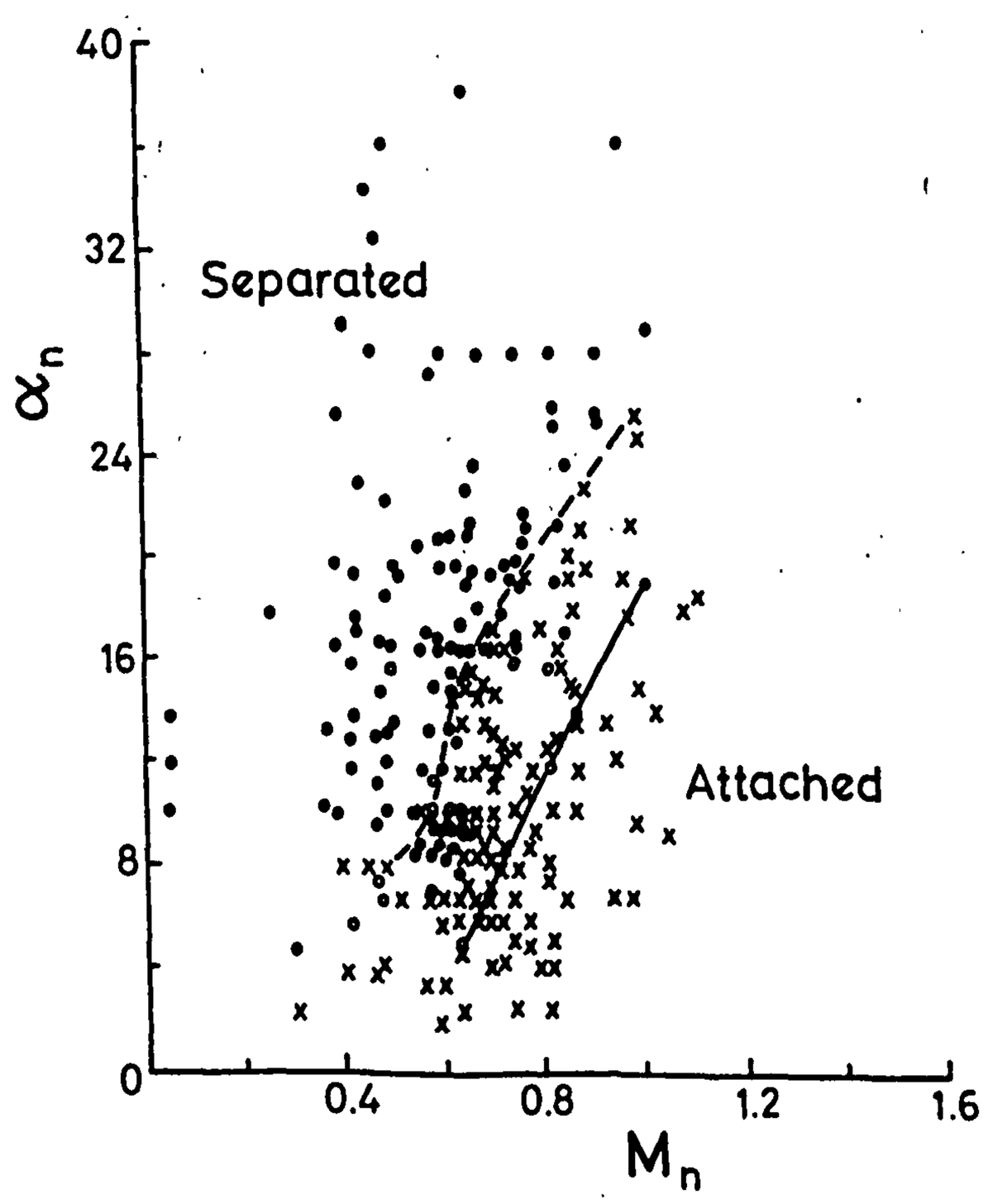

Fig. 25. The experimental boundary between regimes of attached and separated leeside flow. (after Stanbrook and Squire)

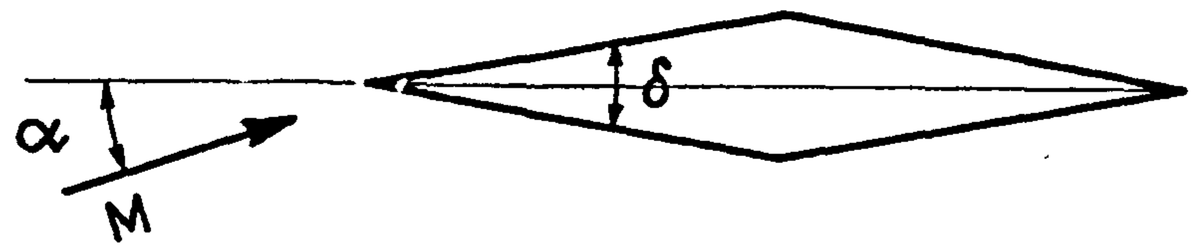

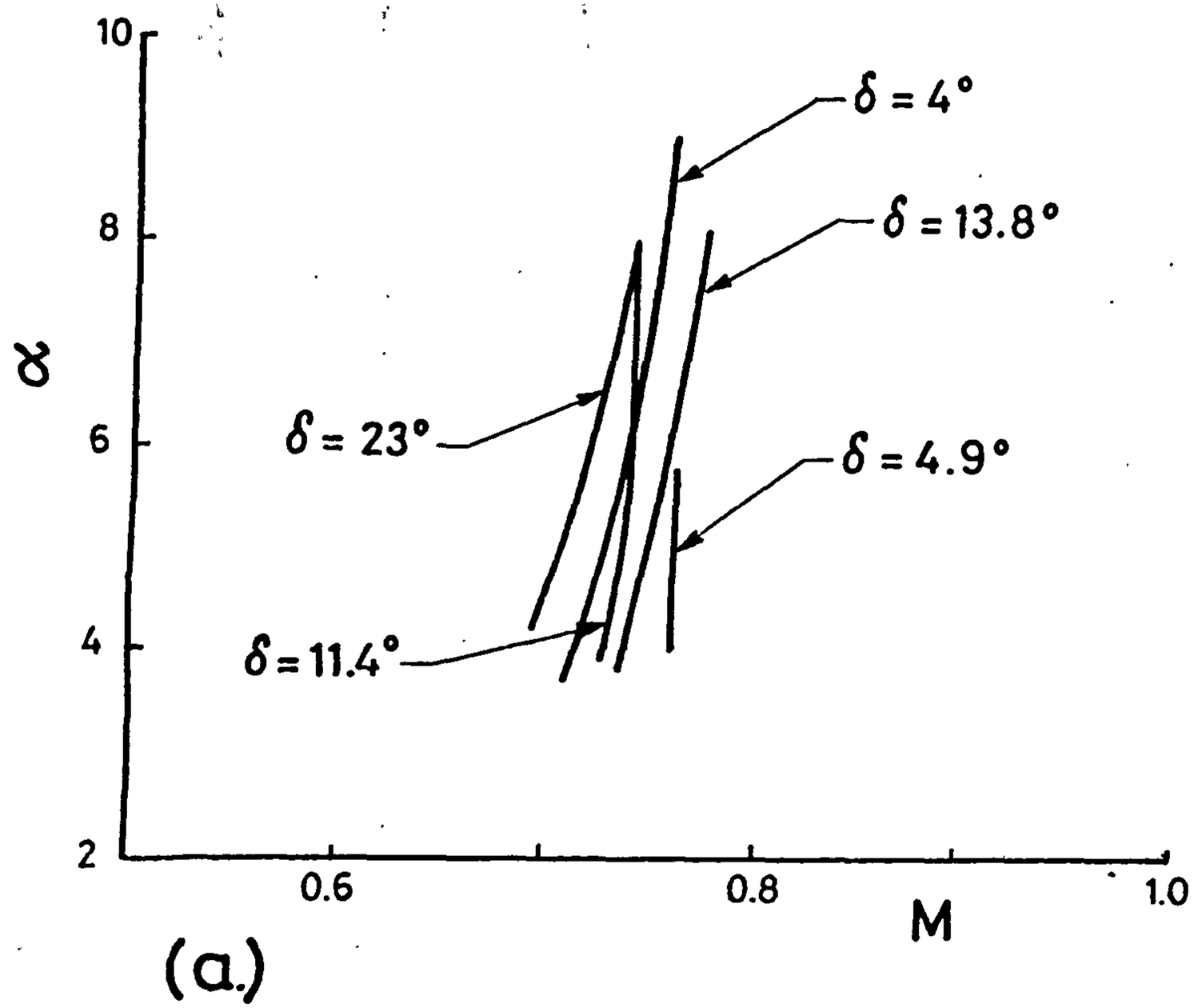

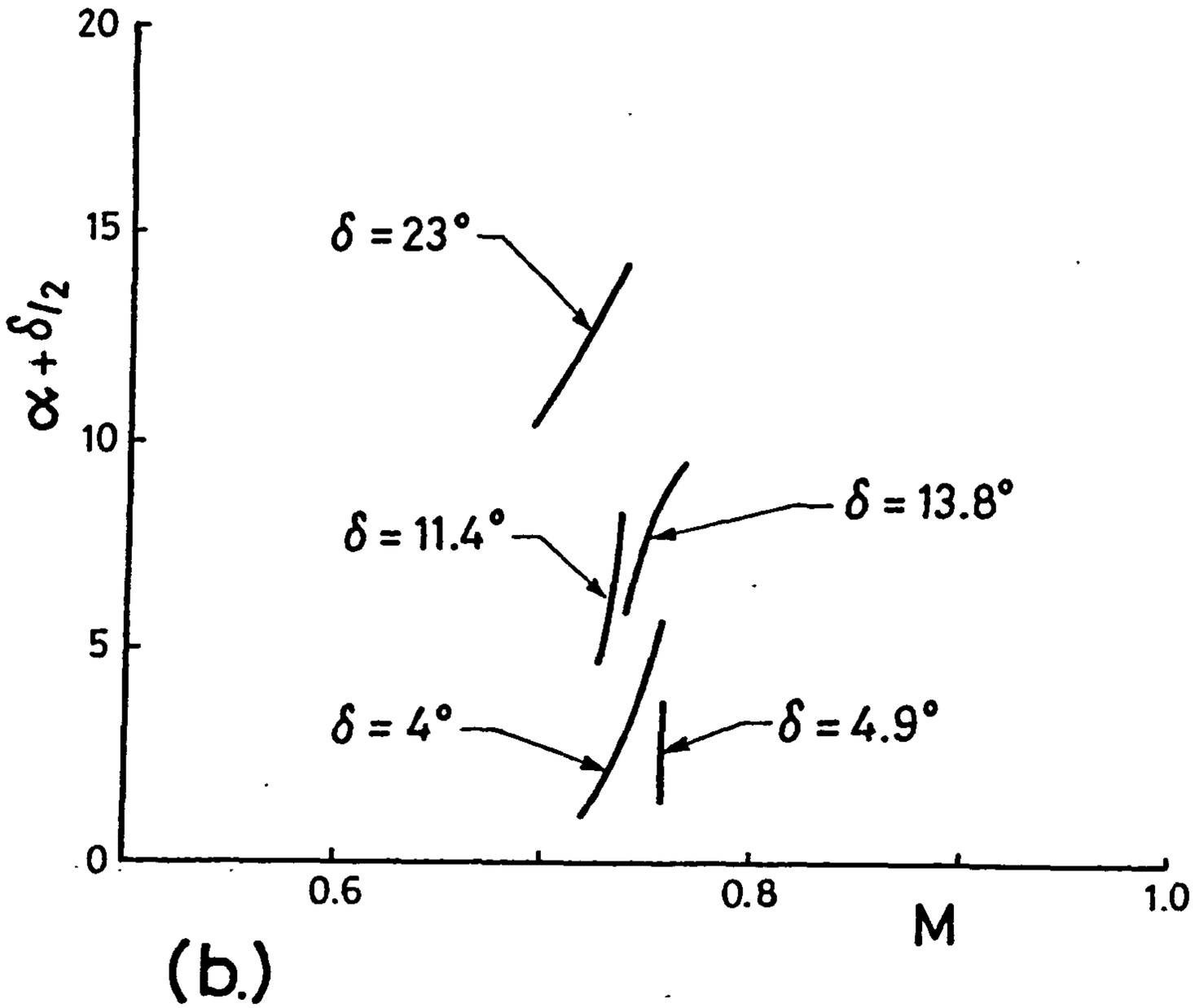

Fig. 26. Separation boundaries for symmetrical two-dimensional aerofoils.

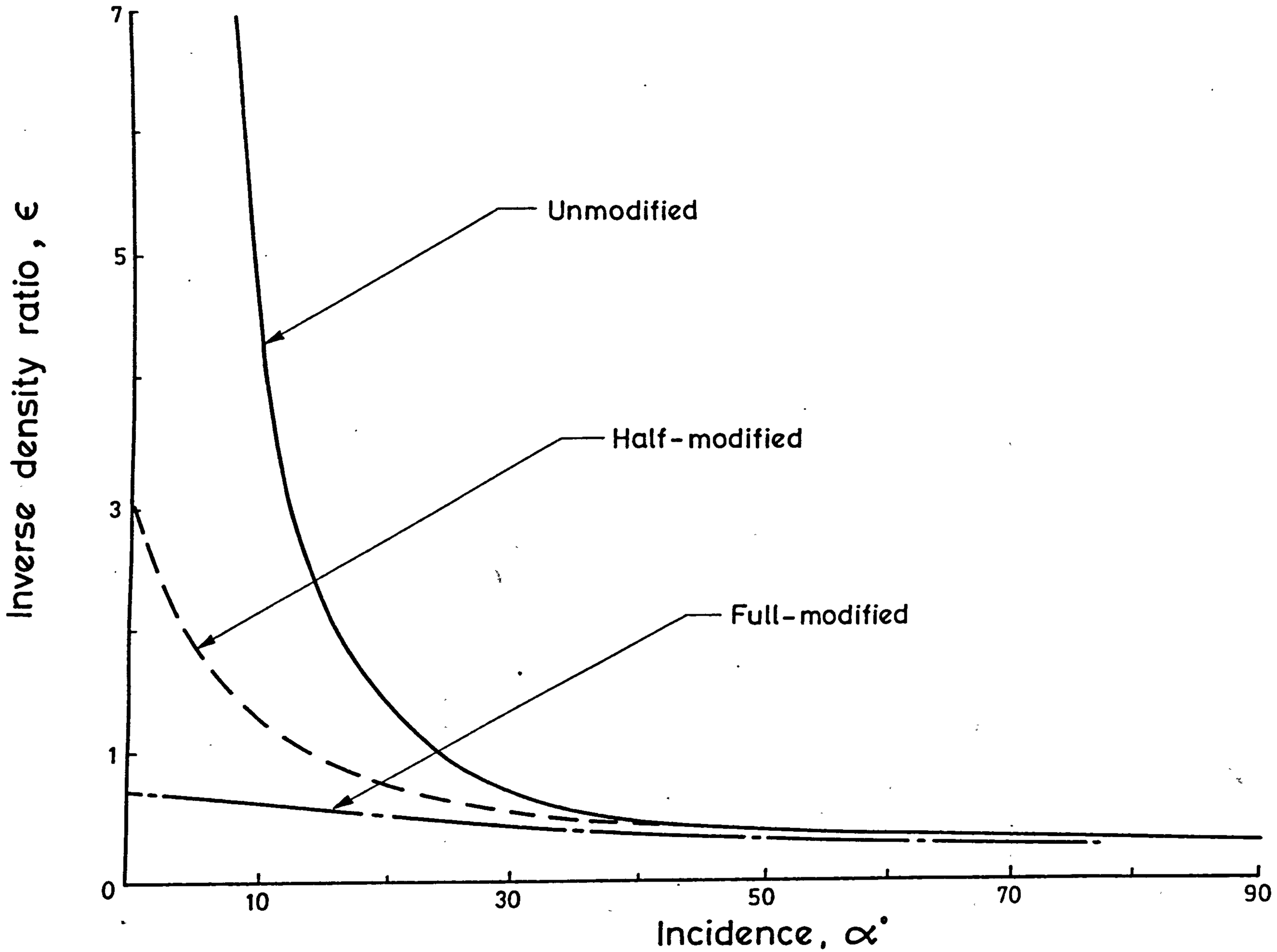

Fig. 27. Inverse density ratio (ϵ) with incidence

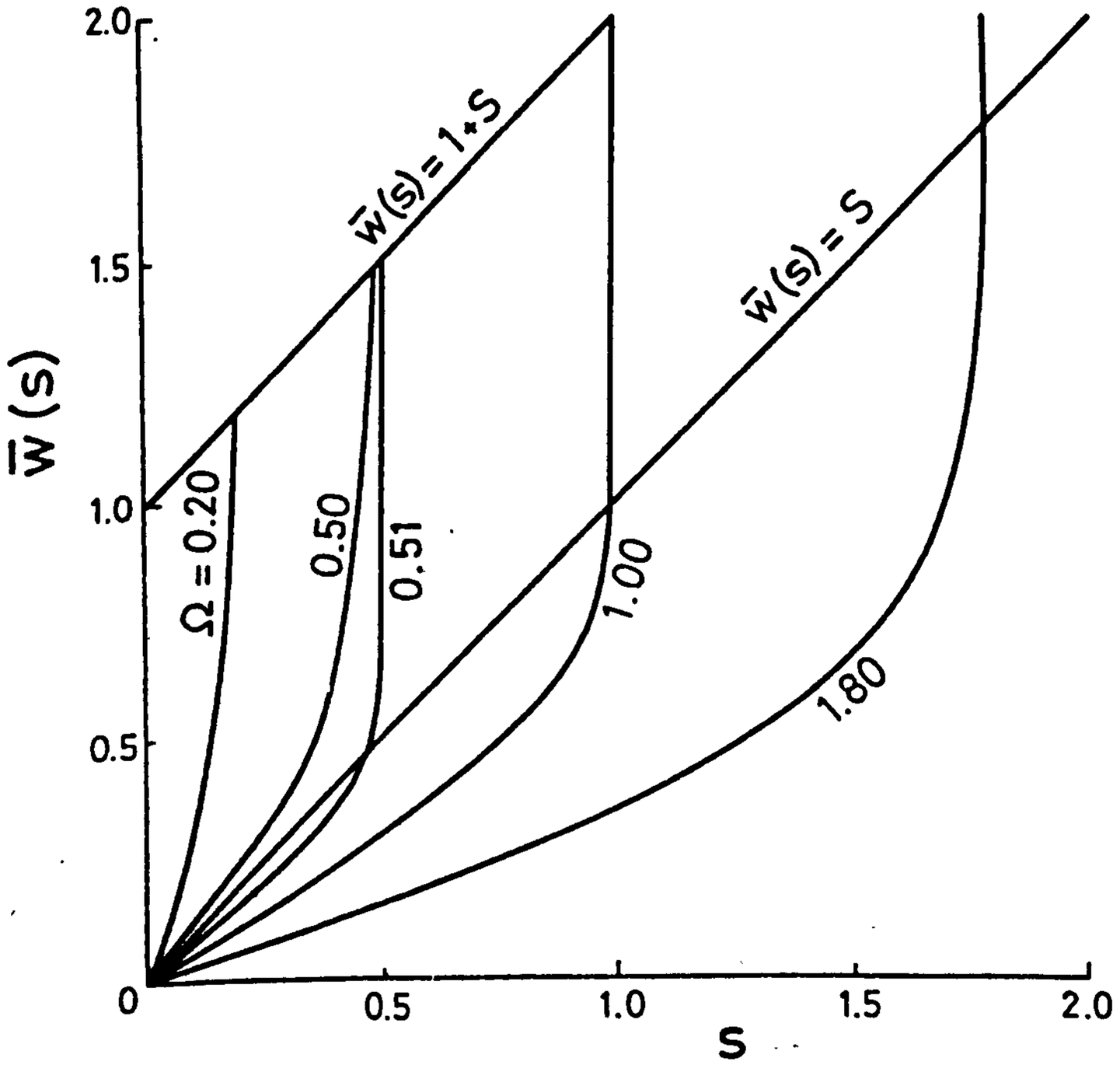

c. Solutions for cross-flow.

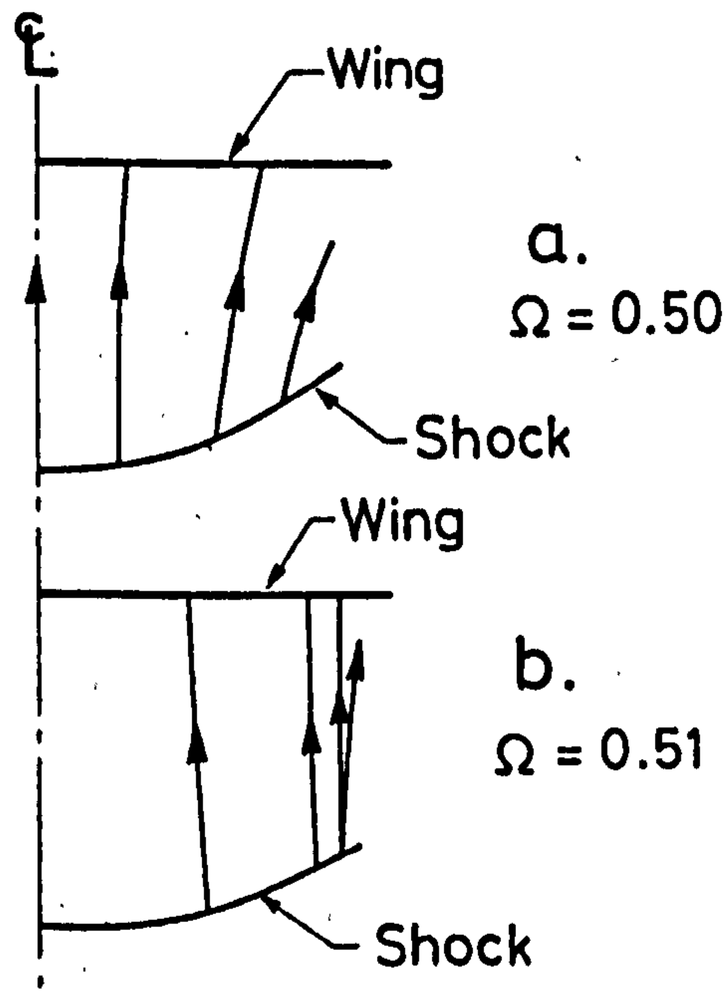

Shock shapes and projected streamlines

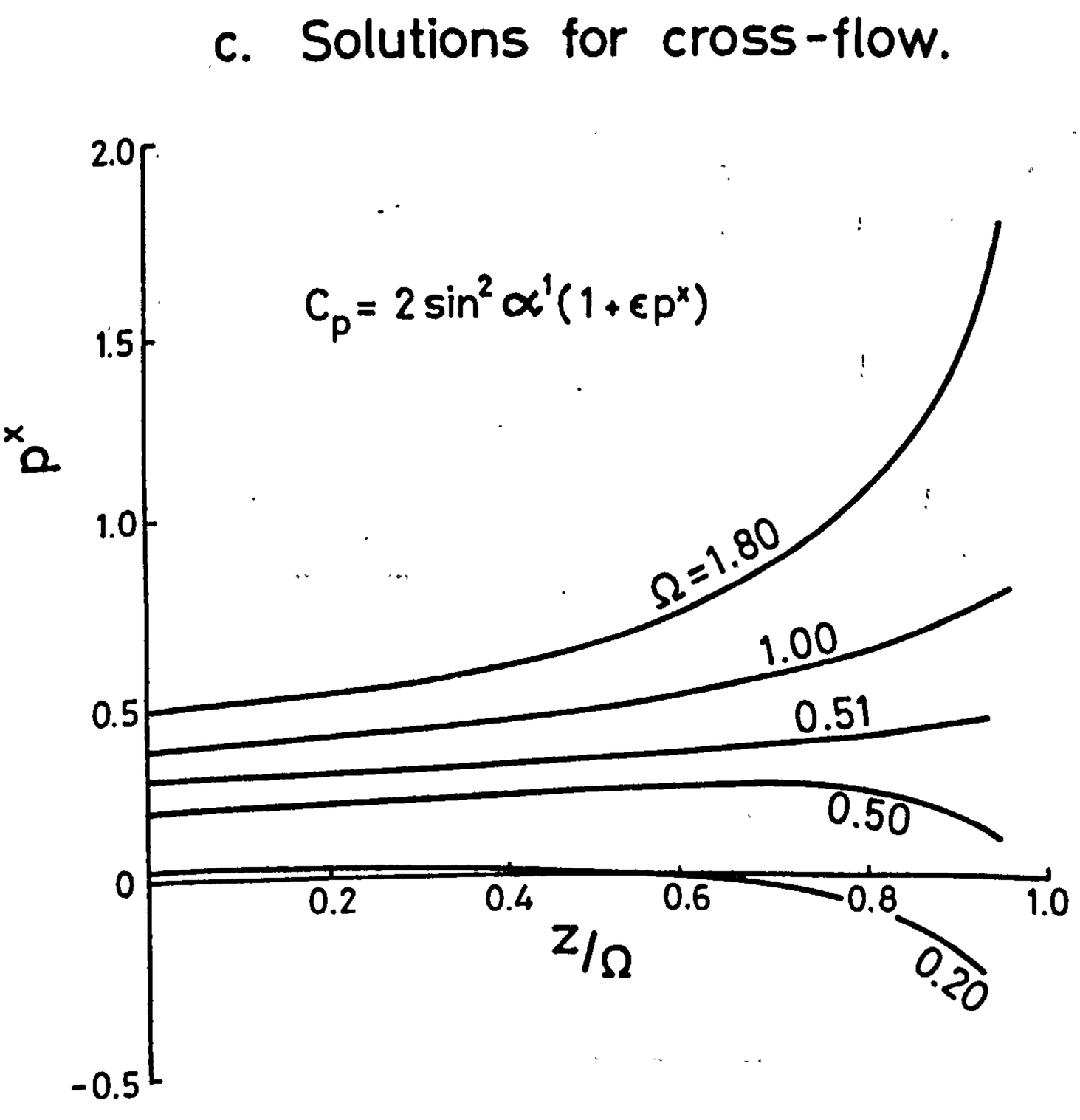

d. Calculated pressure.

Fig. 28. Predictions of Shanbhag's theory for thin wings. (after Squire)

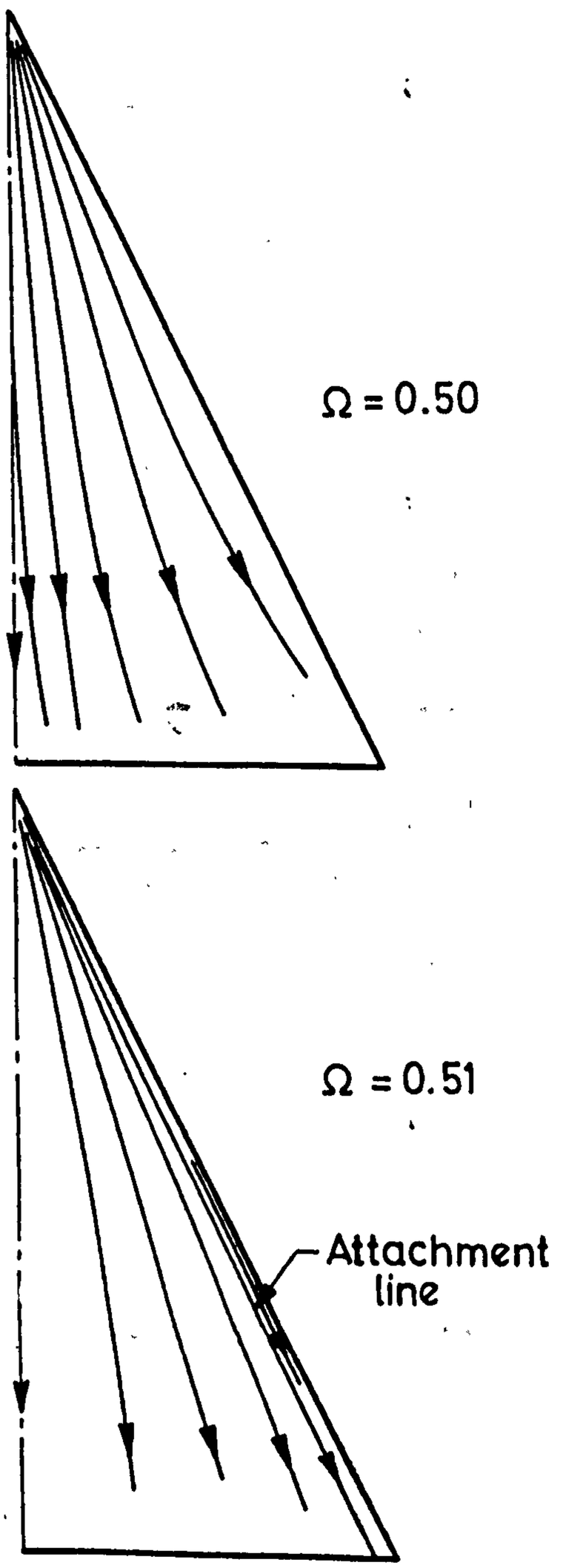

Surface streamlines.

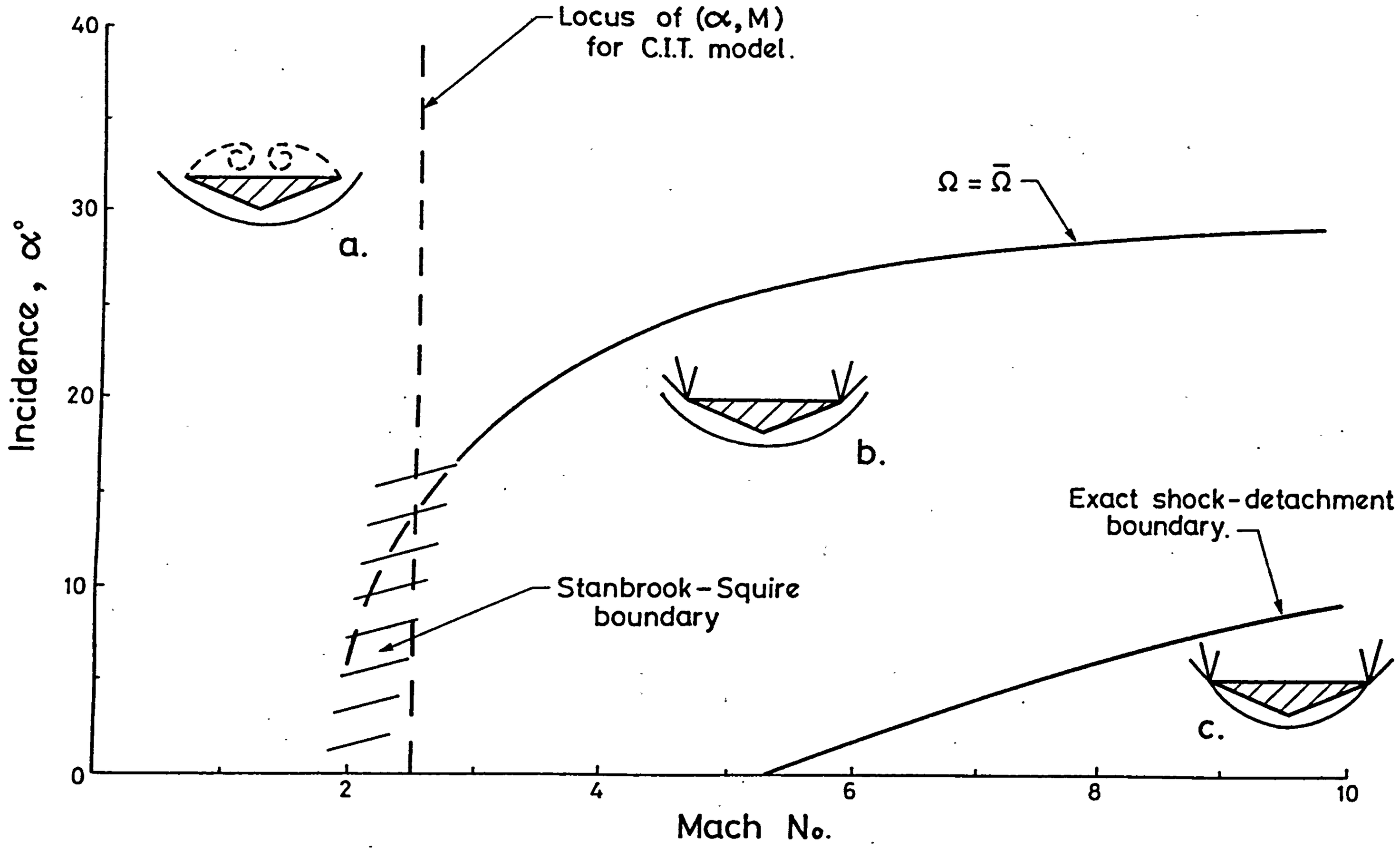

Fig. 29. Predictions of the 'half-modified' theory for the model under investigation.

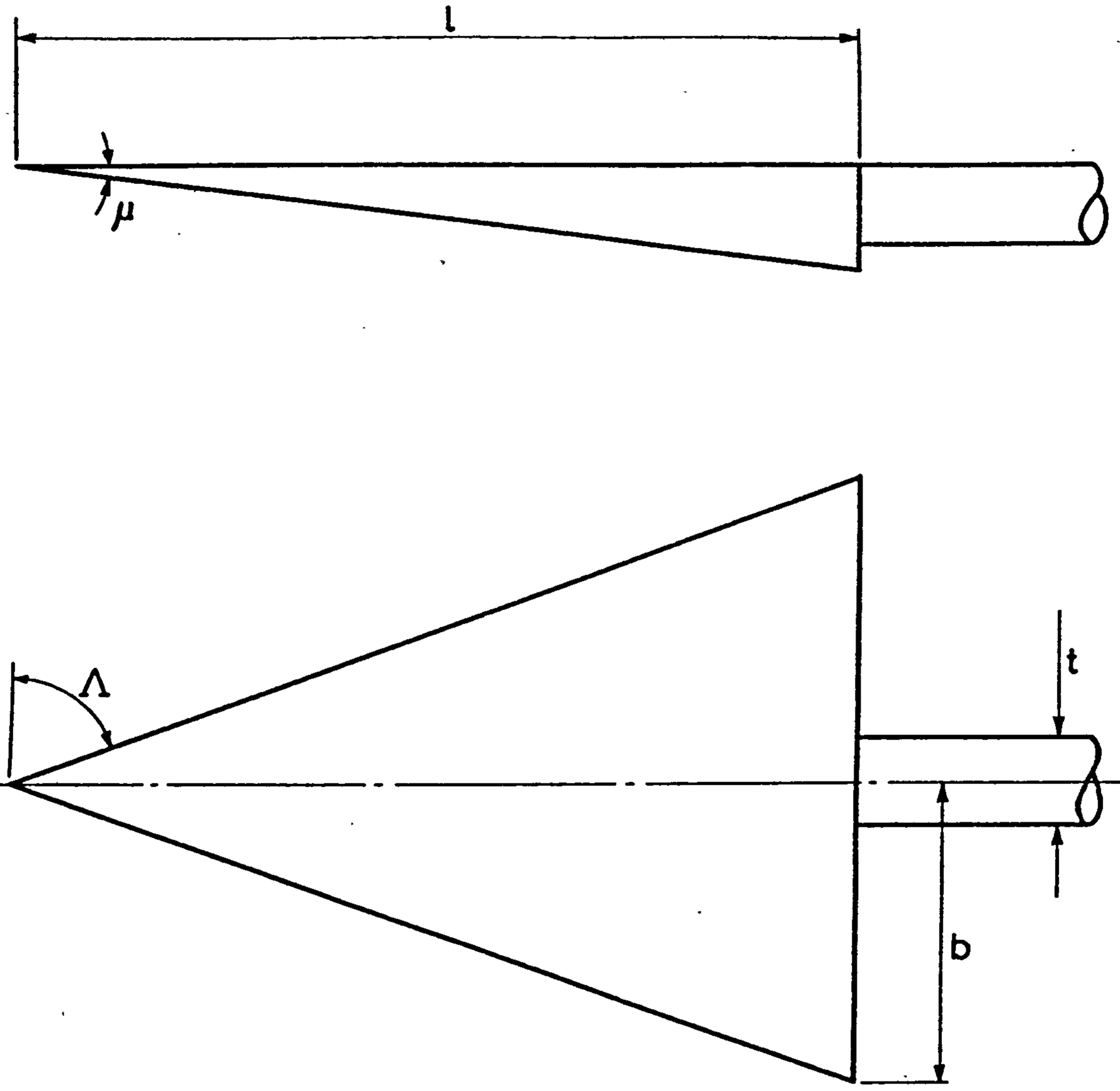

b = 36.4 mm.
h = 13.2 mm
l = 100 mm
t = 10.0 mm
Λ = 70.0°
ψ = 20.0°
μ = 7.5°

Aspect ratio = 1.46

Fig.30. Dimensions of the delta wing models.

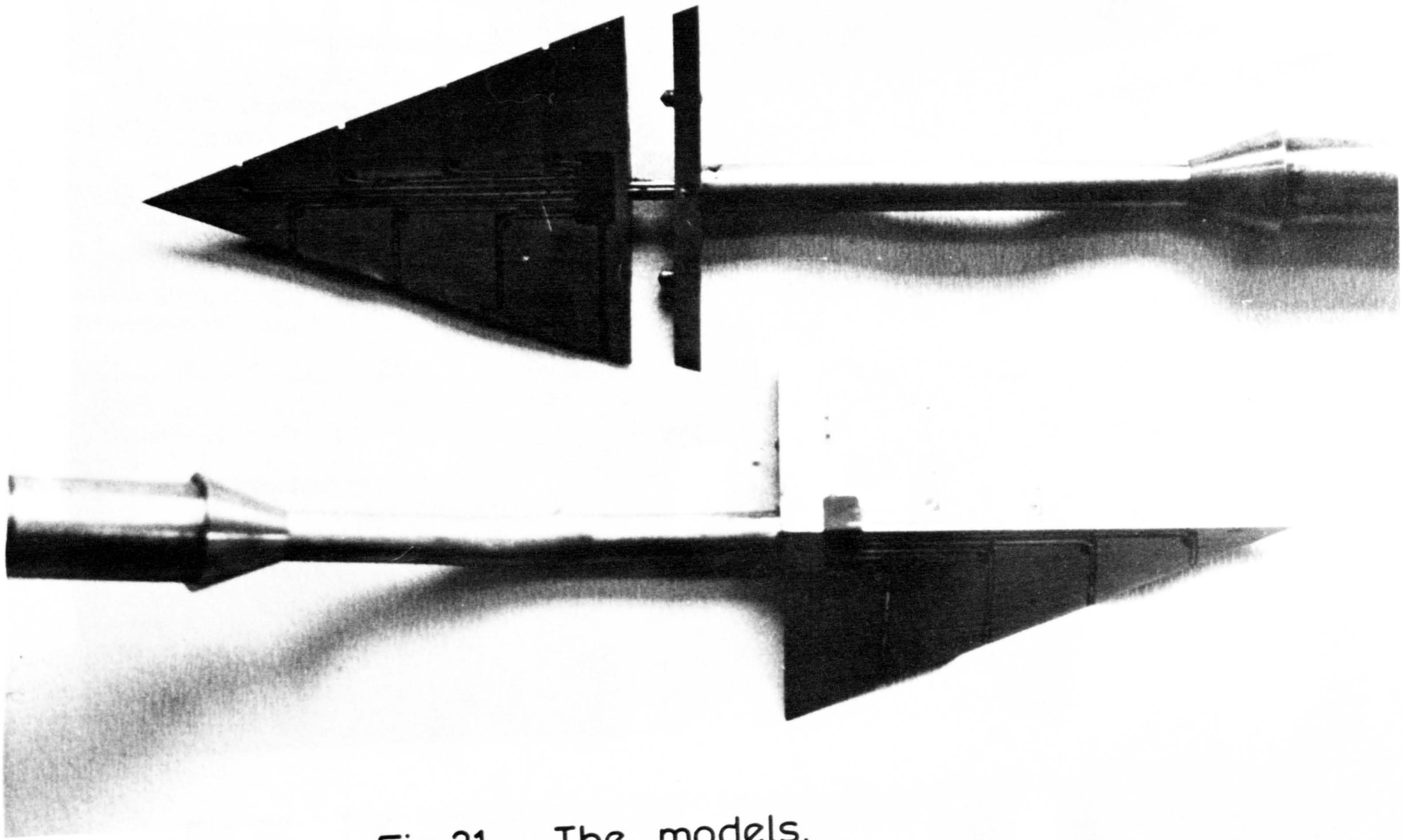

Fig.31. The models.

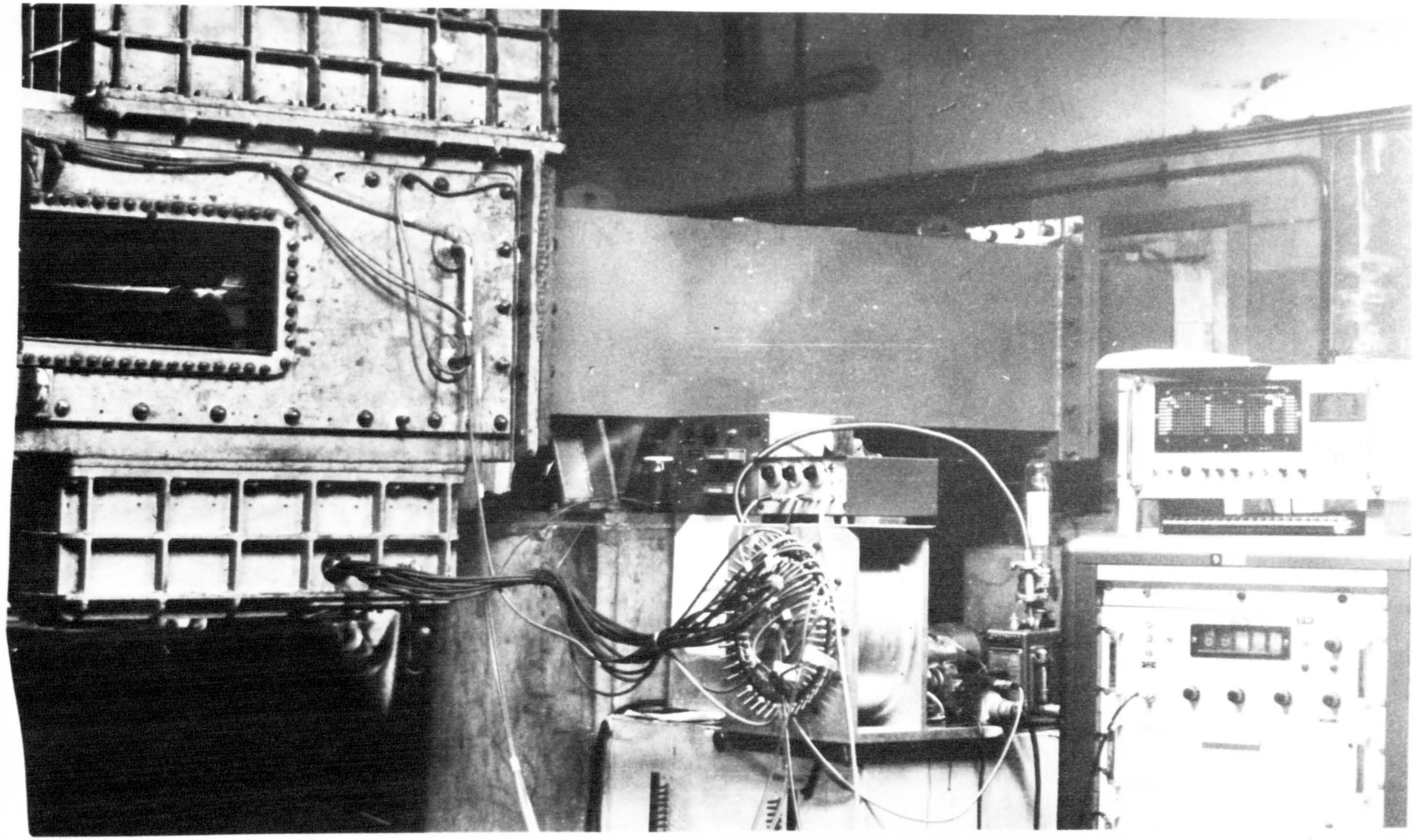

Fig. 32. The working section and pressure scanning switch.

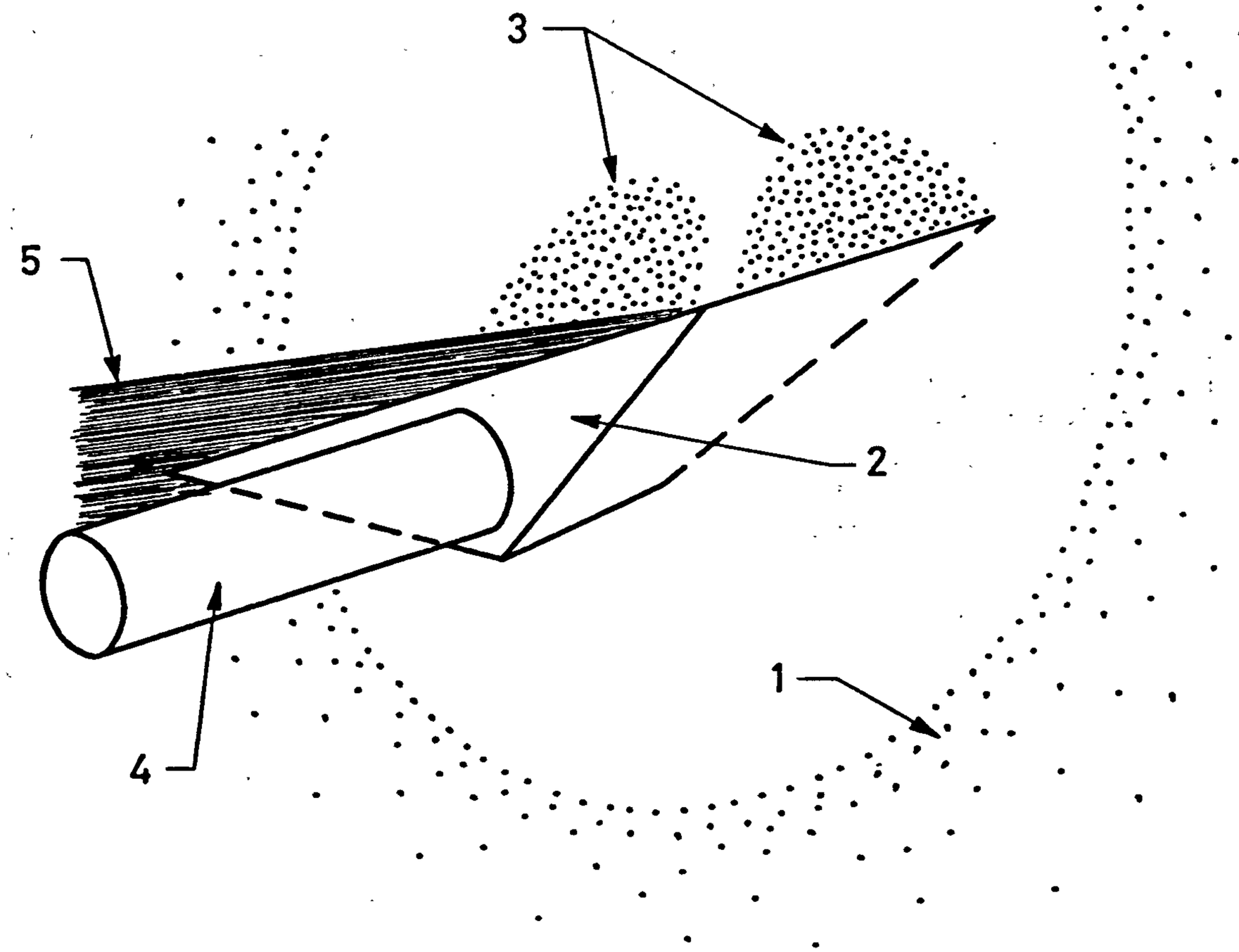

1 Envelope of tip shock
2 Base of model
3 Leeside vortices
4 Model support
5 Shadow of model

View from downstream.

Fig. 33. Vapour screen picture, showing major features.

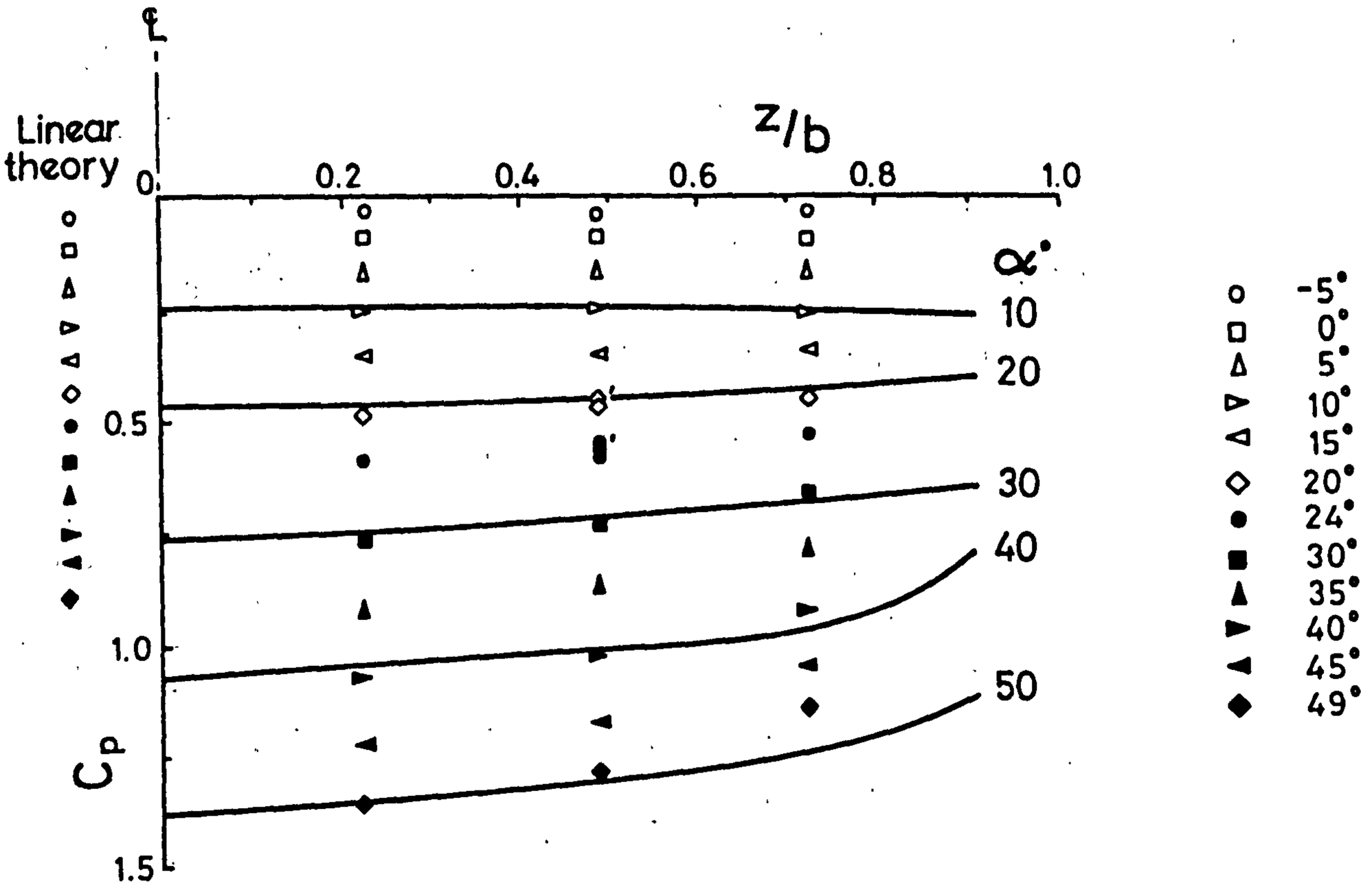

Fig. 34. Compression surface station 1.
(20 mm. from tip) $x/l = 0.2$

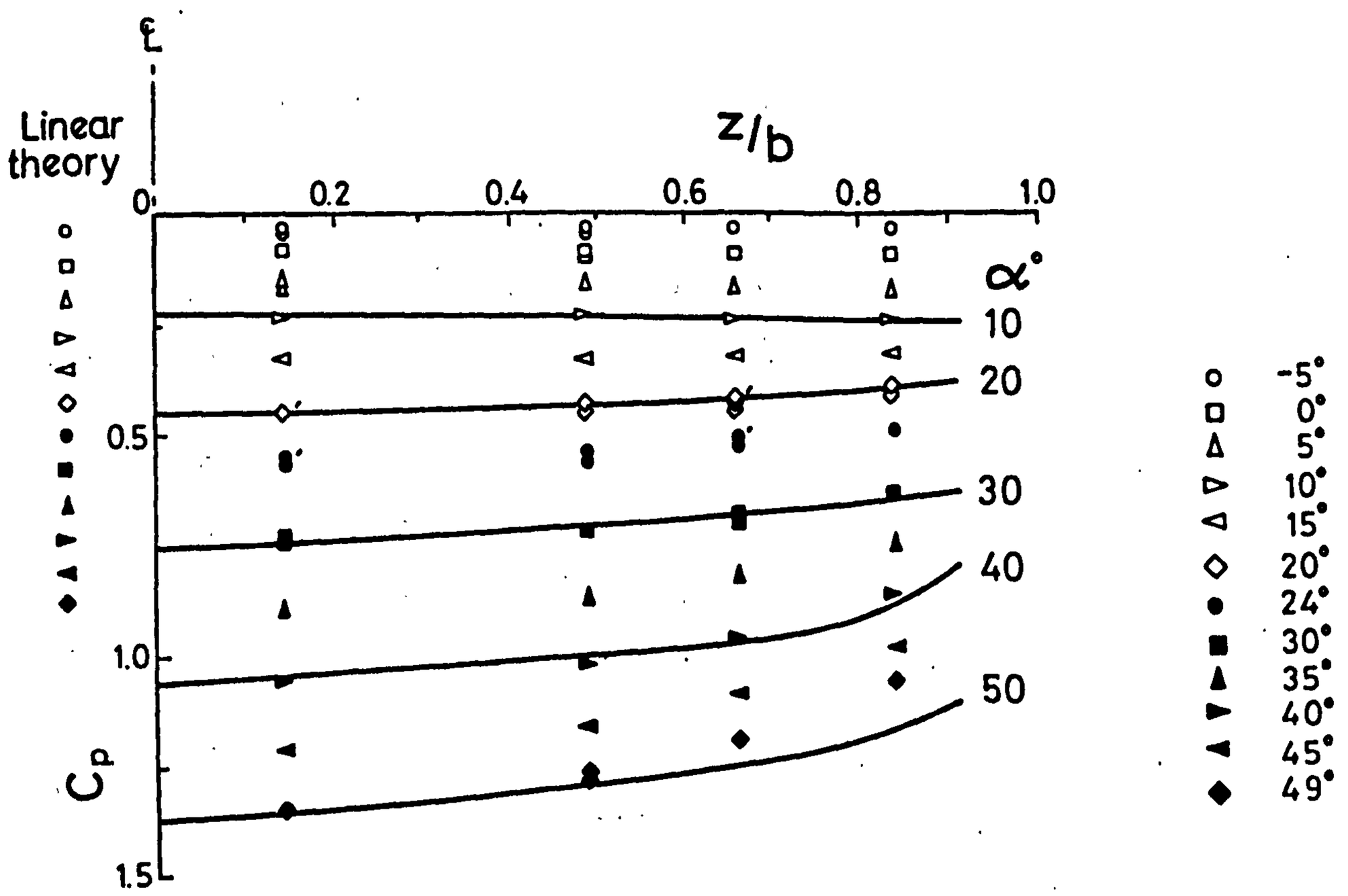

Fig. 35. Compression surface station 2.
(30 mm. from tip) $x/l = 0.3$

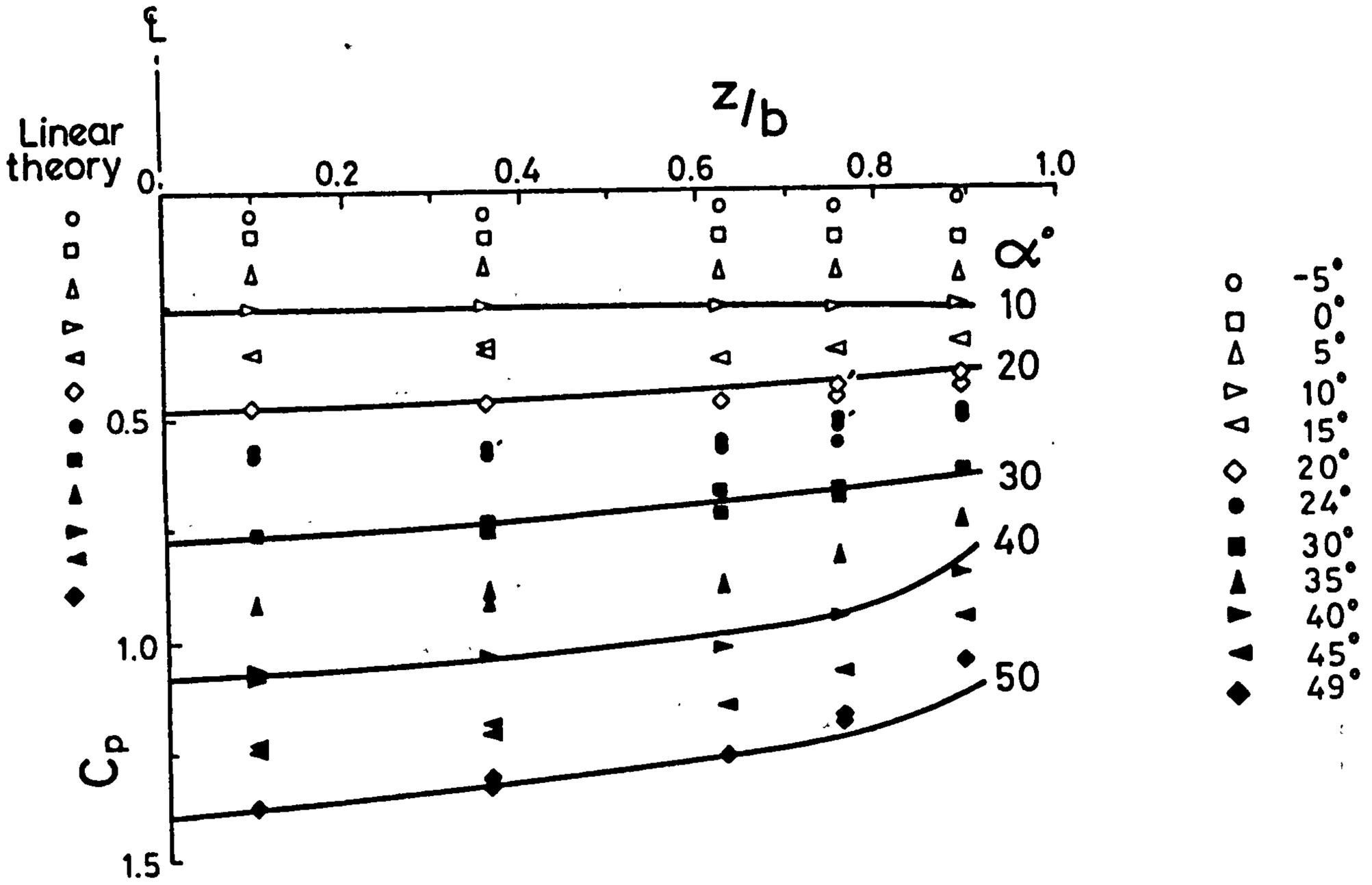

Fig. 36. Compression surface station 3.
(40 mm. from tip) $x/l = 0.4$

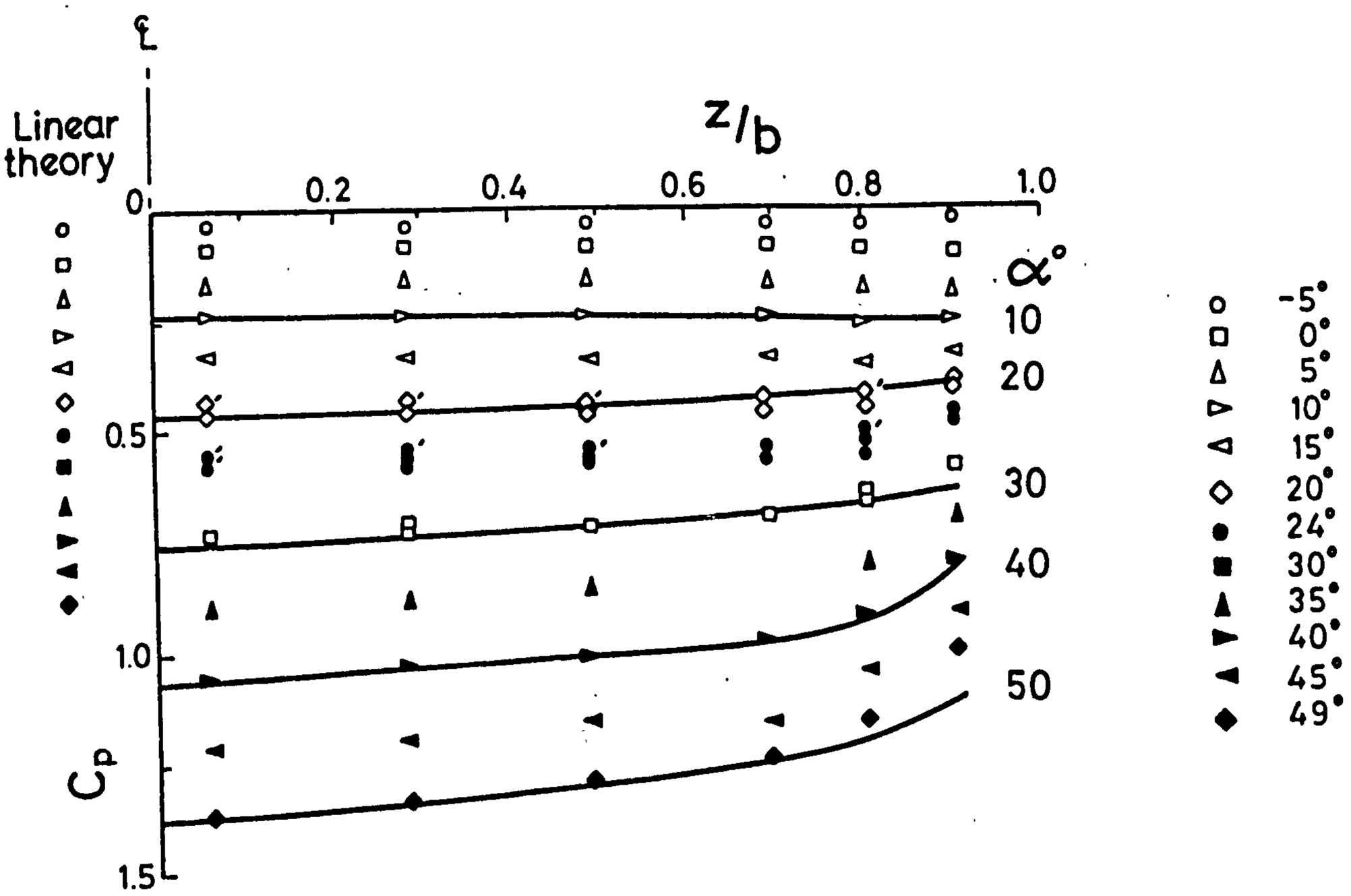

Fig. 37. Compression surface station 4.
(50 mm. from tip) $x/l = 0.5$

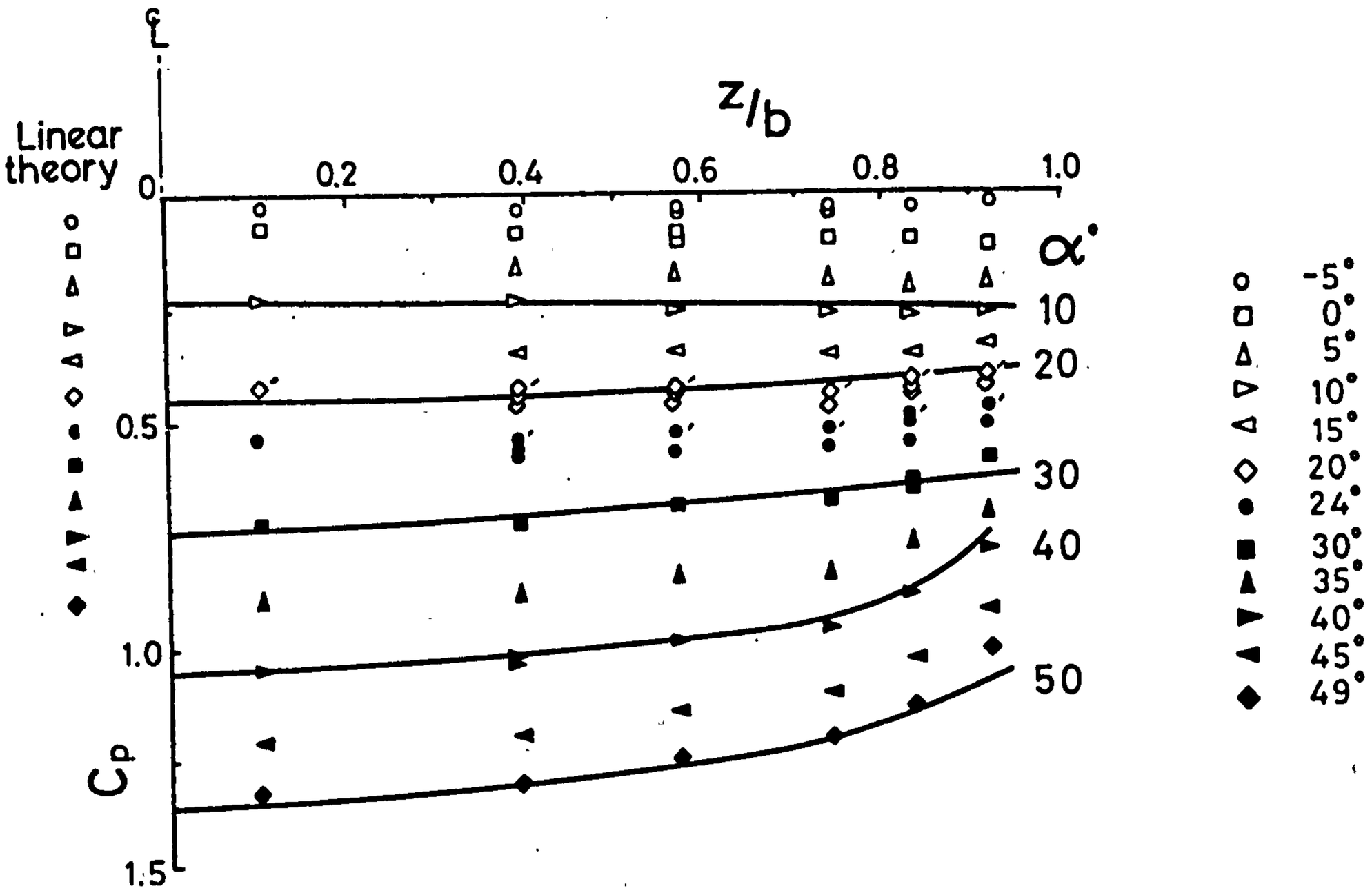

Fig. 38. Compression surface station 5.
(60 mm. from tip) $x/l = 0.6$

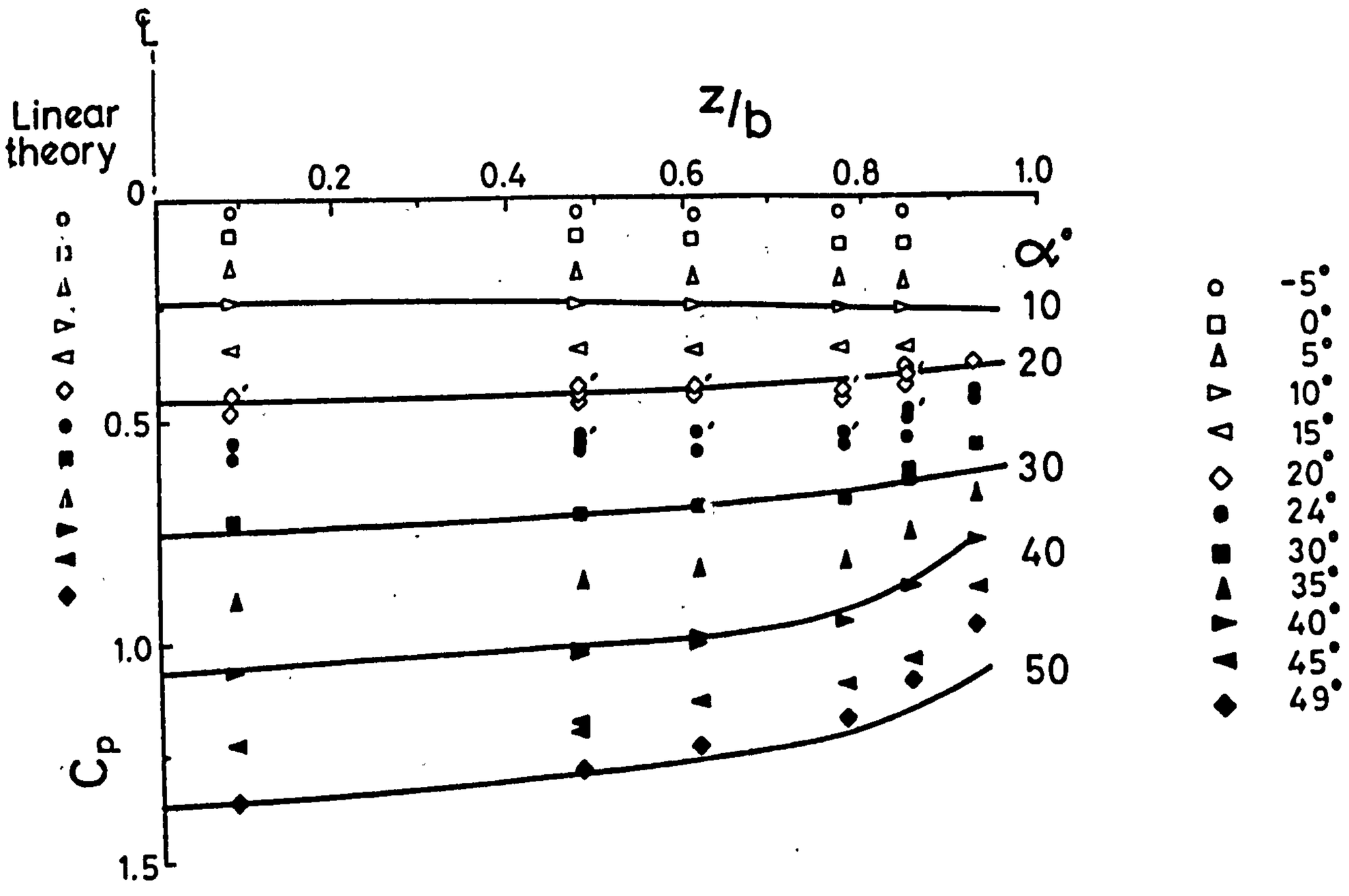

Fig. 39. Compression surface station 6.
(70 mm. from tip) $x/l = 0.7$

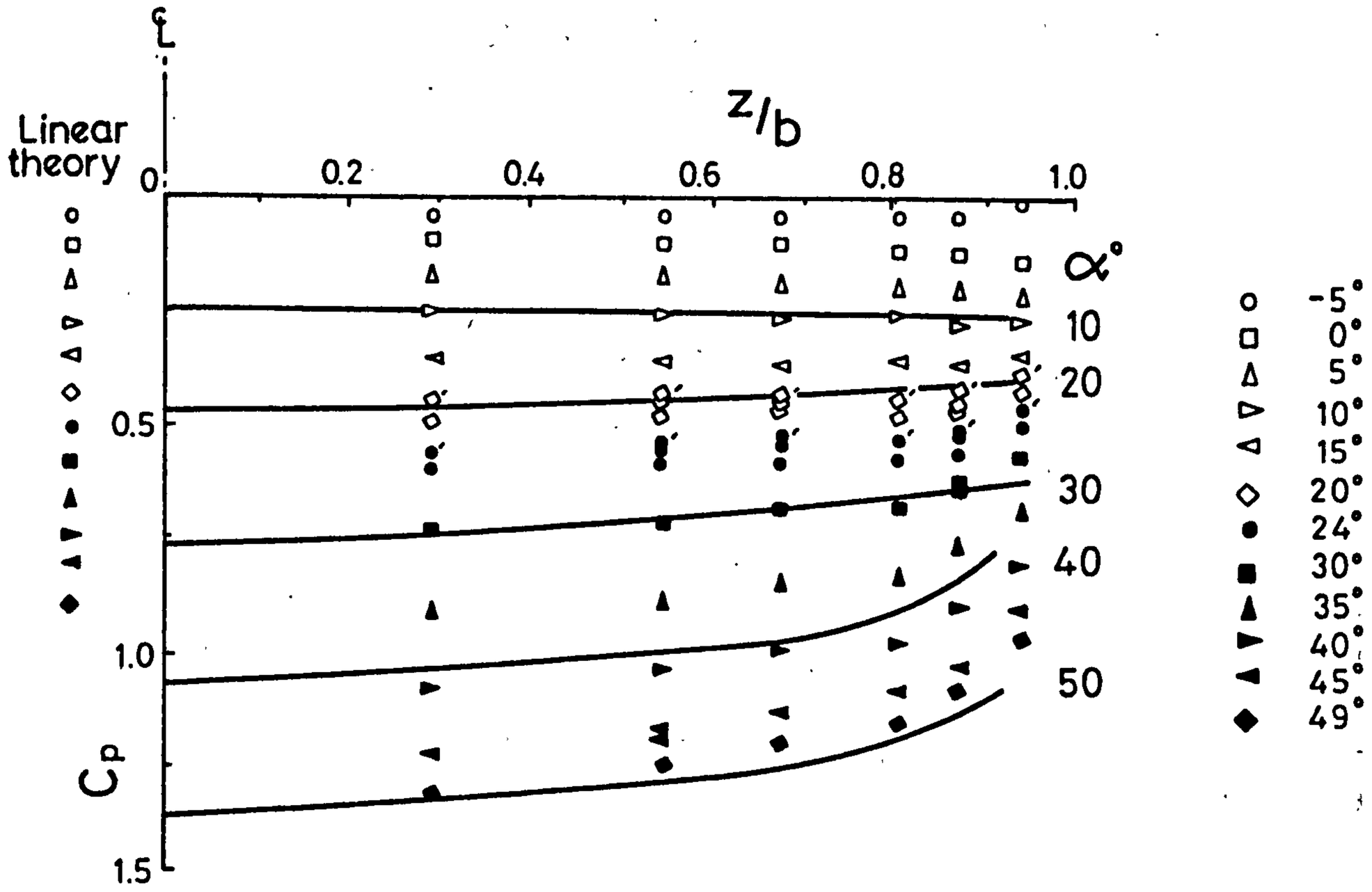

Fig.40. Compression surface station 7.
(80 mm. from tip) $x/l = 0.8$

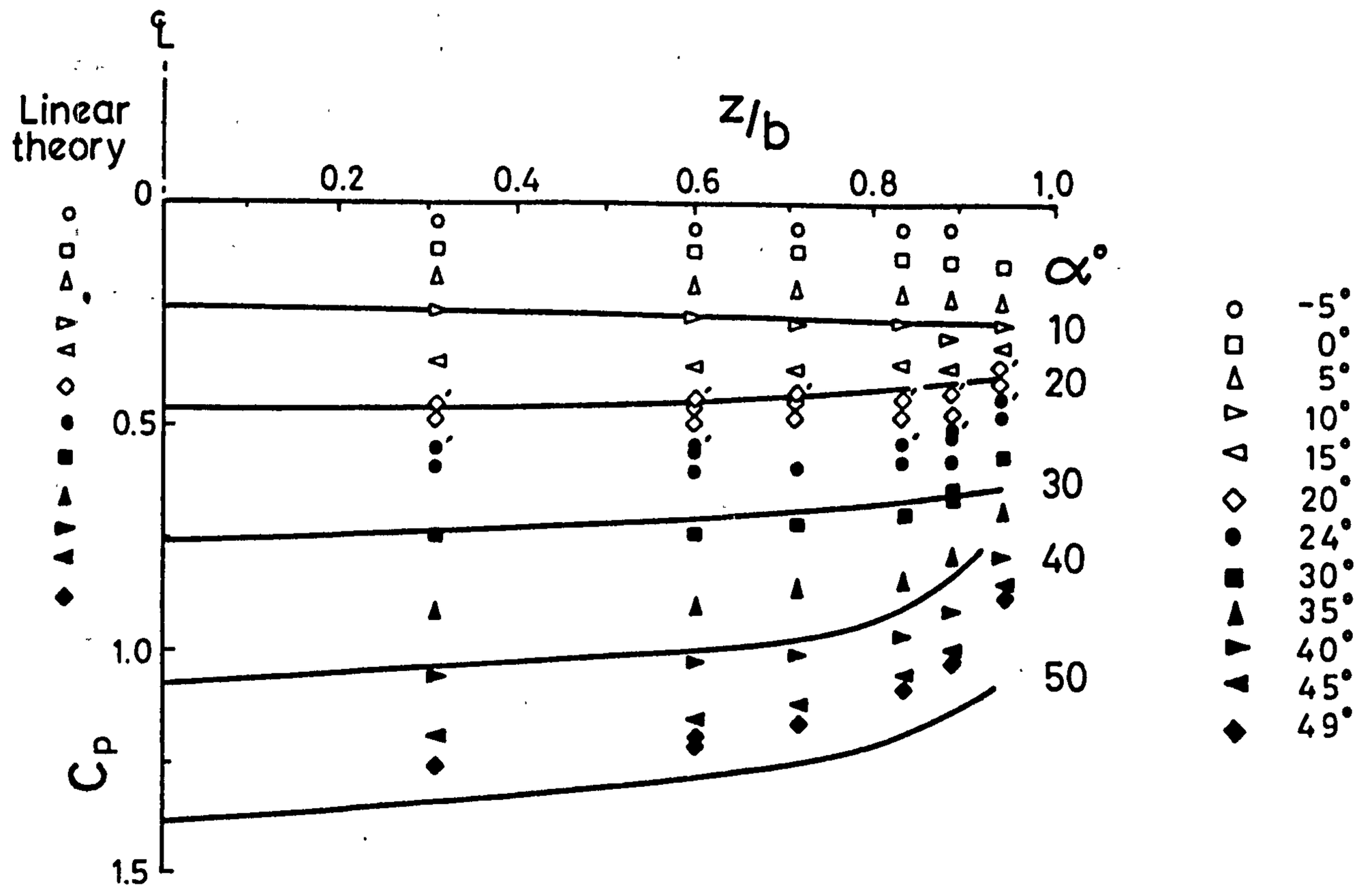

Fig.41. Compression surface station 8.
(90 mm. from tip) $x/l = 0.9$

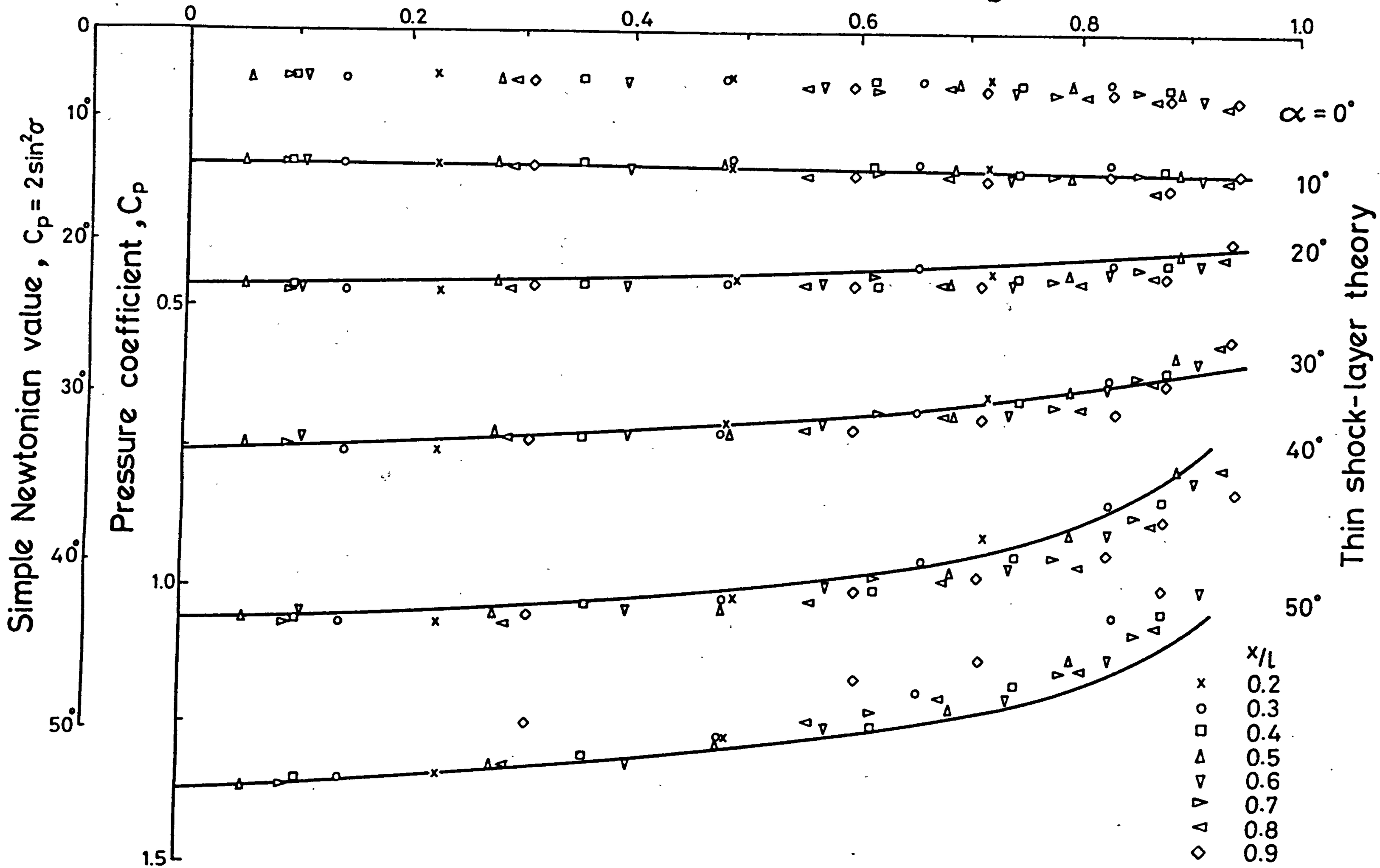

Fig. 42. Combined compression surface pressure distributions.

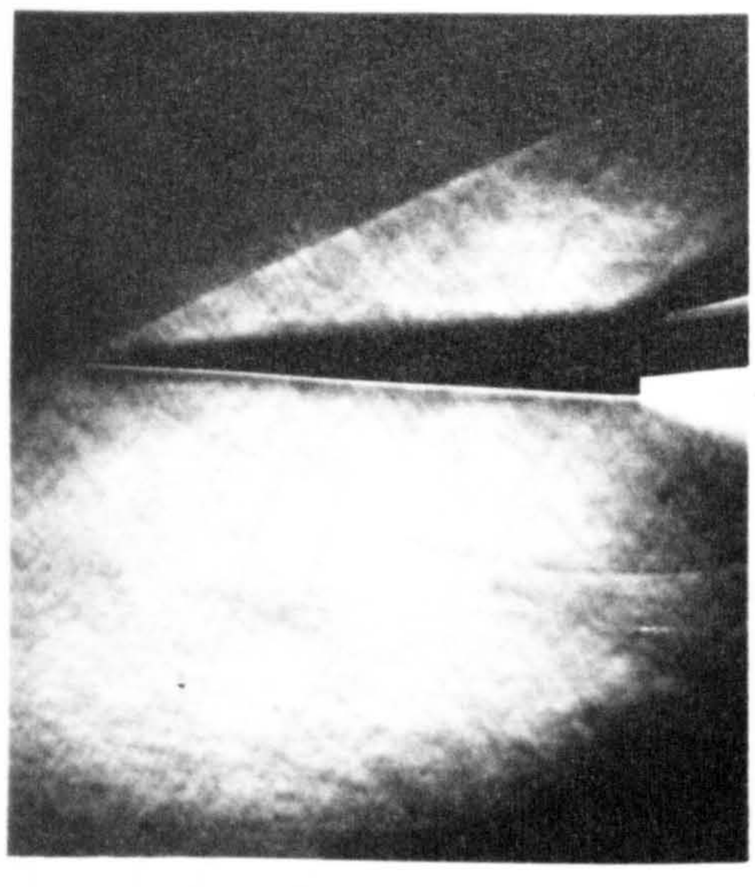

$\alpha = -5^\circ$

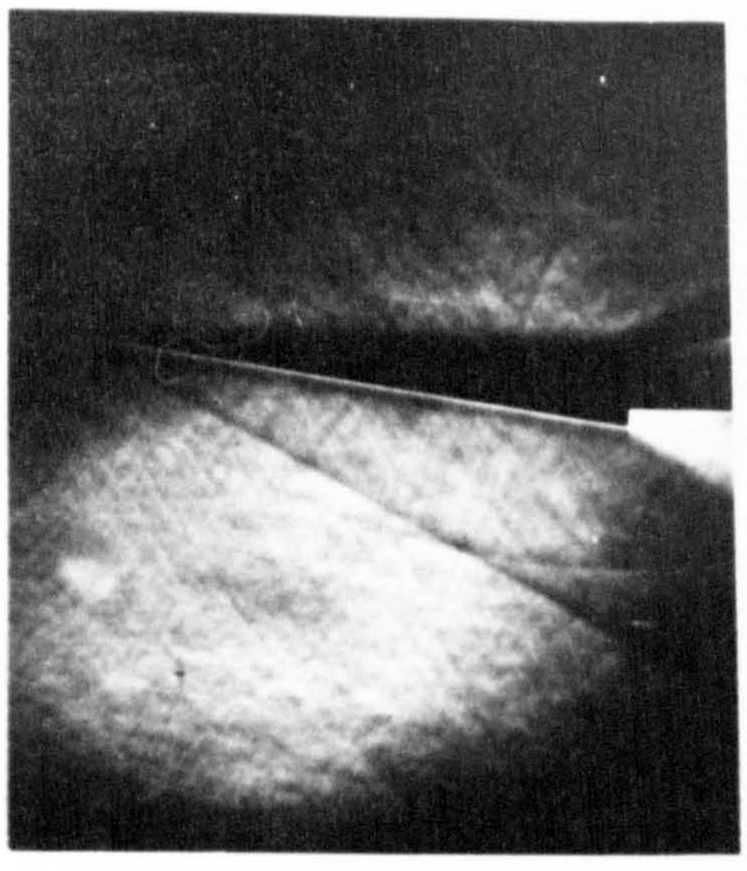

$\alpha = 0^\circ$

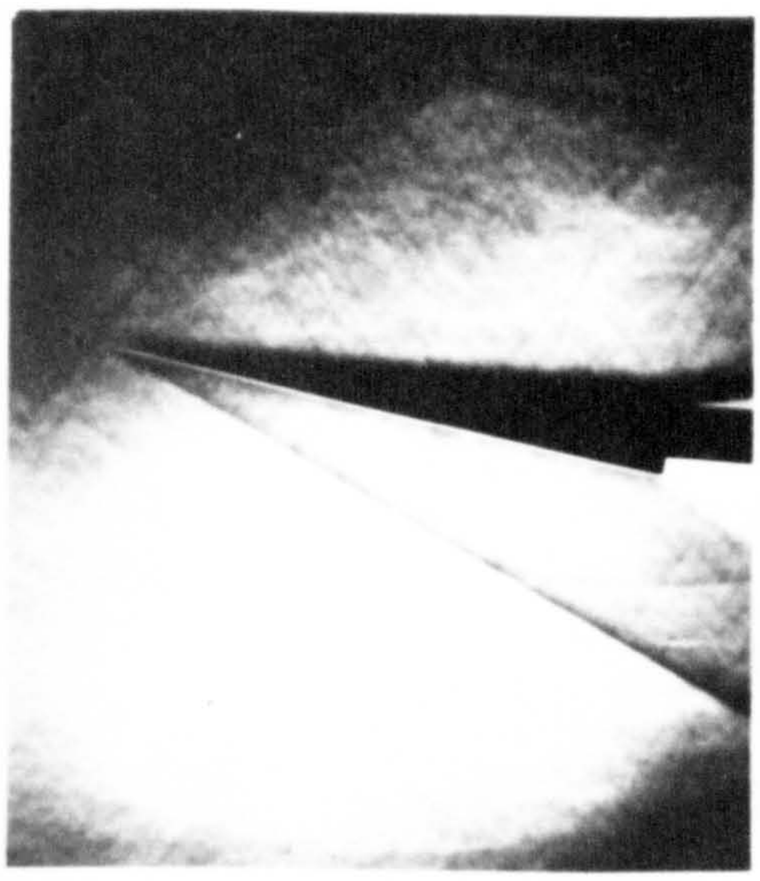

$\alpha = 5^\circ$

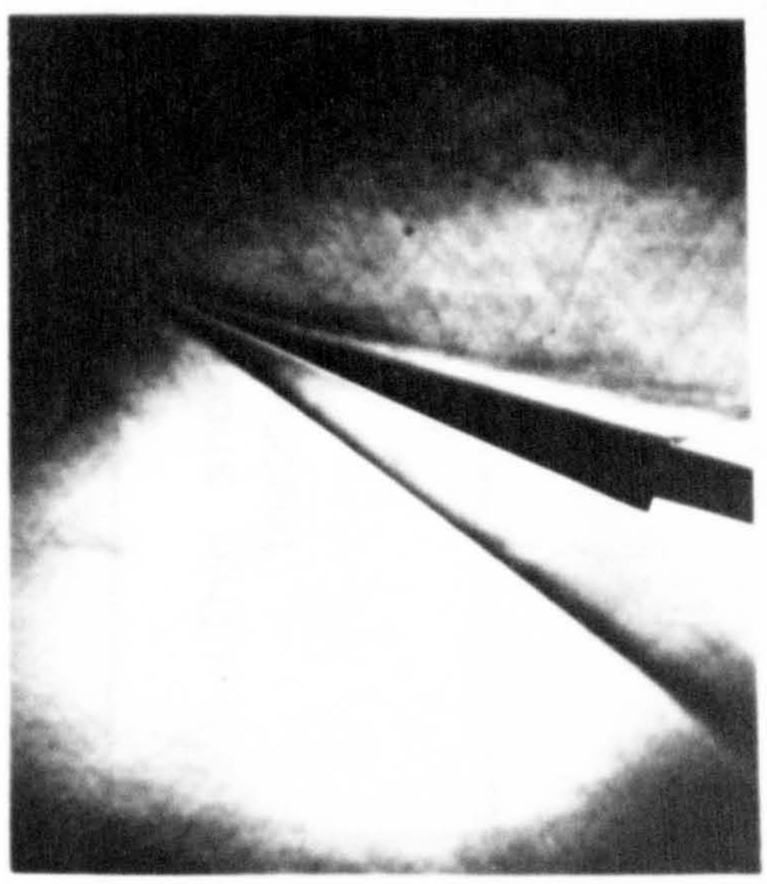

$\alpha = 15^\circ$

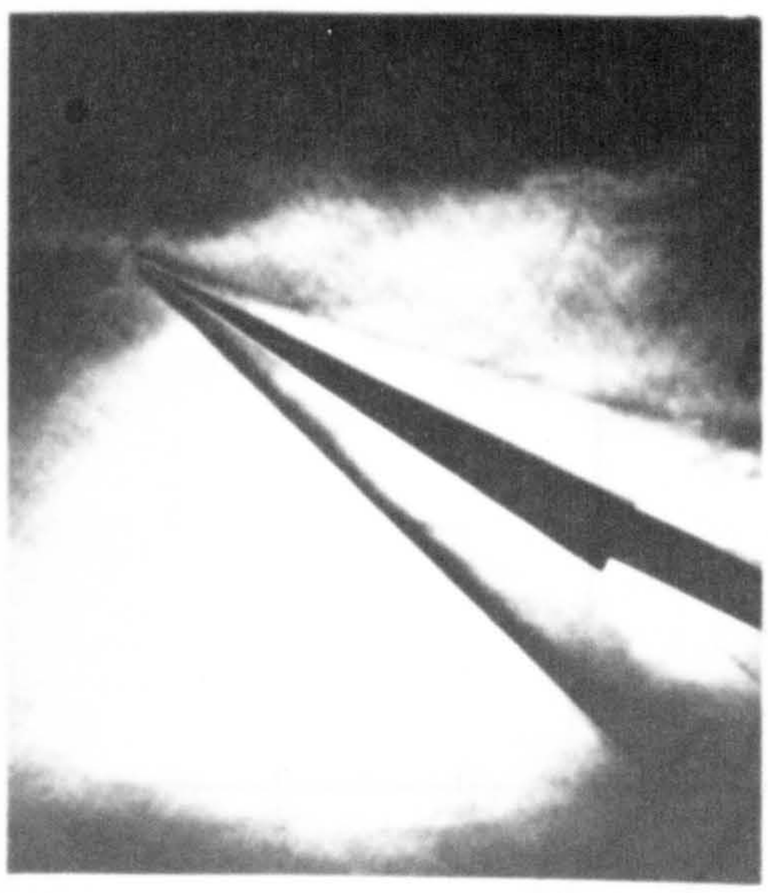

$\alpha = 25^\circ$

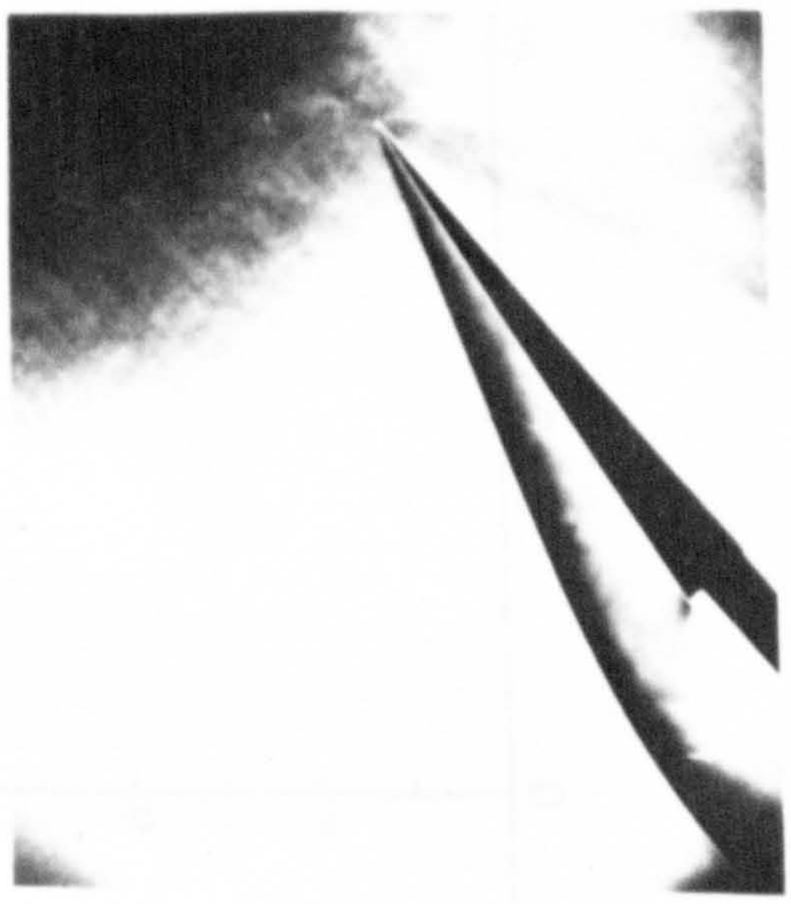

$\alpha = 50^\circ$

Fig. 43. Schlieren photographs, $-5^\circ \leq \alpha \leq 50^\circ$

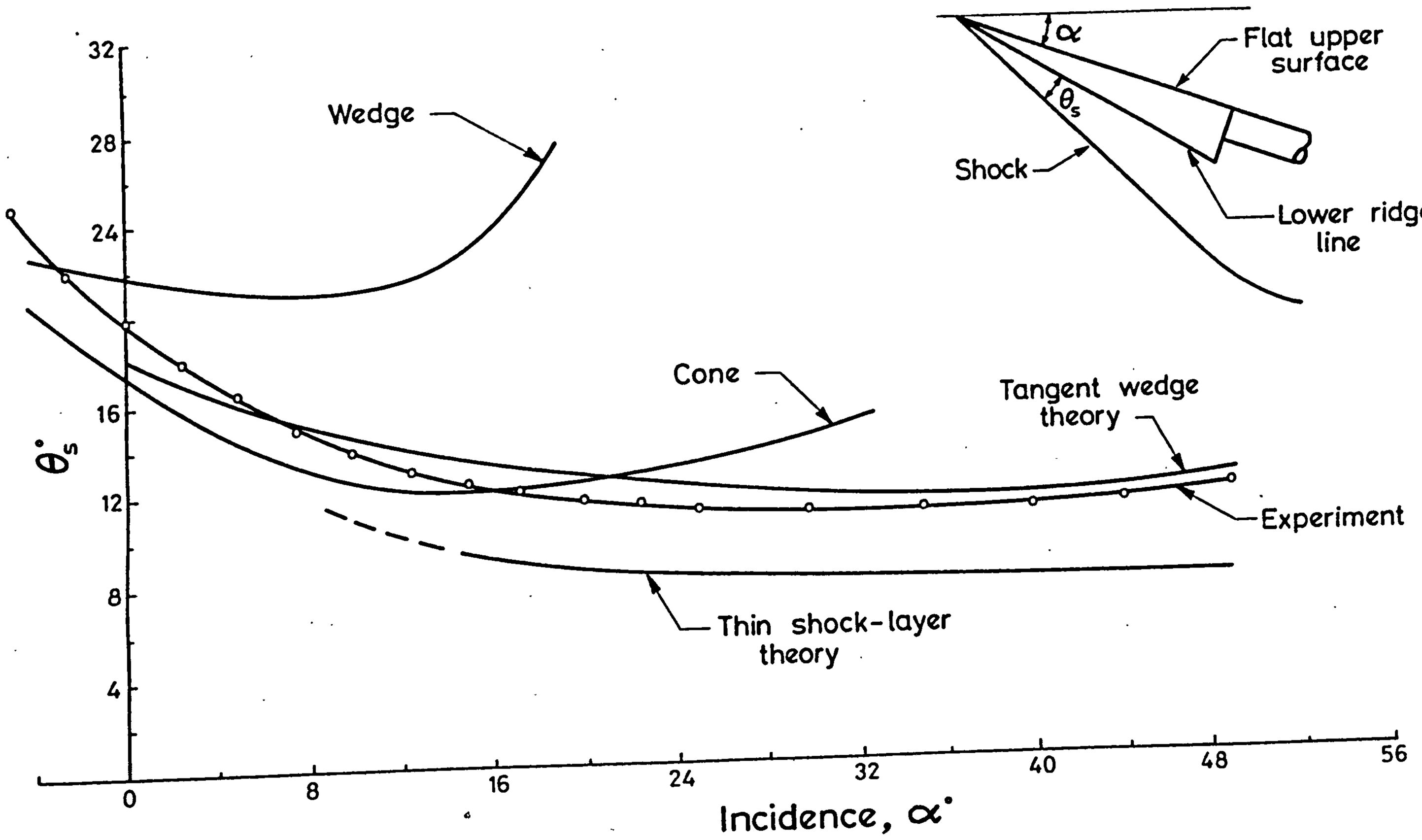

Fig. 44. Variation of shock wave angle with incidence.

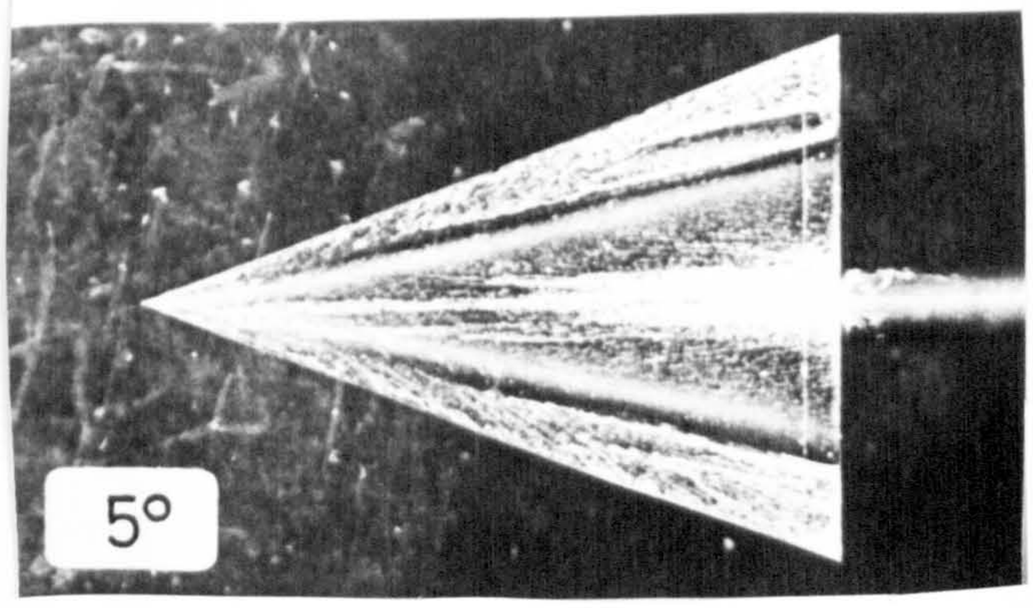

$\alpha = 5^\circ$

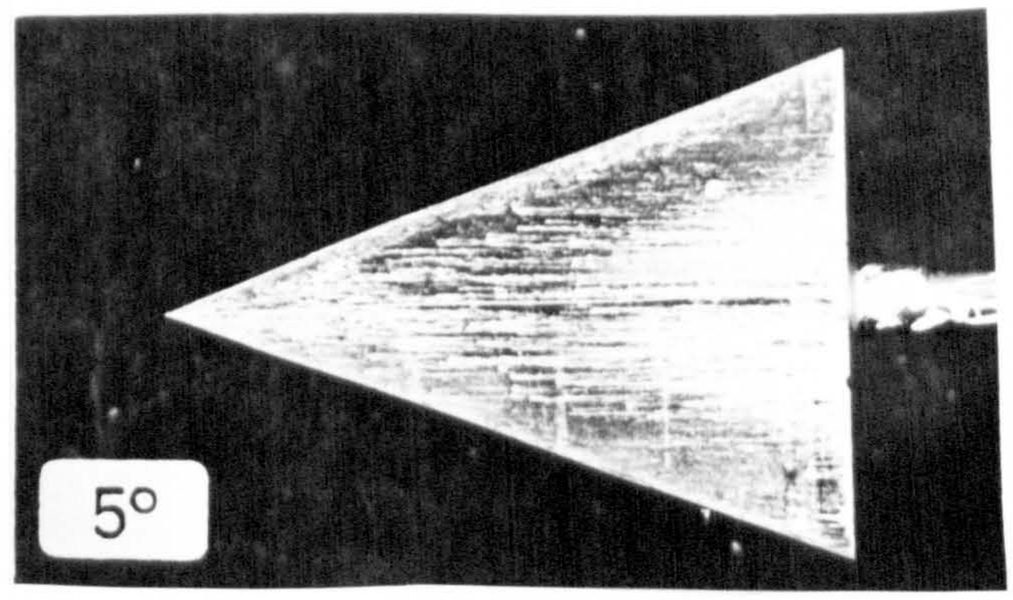

$\alpha = 5^\circ$

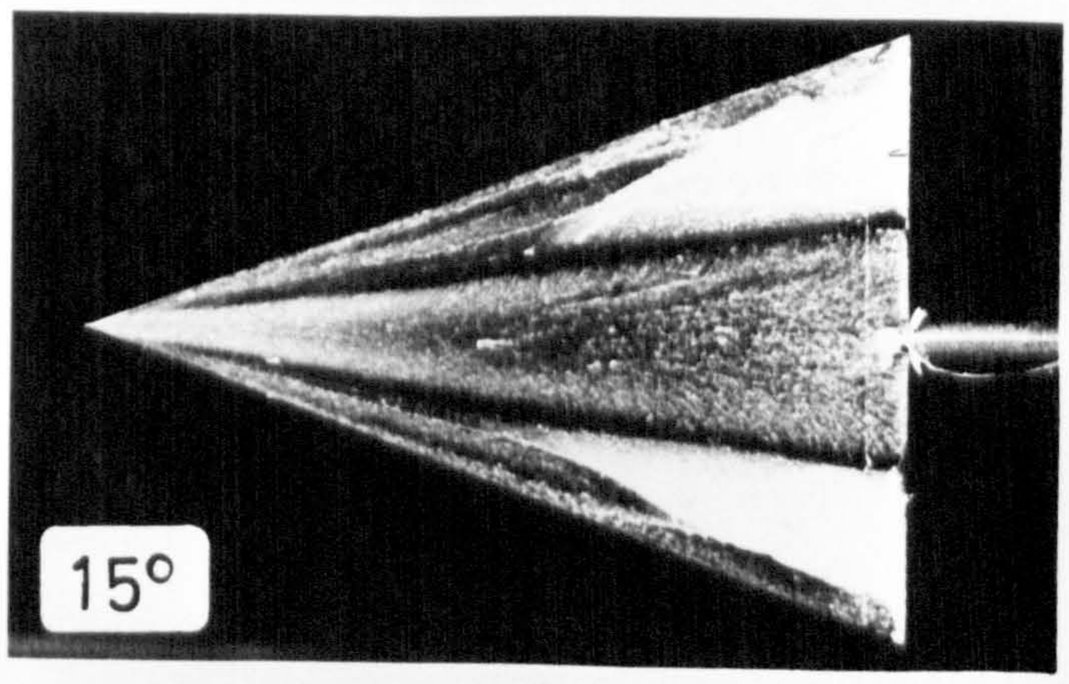

$\alpha = 15^\circ$

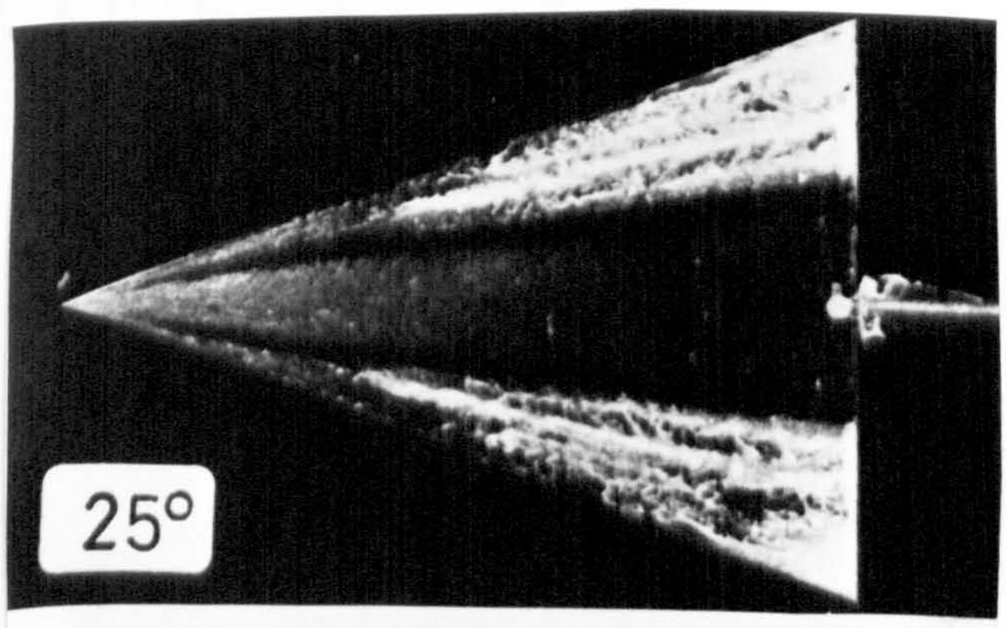

$\alpha = 25^\circ$

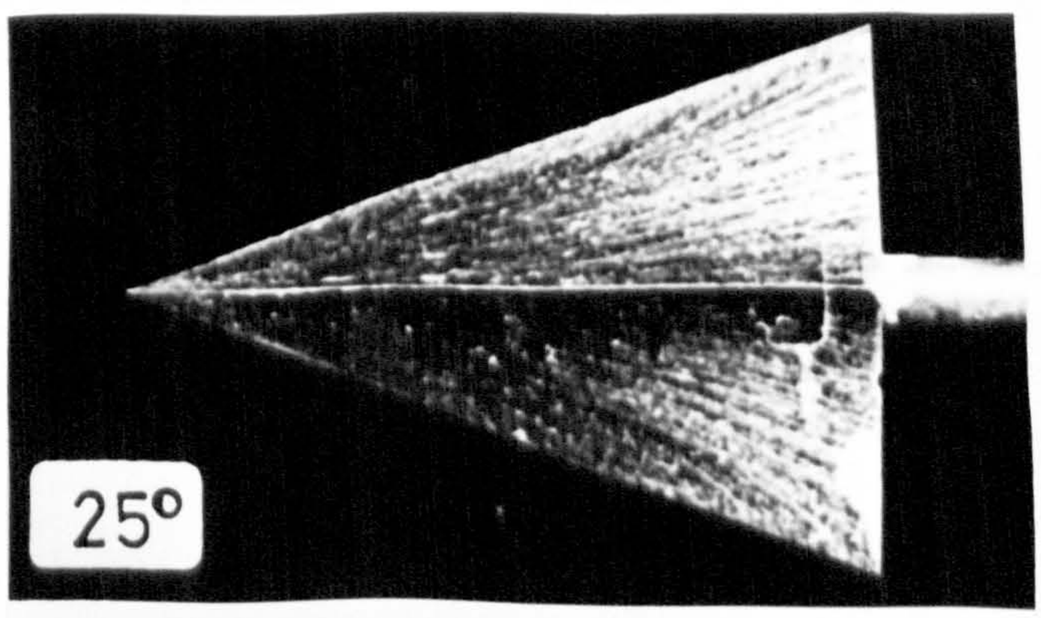

$\alpha = 25^\circ$

Fig. 45. Oil flow photographs.

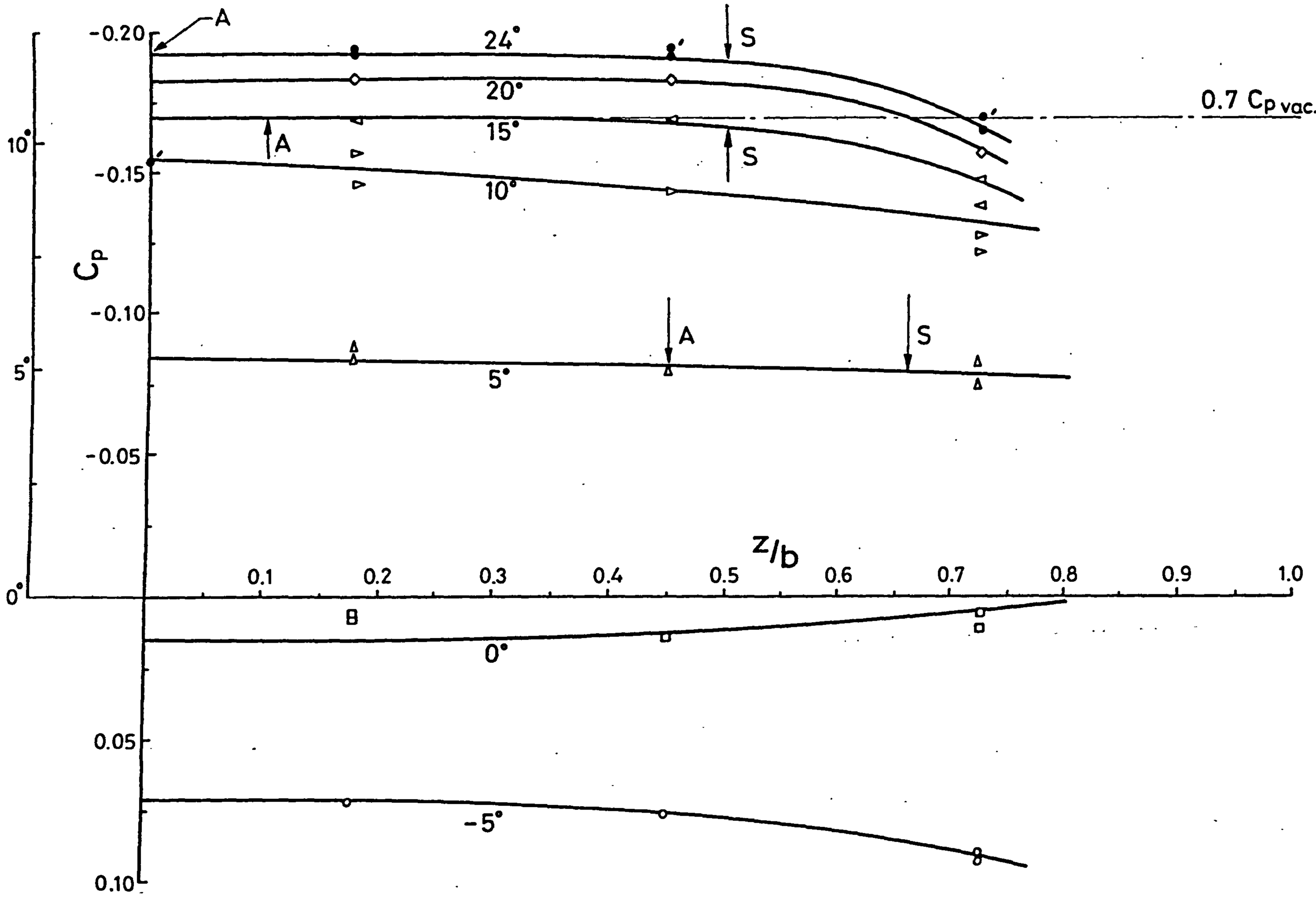

Fig. 46. Expansion surface station 1. (20mm. from tip), $x/l = 0.2$

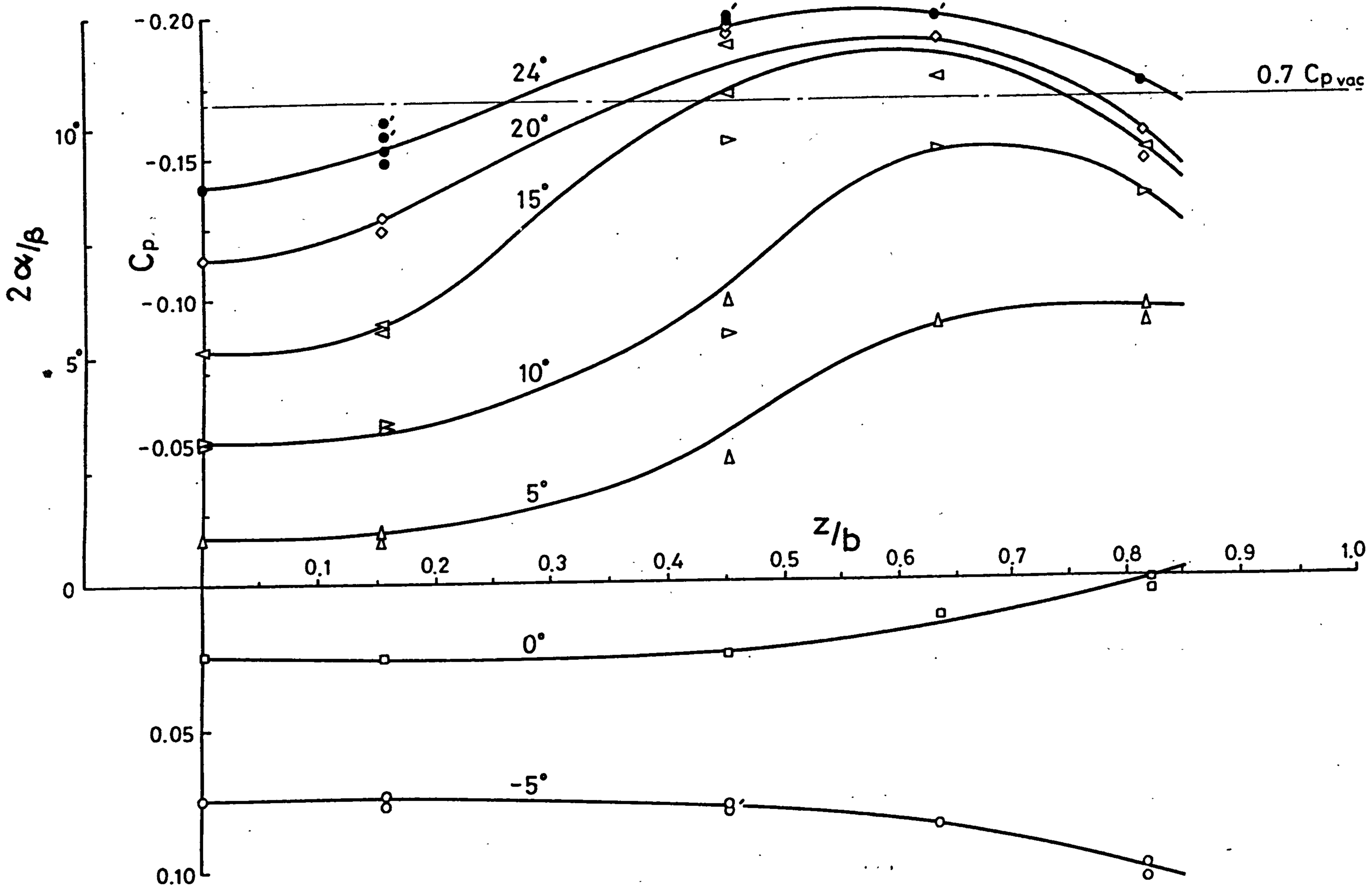

Fig. 47. Expansion surface station 2. (30 mm. from tip), $x/l = 0.3$

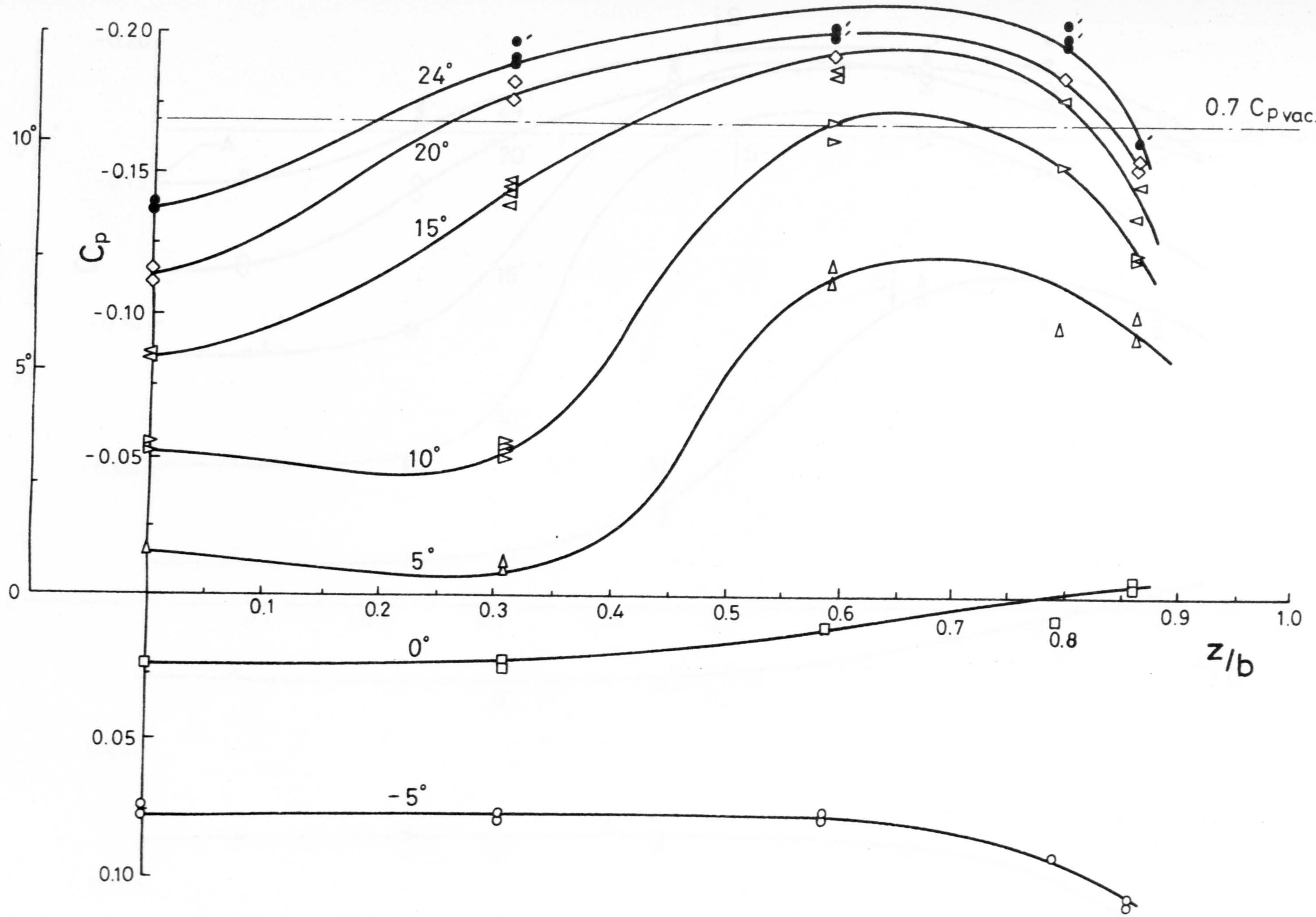

Fig. 48. Expansion surface station 3. (40 mm. from tip), $^{x}/_{l} = 0.4$

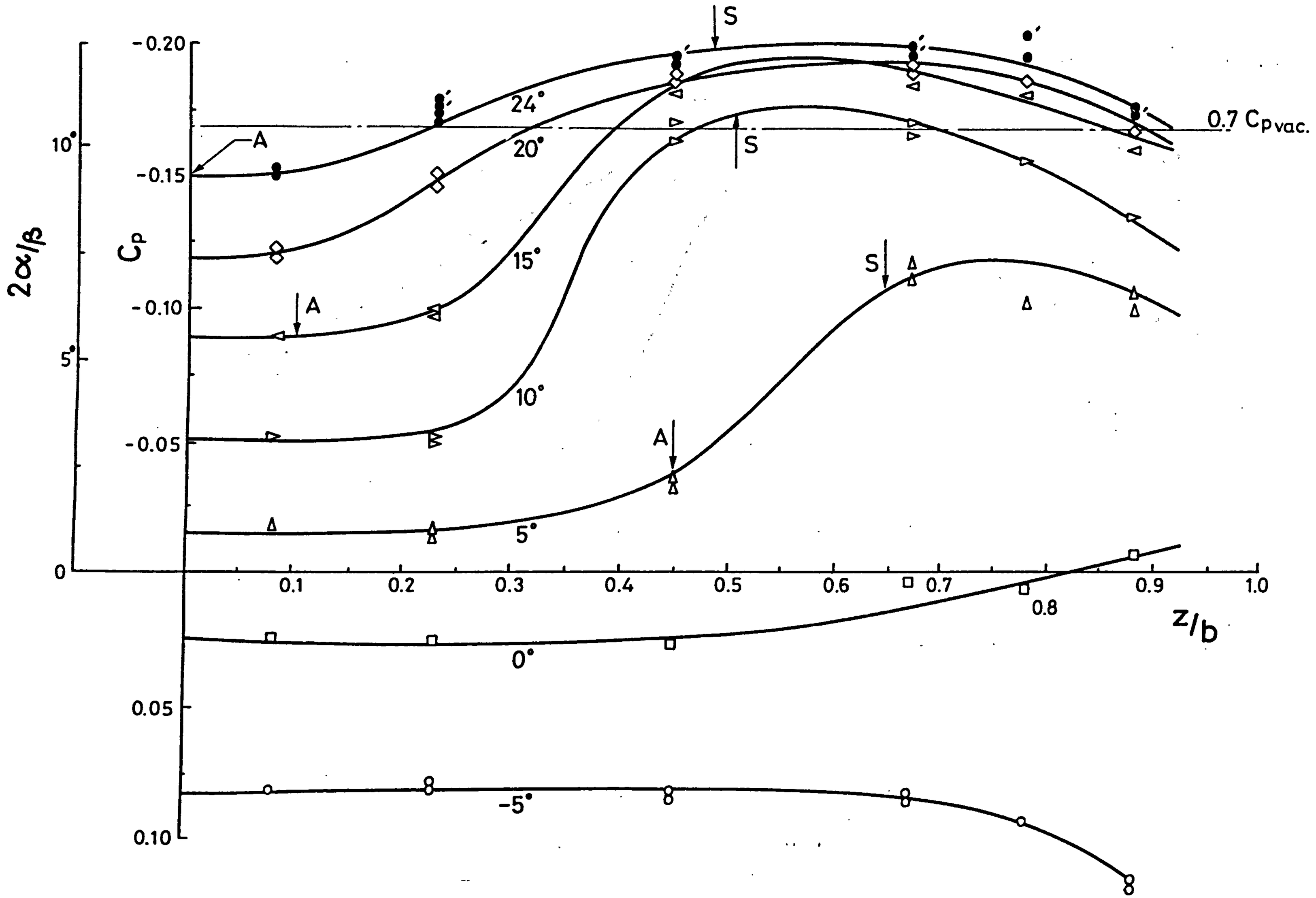

Fig. 49. Expansion surface station 4. (50mm. from tip) , $x/l = 0.5$

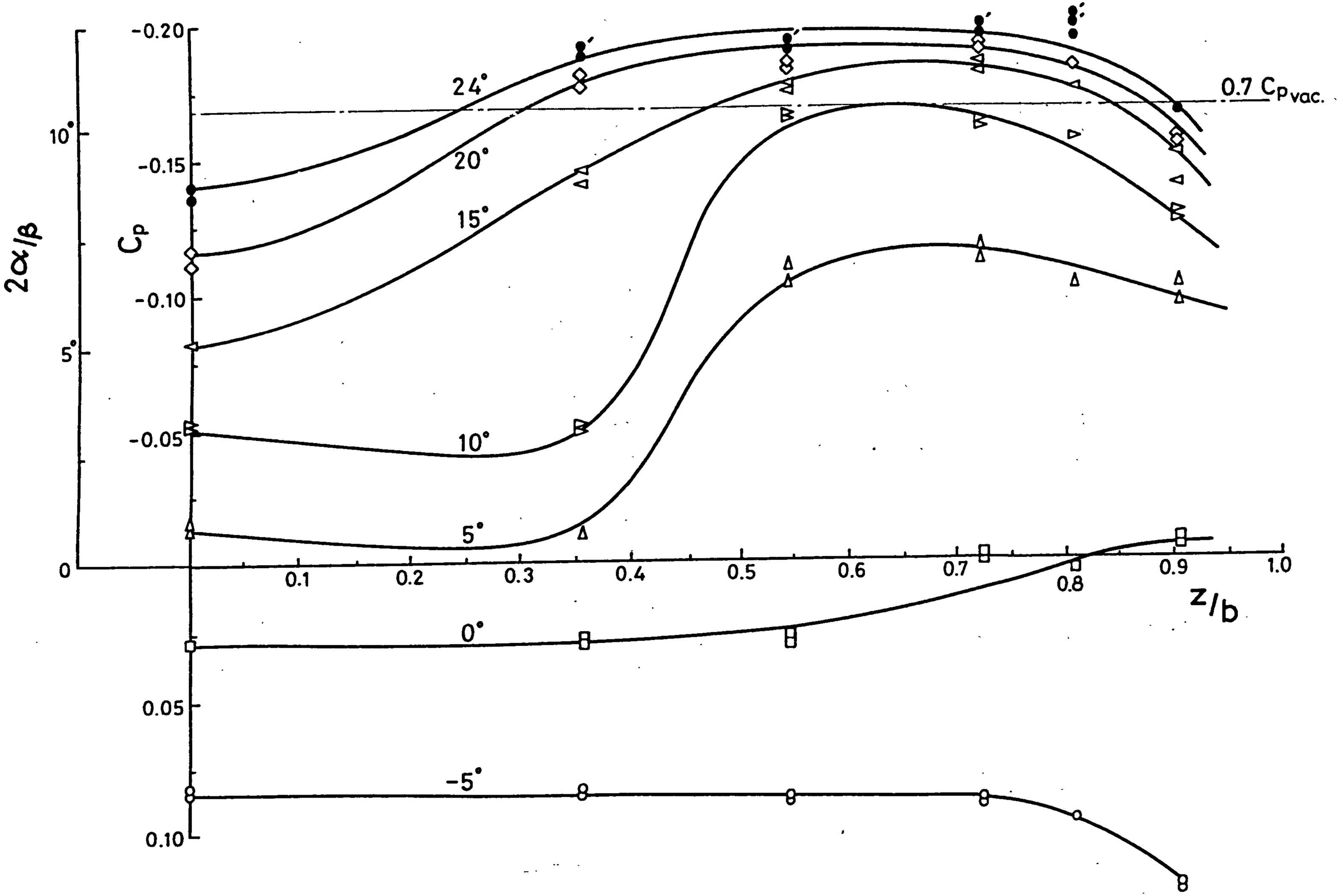

Fig. 50. Expansion surface station 5. (60 mm. from tip), $x/l = 0.6$

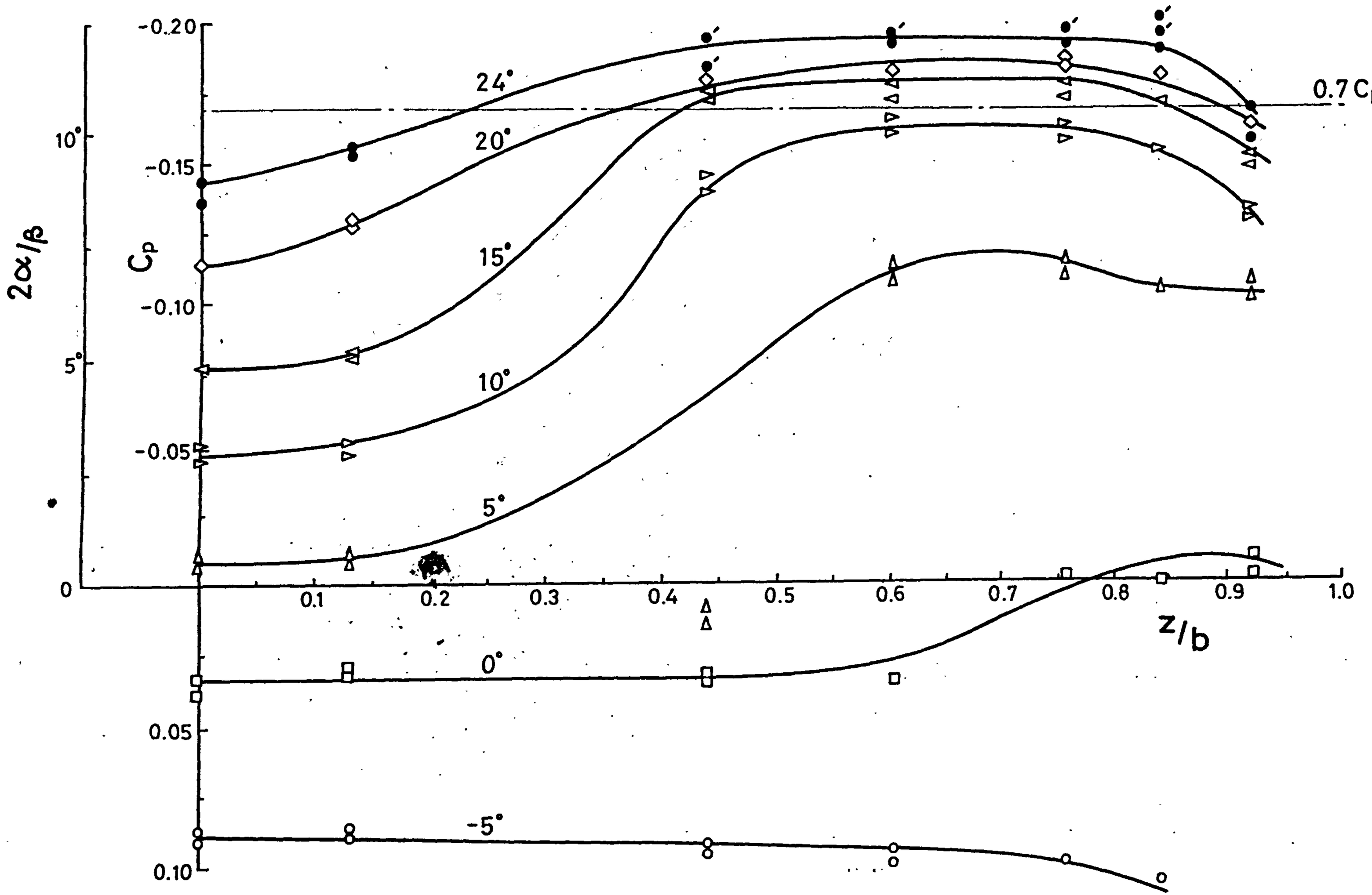

Fig. 51. Expansion surface station 6. (70 mm. from tip), $x/l = 0.7$

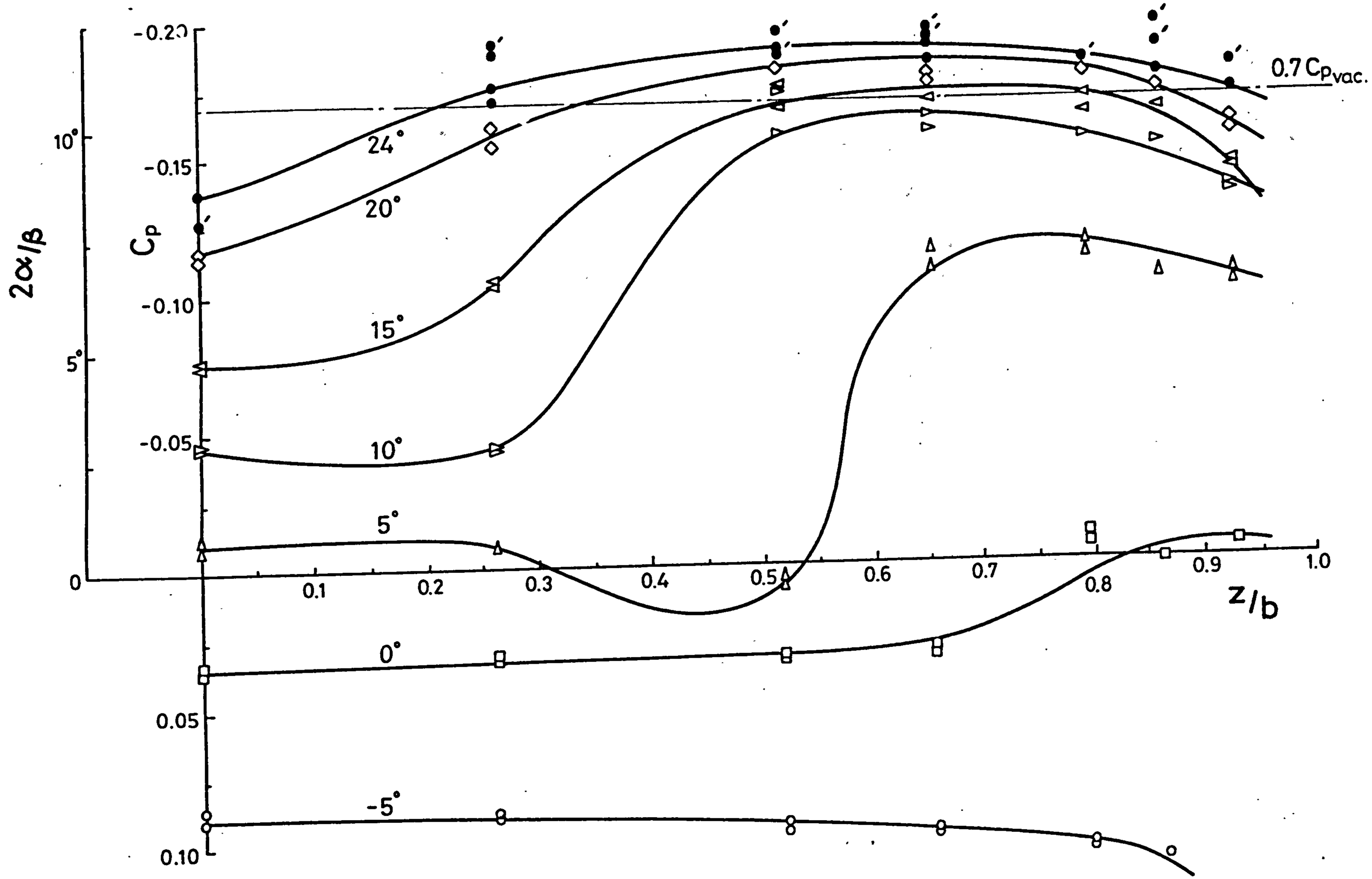

Fig. 52. Expansion surface station 7. (80 mm. from tip) $x/l = 0.8$

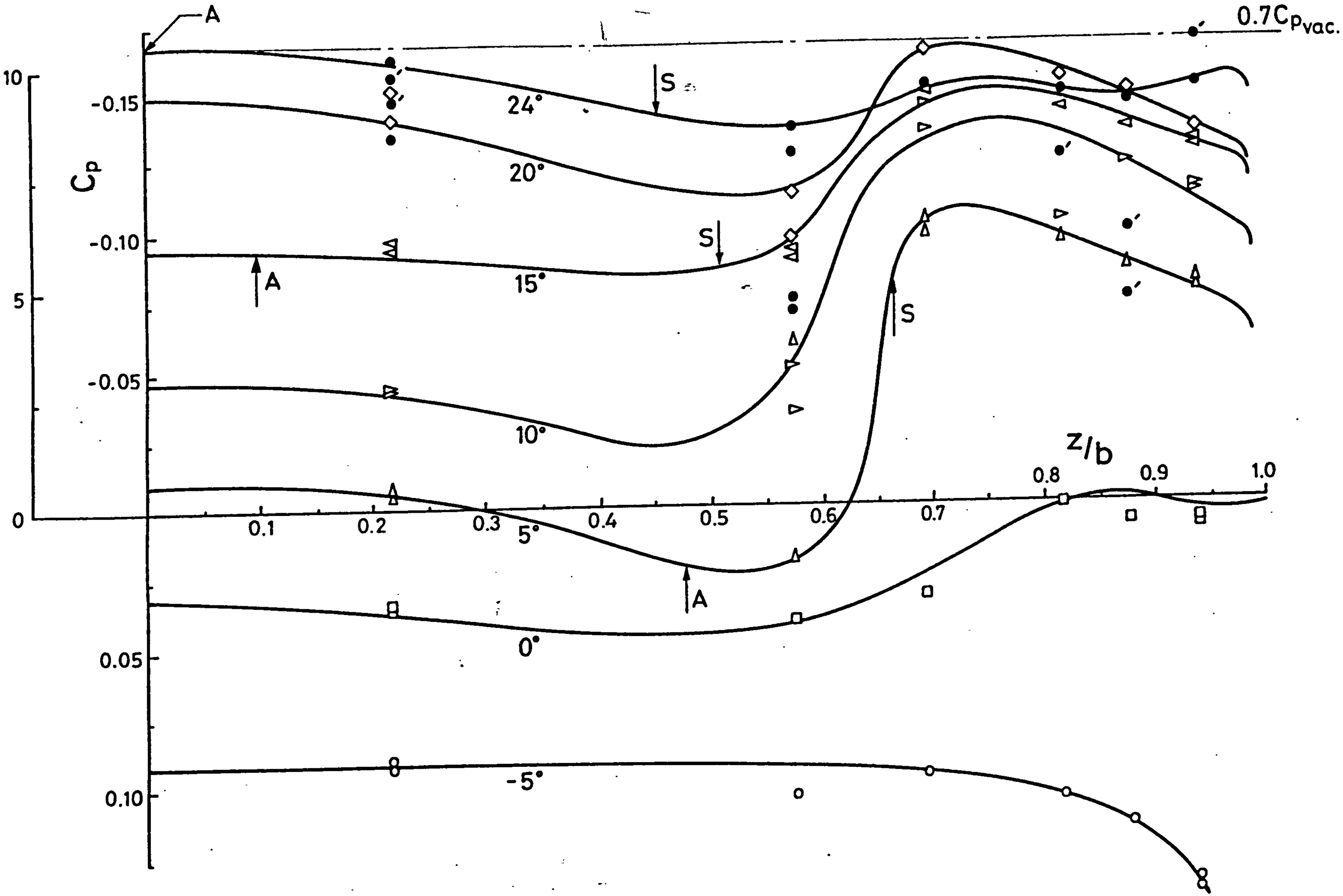

Fig. 53. Expansion surface station 8. (90mm. from tip), $^{x}/_{l} = 0.9$

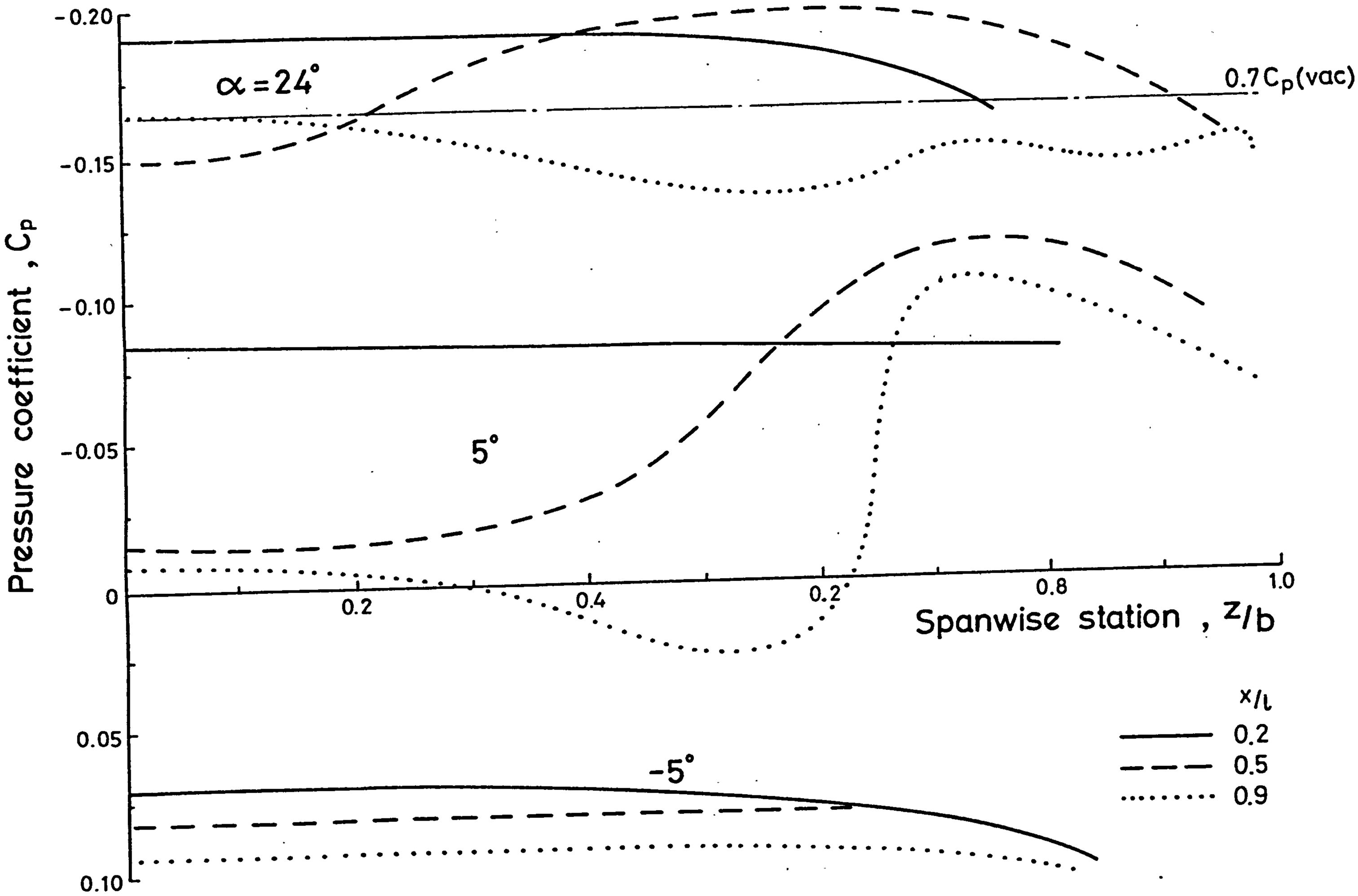

Fig. 54. Variation of pressure with cordwise position.

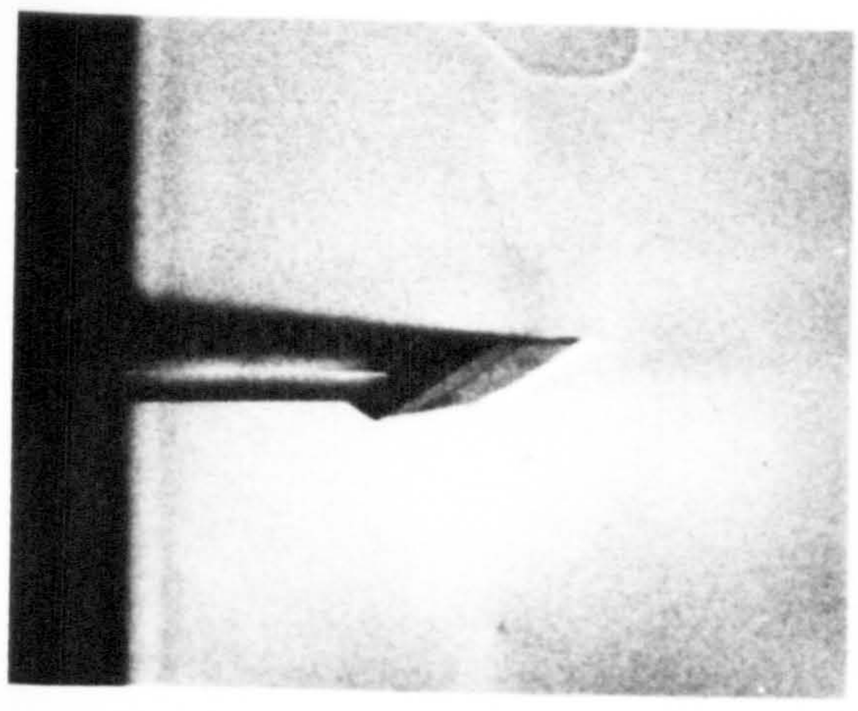

$\alpha = 0°$

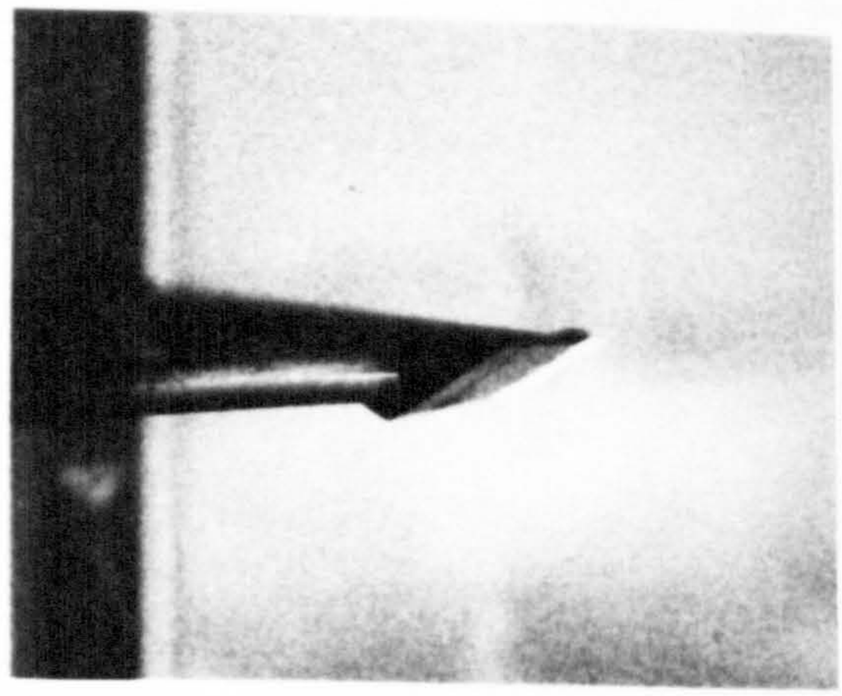

$\alpha = 5°$

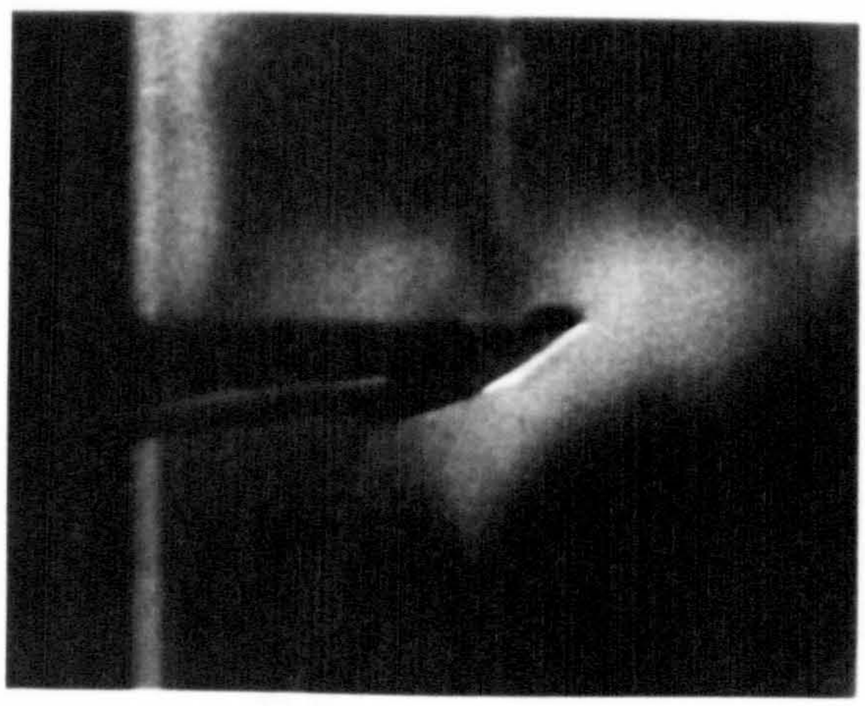

$\alpha = 10°$

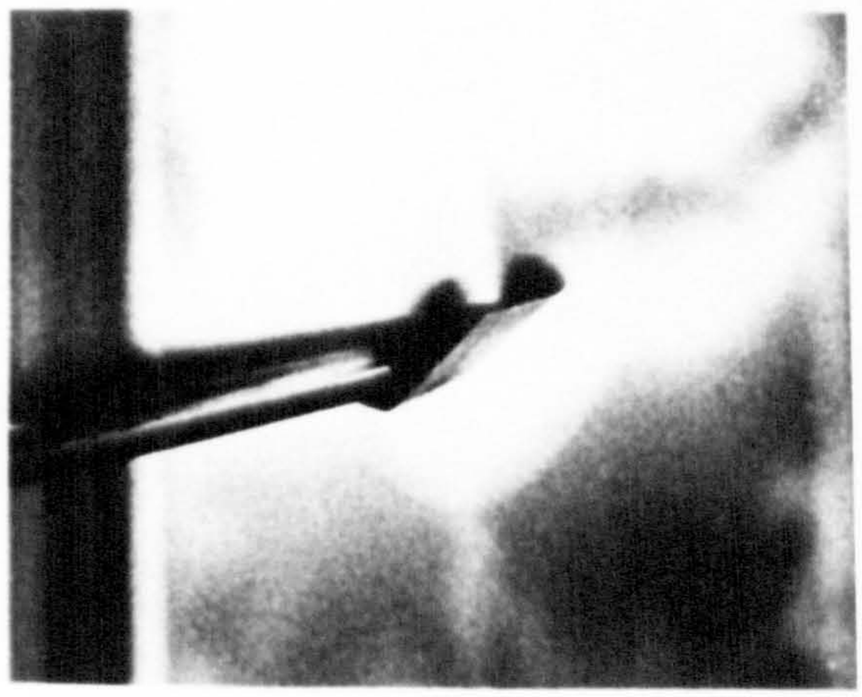

$\alpha = 15°$

$\alpha = 20°$

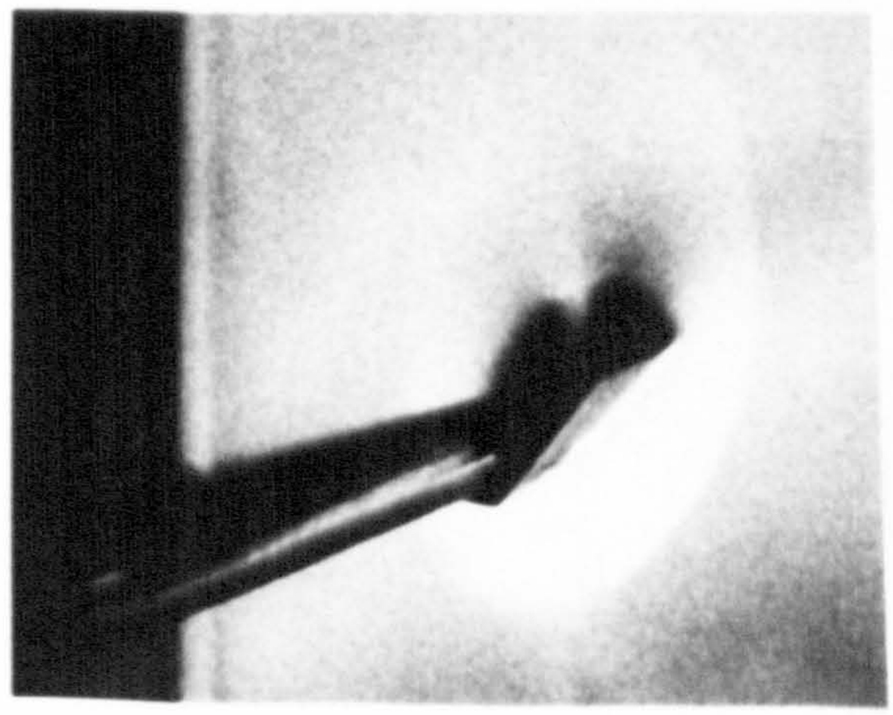

$\alpha = 25°$

Fig. 55. Vapour screen photographs viewed from downstream.

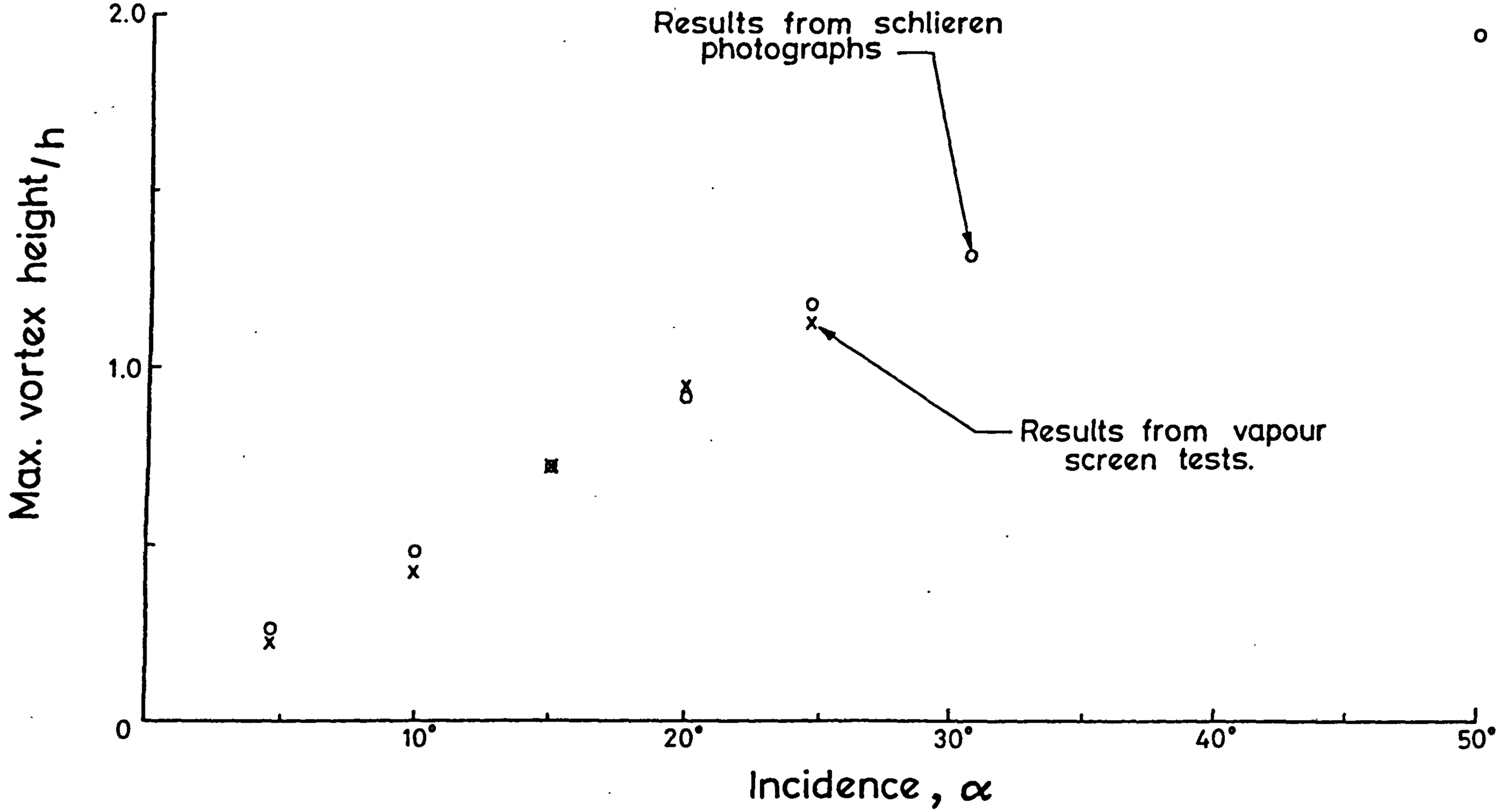

Fig. 56. Variation of vortex height with incidence.

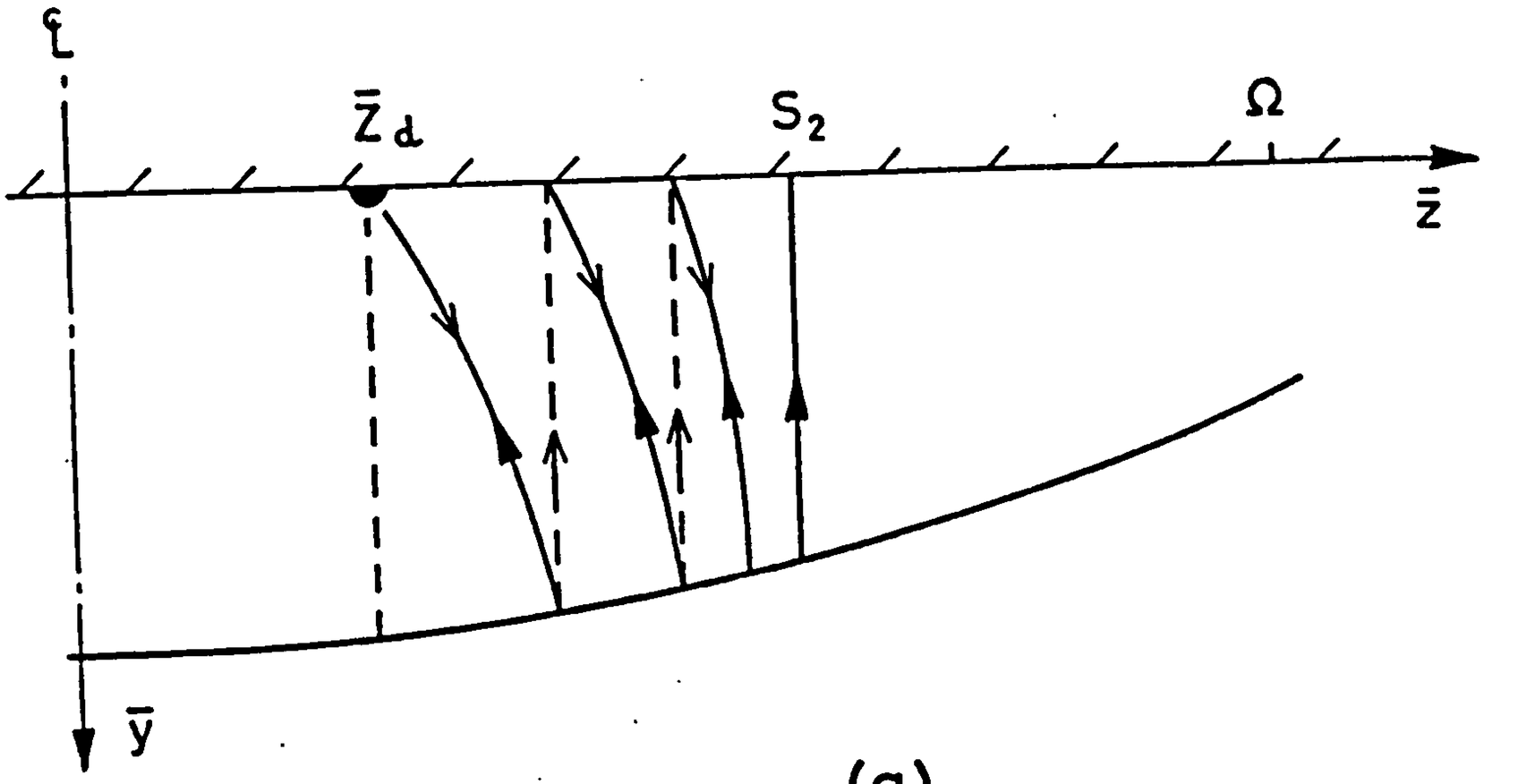

(a)

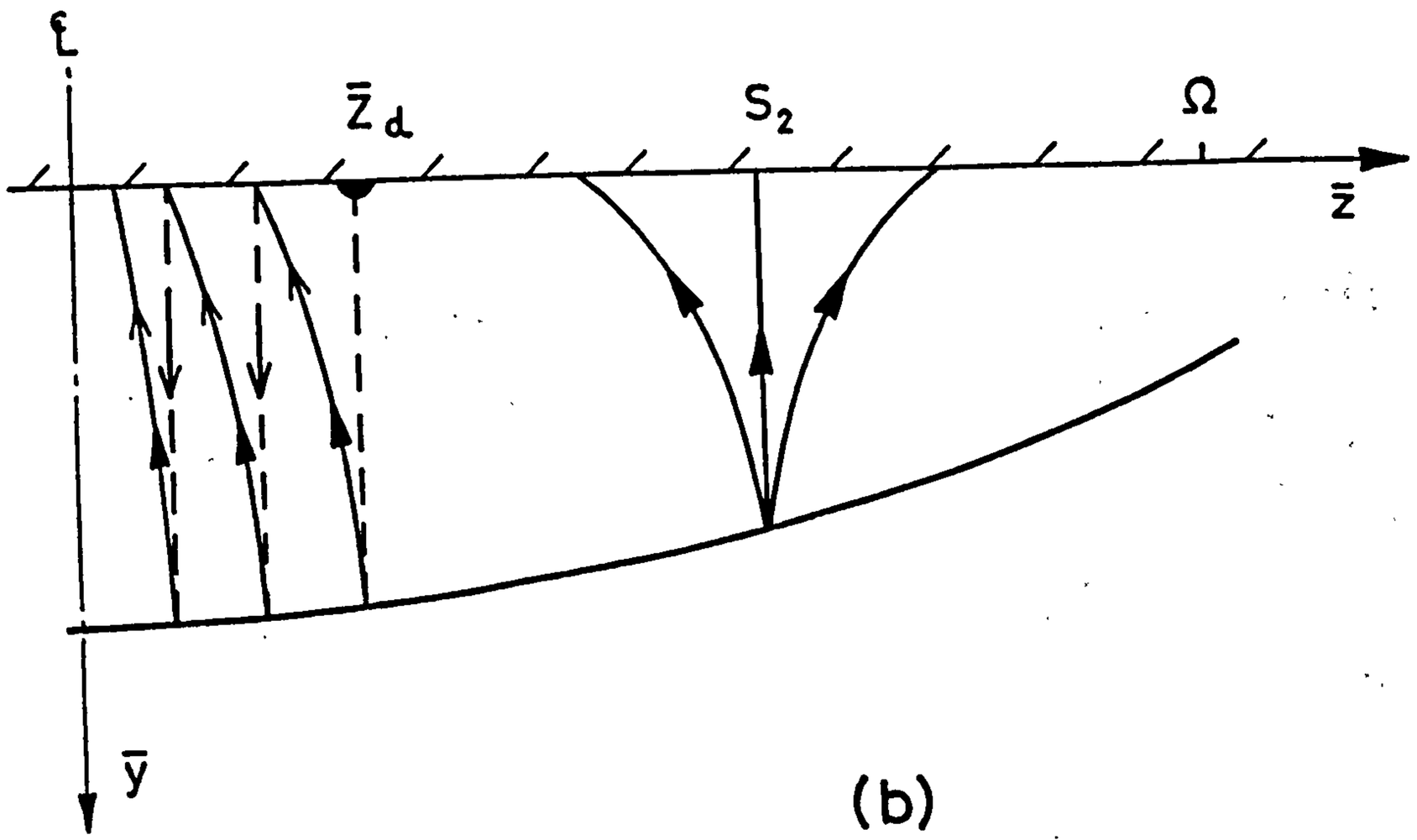

(b)

Fig. 57. The propagation of disturbances in thin shock-layer theory.

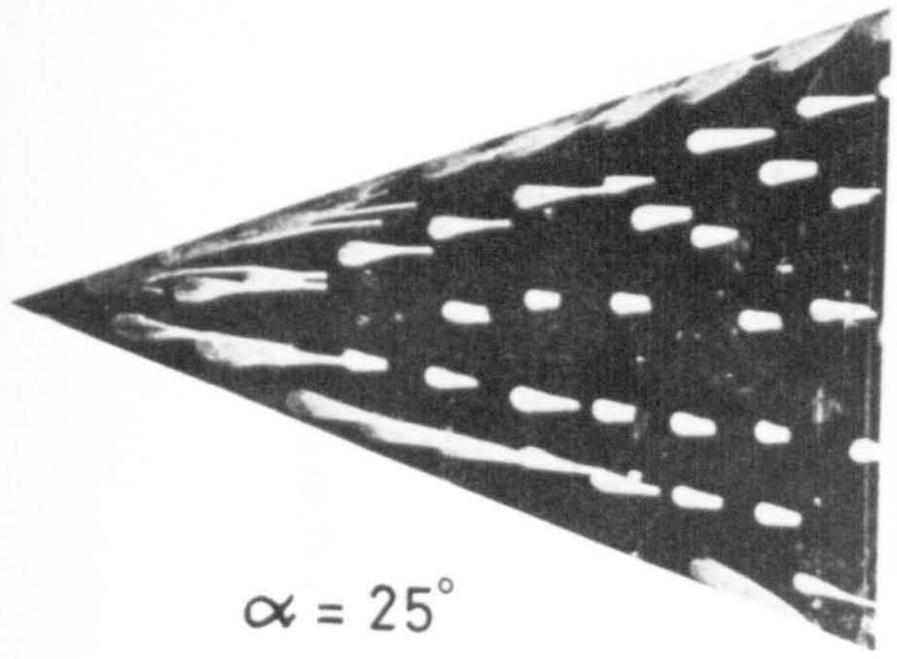

$\alpha = 25^\circ$

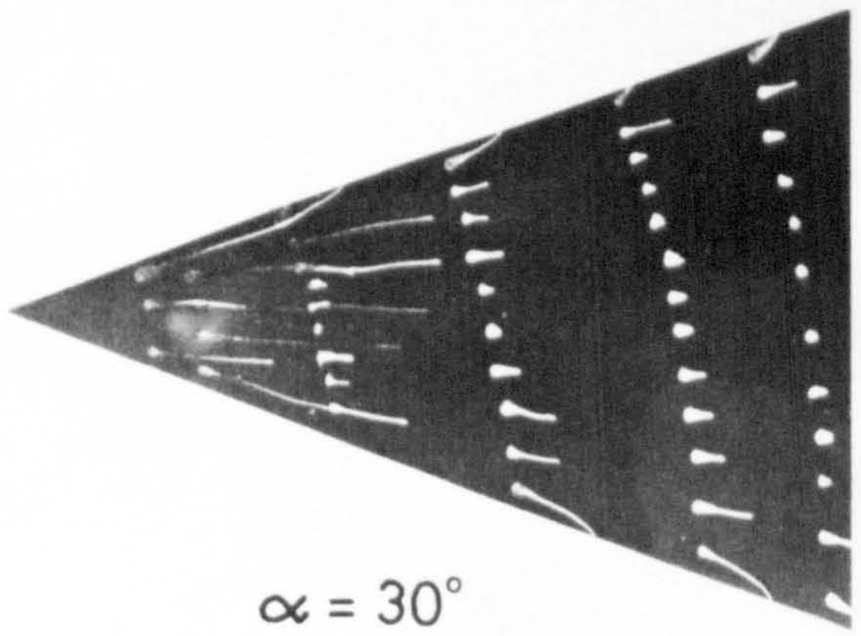

$\alpha = 30^\circ$

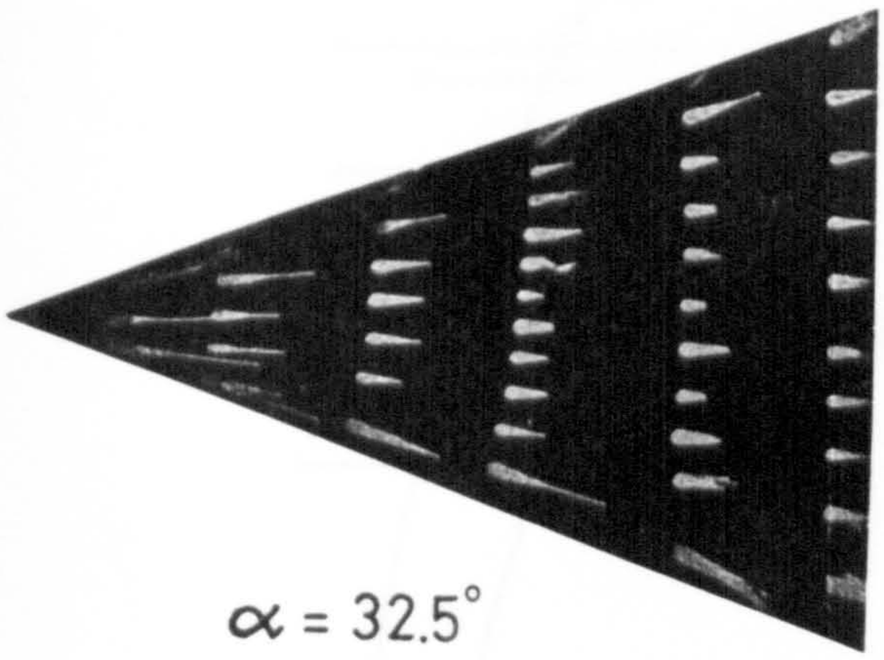

$\alpha = 32.5^\circ$

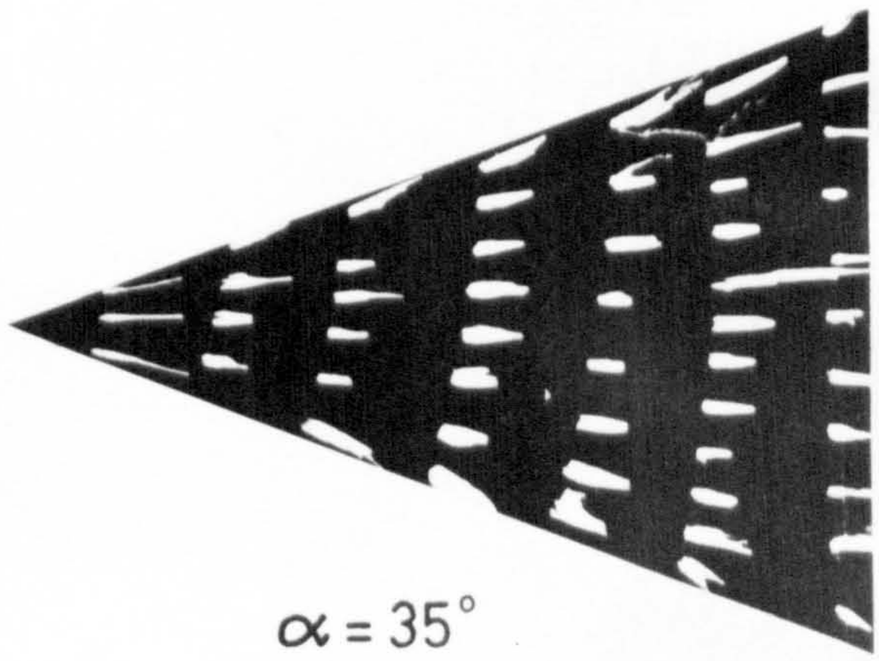

$\alpha = 35^\circ$

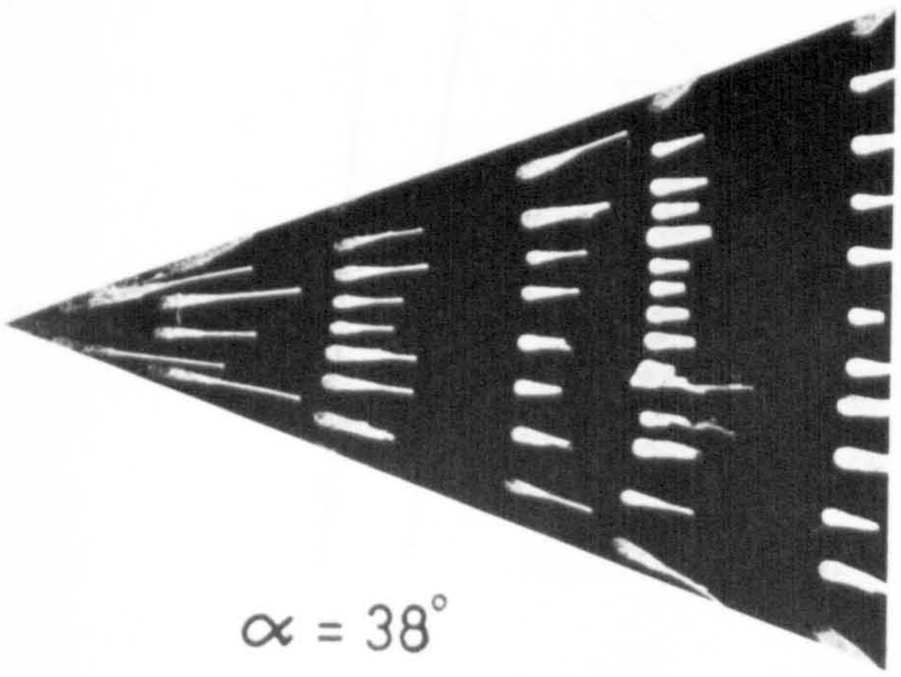

$\alpha = 38^\circ$

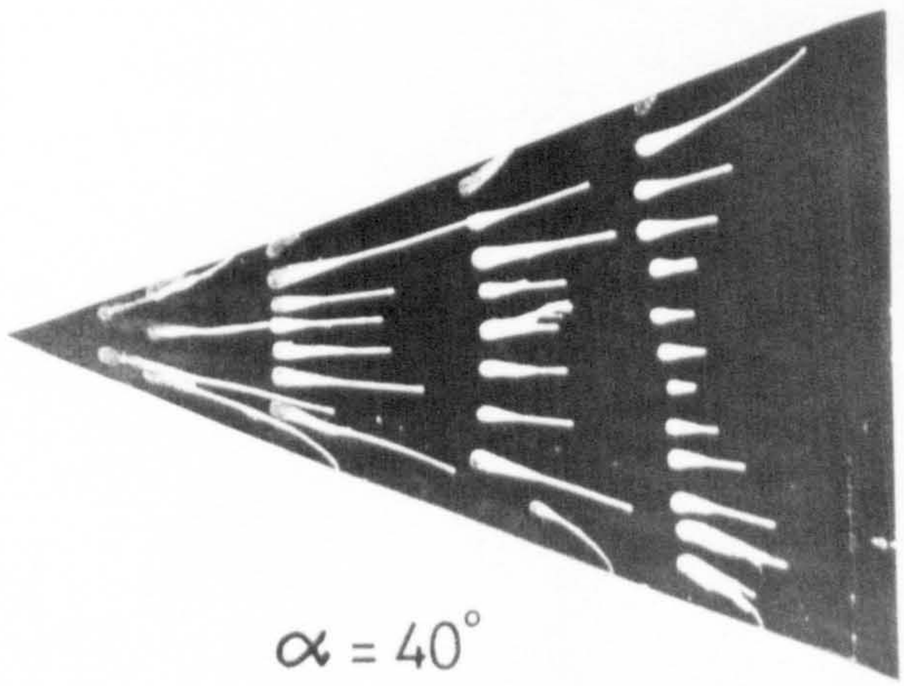

$\alpha = 40^\circ$

Fig. 58. Oil flow on flat compression surface.

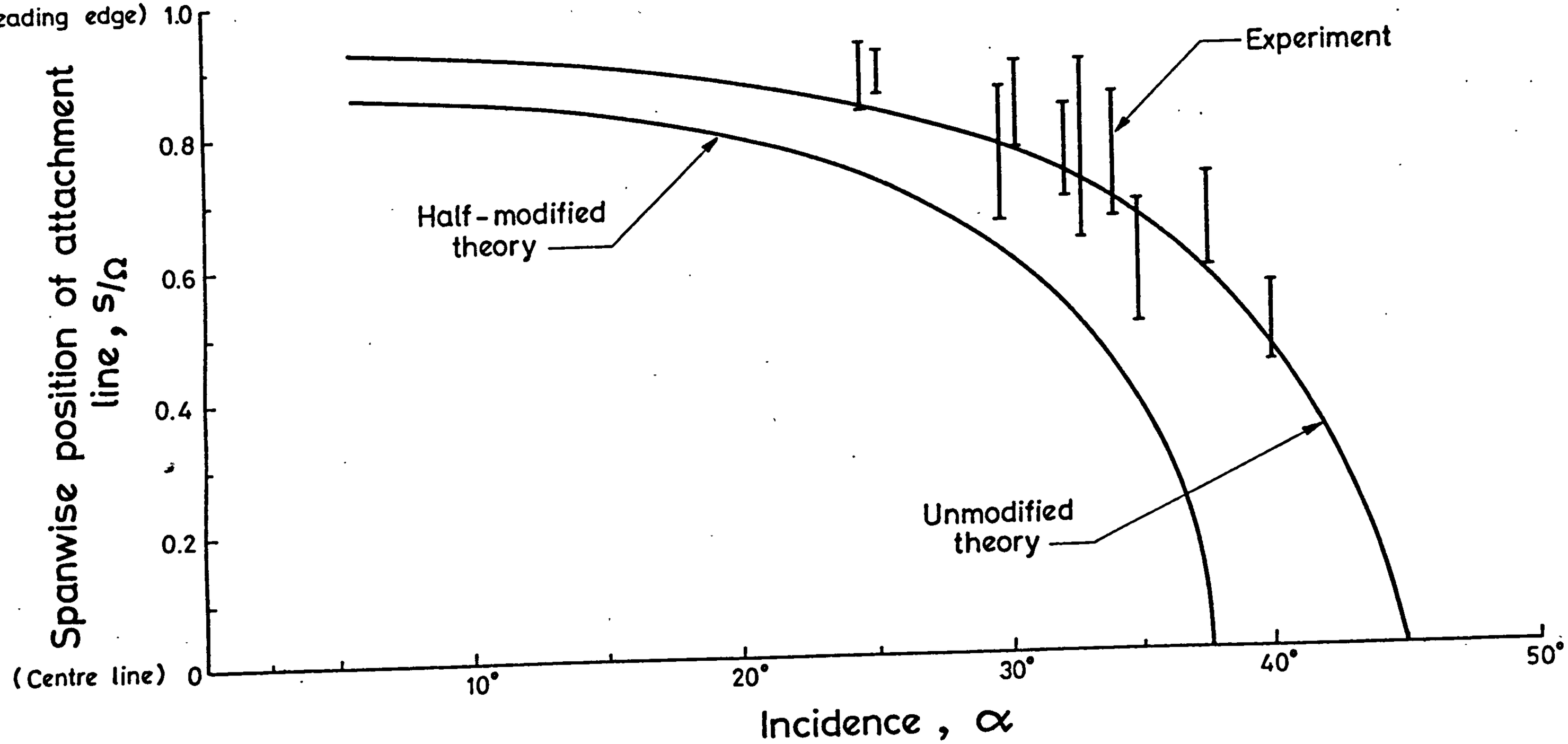

Fig. 59. Movement of compression surface attachment lines.

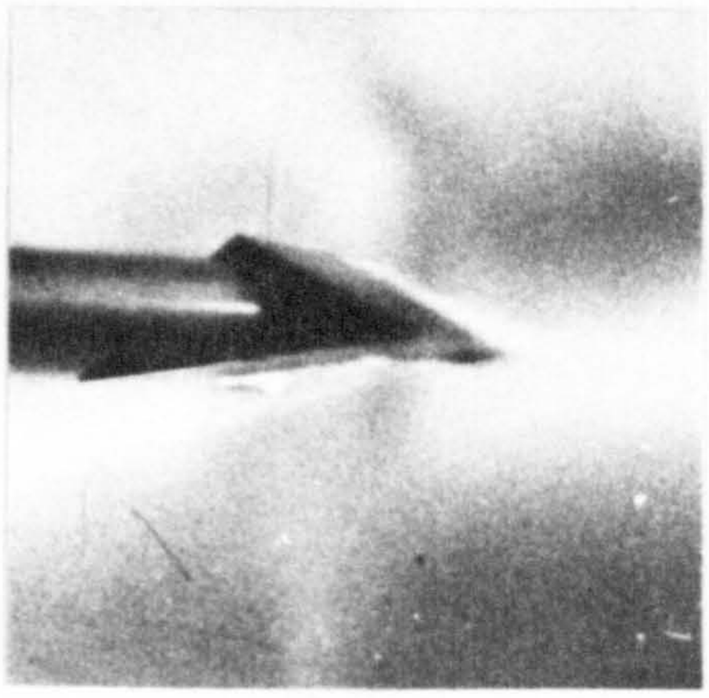

$\alpha = 0°$

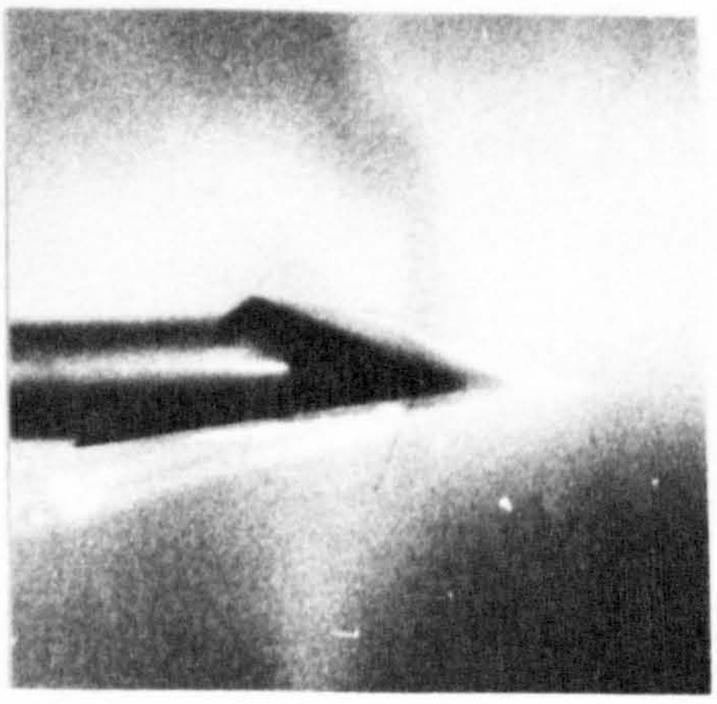

$\alpha = 5°$

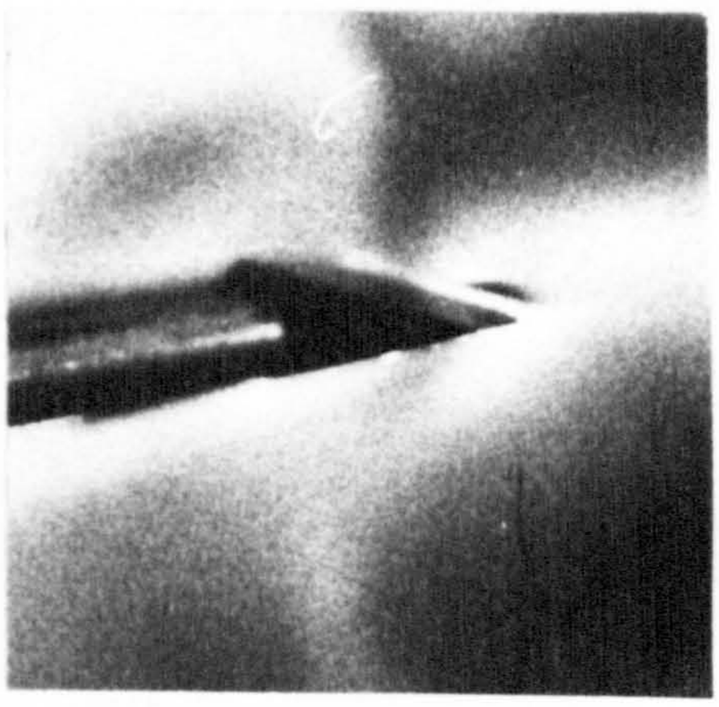

$\alpha = 10°$

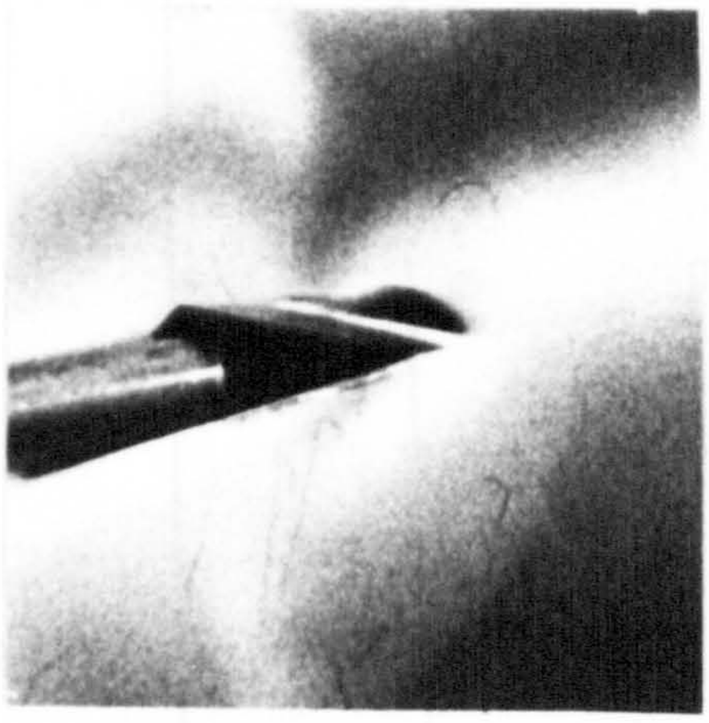

$\alpha = 15°$

$\alpha = 25°$

Fig.60. Vapour screen photographs, flat compression surface.

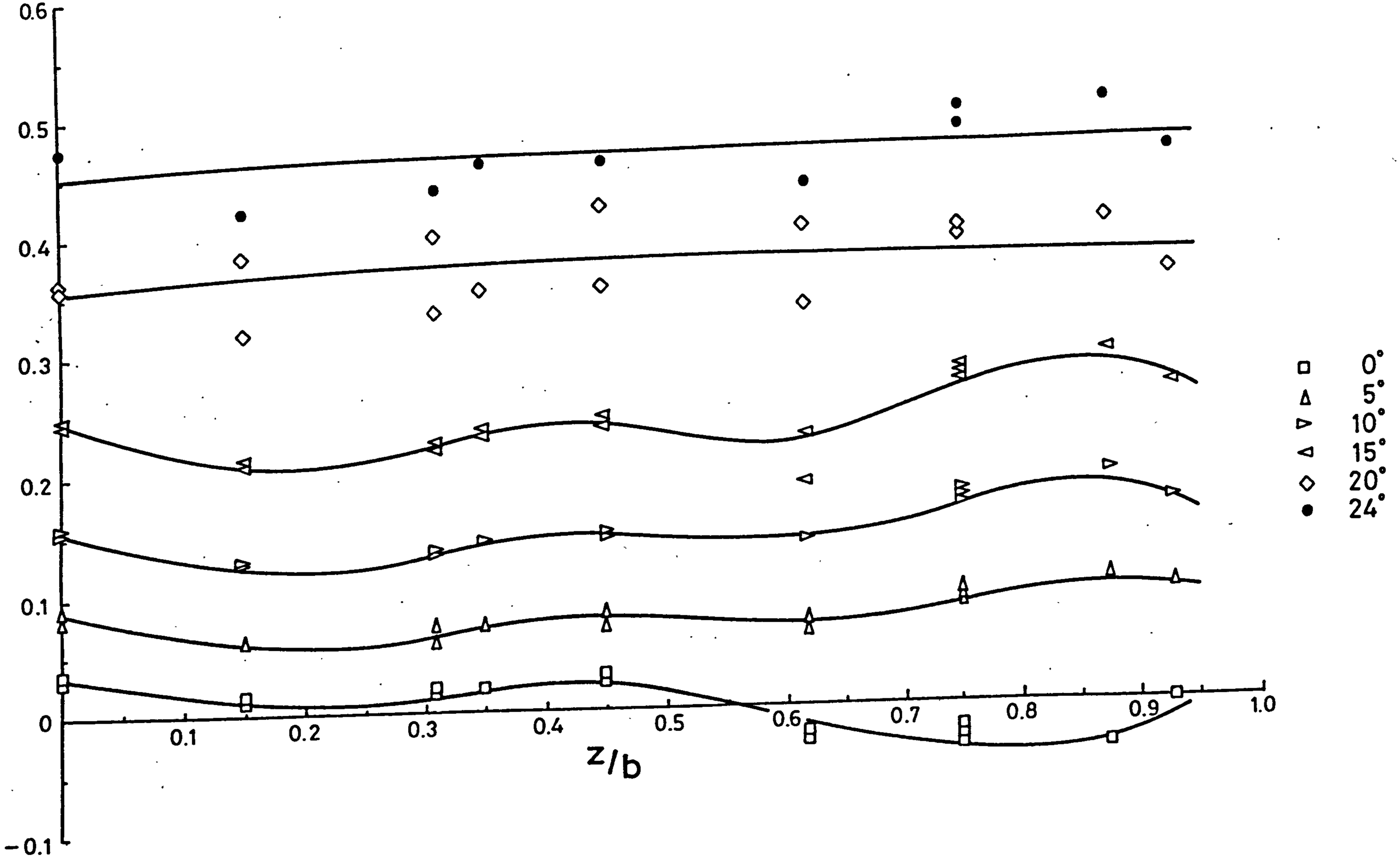

Fig. 61. Combined compression surface distributions.

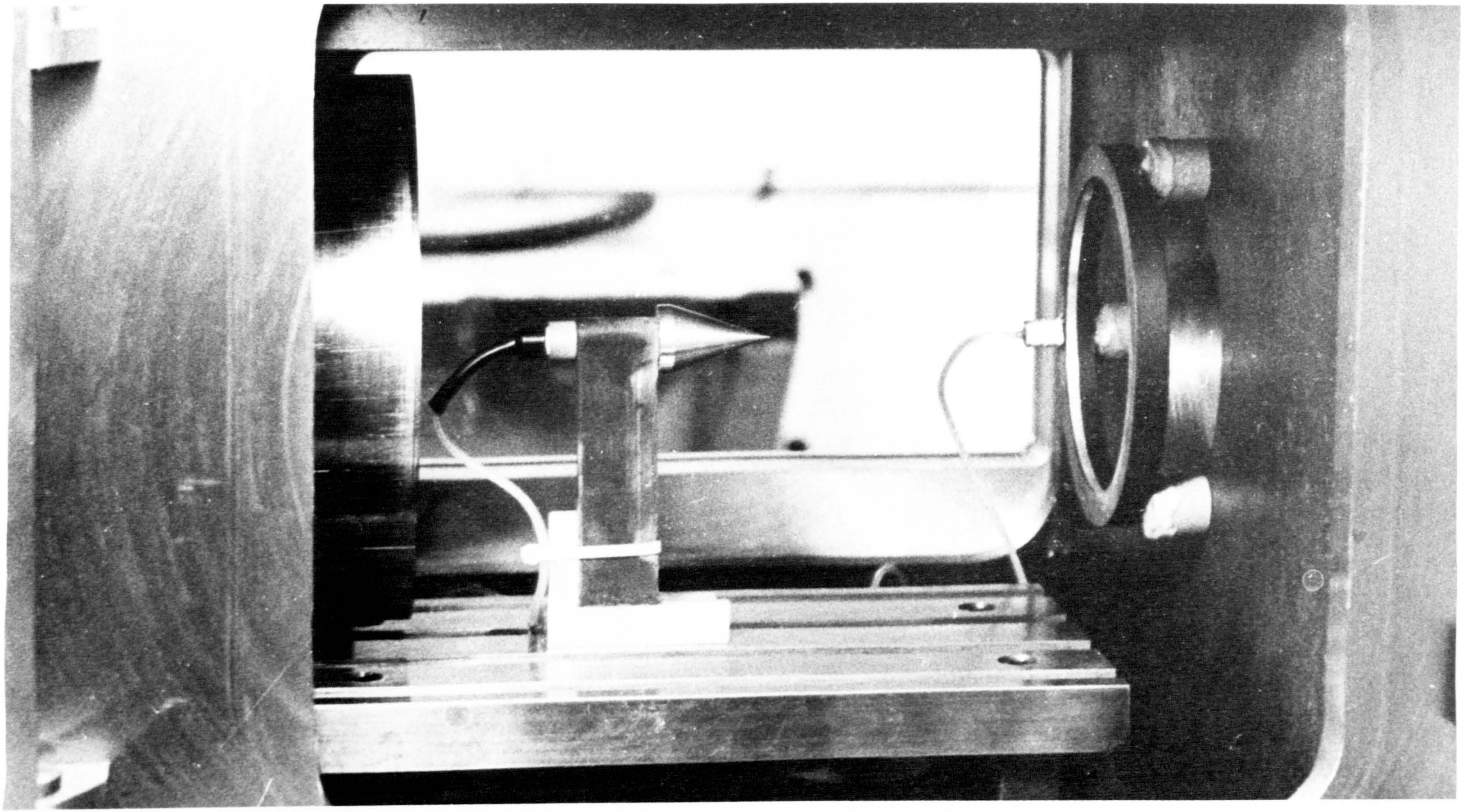

Fig. 62. The working section of the Helium Tunnel.